

**Magneto-Structural Studies of Copper(II) Coordination Compounds Using
1,10-Phenanthroline and 1,4-Phenylene Diacetic Acid Ligands**

by
Azadeh Mehrani

A dissertation submitted to the Department of Chemistry,
College of Natural Science and Mathematics
in partial fulfillment of the requirements for the degree of

Doctor of Philosophy
in Chemistry

Chair of Committee: Dr. Allan J. Jacobson

Committee Member: Dr. Arnold M. Guloy

Committee Member: Dr. Jakoah Brgoch

Committee Member: Dr. Loi Do

Committee Member: Dr. Jeffrey Rimer

University of Houston
December 2019

To my love, Hamid.

Acknowledgment

It was a long and hard journey with lots of ups and downs, and I learned and enjoyed a lot during this fantastic experience. I have received enormous support, passion, and encouragement from very nice individuals. I would like to sincerely and wholeheartedly acknowledge their help and supports. First and foremost, I want to express my deepest appreciation to my advisor, Professor Allan J. Jacobson. The best advisor that I have ever had. I was so fortunate to work in his lab and took advantage of his knowledge and guidance. I would like to express the deepest appreciation for his dedicated help, with constant encouragement and expert advice, and, most importantly, his full support during my Ph.D. research. He was always available, always stayed involved with my project, let me make mistakes, and learn from them. He always had a belief in me that really motivated me to work harder. Not only his professional policies, manner and lab environment, encouraged me through my research, but also his attitude and support during the hardest time of my life kept me enthusiastic about my research. I would have never forgotten the time that his support helped me pursue my dream and continue my study, after being suspended for almost a year as a consequence of my nationality and just because I decide to go back home and visit my family after 3 years which I am so happy about that decision, since, for over 6 years, that was the only chance that all four of us could gather together. I am truly fortunate to have had such an incredible opportunity to work with Dr. Jacobson. I am also very grateful to my dissertation committee members Dr. Arnold Guloy, Dr. Jakoah Brgoch, Dr. Loi Do, and Dr. Jeffrey Rimer for their willingness to take time to review my work and offer their valuable suggestions. I would also like to take another chance to thank Dr. Guloy for his support in my transferring process to my favorite field of study and helping me to start a great chapter of life in the chemistry department.

I would like to express my appreciation for our past and present group members. I would like to thank my mentor in the magnetic study, Dr. Maurice Sorolla, who spent many hours to guide me

through this field and helped me with the magnetic measurements. His guidance, suggestions, and support of my research on many occasions, and answering my countless questions on research and graduate studies are highly appreciated. I would also like to thank Tatyana and Dr. Boris Makarenko for their assistance with the TGA, glovebox and glove bags, and the instrument guidance in the lab. I would like to thank Dr. Xiqu Wang for his help in crystallography and sharing his knowledge and information about synthesis methods. I thank Jem, the great member of our group and my former wonderful labmates, Kannika (my great friend and officemate), Bee, Sam, Julie, and Chris, for a warm and friendly environment. I cannot imagine my accomplishment without our incredible lab manager, Ellen Lee, who has always been there with her kind support and continuous care.

I wish I could express enough of appreciation to Dr. James Korp who taught me the crystallography data collection and guide me through structural analysis. I am thankful of Dr. Joseph Reibenspies from Texas A&M for his support in crystallographic measurements. I am grateful to Dr. James Meen and Karoline Mueller for their assistance in using the SEM, EDX and WDS, and Dr. Alexander Litvinchuk for the Raman measurements. My grateful thanks is also extended to the department staff, including, but not limited to Crystal, Jerry, Roger, and MyTrang. Also, I would like to thank the campus police department for their safe escort during the late-night and early mornings of my schedule.

I want to thank my supportive teacher of my life, Dr. Ayoub Bazgir, who always encourages me with his different ways of problem-solving. I would love to also express my great gratitude toward Dr. Randal Lee for his generous support and encouragement.

Living far from the beloved family was impossible without having my second Houstonian family here, Hamed, Aria, Hamid, Hamed, Sogol, Niusha, Jahandar, Mina, Amin, Pegah, Hesam, Pishi, Pashang, and Gagash. I like to thank my great friends and classmates that made my graduate life pleasurable with their presence, Mohamad, Areej, and Mike. I am grateful for the people who support

me during the first d of my arrival to the US, Arash, Sandra, Asghar, and Shaghayegh. My special thanks go to my incredible friends, Nabil, Peiman, Haleh, Hamideh, Nima, Babak, Ahmad, Amin, Monika, Zahra, Maryam, Reza, Hengameh, Kiarash, Amy, Alan, Helina, Sara, Pouria, Pooria, Maryam, Hosein, Milad and my friends who are far from me now, but their friendship made my heart strong enough to go through this, Mozghan, Sevda, Mehrnoosh, Mahmoud, and Saeideh.

Finally, and most importantly, I am endlessly grateful to my family; my amazing mom, Marjan, the strongest person I have ever known during my whole life, who thought me how to deal with life, my fantastic dad, Kheiroollah, the most supportive and thoughtful person I have ever known, who always backed me up and stood behind me at every stage, and my inspiring and amazing little sister, Atousa, the person who is the blessing of my life; her presence made my life delightful. Their love and support is my most precious possession, and I cannot even describe how grateful I am for having them in my life.

I dedicate my work, to the love of my life and my best friend, my Hamid. If not for his love, sincerity, support, and understanding I could never have gone through this. His attitude toward life and his infinite love opened my heart and soul and ease my way through life.

Abstract

The main focus of this work is on a structural and magnetic study of copper(II) centers chelated by 1,10-phenanthroline (phen) ligands and connected through 1,4-phenylene diacetate (pda) linkers to make the coordination compounds. Their structures and magnetic behavior were determined and the correlation between them was investigated. Using magnetic models based on the structure of the compounds, experimental data were fitted to calculate the coupling constants (J values). Then the coupling constants were assigned to specific $\text{Cu}^{\text{II}} \cdots \text{Cu}^{\text{II}}$ interactions based on the structural geometry.

Seven new copper(II) coordination compounds were synthesized solvothermally. The synthesis conditions were varied to find the optimum conditions to obtain pure phases, in the highest yield, and with the best crystal quality. These copper(II) coordination compounds were characterized by single crystal X-ray diffraction. The compounds $[\text{Cu}_3(\text{phen})_3(\text{pda})_2(\text{H}_2\text{O})^{2+}] \cdot (\text{ClO}_4^-)_2 \cdot (\text{H}_2\text{O})_4$ (**1**), $[\text{Cu}(\text{phen})(\text{pda})] \cdot (\text{H}_2\text{O})_2$ (**2**), and $[\{\text{Cu}(\text{OH})(\text{phen})\}_4] \cdot (\text{ClO}_4)_4$ (**3**) were phase pure and further characterized using IR, Raman, thermogravimetric analysis, powder X-ray diffraction and magnetic measurements. Four other compounds $[\text{Cu}_2(\text{phen})_2(\text{pda})(\text{H}_2\text{O})] \cdot [\text{H}_2\text{pda}] \cdot [\text{ClO}_4^-]_2 \cdot (\text{H}_2\text{O})_4$ (**4.1**), $[\text{Cu}_2(\text{phen})_2(\text{Hpda})_{0.175}(\text{CH}_3\text{CH}_2\text{pda})_{0.825}(\text{H}_2\text{O})] \cdot (\text{H}_2\text{O})_{0.35} \cdot (\text{ClO}_4^-)_2$ (**4.2**), $[\text{Cu}_4(\text{phen})_4(\text{pda})_2(\text{H}_2\text{O})_2] \cdot (\text{ClO}_4^-)_4 \cdot (\text{H}_2\text{O})_2 \cdot (\text{CH}_3\text{CN})_4$ (**5.1**), and $[\text{Cu}_4(\text{phen})_4(\text{pda})_2(\text{H}_2\text{O})_2] \cdot (\text{ClO}_4^-)_4 \cdot (\text{H}_2\text{O})_{0.24}$ (**5.2**). could be synthesized as major phases with the suitable single crystals for structural characterization.

The magnetic data in the trinuclear compound $[\text{Cu}_3(\text{phen})_3(\text{pda})_2(\text{H}_2\text{O})] \cdot (\text{ClO}_4)_2 \cdot (\text{H}_2\text{O})_4$ (**1**), were well described with a 2-J model, with $J_1 = -51.8 \text{ cm}^{-1}$, which is consistent with the structural similarity to copper acetate, and $J_2 = +22.9 \text{ cm}^{-1}$, which follows the Goodenough–Kanamori–Anderson (GKA) rule.

Zigzag chains are found in $[\text{Cu}(\text{phen})(\text{pda})] \cdot (\text{H}_2\text{O})_2$ (**2**). Fitting the experimental data with the Fisher chain model results in two-dimensional magnetic ordering with a long-range intrachain interactions with $J = +2.52 \text{ cm}^{-1}$, and the interchain coupling constant of $zJ = -1.98 \text{ cm}^{-1}$.

The magnetic data in the $[\{\text{Cu}(\text{OH})(\text{phen})\}_4] \cdot (\text{ClO}_4)_4$ (**3**) with a cubane arrangement, were fitted using a 1+1+4 unique model with the $J_1 = -28.0 \text{ cm}^{-1}$, $J_2 = +72.2 \text{ cm}^{-1}$, and $J_3 = -15.3 \text{ cm}^{-1}$. By considering the $\text{Cu}^{\text{II}}\text{-O-Cu}^{\text{II}}$ angles (θ), the magnetic interactions of the two subunits and the four diagonal interactions are consistent with the Hatfield magnetic correlation model in hydroxo-bridged binuclear compounds, and the 2+4 model, respectively.

Due to the interesting structural geometries of four later coordination compounds, their structures were reported. Several compounds were synthesized using phen and pda ligands through this work. The similar stability of these compounds leads to the simultaneous occurrence of different compounds in the same reaction pot. However, three compounds were successfully synthesized in a single-phase, and their magnetic behavior was studied.

Table of Contents

Dedication	ii
Acknowledgment	iii
Abstract	vi
List of Figures	xii
List of Tables	xvi
List of Abbreviation and Acronyms	xvii
List of Symbols	xviii

Chapter 1. Introduction to Copper Compounds

1.1. Transition Metal Complexes.....	1
1.2. Copper Complexes.....	4
1.2.1 Different Oxidation States.....	4
1.2.2. Coordination Numbers and Geometries	5
1.3. Cu(II) Complexes.....	7
1.3.1. Structural Features.....	7
1.3.2. Applications of Copper(II) Complexes	11
1.3.2.1 Transfer, Storage, Removal, and Separation	12
1.3.2.2 Pharmaceutical Properties	13
1.4. Research Motivation	19

Chapter 2. Literature Review on Magnetic Properties of Copper(II) Complexes

2.1. Magnetic Materials in Future Technologies	20
2.2. Magnetic Behavior of Copper(II) Complexes	21
2.2.1. Historical Development.....	22
2.2.2. Intramolecular Magnetic Interactions	23
2.2.3. Mononuclear Copper(II) Compound.....	26
2.2.4. Dinuclear Copper(II) Compounds.....	26
2.2.4.1 Dinuclear Copper(II) Carboxylates	27
2.2.4.2 Di-nuclear Copper(II) Halides	29
2.2.4.3 Dinuclear Copper(II) Compounds with μ -oxo Bridges	30
2.2.4.4 Dinuclear Copper(II) Phosphates	30

2.2.4.5 Long-Range Magnetic Coupling	31
2.2.5. Trinuclear Copper(II) Compounds.....	33
2.2.6. Tetranuclear Copper(II) Compounds	37
2.2.7. Spin Frustrated Systems	40
2.2.8. Polynuclear Copper(II) Compounds	41
2.2.9. Single Molecular Magnets (SMM).....	42
2.2.10 Single-chain magnets (SCM)	43
2.3. Effects of Ligands	44

Chapter 3. Materials, Methods, and Instrumentation

3.1. Synthesis	46
3.1.1. Solvothermal Reactions.....	46
3.1.2. Starting Materials	50
3.1.3. Reaction Containers	51
3.1.4. Ovens.....	51
3.2. Materials Characterization	51
3.2.1. Powder X-ray Diffraction (PXRD)	51
3.2.2. Single Crystal X-ray Diffraction (SCXRD).....	52
3.2.3. Chemical Analysis.....	52
3.2.4. Raman Spectroscopy	53
3.2.5. Infrared (IR) Spectroscopy.....	53
3.2.6. Thermogravimetric Analysis (TGA).....	53
3.2.7. Bond Valence Sum (BVS)	54
3.3. Magnetic Characterization	54
3.3.1. Magnetic Properties.....	54
3.3.2. PHI Program.....	55

Chapter 4. A New Trinuclear Cu(II) Coordination Polymer: Correlation of the Magnetic Behavior with the Crystal Structure

4.1. Introduction.....	56
4.2. Experimental	57
4.2.1. Synthesis of $[\text{Cu}_3(\text{phen})_3(\text{pda})_2(\text{H}_2\text{O})^{2+}] [\text{ClO}_4^-]_2 [\text{H}_2\text{O}]_4$ (1).....	57
4.2.2. Characterization of 1	59

4.2.2.1. Single Crystal X-ray Diffraction (SCXRD)	59
4.2.2.2 Crystal Structure	61
4.2.2.3 Powder X-ray Diffraction (PXRD).....	66
4.2.2.4 Physical Measurements.	67
4.2.3. Magnetic Measurements.....	71
4.2.4. Magneto-Structural Correlations	74
4.3. Conclusion	77

Chapter 5. Two-Dimensional Magnetic Ordering in a One-Dimensional Zigzag Cu(II) Chain Structure

5.1. Introduction.....	78
5.2. Experimental	79
5.2.1. Synthesis of [Cu(phen)(pda)]·(H ₂ O) ₂ (2).....	79
5.2.2. Characterization of 2	80
5.2.2.1. Single Crystal X-ray Diffraction (SCXRD)	80
5.2.2.2 Crystal Structure	82
5.2.2.3 Powder X-ray Diffraction (PXRD).....	85
5.2.2.4 Physical Measurements.	86
5.2.3. Magnetic Measurements.....	88
5.2.4. Magneto-Structural Correlations.....	90
5.3. Conclusion	94

Chapter 6. A Magnetic Study of a New Tetranuclear Copper(II) Complex with a Cu₄O₄ Cubane Core

6.1. Introduction.....	96
6.2. Experimental	99
6.2.1. Synthesis of [{Cu(OH)(phen)} ₄]·(ClO ₄) ₄ (3).....	99
6.2.2. Characterization of 3	100
6.2.2.1. Powder X-ray Diffraction (PXRD).....	100
6.2.2.2. Single Crystal X-ray Diffraction (SCXRD)	101
6.2.2.3. Crystal Structure.	103
6.2.2.4. Physical Measurements.	107
6.2.3. Magnetic Studies	110

6.2.4. Magneto-Structural Correlations	116
6.3. Conclusion	118

Chapter 7. Four New Cu(II) Coordination Complexes Crystal Structure

7.1 Introduction	120
7.2. Copper(II) Binuclear One-Dimensional Coordination Polymer	122
7.2.1. Synthesis of $[\text{Cu}_2(\text{phen})_2(\text{pda})(\text{H}_2\text{O})] \cdot [\text{H}_2\text{pda}] \cdot [\text{ClO}_4^-]_2 \cdot [\text{H}_2\text{O}]_4$ (4.1)	122
7.2.2. Single Crystal X-ray Diffraction (SCXRD)	122
7.2.3. Crystal Structure	125
7.3. Isolated Copper(II) Binuclear Coordination Compound	130
7.3.1. Synthesis of $[\text{Cu}_2(\text{phen})_2(\text{Hpda})_{0.175}(\text{CH}_3\text{CH}_2\text{pda})_{0.825}(\text{H}_2\text{O})] \cdot [\text{H}_2\text{O}]_{0.35} \cdot [\text{ClO}_4^-]_2$ (4.2)	130
7.3.2. Single Crystal X-ray Diffraction (SCXRD)	131
7.3.3. Crystal Structure	133
7.4. Copper(II) Tetranuclear Coordination Polymer in Acetonitrile	137
7.4.1. Synthesis of $[\text{Cu}_4(\text{phen})_4(\text{pda})_2(\text{H}_2\text{O})_2] \cdot [\text{ClO}_4^-]_4 \cdot [\text{H}_2\text{O}]_2 \cdot [\text{CH}_3\text{CN}]_4$ (5.1)	137
7.4.2. Single Crystal X-ray Diffraction (SCXRD)	137
7.4.3. Crystal Structure	139
7.5. Copper(II) Tetranuclear Coordination Polymer in Aqueous Solution	144
7.5.1. Synthesis of $[\text{Cu}_4(\text{phen})_4(\text{pda})_2(\text{H}_2\text{O})_2] \cdot [\text{ClO}_4^-]_4 \cdot [\text{H}_2\text{O}]_{0.24}$ (5.2)	144
7.5.2. Single Crystal X-ray Diffraction (SCXRD)	145
7.5.3. Crystal Structure	147
7.6. Conclusion	152

Chapter 8. Conclusion and Future Work

8.1 Conclusion	154
8.2 Future Work	159
Bibliography	160

List of Figures

Figure 1.1 Different coordination numbers and geometries of copper ion. (a) linear CuCl_2 , (b) CuCl_3^- in KCuCl_3 and NH_4CuCl_3 with the planar structure of $[\text{Cu}_2\text{Cl}_6]^{2-}$, (c) chains of square planar units of CsCuCl_3 , (d) tetrahedral geometry of Cu(I) in $\text{Cs}_3[\text{Cu}(\text{CN})_4]$, (e) square planar geometry of Cu(II) in $(\text{NH}_4)_2[\text{CuCl}_4]$, (f) $[\text{CuCl}_5]^{3-}$ with the square pyramidal geometry, (g) in $\{\text{Cu}[\text{N}(\text{NH}_2)_3](\text{NH}_3)\} \cdot 2\text{PF}_6$ with the trigonal-bipyramidal geometry forced by tetradentate ligand, (h) $[\text{CuCl}_6]^{4-}$ and (i) $[\text{Cu}(\text{H}_2\text{O})_6]^{2+}$ with the octahedral Jahn-Teller distorted geometry.	6
Figure 1.2 Illustration of tetragonal elongation for octahedral complexes.	9
Figure 1.3 J-T distortion effect on copper(II) fluoride bond lengths.	9
Figure 1.4 Two pseudo-Jahn–Teller distortion in six coordinated Cu(II) complexes.	10
Figure 1.5 A porous coordination polymer of $[\text{Cu}(\text{dpa})_2(\text{SiF}_6)]_n$ with or without interpenetration (taken from Reference 84).	13
Figure 1.6 The first metalloid-metal based medicines.	14
Figure 1.7 Some examples of platinum-based drugs.	16
Figure 1.8 Some copper(II) complexes with cytotoxicity effect. [itpy = 4'-(1H-imidazol-2-yl)-2,2':6',2''-terpyridine, bitpy = 4'-(1H-benzimidazol-2-yl)-2,2':6',2''-terpyridine, dmp = 2,9-Dimethyl-1,10-phenanthroline, phen = 1,10-phenanthroline, pyterpy = 4'-(4-pyridyl)-2,2':6',2''-terpyridine, meotpy = 4'-(4-methoxyphenyl)-2,2':6',2''-terpyridine (meotpy)].	18
Figure 2.1 Molecular spintronics is a multidisciplinary field of study (taken from Reference 104).	20
Figure 2.2 Copper(II) acetate monohydrate dimer with the paddlewheel structure.	23
Figure 2.3 (a), (b) Super-exchange magnetic pathway with metal center orbitals and the ligand p orbital are linear, and (c), (d) orthogonal, (e) and (f) the direct magnetic exchange with the δ interaction.	25
Figure 2.4 Different ways that the carboxylato group can bridge between two copper centers. The magnetic interaction between the metal ions are greatest in (a) known as <i>syn-syn</i> and (d). The structures (b) which are known as <i>syn-anti</i> and (c) as <i>anti-anti</i> . The carboxylate in (d) acts as a monoatomic bridging ligand.	28
Figure 2.5 Dinuclear dihalo-bridged Cu(II) complexes' geometries with square pyramids sharing (a) a basal edge, (b) a base-to-apex edge with parallel basal planes, and (c) a base-to-apex edge, but with perpendicular basal planes.	29
Figure 2.6 Connection modes of phosphates to make binuclear copper(II) complexes.	31
Figure 2.7 The dimeric Cu(II) acetate dihydrate paddlewheel with an antiferromagnetic ground-state in both (a) the single-molecule and (b) the metal-organic framework of HKUST-1(taken from Reference 162).	33
Figure 2.8 Trinuclear Cu(II) compounds in linear or triangular structures.	34
Figure 2.9 (a) The linear trinuclear $\{\text{Cu}_3\text{Cl}_4(4\text{-pt})_4(4\text{-Hpt})_2\}^{2-}$ building block of the (b) $[\text{Cu}_3\text{Cl}_4(4\text{-pt})_2(4\text{-Hpt})_2] \cdot 4\text{DMF} \cdot 2\text{MeOH}$ 2-D network, (c) the triangular trinuclear $[\text{Cu}_3(\text{OH})_3(4\text{-pt})_3(\text{DMF})_4]$ building block of the (d) $[\text{Cu}_3(\text{OH})_3(4\text{-pt})_3(\text{DMF})_4] \cdot 5\text{DMF} \cdot 3\text{MeOH}$ 3-D framework, (e) the pore size of $[\text{Cu}_3(\text{OH})_3(4\text{-pt})_3(\text{DMF})_4] \cdot 5\text{DMF} \cdot 3\text{MeOH}$ compared to the (f) pore size of $[\text{Cu}_3(\text{OH})_3(\text{trz})_3 \cdot (\text{H}_2\text{O})_4]$. Color code: copper, blue spheres; oxygen, red spheres; nitrogen, light-blue spheres; carbon, black spheres.	36

Figure 2.10 (a) triangular, (b) linear, (c) butterfly, (d) cyclic, (e) diamond, (e') distorted diamond (f) cyclic-diamond (g) cubane, and (h) ladder-like tetranuclear copper(II) complexes topologies.	37
Figure 2.11 Spin frustration with three antiferromagnetic interactions on trinuclear and with six antiferromagnetic exchanges on tetranuclear cyclic copper(II) complexes.	41
Figure 2.12 Polynuclear copper(II) carboxylate general structures: (a) without bridging ligands; (b) bridging ligands between two copper centers, (c) bridging ligands between copper centers and Oxygen atoms.	42
Figure 2.13 Polynuclear copper(II) ring (x = O, N, F, Cl, Br)	43
Figure 4.1 Schematic description of synthesis method of 1 .	58
Figure 4.2 A view of the asymmetric unit of 1 . Lattice water molecules, perchlorate ions, and hydrogen atoms are removed for clarity. Orange, red, blue, and gray spheres represent copper, oxygen, nitrogen and carbon atoms.	61
Figure 4.3 Geometry around each copper in 1 with thermal ellipsoids at the probability of 50%.	62
Figure 4.4 (a) Three pda ligands in the unit cell direct crystal growth in two directions. (b) The plane is made out of crystal growth in two directions.	64
Figure 4.5 (a) π - π stacking along a-b direction, (b) the hydrogen bond between the coordinated water, lattice water molecules and the two oxygens from pda ligands. Orange, red, blue, and gray spheres represent copper, oxygen, nitrogen and carbon atoms	65
Figure 4.6 Perchlorate groups are located in the empty spaces of the 3-D framework.	66
Figure 4.7 Experimental and simulated powder X-ray diffraction of 1 . The simulated pattern is based on the analysis of the single-crystal X-ray diffraction refined structure.	67
Figure 4.8 TGA and DTG of 1 . The first weight loss corresponds to loss of lattice water and the second drastic weight loss is due to the exothermic decomposition of 1 due to the explosive decomposition of perchlorate.	68
Figure 5.1 View of the asymmetric unit of 2 , with atom numbering and 70% probability thermal ellipsoids. Only one orientation of the disordered water molecules is shown.	82
Figure 5.2 The square planar coordination of the copper ion in 2 .	83
Figure 5.3 One chain of 2 , growing along the c direction. Phen is the blocking chelating ligand, and pda is the bridging ligand.	84
Figure 5.4 Experimental and simulated powder X-ray diffraction of 2 . The simulated pattern is based on the analysis of the single-crystal X-ray diffraction refined structure at -150 °C.	86
Figure 5.5 TGA and DTG of 2 . The first weight loss corresponds to loss of lattice water. The second and third weight loss relates to the decarboxylation and phen ligand dissociation. The last step is the decomposition of 2 . The residual is copper oxide.	87
Figure 5.6 IR spectroscopy of 2 .	88
Figure 5.7 Experimental χT and χ vs. temperature at H = 1 T in the temperature range of 3-300 K. The solid line is the best theoretical fit of the Fisher model to the experimental χT plot.	89
Figure 5.8 $1/\chi$ vs. temperature at 1T magnetic field for 2 . The solid line is the Curie-Weiss fit.	89
Figure 5.9 Schematic view of the two chains of 2 within a layer and determining Cu...Cu distances in a) the bc plane and b) the b direction.	91
Figure 5.10 Schematic view of the three layers of 2 chains and the interchain-interlayer distances between copper ions.	91

Figure 5.11 Two layers of chains in 2 the ac plane while the water molecules are in the middle of the chain layers.	92
Figure 5.12 Localized magnetic orbitals on three nearest copper centers from three interlayer chains display a weak δ -interaction.	94
Figure 6.1 Out-of-plane displacement (τ) of the coordinated atom(s) to the bridging oxygen with respect to the dinuclear subunit plane and the Cu ^{II} -O-Cu ^{II} angle (θ).	97
Figure 6.2 Schematic drawing of different models of Cu(II) cubane complexes.....	98
Figure 6.3 Experimental and simulated powder X-ray diffraction of compound 3 . The simulated pattern is based on the analysis of the single-crystal X-ray diffraction refined structure.	101
Figure 6.4 Coordination environment around Cu(II) centers; polyhedron of the Cu(1) and Cu(2) are distorted square pyramidal and the geometry of the Cu(3) and Cu(4) are distorted octahedral.	103
Figure 6.5 The coordination environment around copper centers (a) without and (b) with the phen ligands.....	105
Figure 6.6 The hydrogen bond of the perchlorates to the μ_3 -hydroxo groups in vertices of the cubane core.	106
Figure 6.7 Packing of 3 with a centrosymmetric space group. The unit cell border is shown with dash lines.....	106
Figure 6.8 TGA and DTG of 3 in the air with a heating rate of 1 °C/min.....	108
Figure 6.9 IR Spectroscopy of 3	110
Figure 6.10 Plots of χ and $1/\chi$ vs. T for 3	111
Figure 6.11 The experimental and best fit theoretical temperature dependence of χT in a field of 1 T for 3	112
Figure 6.12 (a) Cu-O bond lengths and Cu-O-Cu angles (b) Cu...Cu distances of the cubane core of 3	113
Figure 6.13 Schematic view of coupling exchange in 3 , between Cu(1)-Cu(2), J_1 , between Cu(2)-Cu(3), J_2 and between Cu(1)-Cu(3), Cu(1)-Cu(4), Cu(2)-Cu(3), Cu(2)-Cu(4), J_3	115
Figure 6.14 d^9 orbital splitting of square pyramidal and octahedral both with elongation along the z-axis.....	117
Figure 6.15 Schematic view of the magnetic orbitals on copper centers for the predominant exchange pathways in the cubane core consists of two individual subunits. The binuclear subunit coupling exchange pathway consists of each individual copper center and the connected atoms.	118
Figure 7.1 The copper(II) complexes synthesized by Helen Wang using pda and phen ligands. (a) [Cu ₃ (phen) ₃ (pda) ₃ (H ₂ O)](ClO ₄) ₂ (H ₂ O) _x (HW1), (b) [Cu ₂ (phen) ₄ (pda)](ClO ₄) ₂ (HW2), and (c) [Cu ₄ (phen) ₄ (pda) ₂ (OH) ₂](ClO ₄) ₂ (H ₂ O) _x (HW3).....	121
Figure 7.2 Coordination environment around copper centers in 4.1 . Lattice water molecules, perchlorate ions, and hydrogen atoms are removed for clarity. gray spheres represent carbon atoms.	125
Figure 7.3 Geometry around Cu(1) and Cu(2) in 4.1	126
Figure 7.4 The zigzag chain of binuclear units of 4.1 . The hydrogen-bonded phenylene diacetic acid (H ₂ pda) molecule is removed for clarity, and the water molecules and the perchlorate counter ions are shown in two different sides of the figure.	128

Figure 7.5 The tetranuclear unit consists of two binuclear parts connected through two pda ligands. Each binuclear unit contains copper centers with chelating phen ligand bridging by a water molecule and two pda ligands in ac-plane in (a) HW2 structure and (b) 4.1	129
Figure 7.6 The π - π stacking interchain interactions.	130
Figure 7.7 The view of the asymmetric unit of isolated binuclear unit of 4.2 with two different occupancy percentages.	133
Figure 7.8 Geometry around Cu ion in 4.2	134
Figure 7.9. The hydrogen bond between a coordinated water molecule and O4 or O4' in 4.2	136
Figure 7.10 The π - π stacking intermolecular interaction along the c-axis.	136
Figure 7.11 The view of the asymmetric unit of 5.1 with thermal ellipsoids at the probability of 50%. Hydrogen atoms, solvent molecules and counter ions are removed for clarity.	139
Figure 7.12 Geometry around Cu(1) and Cu(2) in 5.1	140
Figure 7.13 Solvent molecules of water and acetonitrile in unit cell and four perchlorate anions in 5.1 . The carbon atoms of the organic ligands are removed for clarity.	142
Figure 7.14 A tetranuclear unit connects to four tetranuclear units through phenylene diacetate (pda) ligands. The pda linkers are shown with filled gray circles.	143
Figure 7.15 The π - π stacking interchain interactions of the aromatic ring in 5.1	144
Figure 7.16 The view of the asymmetric unit of a tetranuclear unit of 5.2 Hydrogen atoms, solvent molecules, and counter ions are removed for clarity.	147
Figure 7.17 Geometry around Cu(1) and Cu(2) in 5.2	148
Figure 7.18 Water molecules and four perchlorate anions in the unit cell of 5.2 . The carbon atoms of the organic ligands are removed for clarity.	150
Figure 7.19 The view of the pda ligands directions in a tetranuclear unit of (a) 5.1 and (b) 5.2	151
Figure 7.20 A tetranuclear unit in 5.2 connects to four tetranuclear units through phenylene diacetate (pda) ligands, making 2-D coordination polymer. The pda linkers are shown with filled gray circles.	151
Figure 7.21 (a) The π - π stacking interactions of the aromatic ring and (b) the hydrogen bond of terminal coordinated water to perchlorate ions in 5.2	152

List of Tables

Table 3.1 Optimizing the amount of initial solution concentration for the synthesis of 1 .*	47
Table 3.2 Optimizing the amount of solvent for the synthesis of 1 . *	48
Table 3.3 Starting reagents for all synthesis techniques	50
Table 4.1 Crystal data and structure refinement for 1 .	60
Table 4.2 Selected bond lengths [Å] and angles [°] for 1	63
Table 4.3 The oxidation states assignment of the copper ions from bond valence sums (BVS) in 1 , and the parameters used for the BVS calculations ^{227,239} .	69
Table 5.1 Crystal data and structure refinement for 1 .	81
Table 5.2 Selected bond lengths [Å] and angles [°] for 1	83
Table 5.3 The oxidation states assignment of the copper ions from bond valence sums (BVS) in 284	
Table 5.4 The parameters used for the BVS calculations.	84
Table 6.1 Crystal data and structure refinement for 3 .	102
Table 6.2 The oxidation states assignment of the copper ions from bond valence sums (BVS) in 3	109
Table 6.3 Parameters used for the BVS calculations for 3	109
Table 6.4 Important bond length and angles for 3 cubane core	114
Table 7.1 Crystal data and structure refinement for 4.1 .	124
Table 7.2 Selected bond lengths [Å] and angles [°] for 4.1	127
Table 7.3 Crystal data and structure refinement for 4.2 .	132
Table 7.4 Selected bond lengths [Å] and angles [°] for 4.2	135
Table 7.5 Crystal data and structure refinement for 5.1 .	138
Table 7.6 Selected bond lengths [Å] and angles [°] for 5.1	141
Table 7.7 Crystal data and structure refinement for 5.2 .	146
Table 7.8 Selected bond lengths [Å] and angles [°] for 5.2	149
Table 8.1 The main syntheses condition with the highest yield of compounds.	156

List of Abbreviation and Acronyms

1,4-ndc	1,4-naphthalene dicarboxylic acetate
2,7-ndc	2,7-naphthalene dicarboxylic acetate
AFM	antiferromagnetic
BVS	Bond Valence Sum
FM	ferromagnetic
GKA	Goodenough–Kanamori–Anderson
IR	Infrared
pda	1,4-phenylene diacetate
phen	1,10-phenanthroline
PXRD	Powder X-ray Diffraction
SCXRD	Single Crystal X-ray Diffraction
THF	Tetrahydrofuran
TGA	thermogravimetric analysis
TIP	temperature-independent paramagnetism
SOMO	singly occupied molecular orbital
VSM	vibrating sample magnetometer

List of Symbols

C	Curie constant
g	Landé g-factor
H	Hamiltonian
J	magnetic coupling
k	Boltzmann constant
N_{α}	Avogadro's number
r	observed bond length
R	agreement factor
S	spin vector value
S	bond valence
S_t	total spin
zJ	interchain interaction exchange
β	electron Bohr magneton
μ_{eff}	effective spin-only magnetic moment
χ	susceptibility
θ	Weiss constant

Chapter 1. Introduction to Copper Compounds

1.1. Transition Metal Complexes

In the field of material science, a better understanding of physical and chemical properties and of the interactions between the individual components is necessary to control the structural features and properties of new materials. Knowledge of the bonding chemistry, reaction mechanisms, and compound structures help to synthesize new materials exhibiting remarkable physical properties such as magnetism¹. The rapid development of crystal engineering of metal-organic complexes during the past decades has resulted in synthesis of numerous new materials with diverse structures and properties. The variety of structures are attributed to how the different metal centers and organic ligand building blocks are assembled². Transition metals are the d and f-block elements, between group 3 and 12 in the periodic table. The f-block elements are called lanthanide metals. The d-block elements have at most two electrons in their outermost s orbital and incompletely filled d orbitals. Unique behavior and specific applications arise from this configuration³⁻⁵.

In transition metal complexes, a transition metal is coordinated to one or more types of ligands. Transition metals exhibit different oxidation states and can interact with neutral or negatively charged molecules. The incomplete d shell allows transition metals to connect to a range of molecules or ions to form metal complexes or coordination compounds. Applications related to the electronic and aerospace industries, catalysis, or medical products indicate the importance of transition metal complexes⁶⁻¹⁰. Copper with the atomic number of 29 has the electronic configuration of $[\text{Ar}] 3d^{10} 4s^1$. The loss of an electron from 4s orbital to complete the 3d orbital makes it more stable because of the lower exchange energy than the pairing energy of orbitals in the s shell.

Furthermore, the sublimation energy and the melting point of copper are higher than alkalis in the same period on account of the metallic bond that the d shell electrons are involved in. These features are responsible for the behavior of copper to make more compounds with covalent bonds and higher lattice energy of them in comparison to others of alkali metals. The next ionization enthalpy energies, though, are lower than that of alkalis, so the formation of II, III, and IV oxidation state in copper needs less energy. Copper can be extracted from ores through leaching with sulfuric acid and refined by electrolysis¹¹.

The important roles of transition metal complexes in biological systems can be categorized in different ways according to their structural, reactive, and enzyme actions. In these categories, the metal complex acts as an enzyme cofactor and redox reaction catalyst, contributing to biological molecules' stability and functions in the transport of oxygen and hydrolysis reactions. Many anti-inflammatories, antibacterial, and anticancer metal complexes have been synthesized and applied since the discovery of cisplatin^{12,13}.

Research interest in polynuclear metal complexes mainly involving polydentate ligands, has been growing in recent decades because of a wide range of applications, primarily those related to unique magnetic properties. Revealing the fundamental magneto-structural correlations is the main research aim in this field. The research area offers a useful pathway to new types of magnetic materials¹⁴⁻¹⁹.

As a transition metal, copper is the first choice as a conductor for electrical applications, due to excellent electrical and thermal conductivities, combined with its high ductility, good formability and malleability, high strength, and outstanding resistance to corrosion. Alloying with appropriate elements changes the mechanical properties of copper for use in other different electrical applications. The most famous alloys with copper as the principal component are bronze and brass, in which the alloying

elements are tin and zinc, respectively. Alloying with nickel in cupronickel improves the strength and enhances corrosion resistance to seawater²⁰⁻²⁴.

Due to the various coordination numbers, geometries, and oxidation states, copper ions can adopt diverse topologies and form mono or multinuclear metal-organic complexes with different structural features and properties. Copper complexes have been shown to function as antibacterial, anti-inflammatory, and antiviral and antitumor agents with reduced side effects and toxicity, and to possess different modes of action compared to uncomplexed medicines. The mechanism of antibacterial and antiviral activity of copper-based complexes is only partly understood. Based on a theory the viral nuclei go through a degradation process in touch with copper ions. This would be more discussed in Section 1.3.2.2. Copper is a vital element in biochemical organisms, specially in metalloenzymes²⁵. The development and study of copper complexes are useful in designing and producing new compounds that have chemotherapeutic potential^{12,26}. The polynuclear compounds containing copper(II) ions with a single electron in the d shell have specific magnetic properties. The fascinating magnetic properties depend on their structure, the pathway, and the type of exchange interactions between the centers that hold unpaired electrons and are magnetically active. Their magnetic features arise from interactions between metal centers with unpaired d electrons. Owing to the single-molecule magnetism properties of polynuclear compounds, they could be used as single-molecular transistors and molecular magnetic memories. The molecular magnetism in polynuclear compounds containing metal centers with single electrons results from the short distance between metal centers and metal-metal magnetic interactions²⁷⁻²⁹.

1.2. Copper Complexes

1.2.1 Different Oxidation States

Copper most common stable complexes exist as Cu^{+1} and Cu^{2+} ; Cu^{3+} complexes are scarce^{19,30}. Copper(I) with a d^{10} configuration should be more stable than copper(II) with a d^9 system. Stability is a relative concept, as in aqueous solution, copper(I) is unstable relative to copper(II) and disproportionates to copper(II) and metallic copper. Although copper(I) is more stable than copper(II) in a non-aqueous solvent like acetonitrile.

The stability of a copper oxidation state in a complex depends upon the donor's hard or soft nature. Cu(I) as a soft metal ion prefers to link to a soft donor ligand like iodine or sulfur atoms. On the other hand, Cu(II) is a hard metal ion and makes stable complexes linking to the hard ligands, such as oxygen or nitrogen atoms. Among the copper halides, although CuI and CuF_2 are stable, CuF and CuI_2 are thermodynamically unstable and have never been isolated³¹⁻³³.

Cu(III) complexes are not stable but are considered as biological or homogeneous catalysis intermediates. To stabilize Cu(III) complexes constraining the coordination environment around copper to be square planar by using tetradentate anionic ligands was a strategy first used by Mergerum *et al.*^{34,35}. Rich coordination chemistry has been developed by discovering a few ligands that can stabilize copper(III) complexes³⁶⁻³⁸. In recent years, Cu(IV) species have been postulated as intermediates in oxidation catalysis. The spectroscopic data on these species, despite the importance of high oxidation states of copper ions, are scarce^{39,40}. The first Cu(IV) coordination compound of cesium hexafluorocuprate(IV) was synthesized in 1973 by mixing $\text{Cs}_2[\text{CuF}_6]$, cesium fluoride, and fluorine at high pressure^{41,42}. The Cu(IV) complexes in pure form are found in fluorides, and mixed with Cu(III) forms are observed in oxides^{43,44}.

1.2.2. Coordination Numbers and Geometries

The coordination numbers and geometries of copper ions in copper compounds influence function and reactivity in biological and environmental systems. Copper ions adopt different coordination numbers (CN) from 2 to 6. The geometry of Cu(I) and Cu(II) with the same CNs could be different. For instance, with a CN of 4, Cu(I) ions mostly adopt tetrahedral geometry with the sp^3 hybridization. Cu(II) compounds demonstrate various geometries, including tetrahedral, square planar, and trigonal bipyramidal^{45,46}. Some examples of different coordination numbers and geometries can be seen in Figure 1.1.

The preferred geometries of Cu(II) ions are square planar, square pyramidal, or axially distorted octahedral by the Jahn-Teller effect. However, Cu(I) with filled d^{10} configuration has no preference based on ligand field stabilization energy (LFSE) geometry. On the other hand, the geometry of the ligand field influences the oxidation state of copper. Cu(II) would not bond with ligands, which impose tetrahedral geometry, so the reduction potential is more positive in favor of Cu(I)⁴⁷. The geometry preference also is using for differentiating Cu(II) from Zn(II) which with a d^{10} configuration preferred geometry. Zn(II) tetrahedral complexes are common⁴⁸. The geometry affects the physical properties of the compound. Two newly reported Cu(II) complexes with chloride ligand in the form of bridging and a separated ligand show different magnetic behavior. The monomer with $[Cu(tdp)Cl_2]$ (tdp = tris(3,5-diisopropyl-1-pyrazolyl)methane) composition is diamagnetic, however the dimer unit $[Cu(tdp)(\mu-Cl)]_2(ClO_4)_2$ has a ferromagnetic interaction⁴⁹.

Cu(III)-aqua and Cu(III)-amine complexes are not stable species and rapidly decay. Cu(III) complexes of macrocyclic amines have been prepared by an electrochemical method in acetonitrile solution but they undergo spontaneous reduction to Cu(II). Accessing highly oxidizing ions strongly depends on the nature of the donors and the ligand ability to force square-planar geometry^{19,36}. Most of Cu(III) complexes coordination geometries are square planar or square pyramidal which is

consistent with the d^8 electronic configuration of Cu(III). Reported Cu^{3+} complexes are limited in number, and in octahedral geometry, they exhibit paramagnetic properties^{30,50}.

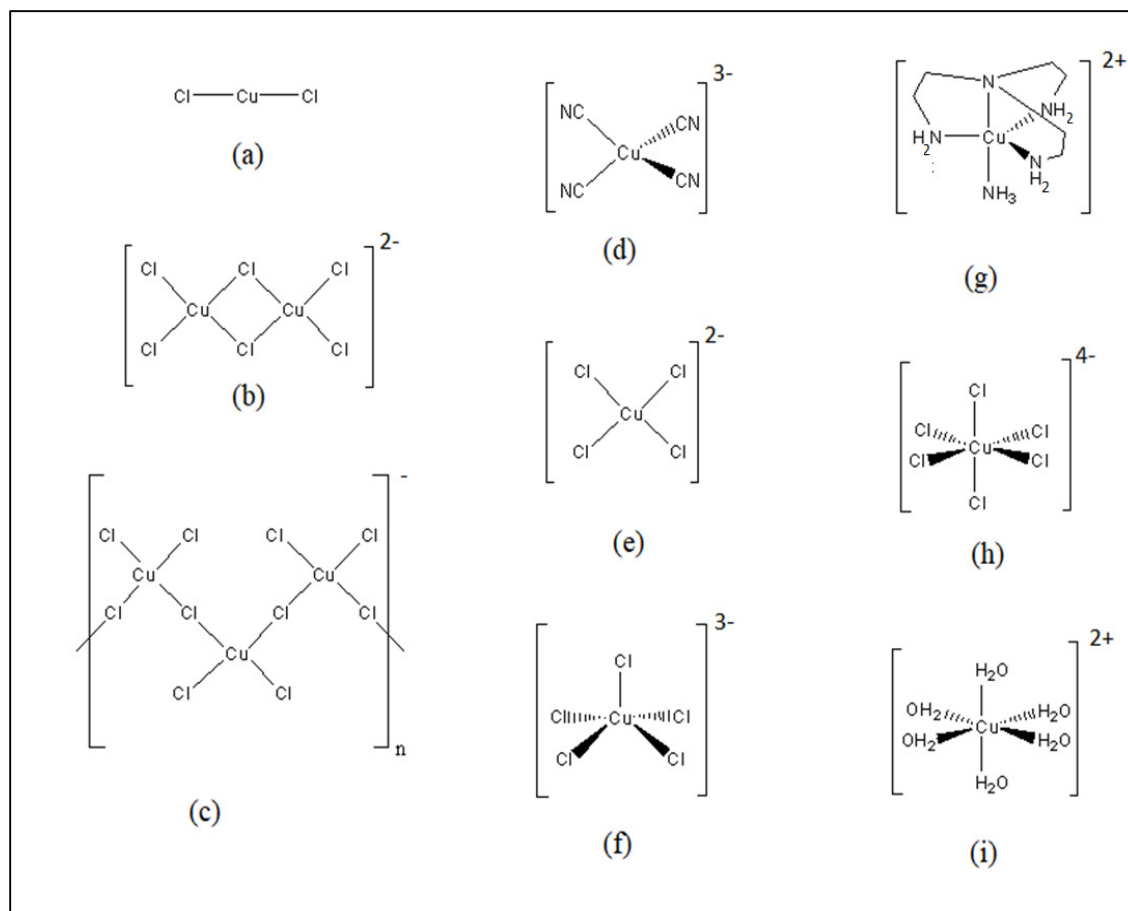


Figure 1.1 Different coordination numbers and geometries of copper ion. (a) linear CuCl_2 , (b) CuCl_3^- in KCuCl_3 and NH_4CuCl_3 with the planar structure of $[\text{Cu}_2\text{Cl}_6]^{2-}$, (c) chains of square planar units of CsCuCl_3 , (d) tetrahedral geometry of Cu(I) in $\text{Cs}_3[\text{Cu}(\text{CN})_4]$, (e) square planar geometry of Cu(II) in $(\text{NH}_4)_2[\text{CuCl}_4]$, (f) $[\text{CuCl}_5]^{3-}$ with the square pyramidal geometry, (g) in $\{\text{Cu}[\text{N}(\text{NH}_2)_3](\text{NH}_3)\} \cdot 2\text{PF}_6$ with the trigonal-bipyramidal geometry forced by tetradentate ligand, (h) $[\text{CuCl}_6]^{4-}$ and (i) $[\text{Cu}(\text{H}_2\text{O})_6]^{2+}$ with the octahedral Jahn-Teller distorted geometry.

Accompanied by stability in aqueous solutions and flexibility of the coordination chemistry, the copper(II) ion has is able to coordinate with various ligands, especially with the ones with oxygen and nitrogen donors. Considerable attention has been given to experimental and theoretical research on coordination chemistry of copper(II) and the synthesis of new materials with diverse applications using this unique metal ion.

1.3. Cu(II) Complexes

The synthesis of Cu(II) complexes by using a variety of ligands, linkers, and building blocks has made considerable progress. From simple complexes to coordination polymers and supramolecular compounds and even biomaterials, Cu(II) ion plays an influential role in determining the properties of the compound. Due to flexible coordination geometry, low toxicity, bioactivity as well as high stability and solubility, low cost and versatility, synthesis, characterization, and analysis of copper(II) compounds have received much interest.

1.3.1. Structural Features

The spectroscopic and stereochemistry properties of Cu^{2+} complexes are commonly understood in terms of Jahn-Teller coupling. When the geometry and electronic structure are changing as a function of temperature the effect termed the dynamic Jahn-Teller effect. The consequence of the interaction between electronic degeneracy and coupling to the lattice, i.e., unconventional local electron–lattice interactions results in the Jahn–Teller effect. Interest in this area has been motivated by the suggestion that superconductivity in copper oxides, dynamic Jahn-Teller coupling may be a novel and much stronger glue for electron pairing than conventional Bardeen–Cooper–Schrieffer (BCS) electron-phonon coupling in the underlying the behavior of high-temperature superconductors.

Furthermore, this suggests that the fluctuation of certain copper proteins electron paramagnetic resonance (EPR) spectra with temperature is due to the dynamic vibronic coupling effects⁵¹.

Six coordinated Cu(II) complexes show the Jahn-Teller (J-T) effect⁵². This effect denies the presence of stability and degeneracy simultaneously unless in a linear environment. The d^9 electron configuration of Cu^{2+} in an octahedral environment leads to the removing of the degeneracy of two e_g molecular orbitals of an octahedron. Distortion of these types of complexes occurs along one of the fourfold axes, labeled as the z -axis, and lower the overall energy. The common distortion is the elongation of bonds between Cu^{2+} and ligands along the z -axis, however, occasionally compression of bonds occurs due to this distortion. The direction of distortion is not predicted by the J-T theorem . The copper(II) octahedral compounds with the Jahn-Teller elongations of the stabilized z component orbitals are well-documented (Figure 1.2)⁵³⁻⁵⁶.

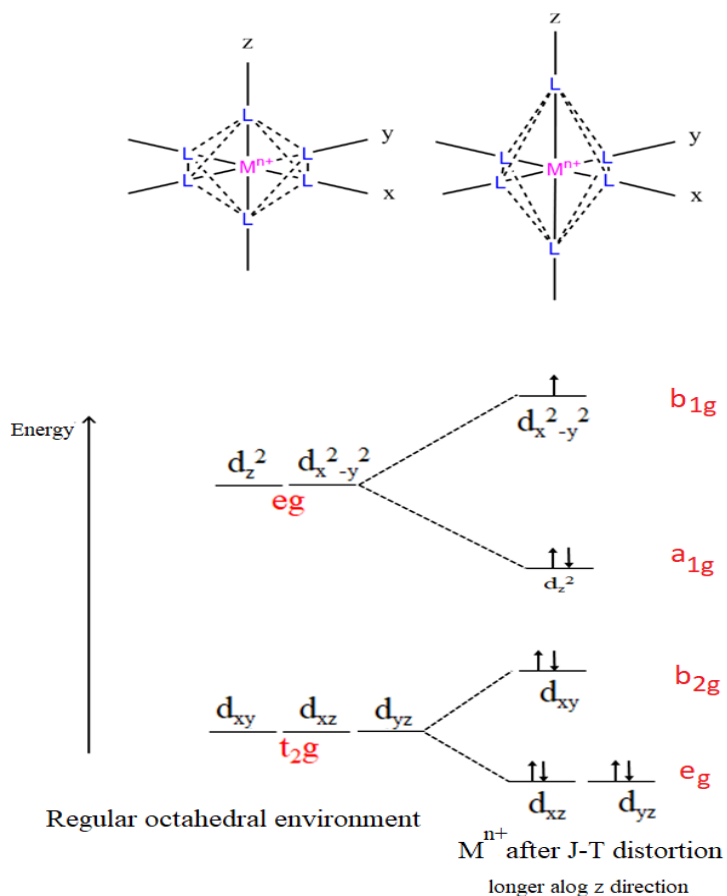


Figure 1.2 Illustration of tetragonal elongation for octahedral complexes.

Many examples of Cu(II) six coordinated complexes with different coordination environments (CuO₆, CuN₆, CuS₆, and other) have been reported by Malcolm A. Halcrow⁵⁷. A classic example of this type is copper(II) fluoride, as shown in Figure 1.3.

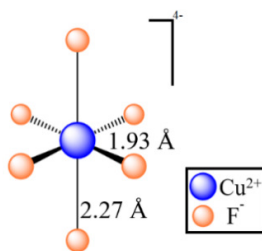


Figure 1.3 J-T distortion effect on copper(II) fluoride bond lengths.

The above argument only applies to complexes with Octahedral symmetry. The other reason for breaking the degeneracy is an unsymmetrical geometry. Another type of distortion in copper six coordinated complexes with $[\text{CuX}_2\text{L}_4]$ compositions is called the ‘pseudo-Jahn–Teller’ distortion (also known as second-order Jahn-Teller effect). Two examples of coordination environments around copper in such the structures are CuN_4O_2 , and CuO_4N_2 (Figure 1.4)⁵⁸.

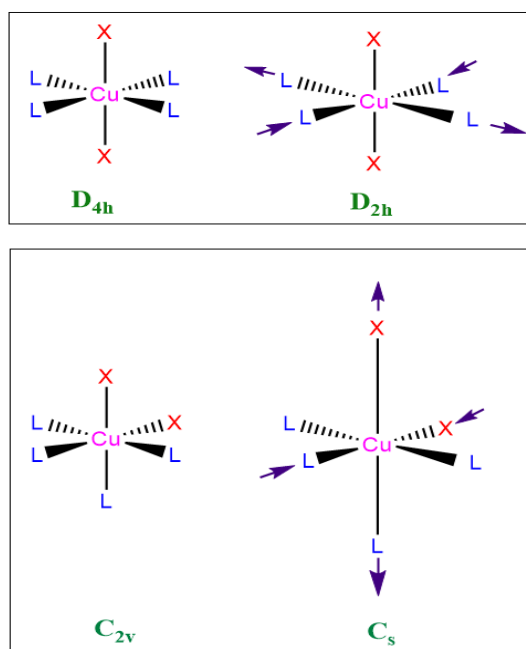


Figure 1.4 Two pseudo-Jahn–Teller distortion in six coordinated Cu(II) complexes.

A list of such distortions of Cu(II) six coordinated complexes is available in Halcrow’s review (see the supplementary file of mentioned review article)⁵⁷.

The electronic paramagnetic resonance (EPR) study was the first experimental evidence of the first and second Jahn-Teller effects in Cu(II) octahedral complexes. The interest of this study is due to the possible role of vibronic coupling in modifying the spectroscopic and electronic properties of the active sites of Cu(II) complexes^{59,60}. The first study on the 6-coordinated complexes was the hexakis using monodentate ligands, such as $\text{Cu}(\text{OH}_2)_6^{2+}$. The J-T distortion was determined from the static EPR of $[\text{Cu}(\text{ptz})_6](\text{BF}_4)_2$ (ptz = 1-propyltetrazole)⁶¹. $[\text{CuCl}_6]\text{Cl}_4$ EPR study has also shown two trans

longer bonds and four shorter Cu-Cl bonds⁶². An EPR study on Cu(en)_3^{2+} (en is a bidentate tris(ethylenediamine) ligand) also showed tetragonal distortion⁶³.

The favored geometry for 5-coordinated copper(II) is square pyramidal, however, both square pyramidal (SP) and trigonal bipyramidal (TBP) geometries could be seen occasionally. A newly reported complex $\{\text{Cu(hbp)(phen)}\}[\text{Cu(hbp)(phen)}]\cdot 5\text{H}_2\text{O}$ [$\text{H}_2\text{hbp}=3\text{-}[(2\text{-hydroxy-benzylidene)-amino]-propionic acid, phen = 1,10\text{-phenanthroline}]$] is a cocrystal of $[\text{Cu(hbp)(phen)}]$ composition with SP and TBP geometries within a unit cell⁶⁴.

The electron configuration for square pyramidal geometry is similar to the elongated octahedral geometry along the z -axis. The same reason for less ligand orbital overlap in z -direction applies for this geometry with the assumption of an infinite bond distance exists along the z -direction.

Most of the geometries around copper(II) complexes are distorted from the above geometries based on ligand functional groups and the multidentate bonds that force the complex into a specific geometry.

1.3.2. Applications of Copper(II) Complexes

The complexes of Cu(II) have wide applications in the food and dye industries, catalysis, as fungicides, agrochemicals, pharmaceuticals, and biologicals. Copper(II) complexes not only play a role in the development of modern coordination chemistry, stereochemical models, and transition metal coordination chemistry, but also, they can be found at key points in the progress of inorganic biochemistry, catalysis and optical properties⁶⁵⁻⁶⁷. The unique electron configuration of copper(II) creates a magnetically active ion that, in interaction with other active ions shows special magnetic properties. Polynuclear copper(II) compounds can be used as molecular magnets^{68,69}.

The discovery of superconductivity in La_2CuO_4 with the threshold temperature of 35 K in 1986,⁷⁰ earned Bednorz and Müller a Nobel prize in physics. Numerous studies have been conducted over the past decades since the discovery of the high- T_c cuprate layer superconductor⁷¹⁻⁷⁷.

Transition metals are used as catalysts for numerous chemical reactions. One class of heterogeneous catalysts are organometallic catalysts that consist of a central metal ion that is surrounded by organic ligands. Recently, remarkable progress has been made in the development of Cu-catalyzed C-heteroatom bond-forming reactions⁷⁸. The formation of numerous types of chemical bonds are catalyzed by Cu(II) complexes. Furthermore, many oxidation reactions are regioselectivity copper-catalyzed^{79,80}. Different ligands bound to copper catalyst sites result in different yields of products, and to form the desired product in its highest yield, a specific complex of copper needs to be selected^{78,81}.

The applications of copper(II) coordination compounds are discussed in this chapter. Porous coordination polymers (PCP) and specifically metal-organic framework (MOF), are good candidates for media transferring, gas storage, etc. The pharmaceutical properties of coordination compounds make them suitable for medical applications. The magnetic properties of copper(II) compounds are discussed comprehensively in the second chapter.

1.3.2.1 Transfer, Storage, Removal, and Separation

Copper(II) complexes play an influential role in supramolecular and metallosupramolecular chemistry development. The design and synthesis of supramolecular metal-organic coordination compounds has been extensively studied because of their fascinating and diverse structures. To assemble desired and specific network topologies with potentially interesting properties, selecting suitable molecular building blocks for applications such as drug delivery or regenerative medicine is important^{82,83}.

Porous coordination polymers (PCP) among supramolecular compounds have been widely studied because of their variety of applications in gas storage, host-guest chemistry, and ion exchange. Recently interesting Cu(II) PCPs were synthesized Zaworotko et al. by choosing the linkers SiF_6^- and 4,4-dipyridylacetylene (dpa)⁸⁴. A 3D pillared layer structure $[\text{Cu}(\text{dpa})_2(\text{SiF}_6)]_n$ (Figure 1.5) is formed when a two-dimensional layer of $\text{Cu}(\text{dpa})_2$ is pillared by SiF_6^- to form. This compound is one of the best sorbents for CH_4 and is highly selective for taking up CO_2 compared to CH_4 and N_2 . The pore size could be changed by double interpenetration to form a compound related to the non interpenetrated primitive-cubic form.

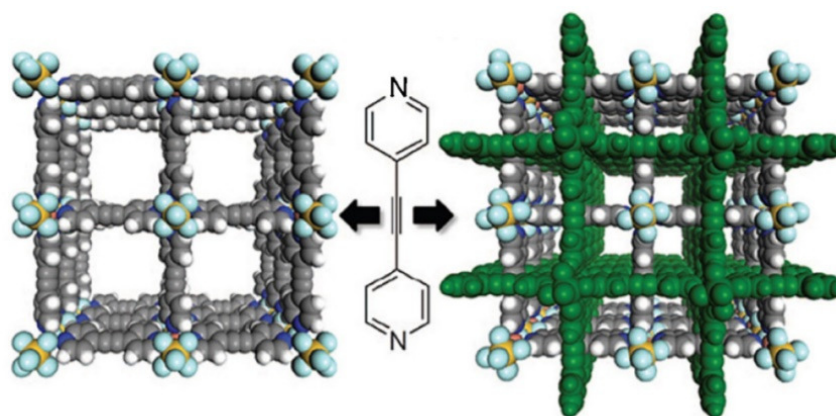


Figure 1.5 A porous coordination polymer of $[\text{Cu}(\text{dpa})_2(\text{SiF}_6)]_n$ with or without interpenetration

(Taken from Reference 84)⁸⁴.

Another interesting example of copper metal-organic framework (MOF) is $[\text{Cu}(\text{tba})_2]_n$ (tba = 4-(1H-1,2,4-triazol-1-yl)benzoate) which has CO_2 adsorption and separation selectivity over $\text{CH}_4/\text{H}_2/\text{O}_2/\text{Ar}/\text{N}_2$ gases. The kinetic and thermodynamic Single-Crystal to Single-Crystal (SCSC) transformations are a fascinating ability, can be seen in this compound⁸⁵.

1.3.2.2 Pharmaceutical Properties

Metal ions as electron-deficient cations in biological systems are attracted to electron-rich biological molecules such as proteins and DNA. Biological systems themselves provide numerous cases of ligands that bind metal ions to perform vital biological functions, Iron metalloprotein hemoglobin for instance that carries oxygen to organs. Based on these compatible complexes, drug designs were formed to react with biological molecules in desired ways⁸⁶.

The pioneers for metal-metalloid based drugs were Arsphenamine, also known as Salvarsan drug that was the first effective treatment for syphilis introduced at the beginning of the 1910s, and was also used to treat trypanosomiasis. Aurothioglucose, also known as gold thioglucose, was formerly used to treat rheumatoid arthritis. The sodium aurothiopropanate sulfonate, also known as Aurotioprol, used as antirheumatic agent (Figure 1.6). Discovering arsphenamine, based on the work of Paul Ehrlich (1854–1915) in Germany initiate the concept of modern chemotherapy. Ehrlich received the Nobel prize in Physiology for his contributions to immunology^{87–89}.

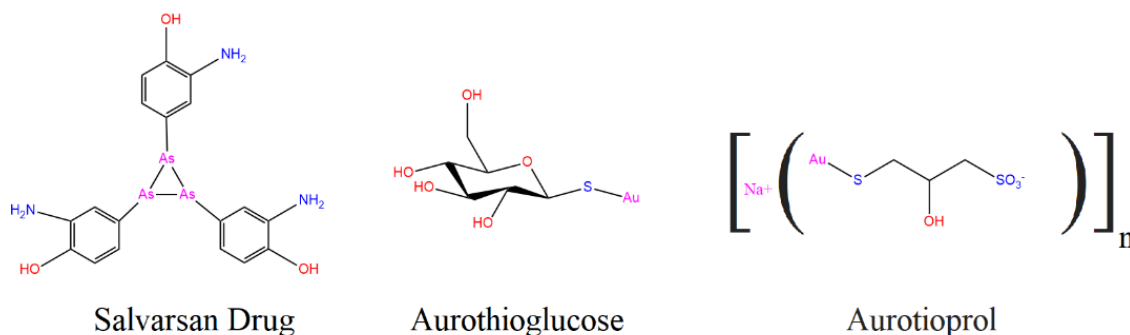


Figure 1.6 The first metalloloid-metal based medicines.

The medical accomplishments such as fungicidal, anti-inflammable, antimicrobial, antibacterial, and chemotherapeutic activities of copper and identification of its complexes as *in vitro*

and *in vivo* bioactive compounds aroused an ever-increasing interest. Copper complex medicines act by a different pathway compared to platinum-based or uncomplexed drugs. The novel generation of highly active drugs with minimal side effects resulting from development of copper complex agents as potential drugs for therapeutic intervention in various diseases and the vast array of statistics available for their bioinorganic properties could add significant value to the current clinical research and practice. A huge number of Schiff's base copper complexes are potential models of biological compounds⁶⁹. Schiff's bases with the general structure of $R_2C=NR'$ ($R' \neq H$) are secondary imine ligands which are good linkers and by changing the R groups as aryl or alkyl groups they demonstrate different properties.

Antibacterial activity against *Escherichia coli*, *Staphylococcus aureus*, *Klebsiella pneumoniae*, *Mycobacterium Smegmatis*, *Pseudomonas aeruginosa*, *Enterococcus cloacae*, *Bacillus megaterium*, and *Micrococcus luteus* were detected using Cu(II) complexes with bidentate Schiff bases derived from 2-pyridine carboxaldehyde, 3-amino-5-methyl isoxazole with 5-methyl furan-2-carboxyaldehyde, 5-methyl thiophene-2-carboxaldehyde and pyridine-2-carboxaldehyde, respectively, coordinate to Cu^{2+} through the azomethine nitrogen, furfural oxygen, thiophene sulphur, and pyridine nitrogen^{90,91}. The mechanism of bacterial activity of copper complexes is not clear yet, however some suggested mechanisms are reported. The copper(II) complexes are found to generate reactive oxygen species. They interact with the membrane protein of the bacteria cell wall that causes the release of intracellular material. They also found that to act as an efflux inhibitor in bacterial cells, distort DNA and protein structures and disrupt biochemical processes. These studies proposed that multimodal action by copper complexes causes bacterial cell death b. To distort the DNA and protein of the targeted systems Cu(II) nanoparticles may interact with phosphorus and sulfur-containing biomolecules. The biochemical disruption processes are the hypothetic antibacterial activity mechanism against *E. coli*, *Staphylococcus aureus*, and *Pseudomonas aeruginosa*⁹².

Later on, Rosenberg⁹³, in 1967, examined the consequence of an electrical field on bacterial growth by inhibition of cell division. Further studies showed that the effect was not because of the electrical field but was due to the formation of cis-dichloro diamine platinum(II), i.e., cisplatin from the platinum electrodes. Modern chemotherapy research was influenced by the discovery of the cytotoxicity of cisplatin⁹³ against different cancer cell lines and the development of its congeners⁹⁴. Cisplatin was the first metal-containing compounds showed the anti-cancer activity efficient for several types of solid tumors. Platinum-based drugs cisplatin, carboplatin and oxaliplatin then were widely used in the therapy of human neoplasms (Figure 1.7). The effectiveness of cisplatin, however, was limited by toxic side effects, and tumor resistance results in the secondary malignancies⁹⁵. The efforts for developments of new platinum anticancer complexes has not reached the clinical applications so far. Only nedaplatin and lobaplatin received have regional approval^{87,96}.

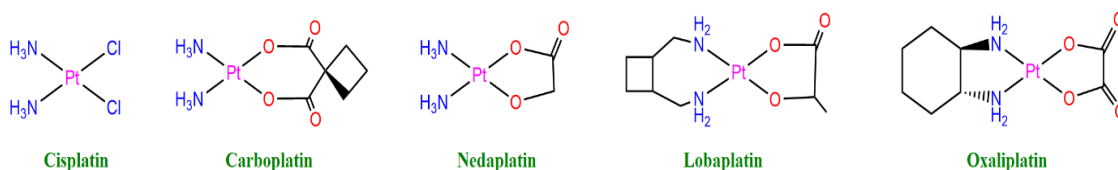


Figure 1.7 Some examples of platinum-based drugs.

Numerous metal complexes have been discovered effectively function against several diseases, however because of the high level of toxicity or drug resistance conditions they were not applicable in clinical tests. Though, copper displays a substantial biochemical role as a vital trace metal or an essential base of exogenously engaged compounds in a human's body. Among many metal complexes applicable in pharmacological purposes Cu(II) complexes play very important roles in biological activities in the human body as well as applicability in pharmacy, medicine, agronomy, and nutrition. Their biological applications have drawn specific attention due to various coordination modes and

bonding to targeted chelating agents. They bond to albumin, ceruloplasmin, or other proteins in the past and flexible bonding to other ligands of different types and making compounds that interact with biomolecules such as nucleic acids and proteins later brings together the multifaceted role. Copper(II) complexes with amino acids are models to study the effects of drugs that lowering the toxic effects of some metal ions. Copper complexes have a cytotoxicity effect with less toxicity than cisplatin medicines (Figure 1.8). The discovery of cisplatin ($\text{cis-}[\text{Pt}(\text{NH}_3)_2\text{Cl}_2]$) and its analogs play a significant role in the development of the metal complexes and inorganic compounds in medical manufacturing^{86,97-102}.

The role of copper(II) as an active site of innumerable metalloproteins biological systems and for numerous catalytic processes in living organisms involving electron transfer reactions or the initiation of some antitumor materials is inevitable.

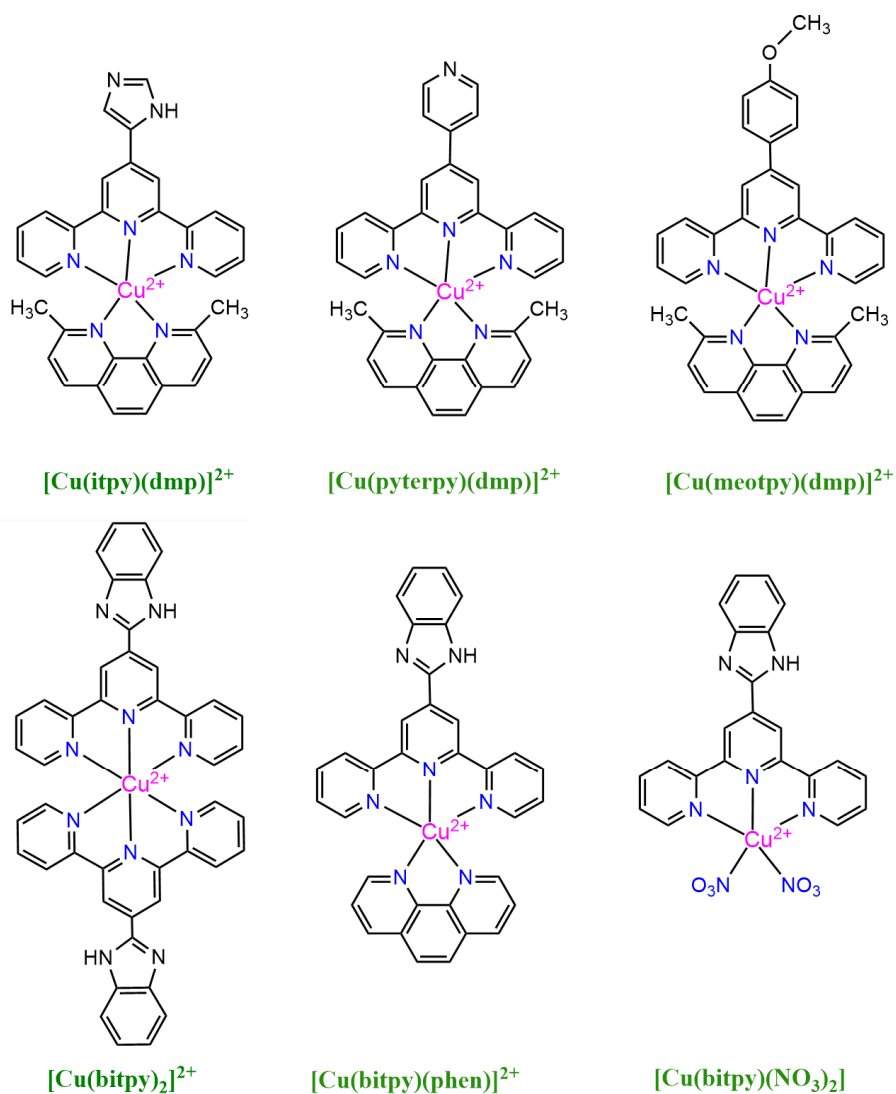


Figure 1.8 Some copper(II) complexes showing cytotoxicity effect. [itpy = 4'-(1H-imidazol-2-yl)-2,2':6',2''-terpyridine, bitpy = 4'-(1H-benzimidazol-2-yl)-2,2':6',2''-terpyridine, dmp = 2,9-Dimethyl-1,10-phenanthroline, phen = 1,10-phenanthroline, pyterpy = 4'-(4-pyridyl)-2,2':6',2''-terpyridine, meotpy = 4'-(4-methoxyphenyl)-2,2':6',2''-terpyridine (meotpy)].

1.4. Research Motivation

In this work, seven new coordination compounds, and their structural properties are reported. The motivation to synthesis the title compounds was the successful synthesis and structure determination of similar copper complexes: $[\text{Cu}_2(\text{cca})(\text{phen})_4](\text{ClO}_4)_2(\text{H}_2\text{O})_{5.5}$, and $[\text{Cu}_2(\text{OH})(\text{oda})(\text{phen})_2](\text{ClO}_4)$, (cca = 4-carboxycinnamate, phen = 1,10-phenanthroline, oda = octanedioate). The compounds were evaluated by collaborators in Texas Medical Center for their anticancer efficacy and were found to exhibit remarkable activities against liver and pancreatic cancer cells¹⁰³.

The research interest in anticancer compounds based on transition metals is increasing, aiming at better pharmaceutical properties, and less severe side effects¹². In this respect, the synthesis of similar complexes with bridging dicarboxylate linkers and different bridging modes was of interest. This was the starting point for the motivation to synthesis similar compounds with anticancer properties. In the course of the project, it was discovered that it is possible to make compounds containing mono-, bi, or polynuclear units with interesting structural features. Therefore, the focus has changed to magnetic measurement. The focus on future work is going to be a cancer treatment evaluation.

Chapter 2. Literature Review on Magnetic Properties of Copper(II) Complexes

2.1. Magnetic Materials in Future Technologies

The world has been revolutionized in the past fifty years by electronics and by exploring a fundamental property of electrons, their charge. The manipulation of another fundamental property of an electron, spin, is now being applied in electronic devices. The spin-based electronics, “spintronics” is the study of the electron’s intrinsic spin in solid-state devices and requires a wide knowledge over spin control and transport. Electronic microprocessors can be replaced with faster and more reliable devices that decrease energy consumption and heat production¹⁰⁴. The polarized spin of the electron is what makes the material magnetic, and the spin current is necessary to read and write on a magnetic memory. Certain types of materials that enable control of the flow of the current of spin-polarized electrons will lead to new devices. The new type of solid-state storage devices can move information faster, more energy-efficiently and with less heat dissipation. The first magnetic memories with the smaller size, that will allow us to improve data storage capacity may become a part of mobile phone and computers within just a few years¹⁰⁵.

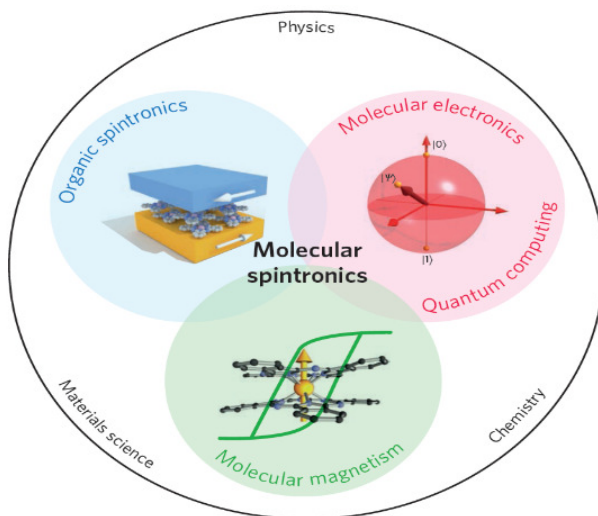


Figure 2.1 Molecular spintronics is a multidisciplinary field of study (Taken from Reference 104)¹⁰⁴.

The working principle and discovery of giant magnetoresistance brought a breakthrough in gigabyte hard disc drives and led the Nobel Prize in 2007 in Physics. The application is going to be seen in the next generation of low-power, ultrafast memories. Besides the traditional spintronics materials, in a search for new materials, molecular magnets have been proposed to perform spintronic functions in conventional applications and beyond. Molecular magnetic materials, and in particular, single-molecule magnets can establish a fundamental link between the contemporary evolution of the field of spintronics and molecular electronics. The study of magnetic exchanges in molecular materials to controlling the magnetic coupling in molecular spintronics is a challenge to build efficient devices^{106,107} (Figure 2.1). The contribution of this work in this novel field of research is the study on the molecular magnetism.

2.2. Magnetic Behavior of Copper(II) Complexes

The magnetic properties of molecular materials have been studied during the past decades in the field of material science and chemistry. The magnetic properties of a compound depend upon the electron configuration of the metal center. Copper(I) with the d^{10} electronic structure is diamagnetic. The copper(II) ion has the ground state of $3d^9$ electron configuration. The unpaired electron in its d shell is responsible for the paramagnetic behavior and the magnetic moment close to the spin-only value, 1.73 B.M, regardless of the specific bonding. The magnetic moment is given by $\mu_{\text{eff}} = \sqrt{4S(S + 1)}$, in which S is the ground state total spin value. The observed values of the magnetic moment for Cu^{2+} compounds with ionic or weak covalent bonds are 1.9-2.2 B.M., and for strong covalent bonds is 1.72-1.82 B.M¹⁰⁸. Copper(II) compounds with magnetic moments less than 1.73 B.M are unusual.

2.2.1. Historical Development

Copper(II) carboxylate dimers play an important role in the study of the magnetic interaction of polynuclear complexes of the first-row transition metals both from historical and theoretical viewpoints. Lifschitz and Rosenbohm¹⁰⁸, in 1915, noticed that the compound copper(II) acetate monohydrate has a much lower molar susceptibility at room temperature than a mononuclear copper(II) compound. Further magnetic measurements confirmed this abnormally low magnetic moment. Later, in 1951, Guha¹⁰⁹, measured the magnetic susceptibility of a single crystal of $\text{Cu}(\text{OAc})_2 \cdot \text{H}_2\text{O}$ (OAc = acetate) from 83 to 304 K and found a maximum in the magnetic susceptibility as a function of temperature. In the following year, Bleany and Bowers¹¹⁰ measured the ESR spectra of a single crystal and explained the results and the experimental data of Guha by assuming direct exchange coupling between a pair of copper(II) atoms. The exchange coupling constant J was calculated to be -315 cm^{-1} . Later, the J value determined to be -292.2 cm^{-1} from measurements of the magnetic susceptibility from 4.2 to 300 K. The χ value is negligible below 100 K and reaches its maximum around 265 K. An increase in χ is observed on cooling below $\sim 50 \text{ K}$ due to the presence of noncoupled copper(II) atoms. This effect is not intrinsic.

Niekerk and Schoening¹¹¹ a year later determined the very unusual cage-type dimeric structure of this compound. The $\text{Cu} \cdots \text{Cu}$ separation was measured as 2.64 \AA . This observation led to the beginning of research activity on the magnetic behavior of polynuclear metal complexes. Diaqua tetraacetato dicopper(II) adopts the paddlewheel structure. The coordination environment around each copper(II) ion is square pyramidal. The basal planes are occupied by oxygen atoms from acetato groups; water molecules occupy the apical positions. The four acetato groups bridge the metal atoms, and the two basal planes are parallel to each other. The molecular symmetry is close to D_{4h} . The Cu-O length of basal position is 1.97 \AA , and the apical Cu-OH₂ bond distance is 2.20 \AA (Figure 2.2).

A Cu-Cu distance in clusters of 2.40–2.55 Å is considered as a bond¹¹², and the separation between copper atoms in Cu₂(OAc)₄(H₂O)₂ is greater and consequently, the two opposing spins rather than canceling each others magnetic moment in a bond, exchange couple. This was a critical step in the development of modern theories for antiferromagnetic coupling.

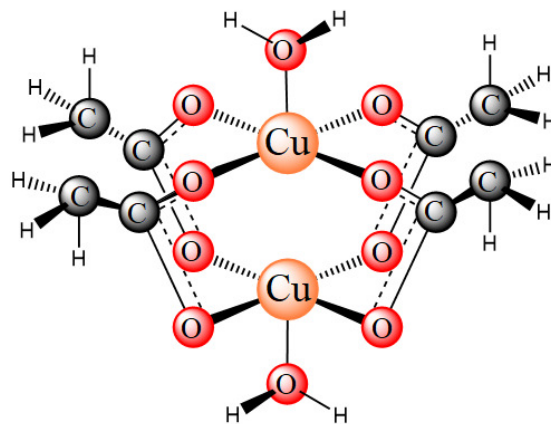


Figure 2.2 Copper(II) acetate monohydrate dimer with the paddlewheel structure.

2.2.2. Intramolecular Magnetic Interactions

The design of magnetic materials requires an understanding of the magnetic properties of polynuclear metal complexes in which at least two centers bear unpaired electrons. The interaction between the magnetic centers can be described by an effective spin-only Hamiltonian, namely the Heisenberg-Dirac-Van Vleck Hamiltonian (Equation (2.1))¹¹³⁻¹¹⁵ :

$$H = -\sum_{i,j} J_{ij} S_i S_j \quad (2.1)$$

That J_{ij} is the magnetic coupling between the magnetic ions i and j . This equation for the systems with two active centers is $H = -JS_1S_2$. The magnetic coupling for the systems in which the active centers contain one unpaired electron ($M_s = \pm 1/2$) is the energy difference between the singlet and triplet state; $J = {}^1E - {}^3E$. A positive J value indicates that the ground state is a triplet, and the coupling is

ferromagnetic; a negative sign corresponds to a singlet ground state with an antiferromagnetic interaction between metal ions. The sign and magnitude of J depend upon the nature of the interaction between the magnetic centers¹¹⁶.

The copper(II) acetate dimer is a prototype of polynuclear copper(II) compounds with $\text{Cu}\cdots\text{Cu}$ magnetic interactions. Martin *et al.*¹¹⁷ have studied the magnetic susceptibility of a series of alkyl carboxylic acid copper(II) complexes and show that there is a direct interaction between the copper ions in the dimeric copper acetate structure in which the copper ions are bridged by four acetate groups with the exception of the formate complexes.

The magnetic interaction between the paramagnetic centers occurs through space. The term “magnetic orbitals,” is commonly used to describe the type of magnetic interaction and refers to localized orbitals containing the unpaired electrons on the magnetic centers partially delocalized onto the bridging ligands¹¹⁸. The overlap of magnetic orbitals and their symmetry is used to explain and predict the magnetic properties of polynuclear species¹¹⁹. The magnetic orbital method assumes that either δ interactions or indirect σ bonding interactions are involved between the pairs of metal atoms. The δ -interaction between metal d orbitals is called the direct exchange. The parallel magnetic orbitals of the metal centers would increase the direct magnetic exchange pathway contribution. However, if the magnetic interaction occurs through the overlap of metal d orbitals with the bridging ligand p orbitals, the pathway is called super-exchange. The schematic view of magnetic orbitals in each pathway is shown in Figure 2.3.

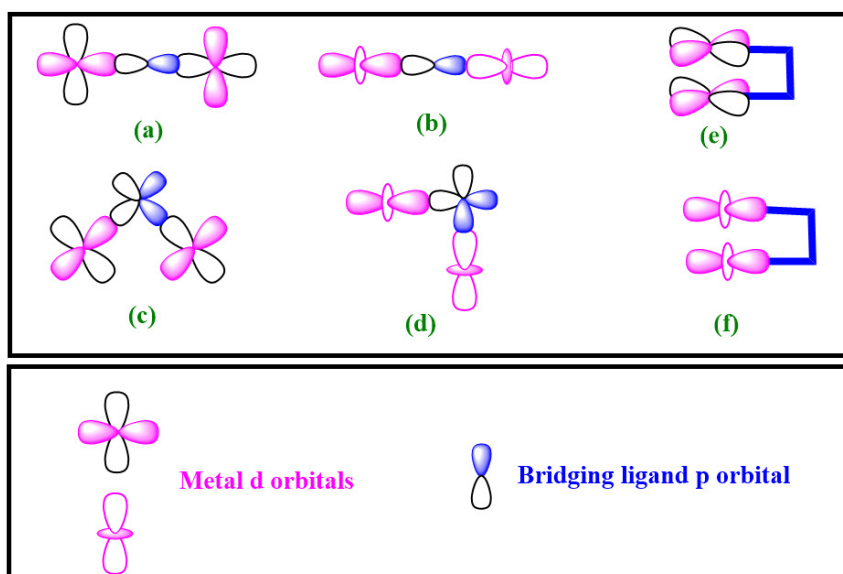


Figure 2.3 (a), (b) Super-exchange magnetic pathway with metal center orbitals, and the ligand p orbital are linear, and (c), (d) orthogonal, (e) and (f) the direct magnetic exchange with the δ -interaction.

In the super-exchange pathway, there is a spin coupling between the cationic metal center and the anionic intermediate, and according to the Goodenough-Kanamori-Anderson (GKA)¹²⁰⁻¹²³ rules, the pathway results in different interactions based on the angles between orbitals. A model developed by Anderson¹²⁴ and a semi-empirical statement proposed by Goodenough-Kanamori describes the GKA rule. Based on this rule if the lobes of metal orbital and the bridging ligand directly point toward each other to have a reasonable overlap, the exchange is antiferromagnetic (AFM), and if orbitals are orthogonal to one another the interaction between centers are ferromagnetic (FM)^{122,125}.

2.2.3. Mononuclear Copper(II) Compound

Mononuclear copper(II) compounds have normal magnetic behavior. Only very small interactions between copper(II) centers exist in separated mononuclear complexes, and they obey the Curie-Weiss law¹²⁶⁻¹²⁹. The Curie-Weiss law for paramagnetic substances is $\chi_m=C/(T-\theta)$ where χ_m is the molar magnetic susceptibility, C and θ are the Curie and Weiss constants, respectively, and T is the absolute temperature. However, coordination polymers that contain mononuclear Cu(II) cores or complexes that are connected through hydrogen bonds exhibit weak interactions between copper centers. In the mononuclear [Cu(bpm)(ox)(H₂O)] (bpm = 2,2-bipyrimidine, ox = oxalate), a one dimensional chain structure is formed with intermolecular hydrogen bonding between H₂O and ox. The magnetic susceptibility measurement displays a weak antiferromagnetic interaction. Ferromagnetic coupling is observed for mononuclear [Cu(tpd)(dca)(H₂O)] (tpd = 4-terpyridine, dca = dicyanamide) with the hydrogen bonding between H₂O and tpd of the next molecule¹³⁰. The compound [Cu(pim)] (pim = N,N'-(propane-1,3-diyl)bis(1-(imidazolate-2-yl)methanimine)) has a zigzag chain polymeric structure in which the copper ion in each monomer sequentially bridged by the nitrogen atoms of the imidazolate groups. The Cu-Cu distance is 5.993 Å, and weak antiferromagnetic interaction between copper ions occurs through the imidazolate bridges¹³¹. The bridging ligands with aromatic rings produce dinuclear copper(II) complexes with long-range magnetic coupling. This will be discussed in more detail in Section 2.2.4.5.

2.2.4. Dinuclear Copper(II) Compounds

Much experimental and theoretical research has been carried out to explain the mechanism of magnetic exchange coupling in polynuclear complexes. Dinuclear systems are the most frequent target due to their relative simplicity that permits the analysis of magneto-structural correlations for the prediction of magnetic properties.

Hatfield *et al.*^{116,132} started to study the magnetic behavior of copper(II) dimers with a variety of compositions. They also systematically studied copper(II) halide dimers with salicylaldimine¹³³. Eventually, they have focused on copper(II) carboxylate dimers^{134,135}. The magnetic behavior investigation of binuclear metal complexes has been extensively studied from their research. For the copper(II) dimers with a pair of spin 1/2 interacting ions, the magnetic susceptibility data, obey the modified Bleaney-Bowers Equation (2.2):

$$\chi_A = \frac{N\alpha g^2 \beta^2}{3kT} \left[1 + \left(\frac{1}{3} \right) \exp \left(\frac{-2J}{kT} \right) \right]^{-1} (1 - \rho) + \frac{N\alpha g_i^2 \beta^2}{4kT} \rho + \text{TIP} \quad (2.2)$$

In Equation (2.2), ρ is the molar fraction of coupled species, the second term is an "impurity" which is assumed to follow the Curie law ($\chi=C/T$), and has the same molecular weight and g-factor as the actual compound, TIP is the temperature-independent paramagnetism, g is the Landé g-factor (gyromagnetic ratio), $N\alpha$ is the Avogadro constant, k is the Boltzmann constant, T is the temperature, and β is electron Bohr magneton.

Many classes of dinuclear copper(II) compounds, including the dinuclear copper(II) carboxylates, halides, and phosphates, are well documented¹³⁶⁻¹⁴⁵. The other common dinuclear copper(II) compounds are the μ -hydroxo bridged dinuclear complexes¹¹⁶.

2.2.4.1 Dinuclear Copper(II) Carboxylates

The carboxylate anion is an adaptable ligand because each carboxylate oxygen ion has two lone pairs. Thus, several coordination modes are possible. Carboxylate anion may bind to metal ions to form polynuclear complexes in one of four ways shown in Figure 2.4.

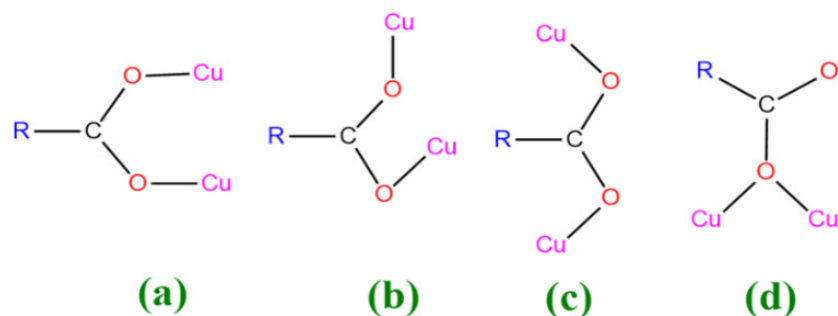


Figure 2.4 Different ways that the carboxylato group can bridge between two copper centers. The magnetic interaction between the metal ions are greatest in (a) known as *syn-syn* and (d). The structures (b) which are known as *syn-anti* and (c) as *anti-anti*. The carboxylate in (d) acts as a monoatomic bridging ligand.

Copper acetate has a structure corresponding to *syn-syn*, while the structure of copper formate tetrahydrate is *syn-anti* and a form of anhydrous copper formate has the structure of type *anti-anti*¹⁴⁶. The *syn-syn* type is the most common type of carboxylate bridging ligand. In the coordination geometry, by involving one of the lone pairs of the oxygen atom, the dinuclear copper(II) complex would form. By second lone pair donation from the same oxygen atom to another metal ion the polynuclear structure is formed. The further discussion on these structures is in the polynuclear Section, 2.2.8.

Many copper(II) carboxylate complexes have been structurally characterized, and their magnetic properties have been measured. The wealth of experimental data on these compounds permits a detailed investigation of the different factors that influence the exchange interaction between the metal centers. The different coordination modes of carboxylates, along with the choice substituent (R), the axial ligand (L), and the number of bridging ligands all influence the specific magnetic properties¹⁴⁷.

2.2.4.2 Di-nuclear Copper(II) Halides

The structural features and magnetic behavior of dihalo-bridged Cu(II) complexes have been studied for many years¹⁴⁸. The metal atoms in dihalo-bridged Cu(II) complexes are usually five- or four-coordinated. Copper ions with square-planar coordination are antiferromagnetic coupling; however, this behavior changes to ferromagnetic exchange¹⁴⁹ when due to the bulky counterion the geometry distorts toward tetrahedral geometry¹⁵⁰. For the five coordinated complexes the common square-pyramidal environment can distort toward trigonal bipyramidal. The dihalo-bridged square pyramidal Cu(II) complexes geometries are shown in Figure 2.5¹⁵¹. These complexes are shown different magnetic behavior based on their structure.

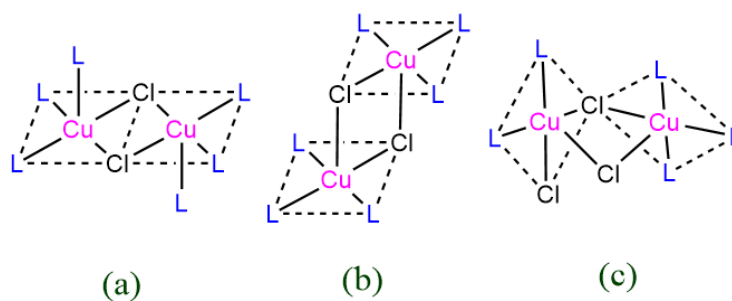


Figure 2.5 Dinuclear dihalo-bridged Cu(II) complexes' geometries with square pyramids sharing (a) a basal edge, (b) a base-to-apex edge with parallel basal planes, and (c) a base-to-apex edge, but with perpendicular basal planes.

Type (a) compound shows a different magnetic behavior depending on the axial ligand. If the axial ligand is a halide, the coupling between copper centers is antiferromagnetic ($-30 < J < -100 \text{ cm}^{-1}$)^{150,152,153}; however, in the presence of N-donor ligands, the interaction is ferromagnetic ($J \sim +40 \text{ cm}^{-1}$).

¹). The coupling constant of type (b) is always small ($-10 < J < +10 \text{ cm}^{-1}$)^{148,154}. Type (c) shows a ferromagnetic behavior ($J = +43 \text{ cm}^{-1}$)¹³⁸.

2.2.4.3 Dinuclear Copper(II) Compounds with μ -oxo Bridges

Monatomic bridges, especially those containing two bridging oxo ligands with a Cu_2O_2 core generated by the bridging hydroxide, alkoxide, and phenoxide ligands have been extensively studied. The relationships between the structural features and the magnetic properties have been established. The existence of this correlation in the hydroxo-bridged compounds is more obvious than for the halo-bridged dinuclear compounds.

According to Hatfield *et al.*,¹¹⁶ a linear correlation exists between the exchange coupling constant (J) and the $\text{Cu}^{\text{II}}\text{-O-Cu}^{\text{II}}$ angle (θ) in hydroxo-bridged copper dimers. The predicted borderline of the transition from antiferromagnetic to ferromagnetic coupling is $\theta \approx 97.5^\circ$. For θ greater than 97.5° , the interaction is antiferromagnetic, and ferromagnetic coupling emerges for θ lower than this threshold value. A similar relationship has been reported for the alkoxo-bridged dicopper(II) complexes with a threshold $\theta \approx 97^\circ$. The effect of the variation of structural factors on the exchange interaction between copper(II) centers in di- μ -methoxo and di- μ -hydroxo dicopper(II) with the general compositions $[\text{Cu}_2(\mu\text{-OR})_2\text{X}_2(\text{NH}_3)_2]$ ($\text{R} = \text{H}$ or CH_3 , $\text{X} = \text{F}$, Cl , Br) were studied by the ab initio MO method and the most effective factor on J -value demonstrated as Cu-O-Cu angle¹⁵⁵.

2.2.4.4 Dinuclear Copper(II) Phosphates

Magnetic exchange interactions in different copper(II) phosphate compounds with the predominant exchange pathway through variable binding modes of the ligand have been studied. Using the 1,1- and 1,3-bridging modes (Figure 2.6) of phosphates permits creating the angle or dihedral

relating to the J values¹⁵⁶. The model for the study was evaluated based on the Kahn–Briat model¹⁵⁷ which tends to describe that the observed magnetic behavior due to the overlap of the magnetic orbitals; the negative J values corresponding to the highest overlap values.

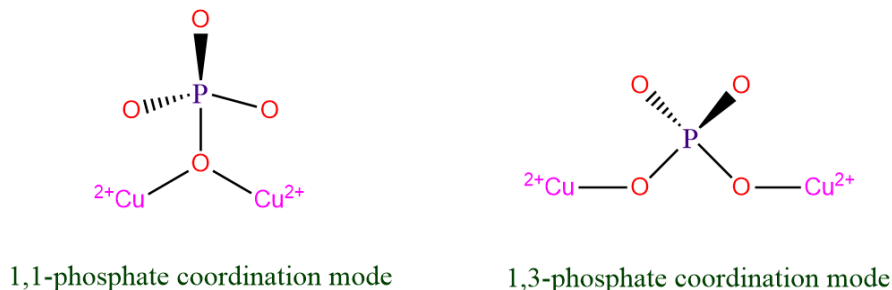


Figure 2.6 Connection modes of phosphates to make binuclear copper(II) complexes.

In the literature, eleven copper(II) phosphates are studied and Cu–O–Cu angle (θ) for the 1,1-bridging mode and the D–P–O–Cu dihedral angle (τ) (D = dummy atom) for the 1,3-phosphate mode was used to establish the correlation. Consistent with the Kahn–Briat model, the larger overlap of the magnetic orbitals resulting from larger angles, leading to a stronger antiferromagnetic coupling¹⁵⁸.

A degree of overlap among magnetic orbitals always exists within the different bonding modes of the phosphates and this is in agreement with the antiferromagnetic interactions as primary exchange leading through phosphate bridges. Furthermore, it reveals that a stronger antiferromagnetic interaction is due to a greater overlap surface between the magnetic centres¹⁵⁸.

2.2.4.5 Long-range Magnetic Coupling

Intramolecular interaction with conjugated bridging ligands for long-distance exchanges is called “long-range magnetic coupling”. Two copper(II) complexes with the aromatic bridging ligands of N,N'-1,4-phenylenebis(oxamate) (ppba) and N,N'-4,4'-biphenylenebis(oxamate) (bpba) were studied

with the Cu-Cu distances of 7.91 and 12.19 Å, respectively. The J value for Cu₂(ppba)₂ is reported in the range of -81 to -95 cm⁻¹ and for Cu₂(bpba)₂ is in the range of -8.7 to -11.5 cm⁻¹. The origin of the antiferromagnetic interaction was described as the predominantly π- type orbital pathways through the aromatic bridges^{159,160}. Similar interactions are reported for many compounds¹⁶¹ and there is a list of complexes with similar interaction in the supporting information of the literature¹⁶⁰.

The metal-organic frameworks (MOF) with short distance copper(II) centers exhibit interactions through direct or super-exchange pathways; however, the long-range magnetic coupling may appear between the distant Cu(II) ions. A metal-organic framework, HKUST-1, with the formula of Cu₃(btc)₂(H₂O)₃ (btc = benzene 1,3,5-tricarboxylate) has been synthesized, and its magnetic study revealed that the direct strong antiferromagnetic exchange is similar to its molecular analog, the cupric acetate dihydrate. Further, there is a weak long-range antiferromagnetic order through the btc ligand with Cu-Cu distance more than 8 Å (Figure 2.7)^{162,163}.

The bdc and btc (benzene 1,3,5- tricarboxylate) ligands are the most common ligands through which the long-range magnetic coupling in MOFs occurs¹⁶⁴⁻¹⁶⁶.

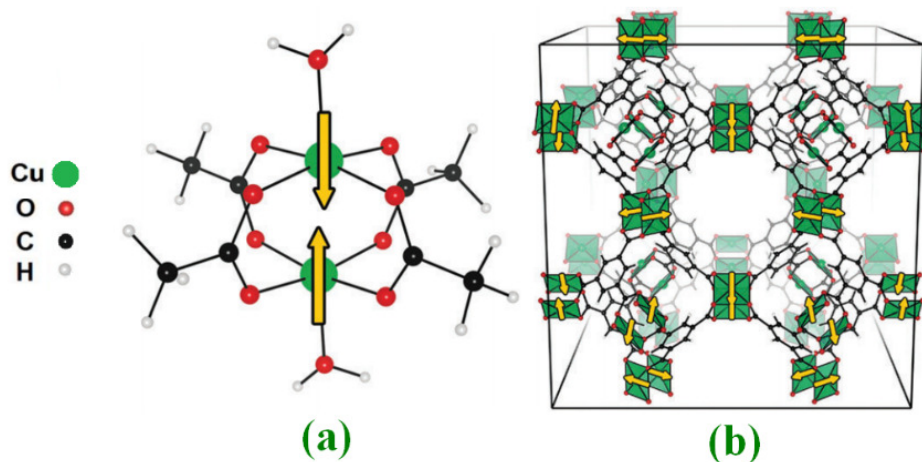


Figure 2.7 The dimeric Cu(II) acetate dihydrate paddlewheel with an antiferromagnetic ground-state in both (a) the single-molecule and (b) the metal-organic framework of HKUST-1(Taken from Reference 162)¹⁶².

2.2.5. Trinuclear Copper(II) Compounds

Depends on the type of ligands, there are some typical structures for trinuclear copper(II) complexes. The two main structural types for copper(II) trinuclear complexes are linear and triangular (Figure 2.8). The structures are shown in Figure 2.8 are the most common structures. The X atoms are mainly the donor atoms (X = O or N) of the ligand. In trinuclear structures, copper(II) centers connect through a multidentate or multi-donors bridging ligands, or the ligands able to hold together two or more metal ions.

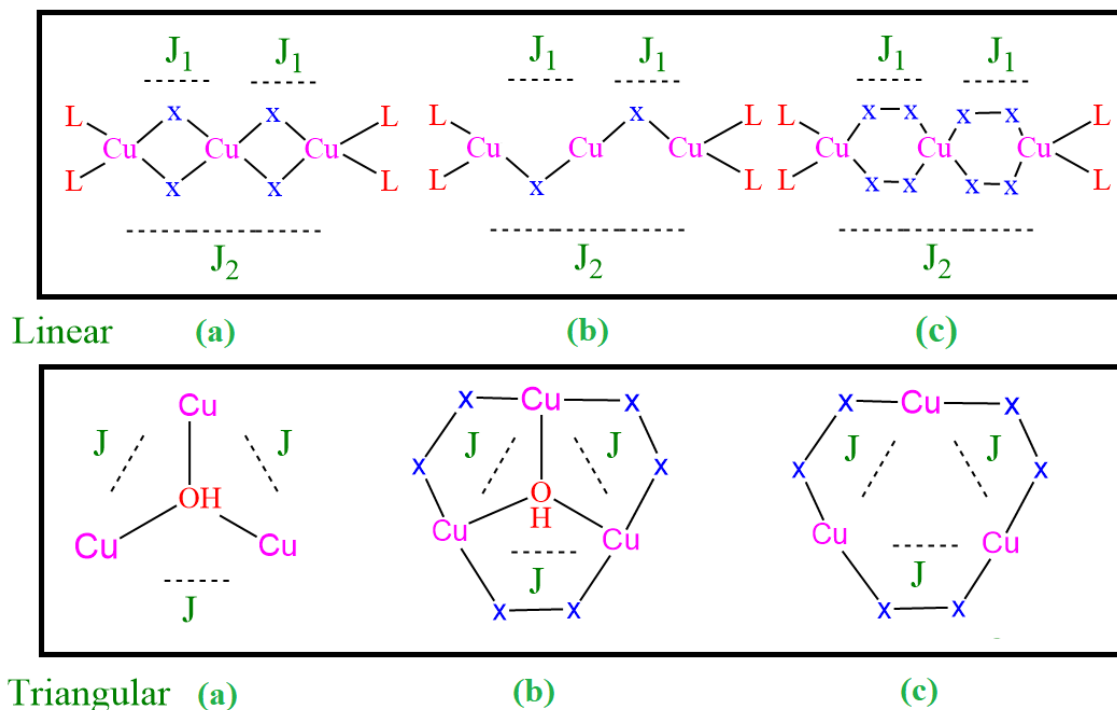


Figure 2.8 Trinuclear Cu(II) compounds in linear or triangular structures.

The linear complex example is $[\text{Cu}_3(\text{mpts})_2(\text{CH}_3\text{COO})_2(\text{OH})_2(\text{dmf})_2]$ (Hmpts = N-(2-methylpyridyl)toluenesulfonylamide) with $J_1 = 93 \text{ cm}^{-1}$ and $J_2 = -5 \text{ cm}^{-1}$, $g = 2.05$. These values are indicative of two strong ferromagnetic (FM) coupling along with short distances and a weak antiferromagnetic (AFM) interaction via the long-distance¹⁶⁷. Other reported compound with the similar interactions of FM and AFM for short and long distances is $[\text{Cu}_3(\text{nyb})_2(\text{HCOO})_2(\text{OH})_2]_n$ (Hnyb=N-pyrid-2-ylmethyl)benzenesulfonylamide)¹⁶⁸. A linear trinuclear copper(II) coordination polymer is $[\text{Cu}_3(\text{adt})_2(\mu_2\text{-OH})_2]$ (H_2adt = 2,4-bis(4-aminobenzoic acid)-6-(dimethylamino)-1,3,5-triazine). The best fitting for the experimental data for this complex gives the $J_1 = 42.39 \text{ cm}^{-1}$, $J_2 = 0$ and $N\alpha = 6 \times 10^{-5} \text{ cm}^3 \text{ mol}^{-1}$, $g = 2.09$ and $z_j = -0.08 \text{ cm}^{-3}$. There is a weak antiferromagnetic (AFM) interaction between the adjacent trimers (z_j) and strong ferromagnetic (FM) interaction within the molecule¹⁶⁹. There are other reported complexes with zero magnetic interaction for long-distance copper centers and AFM behavior for the shorter ones¹⁷⁰⁻¹⁷³. The other type of interaction between

copper(II) centers is the AFM and AFM interaction for short and long distances, respectively. An example of this type is seen in $\text{Cu}_3(\text{msp})_2(\text{CH}_3\text{COO})_4$ (msp = N-methyl-N'-(4-methoxysalicylidene)-1,3-propanediamine)¹⁷⁴. Other than the examples with the bridging ligands in which the x atoms are nitrogen or oxygen atoms; there are halo-bridging structures that are also exhibited the AFM behavior for the J_1 coupling^{172,175}. The Hamiltonian describing the low-lying states for the linear structure is written as $H = -J_1(S_1S_2+S_2S_3) - J_2S_1S_3$ that in many cases the $J_2 = 0$.

The triangular copper(II) complexes are connected through a central component, or through bridging ligands, or both. Plentiful trinuclear triangular complexes possessing a $\text{Cu}_3(\mu_3\text{-OH})$ core have been reported and structurally characterized. In the copper(II) trinuclear complexes that the copper centers are connected through bridging oxygen atoms, the complex exhibits varying degrees of antiferromagnetic behavior¹⁷⁶⁻¹⁸². The bridging ligands connect copper centers by a couple of X donor atoms (X = O or N). In this type of structure, the oxygen is located out of the plane established by the three Cu ions. Many structures are reported in a review paper^{183,184}. The connection also could occur through a Cl atom, holds three copper centers together¹⁸⁵.

These exchanges show the spin-frustrated systems. Most of the polynuclear compounds and especially the cyclic-trinuclear metal complexes can be regarded as geometrically frustrated magnetic exchange models. The frustrated antiferromagnetic compounds which tend to adopt abnormal magnetic ground states remain poorly understood^{186,187}.

The trinuclear Cu(II) complexes are also the building blocks of metal-organic frameworks¹⁸⁸. The 2-D network of $[\text{Cu}_3\text{Cl}_4(4\text{-pt})_2(4\text{-Hpt})_2]\cdot 4\text{DMF}\cdot 2\text{MeOH}$] and the 3-D frameworks of $[\text{Cu}_3(\text{OH})_3(4\text{-pt})_3(\text{DMF})_4]\cdot 5\text{DMF}\cdot 3\text{MeOH}$ and $[\text{Cu}_3(\text{OH})_3(\text{trz})_3\cdot (\text{H}_2\text{O})_4]$ (4-Hpt = 4- pyridyltetrazole, trz = 1,2,4-triazole) are shown in Figure 2.9⁶⁷.

The compounds in Figure 2.9 exhibit antiferromagnetic properties with a linear and equilateral triangle models with the J values of -3.51 , -39.6 cm^{-1} for the (a) and (c) units and the interaction between the adjacent trimers (zJ) values for them in (b) and (d) supramolecular structures are $+0.57$ and -0.59 cm^{-1} . The interaction Hamiltonian used for the linear and triangular trimer is $H = -2J(S_1S_2+S_2S_3)$ and $H = -2J(S_1S_2+S_2S_3+S_3S_1)$, respectively⁶⁷.

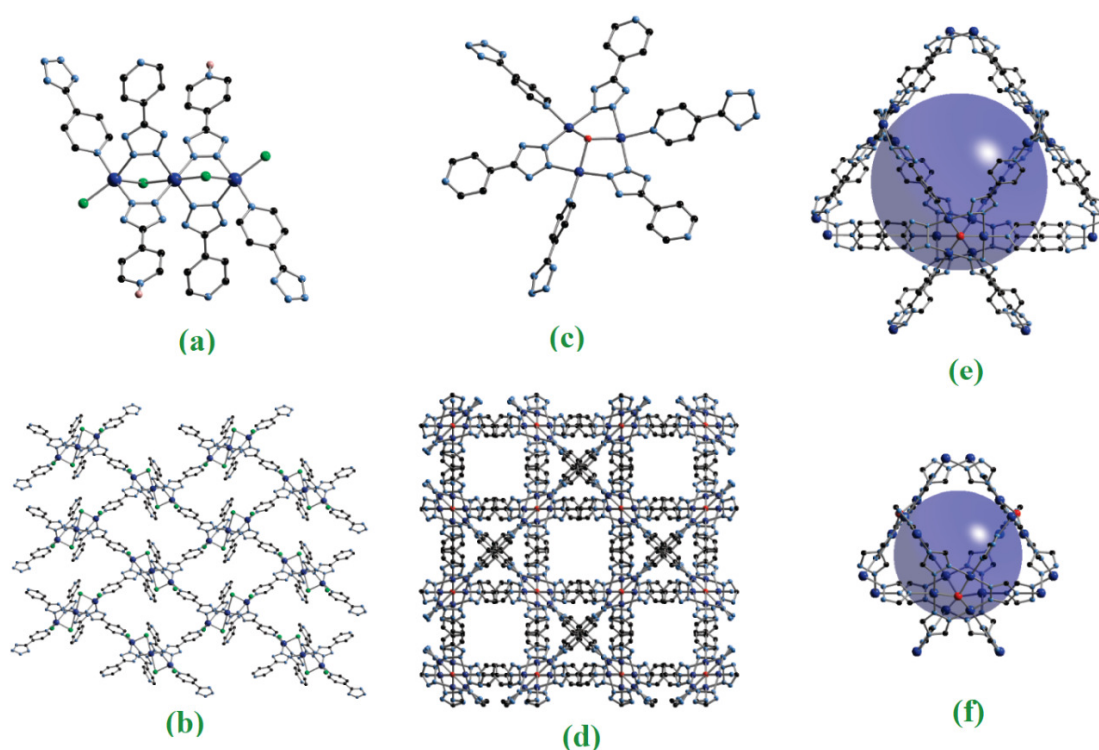


Figure 2.9 (a) The linear trinuclear $\{\text{Cu}_3\text{Cl}_4(4\text{-pt})_4(4\text{-Hpt})_2\}^{2-}$ building block of the (b) $[\text{Cu}_3\text{Cl}_4(4\text{-pt})_2(4\text{-Hpt})_2]\cdot 4\text{DMF}\cdot 2\text{MeOH}$ 2-D network, (c) the triangular trinuclear $[\text{Cu}_3(\text{OH})_3(4\text{-pt})_3(\text{DMF})_4]$ building block of the (d) $[\text{Cu}_3(\text{OH})_3(4\text{-pt})_3(\text{DMF})_4]\cdot 5\text{DMF}\cdot 3\text{MeOH}$ 3-D framework, (e) the pore size of $[\text{Cu}_3(\text{OH})_3(4\text{-pt})_3(\text{DMF})_4]\cdot 5\text{DMF}\cdot 3\text{MeOH}$ compared to the (f) pore size of $[\text{Cu}_3(\text{OH})_3(\text{trz})_3\cdot (\text{H}_2\text{O})_4]$. Color code: copper, blue spheres; oxygen, red spheres; nitrogen, light-blue spheres; carbon, black spheres (Taken from Reference 67)⁶⁷.

2.2.6. Tetranuclear Copper(II) Compounds

The tetranuclear copper(II) complexes crystallize in many different types of structures. The common bridging ligand donors are oxygen and nitrogen atoms (shown as X).

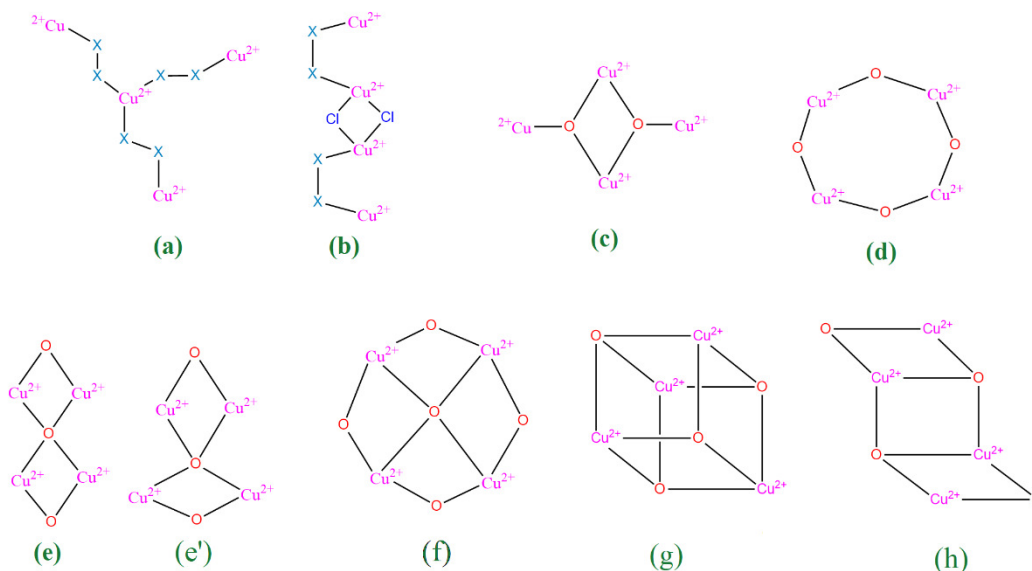


Figure 2.10 (a) triangular, (b) linear, (c) butterfly, (d) cyclic, (e) diamond, (e') distorted diamond (f) cyclic-diamond (g) cubane, and (h) ladder-like tetranuclear copper(II) complexes topologies.

The first type of tetranuclear copper(II) complex is species with a central magnetic ion in which the central ion linked with three peripheral ions through one or more atoms, known as triangular topology (Figure 2.10, a). Two different J values can be considered for this type of structure, one between central ion and the peripheral ones, and the other between each two sideline ions. An example of this type is $(\text{Mn}[\text{Cu}(\text{oxpn})_3]^{2+})$ (oxpn = oxamido- N,N' -3-aminopropane). An antiferromagnetic couple exchange is observed between the central and peripheral ions in magnetic measurement¹⁸⁹.

Another type of structure is the linear type. In the first type structure, the halo bridging ligands link two central coppers together and two other copper ions are bind to them through nitrogen or oxygen atoms of bridging ligands (Figure 2.10, b). A tetranuclear complex with multiple donor atoms and two potentially protic atoms ligand with the formula of $[\text{Cu}_4(\text{onp}_3\text{H})_2\text{Cl}_6(\text{CH}_3\text{OH})_2]$ ($\text{onp}_3\text{H}_2 = \text{O}=\text{C}\{\text{NHN}=\text{C}(\text{Me})(\text{pm})\}_2$, $\text{pm} = 2\text{-pyrimidinyl}$) has two $[\text{Cu}_2(\text{onp}_3\text{H})\text{Cl}_3\text{CH}_3\text{OH}]$ units connected via $\mu_2\text{-Cl}$ bridges to produce a linear tetranuclear copper complex. The presence of a moderate ferromagnetic interaction through chloro bridges and two strong antiferromagnetic exchange coupling via diazines is revealed by magnetic study¹⁹⁰.

Butterfly arrangement is another type of tetranuclear structure that the competition between ferro- and antiferromagnetism occurs within this topology (Figure 2.10, c). We will discuss more this competition and spin frustration later in Section 2.2.7. A butterfly-type structure is tailored for Cu(II) using a tridentate ligand, mta ($\text{H}_3\text{mta} = \text{methanetriacetic acid}$) and bpy (bpy = 2,2'-bipyridine) as a blocking ligand. The $\{[\text{Cu}_4(\text{bpy})_4(\text{mta})_2](\text{ClO}_4)_{2\cdot3}\text{H}_2\text{O}\}_n$ exhibits weak ferromagnetic interactions with $J = +2.27$ ¹⁹¹.

In cyclic tetranuclear complexes, copper(II) centers could connect through oxygen atoms or ligands with longer chains that contain two terminal oxygen donors that link copper centers. There are four equal magnetic interactions along sides and two coupling exchanges along diagonal in equilateral tetrahedrons, or it may consist of combination of classes of equal J values. Two types of cyclic topologies are square-planar and nonplanar (Figure 2.10, d). $[\text{Cu}_4(\text{dmv})_4(\text{H}_2\text{O})_8][\text{ClO}_4]_4\cdot 2\text{H}_2\text{O}$ ($\text{Hdmv} = 1,3\text{-dimethylvioluric acid}$, i.e. 1,3-dimethyl-5-(hydroxyimino)-2,4,6(1H,3H,5H)-pyrimidinetrione) is a planar cyclic tetranuclear complex. The magnetic susceptibility measurement indicates a very strong antiferromagnetic exchange interaction along the oxime bridges. No interactions along diagonals were observed¹⁹². The non-planar example, $\text{Cu}(\text{ava})_4$ displays a weak ferromagnetic interaction along lateral

exchanges with $J=+3.04 \text{ cm}^{-1}$ and no interaction along diagonal copper ions. The ligand *ava* derives from the condensation of DL-valine amino acid with acetylacetone¹⁹³.

There are two types of tetranuclear complexes in which a μ_4 -oxo links four magnetic centers. In the first case, the complex consists of two dinuclear diamonds (Figure 2.10, e). $[\text{Cu}_4(\mu_4\text{-O})(\text{dfba})_2\text{Cl}_4]$ is a tetranuclear complex with antiferromagnetically coupling exchange within dinuclear diamond units and four interdimer ferromagnetic exchanges, where *dfba* is a macrocyclic ligand resulting from the condensation reaction of 1,3-bis(aminopropyl)-tetramethyldisiloxane and 2,6-diformyl-4-methylphenol (Figure 2.10 e)¹⁹⁴. In a distorted structure of this type the magnetic interactions are unequal (Figure 2.10 e'). $[\text{Cu}_4(\text{hmm})_2(\mu_4\text{-O})(\text{OAc})_4]\cdot 2\text{H}_2\text{O}$ (*hmm* = 2,6-bis-[(2-hydroxyethylimino)methyl]-4-methylphenol) is an example of this type (Figure 2.10, e')¹⁹⁵.

The cyclic-diamond type is a combination of the cyclic and diamond topologies with six exchange couplings (Figure 2.10 f). An example of cyclic-diamond type is $[\text{Cu}_4(\text{L})_2(\text{O})(\text{OH})_2(\text{MeOH})_2\cdot(\text{ClO}_4)_2]$ (*HL* = 2,6-bis(pyrrolidinomethyl)-4-methylphenol) with six strong antiferromagnetic exchanges¹⁹². If instead of one oxygen some atoms are sitting in the center of the complex, the interaction through super-exchange pathway gets weaker and the system gets more magnetic diluted. For instance, the reported cyclic-diamond tetranuclear complex with azide μ_4 -1,1,3,3 bridging mode has four weak antiferromagnetic and two very weak ferromagnetic interactions¹⁹⁶.

The cubane-like copper(II) complex consists of two parallel dinuclear planes. The common types of cubane-like tetranuclear complexes are classified based on four long-distance copper-oxygen bonds. If the Cu-O long bonds are sitting within the dinuclear plane, or the complex contains four short, and two long Cu...Cu distances the class is called 4+2 and if the long bonds are the bonds that connect these two planes, or if the complex has two short and four long Cu...Cu distances the class is named 2+4 (Figure 2.10 g). An alkoxo-bridged copper(II) $[\{\text{Cu}(\text{H}_2\text{hbs})\}_4](1)[\text{H}_2\text{hbs} = \text{N}-(2-$

hydroxyethyl)-3,5-di- tert-butylsalicylalimine] complex with a tridentate Schiff base ligand and 4+2 structure has the $J = +28.7 \text{ cm}^{-1}$ for the four short Cu...Cu distances and $J = +7.8 \text{ cm}^{-1}$ for the two long Cu...Cu distances¹⁹⁷.

Ladder/chair-like topology of tetranuclear complex consists of two μ_3 and two μ_2 -oxo bridges (Figure 2.10 h)¹⁹⁸. A strong intradimer antiferromagnetic exchange with $J_1 = 440 \text{ cm}^{-1}$ and two weak interdimer ferromagnetic exchanges with the $J_2 = +0.5$ and $J_3 = +1.7 \text{ cm}^{-1}$ is calculated for $[\text{Cu}_2\text{apmt}(\text{OH})]_2 \cdot 2\text{CH}_3\text{OH} \cdot \text{H}_2\text{O}$ ($\text{H}_3\text{apmt} = 2,6\text{-bis}((2\text{-(acetylamino)phenylimino)methyl) -4\text{-tert-butylphenol})$) with ladder-like structure¹⁹⁹.

2.2.7. Spin Frustrated Systems

In contrast to ferromagnetically coupled molecules, the systems with predominant antiferromagnetic coupling with more than two exchanges, experience phenomenon called spin frustration due to the competing spin interaction¹⁸⁶. Frustration especially occurs in cyclic systems but is not limited to them. The spin frustration term is using for describing the systems with competing antiferromagnetic interactions, even when the competition results in a unique spin ground state¹⁸⁷. When an interaction on one side competing with interaction on the other side, and there is a joint magnetic center sitting in between, the spin of that center experience frustration. When geometry or topology of the lattice purely makes frustration, it is termed geometric frustration. The other way of describing frustration is that it occurs when there is competition between ferromagnetic and antiferromagnetic interaction, and with competition between AFM and FM contributions, most often the former takes over. To some extent, the antiferromagnetic interaction represents a border-line case of a very weak bond. Weakly pairing of magnetic electrons would lower the molecular orbital energies²⁰⁰. Spin frustration in trinuclear complexes most likely occurs in equilateral triangular

structures^{201–204}. The AFM spin frustration can be described in a classical picture with spins are alternately up and down (Figure 2.11).

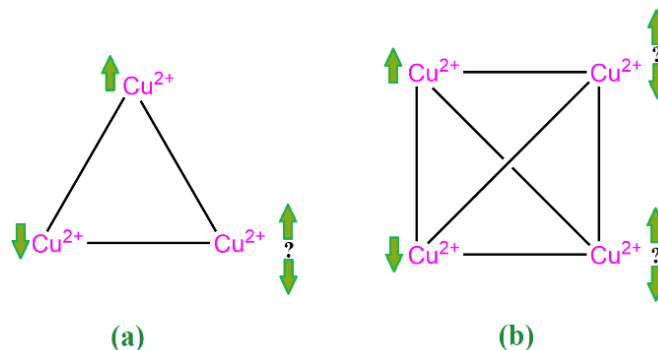


Figure 2.11 Spin frustration with three antiferromagnetic interactions on trinuclear and with six antiferromagnetic exchanges on tetranuclear cyclic copper(II) complexes.

2.2.8. Polynuclear Copper(II) Compounds

The synthesis of various types of polynuclear copper(II) compounds is possible owing to the flexible coordination nature of copper(II) and wide range of bridging ligand such as azide, cyanate, thiocyanate, dicyanamide, that are linking the metal centers to each other²⁰⁵.

As it is discussed in Section 2.2.4.1 carboxylate ligands have several coordination modes due to the two lone pairs on each oxygen atoms. In most structures of coordination geometry, only one of the lone pairs of oxygen atom is involved. However, by donation of the second lone pair to a metal ion another active center can join and the polynuclear structure would generate. $\text{Cu}_2(\text{OOCR})_4$ core is found in several crystal structures reported in the Cambridge Structural Database, that numerous of them are of the type $\text{Cu}_2(\text{OOCR})_4\text{L}_2$. The magnetic measurement on two of type (a) reveals the exhibition of isolated antiferromagnetically coupled dinuclear units, without magnetic interdimer interactions²⁰⁶. L in apical position is the ligand with a nitrogen or an oxygen donor atom (Figure 2.12).

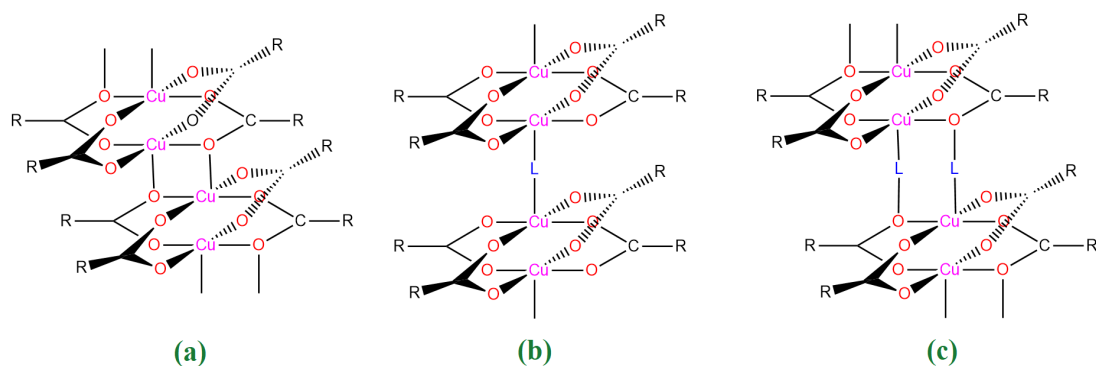


Figure 2.12 Polynuclear copper(II) carboxylate general structures: (a) without bridging ligands; (b) bridging ligands between two copper centers, (c) bridging ligands between copper centers and oxygen atoms.

Many types of one-dimensional chains with zig-zag and ladder configurations, two-dimensional layers, and three-dimensional cages and networks of copper(II) coordination complexes were synthesized and their magnetic behavior has been investigated²⁰⁷⁻²¹⁰. Developing the models and equations gained from the binuclear complexes leads to the understanding of the magneto-structure of the polynuclear copper(II) complexes²¹¹.

2.2.9. Single Molecular Magnets (SMM)

The cyclic polynuclear copper(II) complexes with oxygen, halide or azide linkers drawn specific attention during the past three decades due to the magnetic super-exchange pathways involved in interaction among the magnetic centers (Figure 2.13)²¹². These types of polynuclear complexes are great candidates of single-molecule-magnets (SMM) due to having superparamagnetic behavior at the molecular scale below certain temperatures. Their magnetic moments prefer to direct along a particular axis and their electron spin structures can be tuned to more than one magnetic state. They exhibit

magnetic hysteresis of a pure molecule and retain the state even in the absence of a magnetic field at a low temperature. This characteristic potentially allows them to store information²¹³.

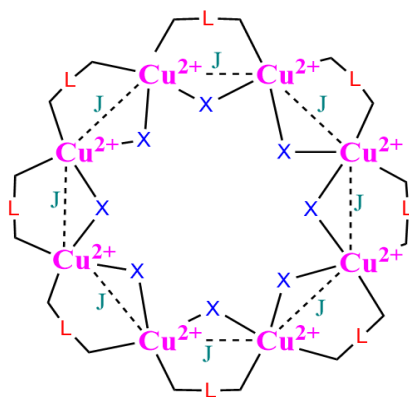


Figure 2.13 Polynuclear copper(II) ring (x = O, N, F, Cl, Br)

The main motivation for studying the magnetic behavior of such systems is the idea that the models provided by chemistry allow detailed analysis of homogeneous systems and can be practiced on inhomogeneous systems²¹⁴.

2.2.10 Single-chain magnets (SCM)

The single-chain magnets (SCM), mainly possess strong intrachain magnetic interaction. These magnetic compounds with their unusual properties are of high interest due to the possibility of potential usage as the molecular magnetic nanowires²¹⁵. The chain magnetic study first time was modeled by Bonner and Fisher²¹⁶ in 1964. Later on, in the same year, Baker and Rushbrook²¹⁷ extended the model with a different method to simplify the calculations.

Fisher model proposed an extrapolation of a magnetic susceptibility calculated for a limited number of magnetic centers for an infinite ring. Fitting the experimental data with the Fisher model for

a carboxylate coordination polymers $[\text{Cu}(\text{H}_2\text{bpta})]_n$, (H_4bpta = 2,2',4,4'-biphenyl tetracarboxylic acid) gives the $J = 9.28(1) \text{ cm}^{-1}$, and $zJ = -0.068(3) \text{ cm}^{-1}$ that indicates a weak ferromagnetic intrachain exchange and a weak antiferromagnetic interchain interactions²¹⁸.

The other polymeric chain structure is $[\text{Cu}(4,3\text{-opybz})(\text{OH})]_n$, [4,3-opybz = 4-(3-pyridyl)benzoic acid N-oxide]. Fitting the experimental data with the Fisher model gives the $J = -137.38 \text{ cm}^{-1}$, $g = 2.11$, $\rho = 0.02$, and $\text{TIP} = 60 \times 10^{-6} \text{ cm}^3 \text{ mol}^{-1}$, where ρ is the molar fraction of coupled species, and TIP is the temperature-independent paramagnetism. Above 150 K this compound follows the Curie–Weiss law. With the fitting, the $C = 0.54 \text{ cm}^3 \text{ K mol}^{-1}$ and $\theta = -219.2 \text{ K}$. The negative θ value and the J coupling interaction indicate the presence of dominant antiferromagnetic coupling between Cu ions²¹⁹.

2.3. Effects of Ligands

Construction of coordination magnetic compounds in a pre-designed and pre-tailored manner to obtain desired features needs a deep knowledge of the ligands involved. There are two different types of ligands²²⁰. The first type is the bridging ligand, linkers, that make the coordination compounds grow. The magnetic interaction between the magnetic centers depends on the type, the length and the geometry of the linkers connect the metal ions. For instance, the aromatic ligands with shorter length could make a stronger interaction between the metal ions in compare with the non-conjugated longer ones. Linkers can bridge between metal centers through their linking motifs and control the overall charge of the system by stabilizing specific oxidation states²²¹. The other types of ligands are blocking co-ligands. These types are limiting the number of coordination sites on a metal ion. In the synthesis of polynuclear complexes, the Blocking and bridging ligands have a significant role²²².

There are two ligands mainly used in this research work. The phenylene diacetic acid (H_2pda) and 1,10-phenanthroline (phen). The pda is a dicarboxylate ligand used as a bridging ligand with a diverse motif of linking to the metal ion. However, phen is used as a blocking ligand in this work¹⁰⁴.

Chapter 3. Materials, Methods, and Instrumentation

3.1. Synthesis

3.1.1. Solvothermal Reactions

In solvothermal reaction, the starting materials are sealed together with a solvent and heated above ambient temperature. In hydrothermal reaction, water is used as the solvent. The hydrothermal method is one of the most ways used to grow crystals of inorganic compounds.

The main advantage of solvothermal reactions is the use of lower temperatures in comparison with solid-state methods. The method is also useful in the synthesis of compounds that decompose at high temperatures. The solvent and high pressure of the sealed system make an appropriate environment for the starting materials to react, and the lower temperature leads to the formation of single-crystals that are large enough to be characterized using the single-crystal X-ray diffraction. The use of low-temperature methods also permits some control over the shape, size, porosity, and morphology of the crystals of crystalline compounds. Different reaction pathways including redox, substitution, and insertion reactions, can lead to the formation of new materials with different topologies^{188,223,224}.

In the one-pot solvothermal reaction, the solubility gradients of the starting materials and the product play a crucial role to form insoluble single crystals. In this regard, finding optimum values of temperature, time, solvent, cooling rate, and pH is important to obtain pure crystalline compounds. Using solvents at low temperatures (between 60 to 250 °C) is an effective method to grow crystals though long reaction times (several days) are usually needed.

In this work, many circumstances were investigated to find the best conditions for making the desired polynuclear coordination compounds. Two important factors that were considered in this

regard was the quality of single crystals and the phase impurity. The yield of the desired compound was another aspect which needs to be considered

The synthesizing method contains two different steps: First, preparing the starting solutions, and second, adding them to each other in order. As well, the optimization process of the synthesizing method contains two stages. At first stage, some variables (concentration of starting solutions, addition order, amount of solvents, pH, and duration) were changed and in the second stage, above variables were kept constant and other variables (temperature, solvent, and amount of starting materials) were altered to make different compounds.

The variables in the first stage were the concentration of starting solutions, the type and amount of solvents, the order of addition of precursors, the time duration, the pH and the temperature.

In the first step, the concentration of starting solutions were investigated in four different conditions, including a, b, c, and d (Table 3.1).

Table 3.1 Optimizing the amount of initial solution concentration for the synthesis of **1**.*

Entry	LiOH.H ₂ O (M)	Phen (M)	Cu(ClO ₄) ₂ .6H ₂ O (M)
a	0.025	0.05	0.05
b	0.05	0.1	0.1
c	0.1	0.2	0.2
d	0.2	0.4	0.4

*1mL of each solution was added to 0.1 mmol of pda ligand to 8mL of the mixture of 1:1 ethanol and water solvent. The reaction mixtures were kept at room temperature for 10 d.

The best concentration of starting solutions for synthesizing **1**, based on the least amount of impurity and highest yield, was gained by using the 0.1M of lithium hydroxide, 0.2M of phen and 0.2M of copper(II) perchlorate hexahydrate (entry c, Table 3.1).

The starting solutions then were added to each other in two different orders. Adding the phen to copper and then mixed it with the pda and lithium hydroxide were results in making the $[\text{Cu}(\text{phen})_2(\text{H}_2\text{O})](\text{ClO}_4)_2^{225}$ as a major phase. Hence, after deprotonation of pda ligand by lithium hydroxide, the **1** was obtained in a single phase by adding the phen ligand followed by adding the copper salt to the whole solution. The amount, type, and ratios of solvents are summarized in Table 3.2.

The optimized amount of solvent by considering the highest yield of product was obtained with adding the 7 mL of solvent, and the least amount of impurity with **1** was obtained by adding the mixed solvents of water and ethanol (Table 3.2).

Table 3.2 Optimizing the amount of solvent for the synthesis of **1**. *

	Solvent		
	Water (mL)	Ethanol (mL)	Water – Ethanol (mL)
Amount of solvent	5	5	2 – 3
	6	6	3 – 3
	7	7	3 – 4
	8	8	4 – 4
	9	9	4 – 5
	10	10	5 -5

* 0.1 mmol of pda ligand was added to 1 mL of 0.1 M LiOH.H₂O, 0.2M phen, and 0.2 M CuClO₄.6H₂O. The reaction mixtures were kept at room temperature for 10 d.

Changing pH was investigated by adding different amount of pda, when the concentration of lithium hydroxide, phen and copper(II) salt were kept constant (0.1 M, 0.2 M and 0.2 M, respectively)

in the mixture of ethanol and water (4 mL : 3 mL) solvent. By studying the different amount of pda ligand which were including 0.4 mmol (pH= 2.42), 0.3 mmol (pH= 2.55), 0.2 mmol (pH= 2.67), 0.1 mmol (pH= 3.28), 0.05 mmol (pH= 2.31), 0.033 mmol (pH= 2.32), 0.025 mmol (pH= 3.35), 0.02 mmol (pH= 4.41), 0.016 mmol (pH= 4.36), the least amount of impurity was obtained in the pH of 3.28 with the 0.1 mmol of pda. It should be noted that the reaction mixtures were kept at room temperature for 10 d.

Three different solvents were investigated in different duration of time, between 3-21 d, while the other variables kept constant. In the mixture of water and ethanol, the best crystal growth and maximum yield happened after 10 d (not a big difference in yield and crystal quality afterward). Also, the best result in acetonitrile and THF was obtained after 7 d.

By optimizing the first group of variables, they were kept constant in the second stage. Changing the second group of variables results in forming different compounds. **1** was synthesized using pda:LiOH:phen:CuClO₄ with the ratio of 1:1:2:2, respectively, in the mixed solvent of ethanol:water (4 : 3) at room temperature. The same ratio of starting material at 80 °C was resulted in forming **1** with the minor phase of **4.2** and **5.2**. The minor phase at 105 °C contained both **4.1** and **5.2**. At 110 °, the major phase was **5.2** containing the two other **1** and **4.1** phases and at 120 °C, the major phase was **4.1**.

In 7 mL acetonitrile, with the same amount of starting materials, the single-phase at 60 °C was compound **1**, however a major phase changed to **5.1** at 70 °C (with the minor phase of **1**). By adding 7mL THF at 60 °C for 7 d, the **4.1** was obtained as the major phase. To form **1** in THF, the ratio of pda:LiOH:phen:CuClO₄ as starting materials has been changed to 1:1:1.25:1.25, respectively.

By changing the ratio of pda:LiOH:phen:CuClO₄ to 1.5:1:1.25:1.25, respectively, compound **4.2** was gained in acetonitrile at 60 °C and in the mixture of ethanol:water (4mL:3mL, respectively) at 80 °C as the major phase.

By changing the ratios of pda:LiOH:phen:CuClO₄ to 0.1:2:2:2, **3** was formed at 80 °C in water and ethanol (Chapter 6). Also, compound **2** was generated by pda:LiOH:phen:CuClO₄ with the ratio of 1:2:1:1 in acetonitrile at 60 °C (Chapter 5).

3.1.2. Starting Materials

Starting reagents for all syntheses are listed in Table 3.1, and they were utilized as purchased. Chemicals were stored in closed containers in the research laboratory. Hygroscopic materials were stored in a vacuum desiccator in closed containers.

Table 3.3 Starting reagents for all synthesis techniques

Compound	Source	Purity
1,10-Phenanthroline *	Alfa Aesar	99%
LiOH·H ₂ O	Aldrich	98%
1,4-Phenyldiacetic acid	Aldrich	97%
2,7-Naphthalenedicarboxylic Acid	TCI	98%
1,4-Naphthalenedicarboxylic acid	TCI	96%
1,4,5,8-Naphthalene tetracarboxylic acid	TCI	60%
Copper(II) perchlorate hexahydrate	Aldrich	98%
Acetonitrile	Sigma-Aldrich	99.9%
Tetrahydrofuran (THF)	Sigma-Aldrich	99.9%

* indicates storage in the desiccator.

3.1.3. Reaction Containers

Solvothermal reactions at 60 to 100 °C were carried out in 30 mL Fisher borosilicate glass polycone black-capped vials. The caps were sealed with Teflon tape. The reactions at the higher temperature used Teflon lined stainless steel autoclave reactors. The Teflon liners were cleaned overnight with a solution of 50% HNO₃ in water at 60 °C, and then were sealed and heated with distilled water at 120 °C.

3.1.4. Ovens

The reactions were performed in Thermolyne 9000 series Electric Convection Lab ovens, fitted with Eurotherm 91e temperature controllers. The cooling or heating rate can be programmed with this controller; a slow cooling ramp rate is necessary to obtain larger crystals. For carrying out reactions simultaneously at exactly the same temperature, the reaction vessels were put in an oil bath in the oven.

3.2. Materials Characterization

3.2.1. Powder X-ray Diffraction (PXRD)

X-ray diffraction is a non-destructive technique to obtain information on the crystal lattice and the atom positions for a material in the form of a polycrystalline sample or a single crystal. The powder X-ray diffraction pattern is a projection in one dimension of many diffracted X-ray beams. Single crystal X-ray diffraction would information in three-dimensional space. PXRD data were collected using a Panalytical X'Pert Pro powder diffractometer with Bragg-Brentano θ - 2θ geometry and monochromatic Cu K α ($\lambda = 1.54178 \text{ \AA}$) radiation at room temperature. The data were collected from $5 < 2\theta < 90^\circ$ for 60 minutes (step size of 0.007° and scan time of at 0.3 s per step). The dry sample was

well ground using an agate mortar and pestle. The fine powder was spread over a zero-diffraction silicon sample holder.

3.2.2. Single Crystal X-ray Diffraction (SCXRD)

Single crystals were picked from the whole sample using an optical microscope. The data were collected using a Bruker Apex-II diffractometer equipped with a CCD area detector and monochromatic Mo K α 1 radiation ($\lambda = 0.71073$). The selected well-faced crystals were covered with vacuum grease and immediately mounted onto the goniometer under the flowing stream of nitrogen at -150 °C. A hemisphere of data was collected overnight with a 6-cm detector distance using a narrow-frame algorithm with scan widths of 0.30 % in omega and exposure times of 40-90 s. The diffraction data were integrated using the Bruker SAINT program, and the intensities corrected for Lorentz factor, air absorption, and absorption due to the variation in the path length through the detector faceplate. The data were scaled, and an absorption correction was applied using SADABS. XPREP program was used to perform unit cell reduction, and determination of possible space groups according to systematic absences and the internal R-value of the data. The crystal structures were solved using direct methods and refined using full-matrix least-squares calculations on F². Thermal parameters were treated anisotropically. The structure solution was performed by using SHELX program package ²²⁶. Compounds **1**, **2**, **3**, **4.1** and **5.1** were refined by Dr. James Korp. (Compound **3** was solved at the same time by Dr. Joseh Reibenspies). Compound **4.2** and **5.2** was refined by Dr. Xiqu Wang.

3.2.3. Chemical Analysis

To confirm the chemical compositions of the bulk with the composition of crystals obtained from single-crystal X-ray diffraction, elemental analysis was performed by Galbraith Laboratories. By

burning a small portion of sample in oxygen, to generate the products of combustion of carbon, hydrogen, and nitrogen (CO_2 , H_2O , and N_2 (or NO_x)). They are separated then and the results in weight percentage were reported. Oxygen is used to pyrolyzes a small portion of sample in an inert atmosphere to make carbon monoxide which is quantified with a thermal conductivity detector. The amount of copper was measured using Inductively Coupled Plasma–Atomic Emission Spectroscopy (ICP-AES). Emitted element-specific spectra of the sample that were heated in plasma are measured by ICP-AES.

3.2.4. Raman Spectroscopy

Raman spectroscopy was measured on a triple Horriba Jobin Yvon T-6400 spectrometer equipped with an optical microscope and a liquid nitrogen-cooled CCD detector using a spectral resolution of 1.5 cm^{-1} . An Ar^+ laser ($\lambda_{\text{las}} = 514.5 \text{ nm}$, 2.41 eV) was used for the excitation. The spectroscopy was performed in the backscattering geometry at room temperature. The incident laser power was kept below 1.0 mW to minimize heating the sample. The measurement was done by Dr. Alexander Litvinchuk.

3.2.5. Infrared (IR) Spectroscopy

Infrared spectroscopy measurements of crushed crystals samples were collected using Bruker Alpha-P spectrometer. A total of 64 scans were recorded and a background spectrum was subtracted.

3.2.6. Thermogravimetric Analysis (TGA)

The thermogravimetric analysis (TGA) and Derivative Thermogravimetry (DTG) was performed on powder samples using a TGA 2050, TA instrument in the range of room temperature to 400-850 °C.

The normal rate of analysis was 1 °C/min; however, due to the explosive decomposition of perchlorate in the samples, a sample was analyzed in a lower rate of heating, 0.1 °C/min.

3.2.7. Bond Valence Sum (BVS)

The bond valence sum rule follows the definition, that an atom valence is equal to the sum of all of the individual bond valences (Equation (3.1))²²⁷. The bond valences are calculated from the observed bond lengths (Equation (3.2)). The r_{ij} is the observed bond length between atom i and atom j , R_0 is a tabulated parameter indicating when the element i has exactly valence 1 what would be the ideal bond length, and b is an empirical constant, typically 0.37 Å.

$$V = \sum(S_{ij}) \quad (3.1)$$

$$S_{ij} = \exp [(R_0 - r_{ij})/b] \quad (3.2)$$

3.3. Magnetic Characterization

3.3.1. Magnetic Properties

The specific magnetic properties of a compound arise from the interaction of magnetic moments of electrons with the applied external field. Paramagnetic materials contain unpaired electrons whereas diamagnetic materials have no unpaired electrons. Ferromagnetism involves cooperatively interacting spins with parallel alignment and which can remain aligned even when the external field is removed; in antiferromagnetism, the spins have antiparallel alignment.

Magnetic susceptibility measurements were performed between 2 and 300 K under an applied field of 0.1 T using a Quantum Design Model 6000 VSM magnetometer. The temperature dependence of magnetization was obtained using zero-field-cooling and field-cooling conditions. Magnetization measurements were performed at 2 K.

Magnetic susceptibility (χ) indicates a material attraction to a magnetic field or repulsion out of it. Standard measurements were the temperature dependence (χ vs T) and the field dependence (M vs H) of a sample.

3.3.2. PHI Program

In order to calculate the magnetic properties of coordination complexes with paramagnetic centers, the computer program PHI was used²²⁸. The program was used to fit the experimental data and calculate the exchange coupling constants (J), the g-factor, the exchange energy increased by the (z) number of interacting neighbors (zJ), temperature-independent paramagnetism (TIP), and the amount of paramagnetic impurities (ρ). Large spin systems and orbitally degenerate complexes, such as d- and f-block ions clusters can be calculated. In 3d ions compared to 4f ions the spin-orbit coupling is much weaker and so the only coupling calculated was the spin-spin coupling. The exchange interaction effective Hamiltonian (H) is parameterized in the PHI program with the Heisenberg-Dirac-Van Vleck Equation (3.3):

$$H = -2J \sum_{i < j}^{i, j \in N} S_i S_j \quad (3.3)$$

Where J denotes the exchange integral between i and j atoms. S_i is the spin vector of atom i .

Chapter 4. A New Trinuclear Cu(II) Coordination Polymer: Correlation of the Magnetic Behavior with the Crystal Structure

4.1. Introduction

Trinuclear copper complexes are attracting attention because of their interesting magnetic properties. In addition, trinuclear copper compounds have the ability to perform DNA strand scission and nuclease-like activity^{168,229}. Using phenylene diacetic acid (pda) as a bridging ligand and 1,10-phenanthroline as a blocking ligand, a new copper(II) complex was synthesized solvothermally.

The magnetic behavior of trinuclear copper(II) complexes has been studied less than that of the binuclear complexes. Here we discuss the synthesis and structure of the coordination polymer $[\text{Cu}_3(\text{phen})_3(\text{pda})_2(\text{H}_2\text{O})^{2+}][\text{ClO}_4^-]_2[\text{H}_2\text{O}]_4$ (**1**), its magnetic behavior, and magneto-structural correlations. The structure is made up of a scalene triangle. The magnetic interactions in this structure are inversely related to the copper ion distances. The interaction between two copper ions at the farthest distance is assumed to be zero. The two other interactions were assumed as binuclear structures and were discussed using two models.

The first interaction was explained using the semi-empirical Goodenough-Kanamori-Anderson (GKA) model^{121,230,231}. Although there are some conflicting reports^{122,232,233}, the GKA model is highly successful in rationalizing magnetic properties on a qualitative level for a wide variety of compounds^{125,234–236}. Briefly, the GKA rules describe the interatomic spin-spin interactions considering electron coupling between magnetic ions through a shared bridging anion (super-exchange). The rule predicts antiferromagnetic behavior when the magnetic ion-ligand-magnetic ion orbitals are parallel to each other. If the orbitals of the magnetic ions and bridging ligand are orthogonal to each other, they do not overlap to reduce the repulsion between the electrons, and therefore following Hund's rule (all of the singly occupied orbitals contain electrons with the same spin) they ferromagnetically interact. The

Cu(1)···Cu(2) interaction with one bridging atom is well illustrated in this chapter. The orthogonality of the bridging ligand orbitals to the magnetic orbitals of these two copper centers result in a ferromagnetic interaction.

The other model was used to describe the Cu(2)···Cu(3) interactions in **1** is the dimeric copper ion units of cupric acetate hydrate with the same bridging O-C-O atoms. Cupric acetate hydrate $[\text{Cu}(\text{CH}_3\text{COO})_2 \cdot \text{H}_2\text{O}]_2$ is an interesting compound due to the exchange coupling between the dimeric units. This compound has a great influence on fundamental polynuclear magnetic studies. The exchange pathway proposed by Bleaney and Bowers¹¹⁰ based on electron paramagnetic resonance (ESR) was the direct magnetic coupling exchange between the copper centers.

4.2. Experimental

4.2.1. Synthesis of $[\text{Cu}_3(\text{phen})_3(\text{pda})_2(\text{H}_2\text{O})^{2+}] [\text{ClO}_4^-]_2 [\text{H}_2\text{O}]_4$ (**1**)

Compound **1** was synthesized by a one-pot hydrothermal reaction. Many attempts result in producing **1**. In the first step, the starting solutions were made. The solution of 6 mmol (2.223 g) of $\text{Cu}(\text{ClO}_4)_2 \cdot 6\text{H}_2\text{O}$ salt was dissolved in sufficient water to make 30 mL of 0.2 M solution. 6 mmol (1.081g) 1,10-phenanthroline (phen) was added to ethanol to make 30 mL of 0.2 M solution. 30 mL 0.1 M of $\text{LiOH} \cdot \text{H}_2\text{O}$ solution was made by adding 3 mmol (0.126 g) salt to water. After the preparation of all three solutions, they were mixed together in order. 0.1 mmol (0.0194 g) of phenylene diacetic acid (H_2pda) was added to 1 mL of the solution of 0.1 M of $\text{LiOH} \cdot \text{H}_2\text{O}$ in the reaction vial. To dissolve the pda, 4 mL ethanol and 3 mL water were added. The mixture was stirred for an hour to make a clear solution (using an ultrasound bath for 20 minutes to dissolve the pda leads in the same result). Then 1 mL of premade phen 0.2 M solution was added to the mixture and shaken well. By adding 1 mL of premade $\text{Cu}(\text{ClO}_4)_2 \cdot 6\text{H}_2\text{O}$ 0.2 M solution, the reaction mixture became blue. The reaction mixture was

capped in a vial and sealed with a Teflon tape. The single phase of **1** was formed from the reaction mixture at room temperature for 10 to 14 d. Acicular blue crystals of **1** formed from reaction mixture as a pure phase, in 65% yield (Figure 4.1).

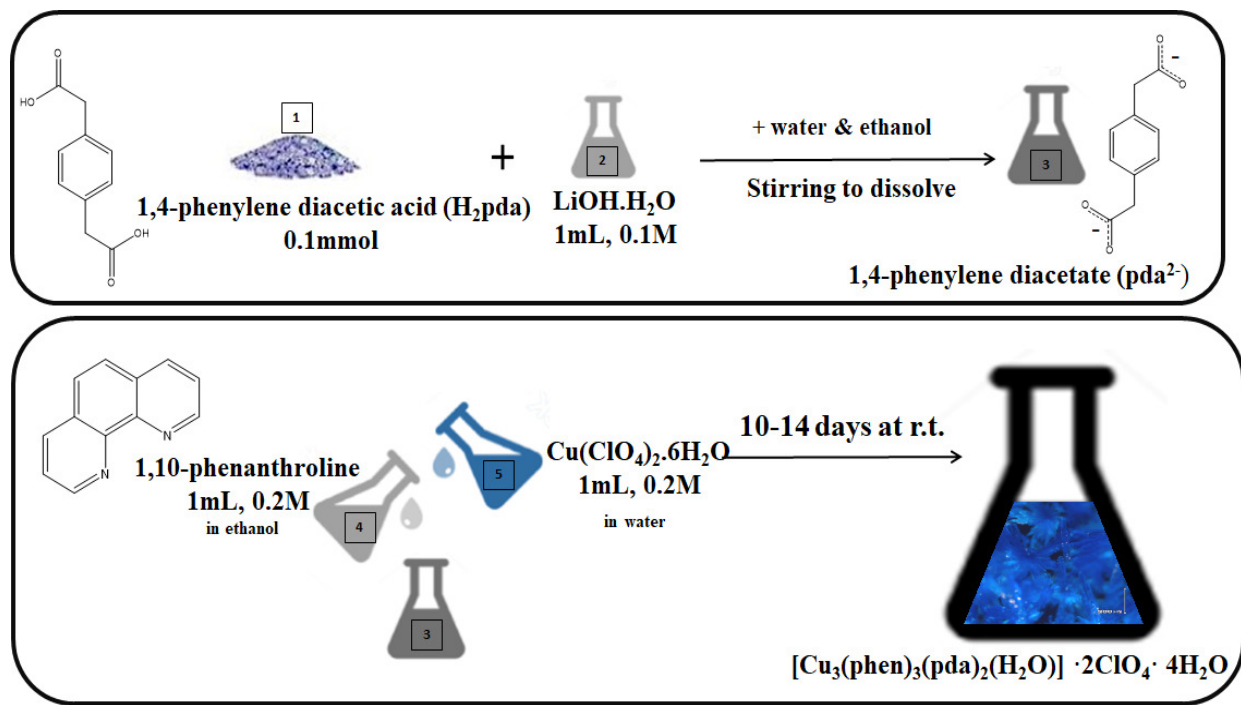


Figure 4.1 Schematic description of synthesis method of **1**.

Reactions under other conditions also result in the formation of **1** (as a single or major phase).

With the same condition when the reaction mixture was heated in the oven at 80 °C in 14d, **1** was also obtained as a major phase. The known minor phases were **4.2** and **5.2** (Structures are discussed in Chapter 7).

By using the same premade solutions and the same amount of starting materials, in tetrahydrofuran (THF) as the solvent at 60 °C for 7d, **1** was produced as a single phase.

Compound **1** can also be made by combining a solution of 0.13 mmol (0.0252 g) pda dissolved in 1.3 mL of a solution of 0.1 M of LiOH·H₂O, 4 mL ethanol and 3 mL water and 1.3 mL of a 0.2 M phen solution and 1.3 mL of 0.2 M solution of Cu(ClO₄)₂·6H₂O. The reaction mixture was heated in a sealed Teflon-lined stainless-steel autoclave at 105 °C for 10 to 14 d. The known minor phase was **4.1**, and **5.2** (Structures are discussed in chapter 7).

Compound **1** was generated in 10 d at 60 °C by adding 0.2 mmol (0.0388 g) of pda to 2 mL of LiOH·H₂O 0.1 M solution and diluting with 7 mL of acetonitrile. Then 1.25 mL of 0.2 M phen solution and 1.25 mL Cu(ClO₄)₂·6H₂O 0.2 M were added. **1** was generated as the major phase, and the known minor phase was **4.2**, and **5.1** (Structures are discussed in chapter 7).

4.2.2. Characterization of **1**

4.2.2.1. Single Crystal X-ray Diffraction (SCXRD)

A blue rectangular single crystal was mounted on the tip of a Micromount mitegen loop. A hemisphere of data (1272 frames at 6 cm detector distance) was collected using a narrow-frame algorithm with scan widths of 0.50% in omega and an exposure time of 40 s frame⁻¹. The data collection crystal was determined to be a multi-domain twin; however, since one large domain predominated and there was not very much overlap with the minor domains, the data were processed as if it was a pure single crystal. The final cell constants of the **1** were refined using 7281 reflections having $I > 4\sigma(I)$, and these, along with other information pertinent to data collection and refinement, are listed in Table 4.2. The Laue symmetry was determined to be -1, and the space group was shown to be either P1 or P-1. The crystal data and structure refinement are summarized in Table 4.2.

Table 4.1 Crystal data and structure refinement for **1**.

Empirical formula	C ₅₆ H ₅₀ Cl ₂ Cu ₃ N ₆ O ₂₁
Formula weight	1404.54
Temperature, Wavelength	123(2) K, 0.71073 Å
Crystal system, space group	Triclinic, P $\bar{1}$
Unit cell dimensions	$a = 10.033(2)$ Å, $b = 13.171(3)$ Å, $c = 22.985(5)$ Å $\alpha = 92.631(2)^\circ$, $\beta = 101.543(2)^\circ$, $\gamma = 109.670(2)^\circ$
Cell Volume	2548.8(4) Å ³
Z, Calculated density	2, 1.677 g/cm ³
Crystal size	0.20 × 0.15 × 0.04 mm ³
Index ranges	$-11 \leq h \leq 11$, $-15 \leq k \leq 15$, $-27 \leq l \leq 27$
Theta range for data collection	0.91 to 25.07°
Absorption coefficient	1.947 mm ⁻¹
F(000)	1434
Reflections collected / unique	15335 / 8768 [R(int) = 0.0162]
Refinement method	Full-matrix least-squares on F ²
Data/restraints/parameters	7281 / 114 / 852
Goodness-of-fit on F ²	1.075
Final R indices [I > 4σ(I)]	R1 = 0.0556, wR2 = 0.1453
R indices (all data)	R1 = 0.0743, wR2 = 0.1596
Largest diff. peak and hole	1.441 and -1.352 e.Å ⁻³

4.2.2.2 Crystal Structure

The main part of the asymmetric unit of the crystal structure of $[\text{Cu}_3(\text{phen})_3(\text{pda})_2(\text{H}_2\text{O})] \cdot 2\text{ClO}_4 \cdot 4\text{H}_2\text{O}$ (**1**) consists of three Cu atoms each attached to a bidentate phenanthroline (phen) ligand, one phenylene diacetate (pda) in a general position, two half-phenylene diacetates situated on inversion centers, and a water molecule. Figure 4.2 shows the asymmetric unit omitting the solvent and the counter ion.

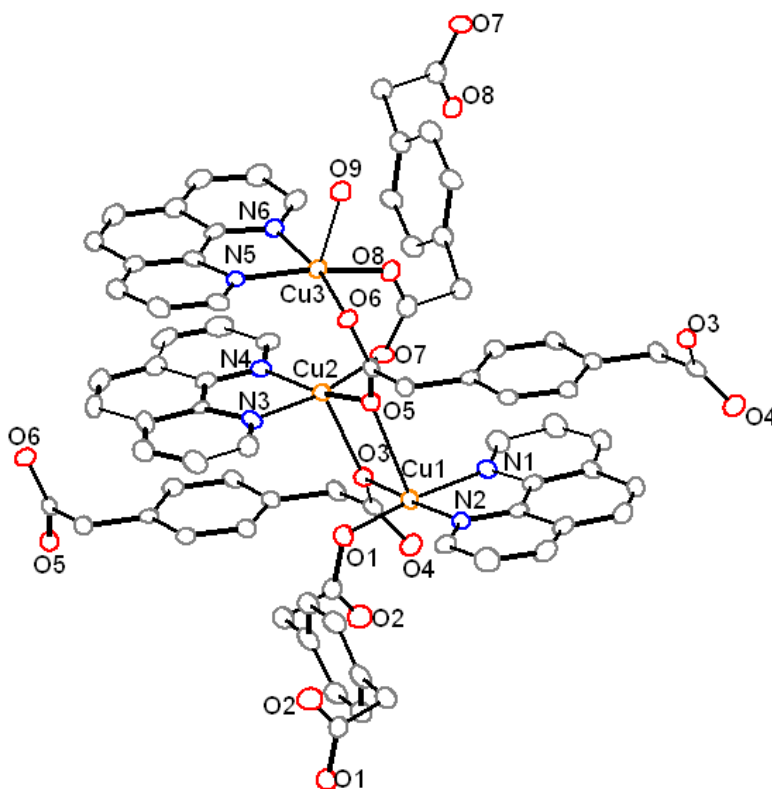


Figure 4.2 A view of the asymmetric unit of **1**. Lattice water molecules, perchlorate ions, and hydrogen atoms are removed for clarity. Orange, red, blue, and gray spheres represent copper, oxygen, nitrogen, and carbon atoms.

The coordination environment around the copper ions is distorted square pyramidal. Each copper ion is coordinated to two nitrogen atoms from the bidentate 1,10-phenanthroline (phen) ligand

in the basal plane of the square pyramid and to three oxygen ions. The three oxygen ions that are connected to Cu(1) and Cu(2) are from three different phenylene diacetate (pda) ligands. Two of oxygen ions that are connected to Cu(3) are from two pda ligands and the apical position is occupied by a water molecule O9 (Figure 4.3). O(5) and O(3) are the bridging oxygen ions between Cu(1) and Cu(2). Cu(3) is connected to Cu(2) through O(5) and O(6) from one bridging pda ligand and O(7) and O(8) from the other one; O5 and O6 also connect Cu(3) to Cu(1).

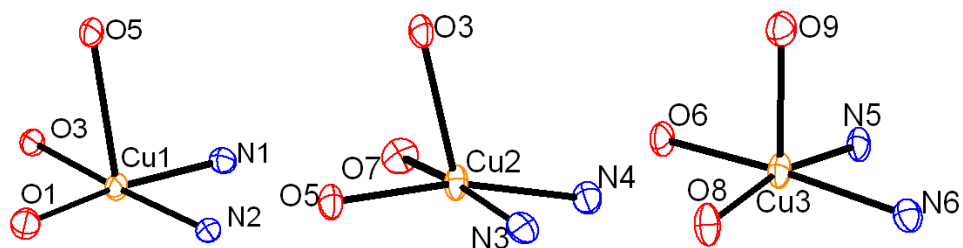


Figure 4.3 Geometry around each copper in **1** with thermal ellipsoids at the probability of 50%.

In these distorted square pyramidal geometries, the copper ions lie above the basal plane towards the apical oxygen ions, and the apical Cu-O bond lengths are longer than the corresponding basal Cu-O bonds. Selected bond lengths [\AA] and angles [$^\circ$] are summarized in Table 4.2.

Table 4.2 Selected bond lengths [Å] and angles [°] for **1**

Cu(1)-O(1)	1.938(4)	O(1)-Cu(1)-O(5)	90.503(15)
Cu(1)-O(3)	1.954(3)	O(3)-Cu(2)-O(5)	79.797(15)
Cu(1)-O(5)	2.465(4)	N(1)-Cu(1)-O(5)	94.308(17)
Cu(1)-N(1)	2.019(5)	N(2)-Cu(1)-O(5)	105.282(17)
Cu(1)-N(2)	2.013(4)	O(7)-Cu(2)-O(3)	87.73(15)
Cu(2)-O(5)	1.969(4)	O(5)-Cu(2)-O(3)	79.81(14)
Cu(2)-O(7)	1.941(4)	N(4)-Cu(2)-O(3)	113.64(16)
Cu(2)-O(3)	2.235(4)	N(3)-Cu(2)-O(3)	100.63(16)
Cu(2)-N(4)	2.003(4)	O(8)-Cu(3)-O(9)	93.26(16)
Cu(2)-N(3)	2.004(5)	O(6)-Cu(3)-O(9)	90.48(15)
Cu(3)-O(8)	1.952(4)	N(5)-Cu(3)-O(9)	98.80(17)
Cu(3)-O(6)	1.974(4)	N(6)-Cu(3)-O(9)	97.68(17)
Cu(3)-O(9)	2.148(4)	Cu(1)-O(3)-Cu(2)	106.92(16)
Cu(3)-N(5)	2.009(5)	Cu(1)-O(5)-Cu(2)	98.35(16)
Cu(3)-N(6)	2.035(5)		

There are three different ligands in the structure of **1**. Water is coordinated to Cu(3) through the oxygen atom. Phen ligands act as bidentate blocking ligands and each occupies two coordination positions of the copper centers through its nitrogen atoms. There are three different pda that act as bridging ligands and connect the copper centers together.

Two, out of three pda ligands in a unit cell cause the crystal to grow in one direction, and the other pda directs the crystal growth to the other direction (Figure 4.4, a). A two-dimensional plane is made out of two-direction crystal growth (Figure 4.4, b). There are two oxygen atoms (O(4) and O(2))

that are not connected to the metal centers. These two atoms are involved in hydrogen bonding along the third direction.

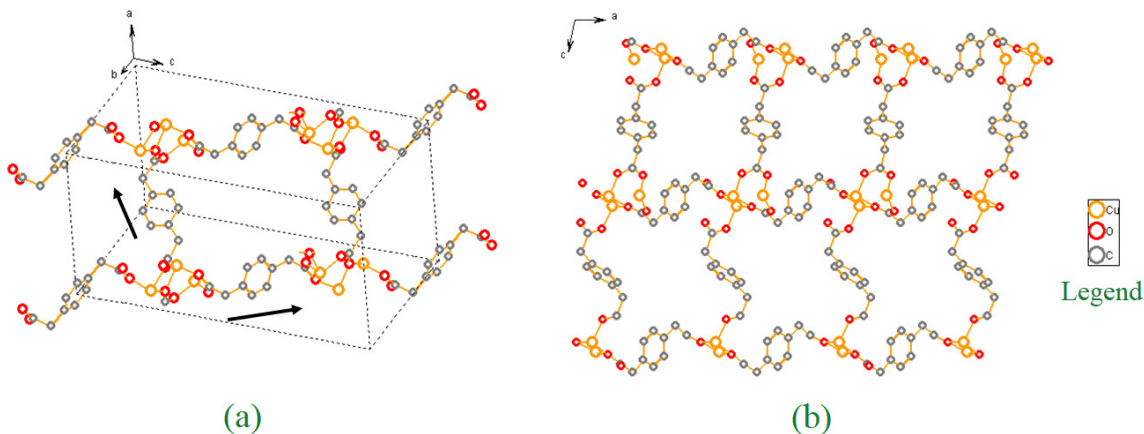
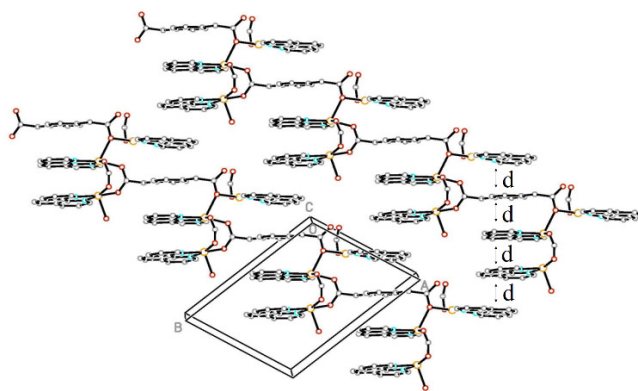


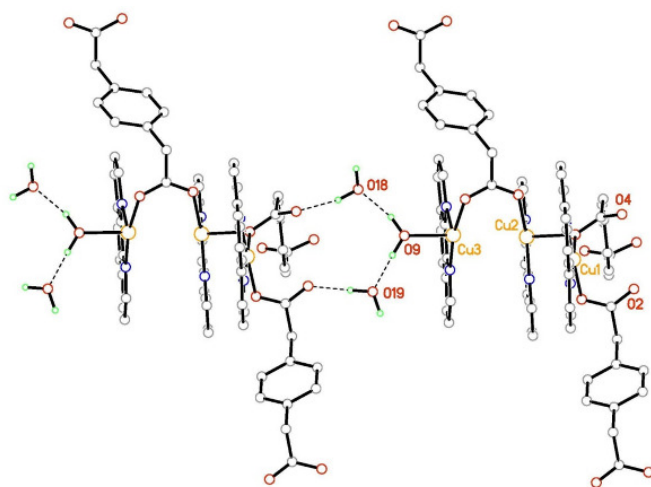
Figure 4.4 (a) Three pda ligands in the unit cell direct crystal growth in two directions. (b) The plane is made out of crystal growth in two directions.

The two-dimensional planes are then linked together via two other forces. The aromatic rings are stacking on top of each other along the [110] direction. The distance between the aromatic planes (d) is $3.3 \leq d \leq 3.5 \text{ \AA}$, which shows strong π - π stacking interaction (Figure 4.5, a).

Hydrogen-bonding also holds the two-dimensional planes together. The hydrogen bonds are between the coordinated water molecule, lattice water molecules, and the two oxygen atoms from pda ligands mentioned above (Figure 4.5, b). The average distance between oxygen atoms in the hydrogen bond is 2.7 \AA and the average $\text{O}\cdots\text{HO}$ angles are 177° . This hydrogen bond reinforces the π - π interaction along the same direction.



(a)



(b)

Figure 4.5 (a) π - π stacking along a-b direction, (b) the hydrogen bond between the coordinated water ($\text{H}_2\text{O}(9)$), lattice water molecules ($\text{H}_2\text{O}(18)$ and $\text{H}_2\text{O}(19)$), and the two oxygens from pda ligands.

Orange, red, blue, and gray spheres represent copper, oxygen, nitrogen and carbon atoms.

Besides the pda ligands, the perchlorate group is responsible for the charge balance of the complex as a counter ion. The two perchlorate groups per unit cell are disordered (Figure 4.6). They are located in the empty spaces within the three-dimensional framework.

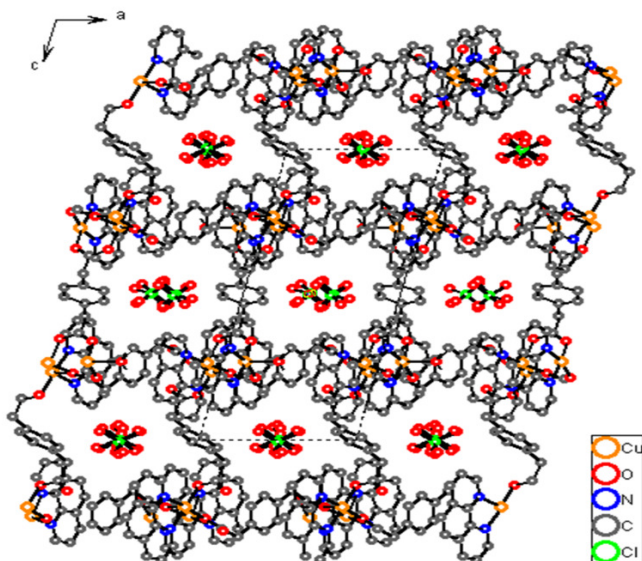


Figure 4.6 Perchlorate groups are located in the empty spaces of the 3-D framework.

4.2.2.3 Powder X-ray Diffraction (PXRD)

The sample from the first reaction was prepared by washing with ethanol and acetone after filtration and then air-dried. The sample then ground using an agate mortar and pestle. The fine powder was spread over a zero-diffraction silicon sample holder. The experimental powder pattern is closely similar to the one simulated from the single crystal data and confirms the phase purity. Small peak shifts occur due to the temperature difference (Figure 4.7) (powder data were collected at room temperature and the single-crystal data were collected at $-150\text{ }^{\circ}\text{C}$).

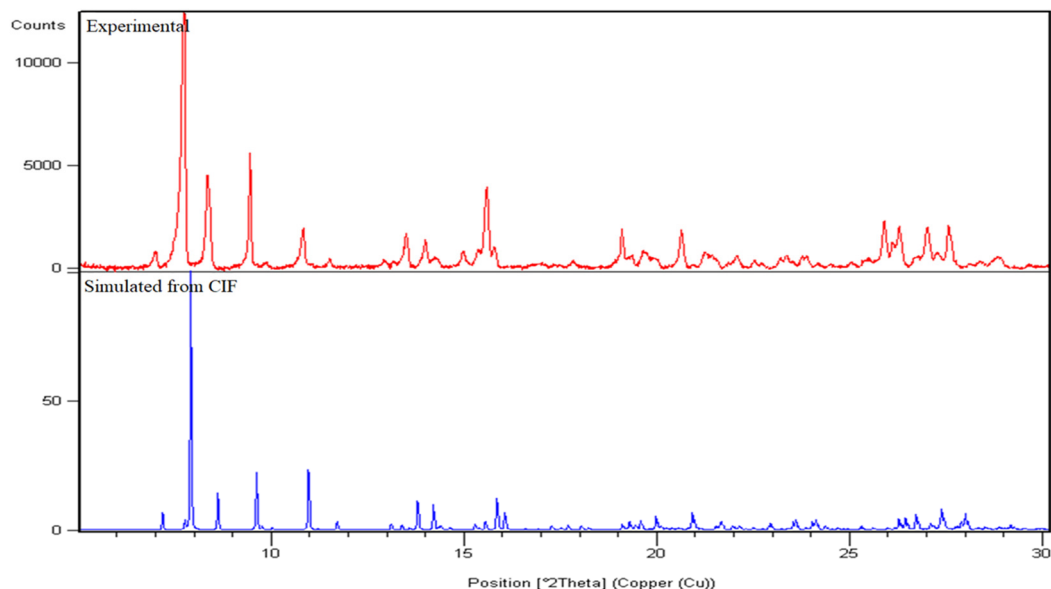


Figure 4.7 Experimental and simulated powder X-ray diffraction of **1**. The simulated pattern is based on the analysis of the single-crystal X-ray diffraction refined structure.

4.2.2.4 Physical Measurements

The C, H, N and Cu values for the **1** composition based on elemental analysis were 47.01%, 3.59%, 5.98% and 14 which are consistent with the calculated percentage of the carbon, hydrogen, nitrogen and copper amounts from the X-ray crystallography that were 47.89%, 3.46%, 6.08% and 13.57 respectively.

Thermogravimetric analysis (TGA) and Derivative Thermogravimetry (DTG) were performed in air at a heating rate of 1 °C/min up to 850 °C (Figure 4.8). The mass loss in the first step is due to the loss of lattice water molecules and not the coordinated ones. The mass loss of 5.2% is consistent with the loss of four water molecules from compound **1**. In the next step due to the perchlorate presence, compound **1** goes through exothermic decomposition, as has been reported^{237,238} for other compounds containing perchlorate ions. Loss of perchlorate as counter ion in the structure leads to breaking down of the whole structure and results in partial loss of the sample from the balance pan.

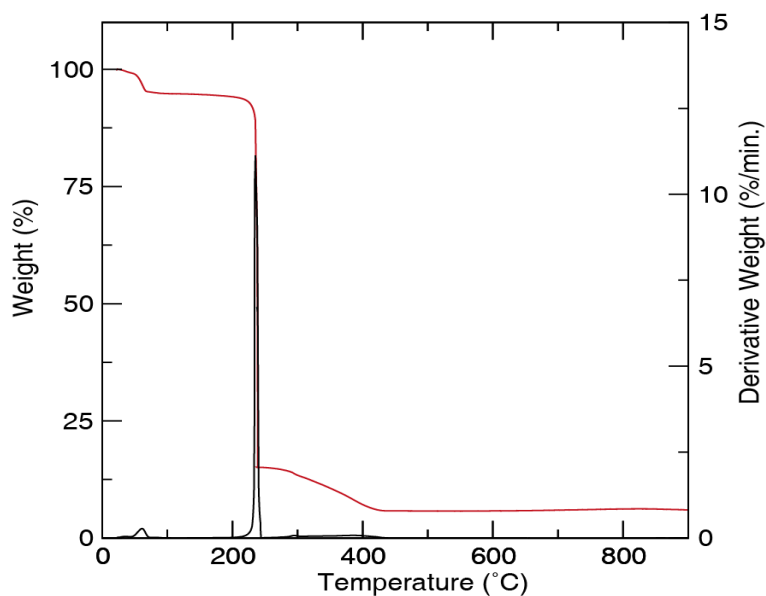


Figure 4.8 TGA and DTG of **1**. The first weight loss corresponds to the loss of lattice water, and the second drastic weight loss is due to the exothermic decomposition of **1** due to the explosive decomposition of perchlorate.

The residual solid after heating to 450 °C was identified as copper(II) oxide by powder X-ray diffraction. The remaining amount of powder (6% CuO per formula unit) was much less than the expected amount (16.9% CuO per formula unit).

The bond valence sum for all three sites was calculated from the bond lengths, based on Equation (4.1) and the tabulated values of R_o and b that are shown in Table 4.3.

$$S_{ij} = \exp[(R_o - r_{ij})/b] \quad (4.1)$$

Table 4.3 The oxidation states assignment of the copper ions from bond valence sums (BVS) in **1**, and the parameters used for the BVS calculations^{227,239}.

site	Bond Valence Sum			Assignment Oxidation State
	Cu(I)	Cu(II)	Cu(III)	
Cu1	1.385	1.906	2.294	Cu(II)
Cu2	1.411	1.981	2.402	Cu(II)
Cu3	1.446	2.000	2.412	Cu(II)

accumulated table of R_o and b				
		Cu ¹⁺	Cu ²⁺	Cu ³⁺
O	R_o	1.504	1.655	1.735
	b	0.37	0.37	0.37
N	R_o	1.63	1.713	1.768
	b	0.37	0.37	0.37

The bond valence sum indicates that the copper ion oxidation state is Cu²⁺ (d⁹) at all three sites. The coordination environment around all three copper ions is square pyramidal with the apical bond length being longer than the basal ones.

FT-IR spectroscopic analysis of **1** is shown in Figure 4.9. The bands of Cu-O and Cu-N are observed at 428.3 and 479.8 cm⁻¹, respectively. Absorption bands at 620 and 718 cm⁻¹ are due to the out of plane bending vibration of CH, =C-H bending vibration appears at 850 cm⁻¹. Also, C-O stretching vibration, C-C stretching vibration, and an absorption band of ClO₄⁻ are overlapped and appear at 1074 cm⁻¹.

The peak at 1223 cm⁻¹ is assigned to stretching vibration of C-N group, C-H bending band is observed at 1356 cm⁻¹, aromatic ring vibration bands are found at 1373-1426 cm⁻¹, the absorption band at 1519 cm⁻¹ is related to C=N stretching vibration, the stretching vibration of C=C has appeared at 1579 cm⁻¹, and COO stretching band finds at 1636 cm⁻¹.

Above 2000 cm⁻¹, CH aliphatic and aromatic stretching bands are present at 2900-3000 cm⁻¹, bound OH is found at 3000-3500 cm⁻¹, and free OH appears above 3600 cm⁻¹²⁴⁰⁻²⁴⁵.

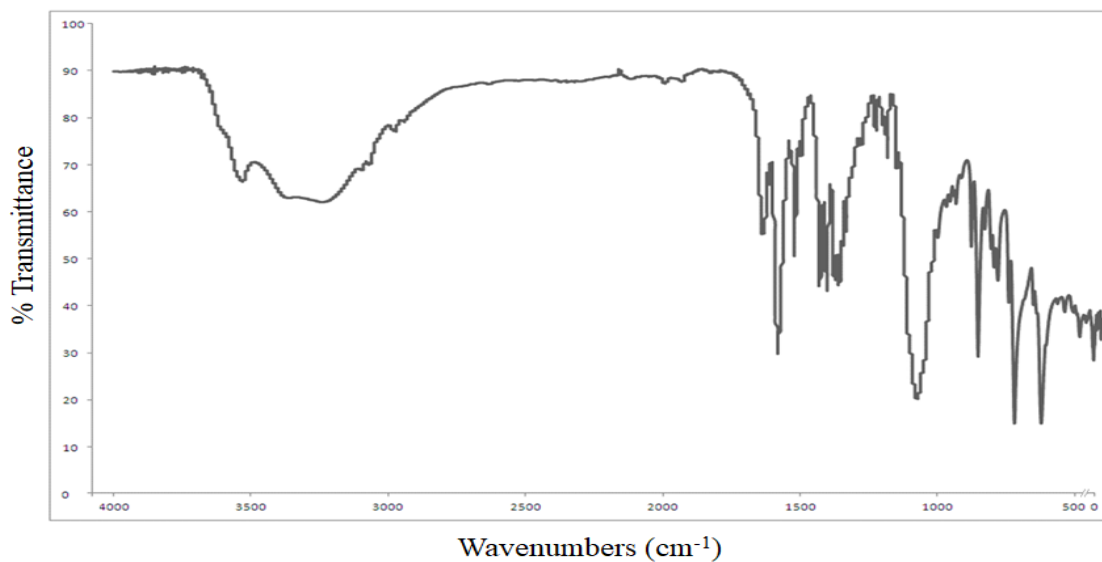


Figure 4.9. IR spectroscopy of **1**.

Functional groups of **1** were confirmed by Raman spectroscopy (Figure 4.10). Characteristic peaks of Cu-O appear at 474, 563 and 744 cm^{-1} , an OH out of plane bending peak is at 934 cm^{-1} , two peaks at 1056 and 1132 are assigned for ring vibrations, a peak at 1313 cm^{-1} is related to C-N stretching, two sharp peaks at 1434 and 1457 are related to ring stretching, and a stretching vibration of COO is found at 1610 cm^{-1} ^{242,246,247}.

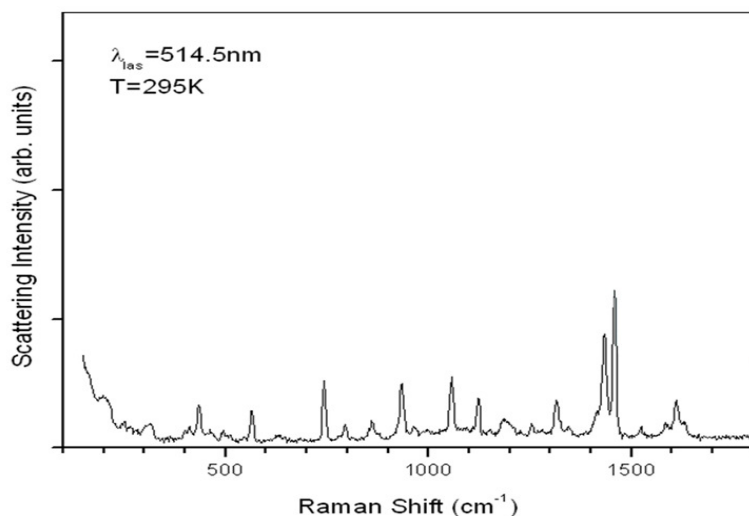


Figure 4.10. Raman spectroscopy of **1**.

4.2.3. Magnetic Measurements

The magnetic susceptibility (χ) per trinuclear Cu(II) coordination complex was measured in a field of 0.1 T in the temperature range of 2–300 K. The temperature dependence of χT product in this temperature range is shown in Figure 4.11, (a). The relationship between the applied magnetic field and the moments can be described in terms of the effective magnetic moment, μ_{eff} . The effective spin-only magnetic moment is calculated from the (4.2) and (4.3) Equations. Equation (4.4) is derived from the (4.2) and (4.3) Equations. T is the absolute temperature, k is the Boltzmann's constant, β is the Bohr Magneton, N_A is Avogadro's number, S is the spin, and χ is the susceptibility. Based on (4.4), the magnetic moment is related to the total number of unpaired electrons.

$$\mu_{\text{eff}} = [(3k/N_A\mu_B^2)\chi T]^{1/2} \approx \sqrt{(8\chi T)} \quad (4.2)$$

$$\mu_{\text{eff}} = g\sqrt{S(S+1)}, \quad g \approx 2 \quad (4.3)$$

$$8\chi T = 4 S(S+1) \quad (4.4)$$

The χT at room temperature is $1.049 \text{ cm}^3 \text{ K mol}^{-1}$ which is slightly lower than that expected spin-only value for three uncoupled $S = 1/2$ spins (calculated $\chi T = 1.125 \text{ cm}^3 \text{ K mol}^{-1}$ for three uncoupled S

= 1/2 centers). However, at low temperature (2K) which the copper centers are coupled, χT is $0.386 \text{ cm}^3 \text{ K mol}^{-1}$ which is close to the value for the $S = 1/2$ ground state (calculated $\chi T = 0.375 \text{ cm}^3 \text{ K/mol}$ for $S = 1/2$ ground state). This shows that two of the spin orientations are parallel to each other but antiparallel to the third one. The ground state total spin was well confirmed by magnetization measurements. Equation (4.5) gives the total spin (S_t) from the saturated magnetization (M_{sat}).

$$M_{\text{sat}} = g S_t \quad (4.5)$$

The spin at each copper site aligns in a way to satisfy the total spin value. In Figure 4.11, (b), $M_{\text{sat}} = 1$ and assuming a g-factor of 2, $S_t = 1/2$ is the ground state.

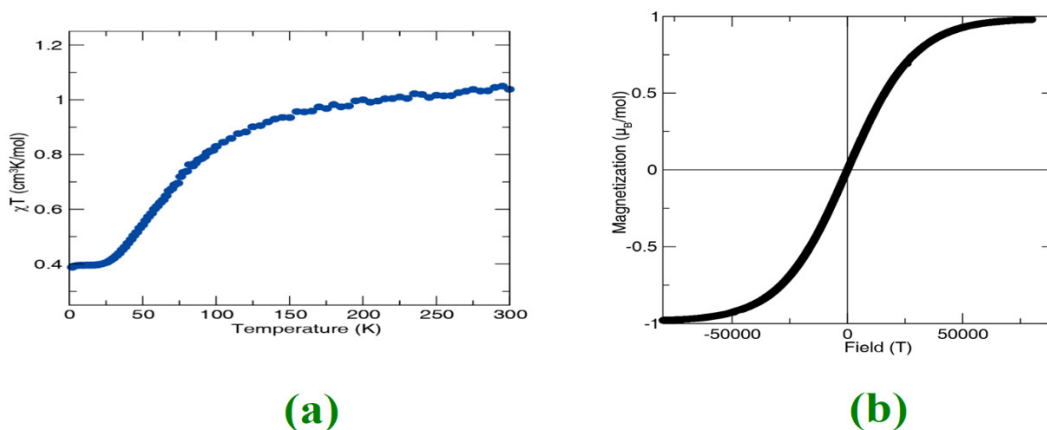


Figure 4.11. (a) Experimental χT data at $H = 0.1 \text{ T}$ in the temperature range of 2-300 K. (b) The magnetization as a function of applied magnetic field at 2 K.

To calculate the coupling constants between copper centers, we used the PHI²²⁸ program. The Equation (3.3) is the Hamiltonian used to fit the experimental data. The Hamiltonian for fitting the experimental data for the 2-J model is described by the Equation (4.6).

$$H = -2J_{12} (S_1 S_2) - 2J_{23} (S_2 S_3) \quad (4.6)$$

The model gave a good fit to the susceptibility and magnetization data at two different temperatures with the J values from the 2-J model of $J_{12} = -51.8 \text{ cm}^{-1}$, $J_{23} = +22.9 \text{ cm}^{-1}$.

Fitting the experimental data with 3-J model with the Hamiltonian in Equation (4.7) gives the J values as $J_{12} = -51.8 \text{ cm}^{-1}$, $J_{23} = +22.8 \text{ cm}^{-1}$, $J_{13} = -0.5 \text{ cm}^{-1}$. This model did not significantly improve the fitting.

$$H = -2J_{12} (S_1 S_2) - 2J_{23} (S_2 S_3) - 2J_{13} (S_1 S_3) \quad (4.7)$$

The distance between Cu(1) and Cu(3) was too long to be considered a significant magnetic interaction. To avoid over parameterizing the model the fitting was done with the 2-J model. The best fit (solid red line) and the experimental data are shown in Figure 4.12.

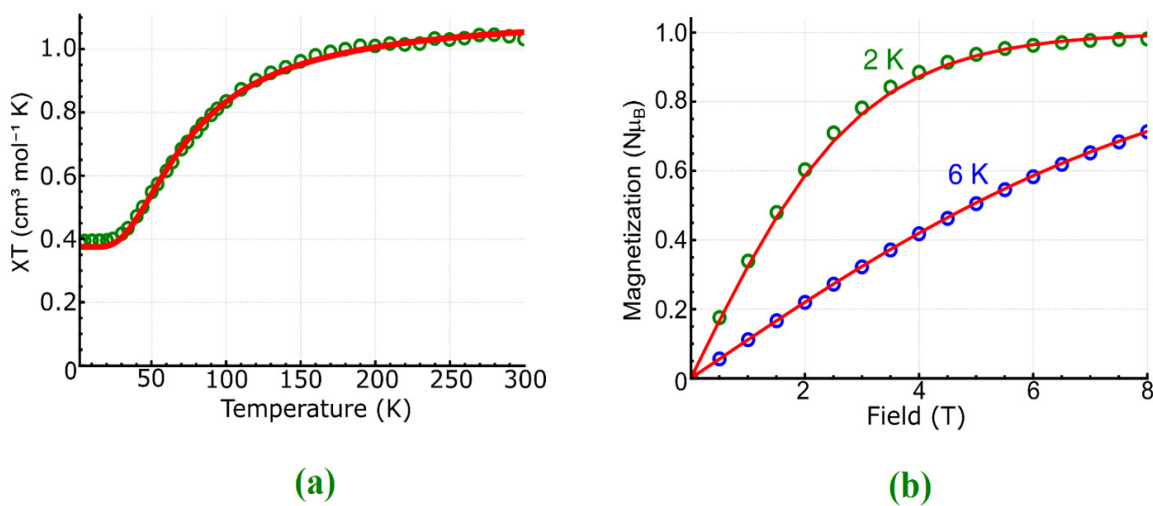


Figure 4.12. Dots are the experimental data, and the solid red lines represent the best theoretical fit for the simultaneous fitting of a) plot of χT vs. T, and b) the magnetization data at 2 and 6 K using the PHI

program for **1**.

4.2.4. Magneto-Structural Correlations

To study the correlation between the exchange coupling constants and the structural parameters, the models based on the previously studied compounds are needed. Owing to the long Cu(1)···Cu(2) distances in **1** (3.3701(1) Å), copper centers do not have sufficient overlap of their wave functions and subsequently not having a direct coupling between moments, however, the one atomic bridge between magnetic centers allow them to go through super-exchange. It has been more than six decades that the Goodenough–Kanamori–Anderson (GKA) rules rationalize the super-exchange magnetic interactions in many complexes. The GKA rules predict an antiferromagnetism interaction when the magnetic orbitals of metal-ligand-metal oriented at a straight angle to have an appropriate overlap and the metal centers have partially filled d shells, and ferromagnetism arises when the magnetic orbitals are at right angle. In compound **1** the orthogonality of the orbitals predicts the ferromagnetic interaction between Cu(1) and Cu(2). The Cu(1)-O(3)-Cu(2) angle is 106.881(17) °, and Cu(1)-O(5)-Cu(2) angle is 98.355(16) °, which are closer to the right angle and therefore no overlap of magnetic orbitals cause the ferromagnetic coupling.

The way the orbitals are overlapping could be described well by magnetic orbitals. The splitting energy of d^9 in square pyramidal geometry with a longer apical bond is shown in Figure 4.13. The magnetic orbital on each copper center is the $d_{x^2-y^2}$ orbital as the singly occupied molecular orbital (SOMO).

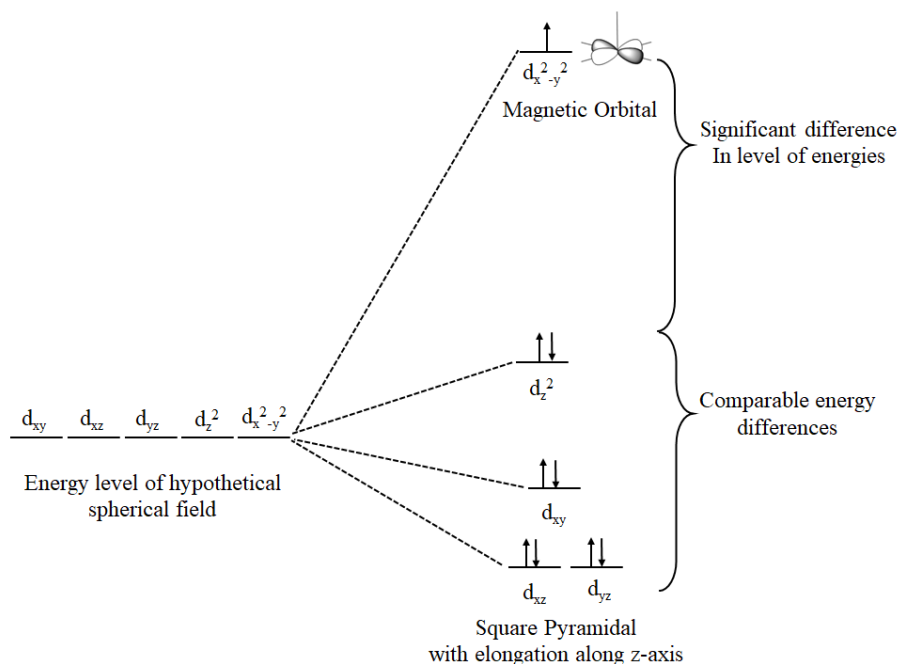


Figure 4.13. The splitting diagram of d^9 in square pyramidal geometry on copper centers with longer apical bonds, showing the $d_{x^2-y^2}$ as a magnetic orbital.

A graphical analysis of exchange interaction in **1** using the magnetic orbital model is shown in Figure 4.14. The magnetic orbitals are the localized-orbital models of exchange interactions. Based on the GKA rule, the orthogonal bridging oxygen orbitals has no overlap with the copper centers that are perpendicular to. Combining the two localized orbitals shows the overall magnetic orbitals.

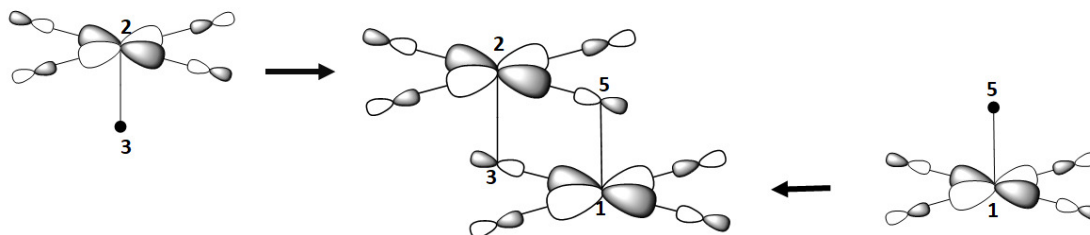


Figure 4.14. Localized magnetic orbitals on Cu(1) and Cu(2) on each side and the overall magnetic orbital to show the super-exchange interaction in the middle of the figure.

The magnetic orbital graphical analysis can be also described with Ginsberg's symbol in (4.8).

$$d_{1x^2-y^2} \parallel p_3 \perp d_{2x^2-y^2}$$

$$d_{2x^2-y^2} \parallel p_5 \perp d_{1x^2-y^2} \quad (4.8)$$

Describing the magnetic behavior using the GKA rule, indicates that orthogonality between the magnetic centers and the bridging atom, predicts the ferromagnetic interaction between Cu(1) and Cu(2) which is consistent with the calculated J values through the PHI program.

The model was used for the study of the Cu(2) and Cu(3) interaction was the dimer copper(II) acetate hydrate. As shown in Figure 4.15, the structure of **1** is similar to that of copper(II) acetate. There were many debates on the type of exchange pathway on cupric acetate^{137,221,248–253}; however the antiferromagnetic coupling with the $J=-296 \text{ cm}^{-1}$ result in the singlet ground state in copper acetate monohydrate dimer.

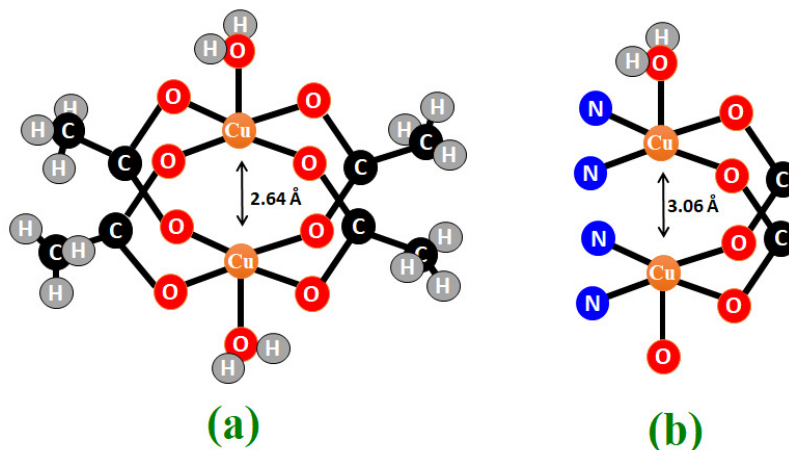


Figure 4.15. The comparison between the structures of (a) copper acetate hydrate dimer and (b) part of the structure **1** which relates Cu(2) and Cu(3).

The distance between copper centers is longer (3.057(1) Å) in **1** than the copper acetate. The planes of basal bonds around copper in copper acetate are parallel to one another, however, in **1** they deviate by 21.9 °. Based on these two comparisons the effect of direct δ -exchange lowered. On the other hand, in copper acetate the super-exchange occurs through four triatomic bridging ligands, however Cu(2) and Cu(3) in **1** are related through only two bridging ligands.

Regardless of the relative magnitudes of the contributions of each exchange type, both reasons cause the J_{23} value would be less than that of copper acetate ($J = -292.2 \text{ cm}^{-1}$), and this is consistent with the observed value of $J_{23} = -51.8 \text{ cm}^{-1}$ for exchange between Cu(2) and Cu(3),-

The energy difference between the ground state and excited state was calculated through the PHI program by having the J values. Low-lying energy state calculation demonstrates that the energy difference between the doublet ground state and the quartet excited state in **1** is 95.5 cm^{-1} .

4.3. Conclusion

$[\text{Cu}_3(\text{phen})_3(\text{pda})_2(\text{H}_2\text{O})^{2+}][\text{ClO}_4^-]_2[\text{H}_2\text{O}]_4$ (**1**) was synthesized using solvothermal reactions under different conditions. The single crystal structure of compound **1** shows a trinuclear coordination polymer. The characterization was confirmed with IR, Raman, TGA and chemical analysis. The Powder X-ray Diffraction indicates compound **1** is a single phase. The three copper centers interact magnetically. Their magnetic susceptibility was measured and the coupling constant between copper centers was determined. A 2-J model fitted well and showed a ferromagnetic interaction through super-exchange between Cu(1) and Cu(2), and the antiferromagnetic interaction between Cu(2) and Cu(3). The magnetic data shows that the total spin of the ground state is $1/2$.

Chapter 5. Two-Dimensional Magnetic Ordering in a One-Dimensional Zigzag Cu(II) Chain Structure

5.1. Introduction

Recently the molecular magnetism field has attracted considerable attention^{254,255}. The possibility now exists to control the structure of materials and design low dimensional magnetic compounds. The single-chain magnets (SCMs) are one of the novel classes of molecular magnets with possible applications in high-density information storage^{256–260}. The SCMs exhibit a very strong intrachain and weak interchain magnetic interactions. One-dimensional (1-D) magnetic ordering is found in compounds with bridging ligands that can effectively transmit magnetic exchange coupling. Typically, diamagnetic separators isolate the chains to prevent them from having strong interchain interactions^{215,261}.

The 1-D chain building blocks are usually assembled from metal magnetic centers combined with appropriate ligands that mediate the magnetic exchange coupling^{262–264}. Polyatomic linkers (e.g., dicyanamide, cyanide, azide, oxalate) have the ability to mediate the magnetic interaction between metal centers and generate long-range magnetic ordering^{265–270}. Studying the magnetic behavior of the 1-D chain magnets provides insights into the long-range transmission of magnetic moment coupling effects^{271,272}. Besides the polyatomic linkers, aromatic bridging ligands provide the same ability^{273–275}. The conjugated bond orbitals of the aromatic bridges are effective in propagating the magnetic exchange interaction of the unpaired electrons in the metal magnetic orbitals^{272,275}.

Here we report on a copper(II) one-dimensional chain magnet with the formula of [Cu(phen)(pda)]·(H₂O)₂ (**2**) (H₂pda = 1,4-phenylene diacetic acid, phen = 1,10-phenanthroline). This compound consists of infinite chains. The chains in a layer (bc-plane) are parallel to each other, and the copper ions are separated by a large distance. The distances between copper centers, however, are

closer than the intralayer-interchain distances. The magnetic data were measured and analyzed for this compound. The Bonner-Fisher²¹⁶ model was used to describe the magnetic behavior of **2**. This model is an extrapolation of the magnetic susceptibility for an infinite ring calculated for a limited number of magnetic ions. Fitting the experimental data with this model gave the same order of magnitude for the intrachain exchange coupling (J) and the interchain coupling (zJ), revealing two-dimensional magnetic ordering. The pda ligand can mediate a weak intrachain ferromagnetic coupling with $J = +2.52 \text{ cm}^{-1}$. The intralayer-interchain copper distances within a bc-layer are too large for significant exchange coupling. The interlayer copper(II) ion distances, however, are close enough to exhibit a weak antiferromagnetic interaction ($zJ = -1.98 \text{ cm}^{-1}$).

5.2. Experimental

5.2.1. Synthesis of $[\text{Cu}(\text{phen})(\text{pda})] \cdot (\text{H}_2\text{O})_2$ (**2**)

Compound **2** was synthesized using a one-pot hydrothermal reaction. $\text{Cu}(\text{ClO}_4)_2 \cdot 6\text{H}_2\text{O}$ (6 mmol, 2.223 g) was dissolved in sufficient water to make 30 mL of 0.2 M solution. 1,10-phenanthroline (phen) (6 mmol, 1.081g) was added to ethanol to make 30 mL of 0.2 M solution. 30 mL of a 0.1 M of $\text{LiOH} \cdot \text{H}_2\text{O}$ solution was made by adding 3 mmol (0.126 g) salt to the water. After the preparation of all three solutions, they were combined with the other reactants in the following sequence. First, phenylene diacetic acid (H_2pda) (0.2 mmol (0.388 g) was added to 4 mL of the solution of 0.1 M of $\text{LiOH} \cdot \text{H}_2\text{O}$ in the reaction vial. Next, 7-10.5 mL acetonitrile was added to the mixture (the final crystals were larger in the more concentrated solutions; however, the amount of impure phase was less in the diluted solutions). The pda particles were dissolved and deprotonated completely in the solution using an ultrasound bath for 20 minutes. Then 1 mL of the phenanthroline solution was added to the mixture and shaken well. Adding 1 mL of $\text{Cu}(\text{ClO}_4)_2 \cdot 6\text{H}_2\text{O}$ solution made the reaction mixture blue. The reaction mixture was capped in a vial and sealed with Teflon tape. The

reaction mixture was heated in the oven at 60 °C for 10 to 14 d. The solution became colorless in 4-7 d. Plate-like dark blue crystals of **2** formed from the colorless reaction mixture, in 70% yield (based on Cu). The minor white impurity phase was removed by washing several times with water at room temperature. The solvent was removed by the gravity filtration and the crystals dried in the air.

5.2.2. Characterization of 2

5.2.2.1. Single Crystal X-ray Diffraction (SCXRD)

All measurements were made with a Bruker DUO platform diffractometer equipped with a 4K CCD APEX II detector. A hemisphere of data (1272 frames at 6 cm detector distance) was collected using a narrow-frame algorithm with scan widths of 0.30% in omega and an exposure time of 80 s frame⁻¹. The data were integrated using the Bruker-Nonius SAINT program, with the intensities corrected for Lorentz factor, polarization, air absorption, and absorption due to variation in the path length through the detector faceplate. The data were scaled, and an absorption correction was applied using SADABS. Redundant reflections were averaged. Final cell constants were refined using 3770 reflections having $I > 4\sigma(I)$, and these, along with other information pertinent to data collection and refinement, are listed in Table 5.1. The Laue symmetry was determined to be 2/m, and from the systematic absences noted the space group was shown unambiguously to be P2₁/c. The asymmetric unit consists of one Cu, 1,10-phenanthroline, phenylene diacetate, and two water molecules, all in general positions. Both water molecules were disordered over two slightly different orientations, with one hydrogen bond in a completely different direction. The water molecules were modeled as ideal rigid bodies. Since there was not enough electron density at the disordered hydrogen atom locations to allow independent least-squares refinement, it was necessary to fix most of the water hydrogen positions based on optimized hydrogen bonding parameters.

Table 5.1 Crystal data and structure refinement for **1**.

Empirical formula	C ₂₂ H ₂₀ Cu N ₂ O ₆
Formula Weight	471.94
Temperature, Wavelength	123(2) K, 0.71073 Å
Crystal system, space group	Monoclinic, P2 ₁ /c
Unit cell dimensions	$a = 9.564(4)$ Å, $b = 17.237(7)$ Å, $c = 12.497(5)$ Å $\alpha = 90^\circ$, $\beta = 108.916(1)^\circ$, $\gamma = 90^\circ$
Cell Volume	1949.13(14) Å ³
Z, Calculated density	4, 1.608 g/cm ³
Crystal size	0.40 × 0.35 × 0.08 mm ³
Index ranges	$-12 \leq h \leq 12$, $-22 \leq k \leq 11$, $-16 \leq l \leq 16$
Theta range for data collection	2.09 to 27.48°
Absorption coefficient	1.166 mm ⁻¹
F(000)	972
Reflections collected / unique	11685 / 4425 [R(int) = 0.0336]
Refinement method	Full-matrix least-squares on F ²
Data/restraints/parameters	3770 / 0 / 276
Goodness-of-fit on F ²	0.987
Final R indices [I > 4σ(I)]	R1 = 0.0274, wR2 = 0.0755
R indices (all data)	R1 = 0.0313, wR2 = 0.0784
Largest diff peak and hole	0.621 and -0.509 e. Å ⁻³

5.2.2.2 Crystal Structure

The asymmetric unit, (Figure 5.1), in the crystal structure of $[\text{Cu}(\text{phen})(\text{pda})]\cdot 2\text{H}_2\text{O}$ (**2**) consists of a Cu ion coordinated by bidentate phenanthroline ligand, a phenylene diacetate (pda) ligand, and two lattice water molecules hydrogen-bonded to the pda free oxygen atoms.

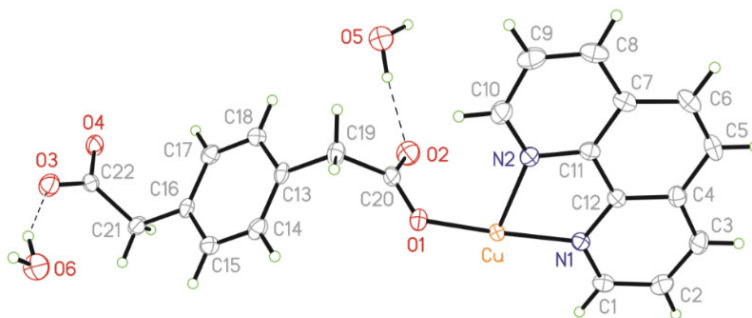


Figure 5.1 View of the asymmetric unit of **2**, with atom numbering and 70% probability thermal ellipsoids. Only one orientation of the disordered water molecules is shown.

The coordination environment around copper ion is a square planar. The nitrogen atoms of the phenanthroline ligand (N1 and N2) and two oxygen atoms from pda ligands (O1 and O4) occupy the four positions (Figure 5.2). The average bond distances of the Cu–N and Cu–O are 2.0254(1) and 1.938(1) Å, respectively. Selected bond lengths [Å] and angles [°] are summarized in Table 5.2. The phen ligand is a bidentate chelating ligand that blocks two positions of the copper ion. The pda ligand acts as a bridging ligand and makes a zigzag chain by connecting two copper centers. Two other oxygen atoms of pda (O2 and O3) form hydrogen bonds with two water molecules (Figure 5.2).

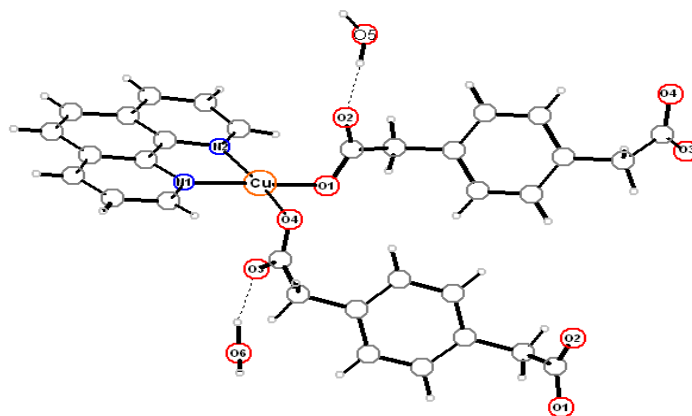


Figure 5.2 The square planar coordination of the copper ion in **2**.

Table 5.2 Selected bond lengths [Å] and angles [°] for **1**

Cu-O(1)	1.9214(12)	O(1)-Cu-O(4)	93.63(5)
Cu-O(4)	1.9544(12)	O(4)-Cu-N(1)	92.42(5)
Cu-N(1)	2.0019(14)	O(1)-Cu-N(2)	92.32(6)
Cu-N(2)	2.0489(14)	N(1)-Cu-N(2)	81.43(5)

The copper(II) ions are connected by pda ligands to form a one-dimensional zigzag chain. The chelating phen ligands block two sites of the copper ions. Depending on the copper position in the chain, the phen ligands attach from top or bottom to the metal ions (Figure 5.3).

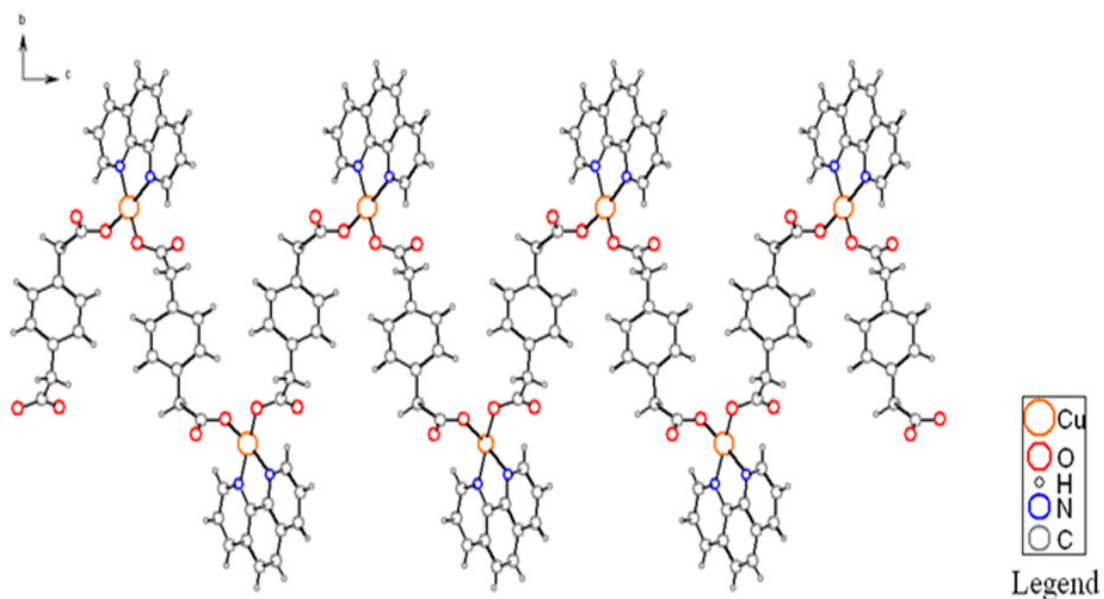


Figure 5.3 One chain of **2**, growing along the *c* direction. Phen is the blocking chelating ligand, and pda is the bridging ligand.

The bond valence sum for the copper site was calculated from the bond lengths, based on Equation (4.1) and the tabulated values of R_0 and b that are shown in Table 5.4. Based on the bond valence sum assessment, the copper oxidation state is as Cu^{2+} (Table 5.3 and 5.4).

Table 5.3 The oxidation states assignment of the copper ions from bond valence sums (BVS) in **2**

site	Bond Valence Sum			Assignment Oxidation State
	Cu(I)	Cu(II)	Cu(III)	
Cu	1.300	1.867	2.144	Cu(II)

Table 5.4 The parameters used for the BVS calculations^{227,239}.

		Cu^{1+}	Cu^{2+}	Cu^{3+}
O	R_0	1.504	1.687	1.735
	b	0.37	0.37	0.37
N	R_0	1.63	1.713	1.768
	b	0.37	0.37	0.37

Although the value for the bond valence sum could be closer to 2 by considering the bond between O(3) and Cu with the distorted square pyramidal geometry, the experimental bond valence between these two atoms is smaller than the number which is defined by Brown²⁷⁶ as a bond. Based on Brown's definition, a bond exists if the experimental bond valence is larger than an arbitrary number of four percent of the copper valence. The experimental bond valence Cu-O(3) (Figure 5.2) is 0.074 which is less than 4% of copper valence (3.7%). It seems, Cu-O(3) may or may not be considered as a bond.

5.2.2.3 Powder X-ray Diffraction (PXRD)

Sample impurity was removed by washing the sample with water ten to fifteen times. Each time the solvent was shaken vigorously, and then the top part of the solvent was decanted. The impurity was solvable in water. The sample stayed in water overnight to ensure removal of all impurities. Washing the sample with acetone or ethanol changed the powder X-ray diffraction. The sample was then ground using an agate mortar and pestle. The fine powder was spread over a zero-diffraction silicon sample holder. The experimental powder pattern is closely similar the simulated pattern from the crystallographic single crystal data and confirms the phase purity. The small peak shifts occur due to the temperature difference (Figure 5.4) (powder data were collected at room temperature, and the single-crystal data were collected at -150 °C).

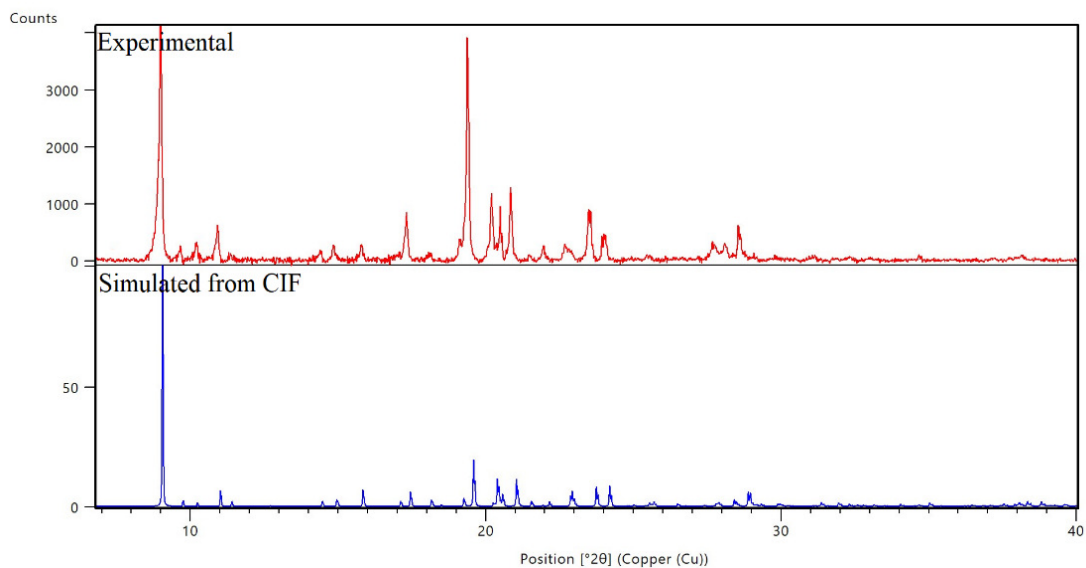


Figure 5.4 Experimental and simulated powder X-ray diffraction of **2**. The simulated pattern is based on the analysis of the single-crystal X-ray diffraction refined structure at -150 °C.

5.2.2.4 Physical Measurements

Elemental analyses of **2** for C, H and N gave values of 55.86%, 4.18%, and 5.89% which are consistent with the calculated percentages of the carbon, hydrogen, and nitrogen amounts from the structure determination namely 55.98%, 4.27%, and 5.93%, respectively.

Thermogravimetric analysis (TGA) and Derivative Thermogravimetry (DTG) were performed in 2% O₂+N₂ at a heating rate of 1 °C/min up to 550 °C (Figure 5.5). The mass loss in the first step is due to the loss of two lattice water molecules (obs. 6.36, calc. 7.61%). The second small step at 220-230 °C may correspond to the decarboxylation of the surface pda ligands of the chains. This step is followed by another weight loss between 230 and 270 °C which is assigned to the loss of the phen ligands (obs. 38.69, calc. 38.13%). The thermal decomposition of the chain starts gradually at 350 °C and continues to 500 °C. The ~17% residue at 550 °C was identified by powder X-ray diffraction as

CuO (calc. 16.9%). Similar TGA trends were reported for other frameworks with the pda linkers and a blocking ligand^{277–279}.

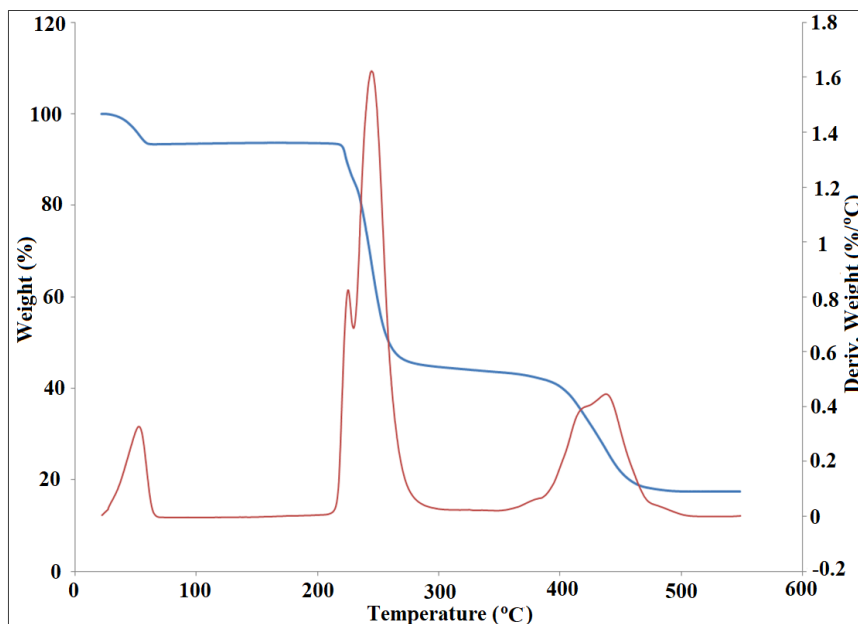


Figure 5.5 TGA and DTG of **2**. The first weight loss corresponds to the loss of lattice water. The second and third weight loss relates to the decarboxylation and phen ligand dissociation. The last step is the decomposition of **2**. The residual is copper oxide.

FT-IR spectrum of **2** is shown in Figure 5.6. The bands of Cu-O and Cu-N are detected at 430 and 490 cm^{-1} , respectively. Absorption bands at 618 and 734 cm^{-1} are related to the out of plane bending vibration of CH. =C-H bending vibration is observed at 849 cm^{-1} , also C-O stretching vibration, and C-C stretching vibration appears at around 1025-1106 cm^{-1} . The peak at 1225 cm^{-1} is assigned to stretching vibration of C-N group, C-H bending band is observed at 1340 cm^{-1} , aromatic ring vibration bands are detected at 1374-1424 cm^{-1} , and the absorption band at 1561 cm^{-1} is due to C=N stretching vibration. The stretching vibration of C=C can be seen at 1587 cm^{-1} , and COO stretching band is observed at 1688 cm^{-1} . Above 2000 cm^{-1} , CH aliphatic stretching bands can be seen

at 2967 cm⁻¹, CH aromatic stretching bands appears at 3070 and 3095 cm⁻¹, and OH is found above 3270 cm⁻¹ 240–245.

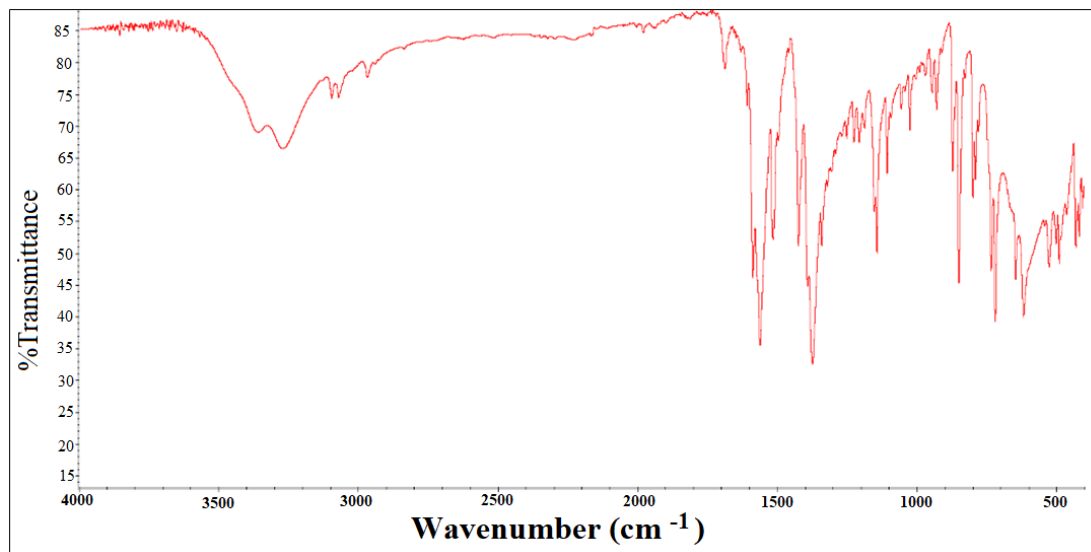


Figure 5.6 IR spectroscopy of **2**.

5.2.3. Magnetic Measurements

The magnetic susceptibility (χ) of **2** per Cu(II) coordination complex was measured in a field of 1 T in the temperature range of 3–300 K. From Equation (4.4), [$8\chi T = 4 S(S+1)$], the χT at 300 K ($0.319 \text{ cm}^3 \text{ K} \cdot \text{mol}^{-1}$) per copper(II) site is lower than expected for a paramagnetic system with $S = 1/2$ ($0.375 \text{ cm}^3 \text{ K} \cdot \text{mol}^{-1}$).

The data were analyzed using the Bonner and Fisher²¹⁶ model. The susceptibility expression proposed by Bonner and Fisher for Heisenberg $S = 1/2$ for the intrachain coupling exchange is based on the spin Hamiltonian (Equation (5.1)), where J is the exchange interaction of adjacent Cu(II) ions connected via bridging ligand.

$$H = -J \sum_{i,j \in N}^{i < j} S_i S_j \quad (5.1)$$

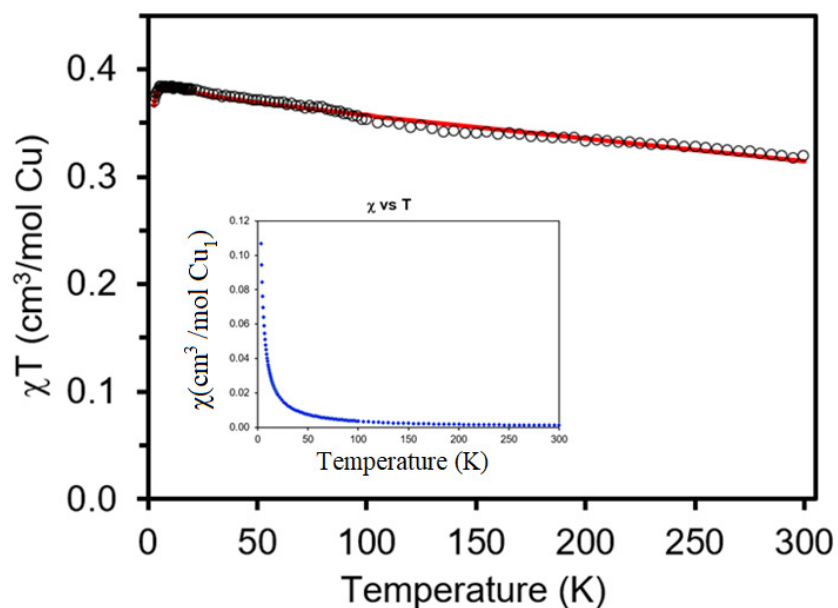


Figure 5.7 Experimental χT and χ vs. temperature at $H = 1$ T in the temperature range of 3-300 K. The solid line is the best theoretical fit of the Fisher model to the experimental χT plot.

The χ^{-1} vs. T plot is shown in Figure 5.8. This plot above 100 K follows the Curie-Weiss law ($\chi_M = C/(T - \theta)$) with the $C = 0.305 \text{ cm}^3 \text{ mol}^{-1} \text{ K}$ and $\theta = +16.198 \text{ K}$. The positive Weiss constant suggests a weak ferromagnetic intrachain exchange between Cu(II) centers.

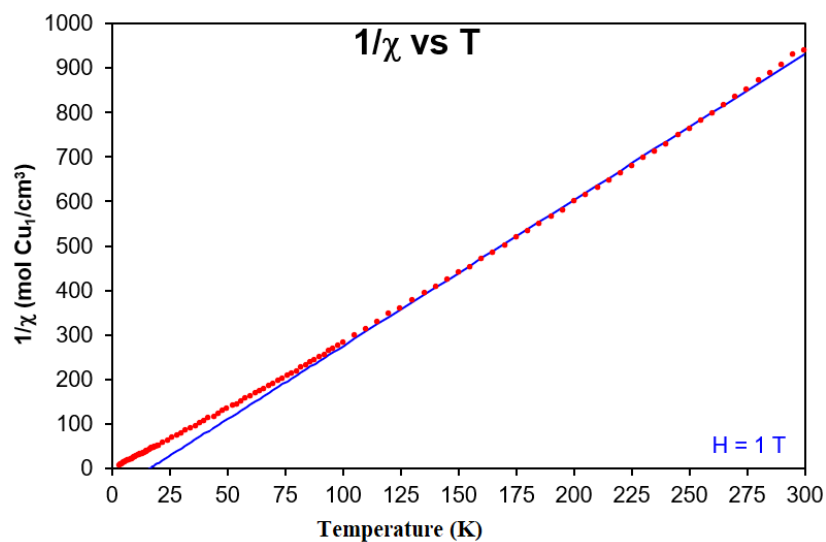


Figure 5.8 $1/\chi$ vs. temperature at 1T magnetic field for **2**. The solid line is the Curie-Weiss fit.

5.2.4. Magneto-Structural Correlations

It is necessary to understand the arrangement of copper ions to interpret the magnetic interactions. There are more than 20 different distances shorter than 15 Å between the copper ions; however, there is only one referring to the distance between magnetic sites through a bridging ligand.

To consider a magnetic interaction between two cores, they need to have a specific relationship to each other. First, the copper wave functions have to have a sufficient overlap to subsequently have a direct coupling between their moments. Second, the longer-range coupling magnetic interactions between distant metal centers (beyond nearest-neighbors) are allowed across extended bridging ligands^{159,162,275}. To be able to understand the relationship between the copper centers, we need to take a closer look at the relationship between the chains. Figure 5.9 and 5.10 shows how the copper centers associate through the structure.

According to these schemes, the association between the copper center distances based on their positions in the chains is defined in three different categories. The intrachain distances are defined for Cu...Cu distances within a chain and specifically those connected through the bridging ligands. The intralayer-interchain distances are the distances between the chains within a layer. The interlayer-interchain (for simplicity: interchain) distances indicate the distances between the bc-plane layers.

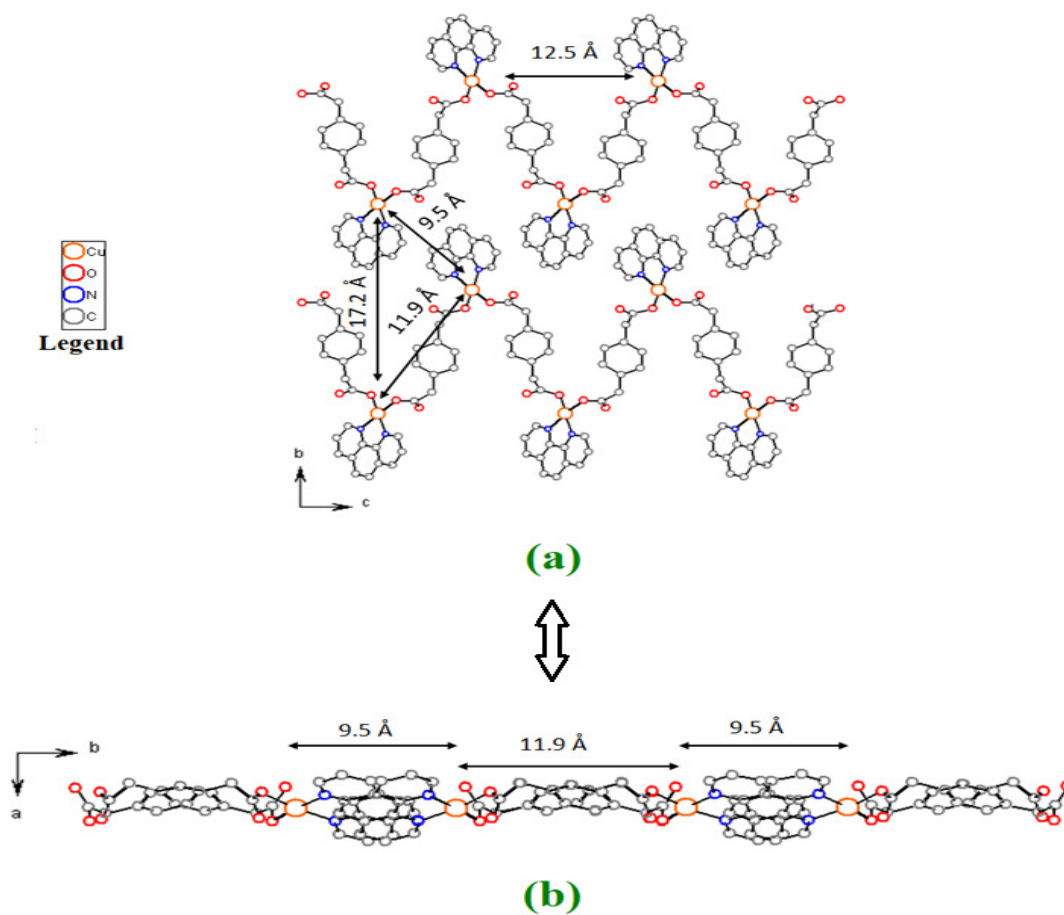


Figure 5.9 Schematic view of the two chains of **2** within a layer and determining Cu···Cu distances in
a) the bc plane and b) the b direction.

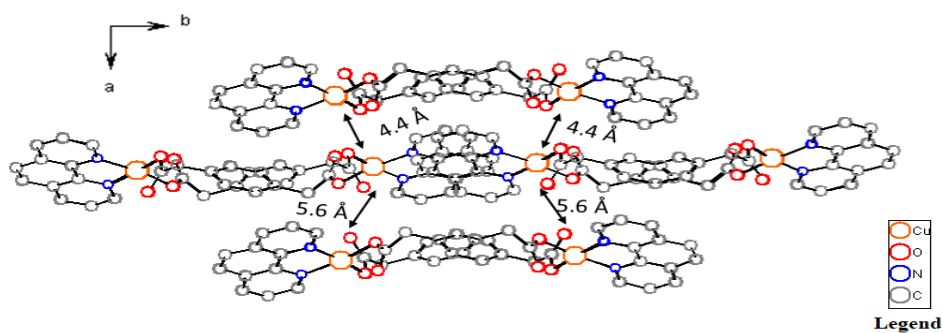


Figure 5.10 Schematic view of the three layers of **2** chains and the interchain-interlayer distances
between copper ions.

The intrachain distance between copper ions across pda ligand is 11.885(5) Å. The shortest Cu...Cu interchain distances are 4.423(3) Å. The solvent molecules are located in the spaces between the chains connecting with a hydrogen bond to the oxygen of the pda ligand (Figure 5.11).

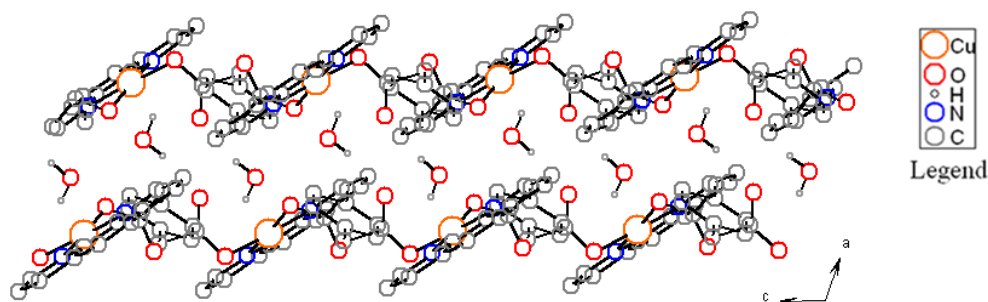


Figure 5.11 Two layers of chains in **2** the ac plane while the water molecules are in the middle of the chain layers.

$\theta > 0$ and $J > 0$ indicate that there is an intrachain ferromagnetic coupling exchange between neighboring Cu(II) ions. The comparable interchain interaction strength (zJ) with the intrachain interaction (J) value demonstrates that the interchain interaction is as considerable as the intrachain coupling exchange, which leads to a two-dimensional magnetic ordering.

The intrachain long-range magnetic coupling with the intervening bridges are well-documented^{159–162,275,284–286}. In most cases, the magnetic interaction between the Cu(II) centers is mainly transmitted through extended π -conjugated aromatic bridges with the para-substitution pattern.

The intrachain interaction with the $J = +2.52 \text{ cm}^{-1}$ in **2**, through para-phenylene diacetate bridge, is a weak, but not negligible, ferromagnetic interaction. Having a p-phenylene spacer along the chain helps the magnetic communication between distant copper(II) centers (11.9 Å in Figure 5.9).

One of the longest reported distances between copper centers in $(n\text{Bu}_4\text{N})_4[\text{Cu}_2(\text{dpeba})_2]\cdot 4\text{MeOH}\cdot 2\text{Et}_2\text{O}$ (dpeba = N,N'-4,4'-diphenylethynebis(oxamate), $n\text{Bu}_4\text{N}$ = tetra-n-butylammonium) is 15 Å in which the magnetic interaction is $J = -3.9 \text{ cm}^{-1}$ ²⁷⁵. The weaker intrachain interaction ($J=+2.52 \text{ cm}^{-1}$) in **2** may occur due to a broken conjugation (a sp^3 carbon) along the chain.

The other magnetic interaction in **2** structure, is the interchain coupling exchange. The zJ value could be assigned to the nearest interlayer-interchain copper(II) ions with distances of 4.4 Å (Figure 5.10). To avoid over parametrizing the model, one interaction was considered between the chains, assuming the interchain magnetic interactions of the copper ions are the same.

Based on the splitting diagram of d^9 orbital in the square planar field, the magnetic orbital of copper(II) ion with an unpaired electron is the $d_{x^2-y^2}$ orbital. Although there is no bridging ligand in between the chains, the parallel planes of the square planar copper centers allow them to have a coupling exchange. The planes are not exactly on top of each other, and a small shift may reduce the magnetic coupling strength. This would lead to a weak magnetic δ -interaction of $d_{x^2-y^2}$ orbitals. A graphical analysis of interchain exchange interaction (zJ) based on the copper site locations and geometries is shown using the magnetic orbital model in Figure 5.11. The magnetic orbitals are the localized-orbital models of exchange interactions.

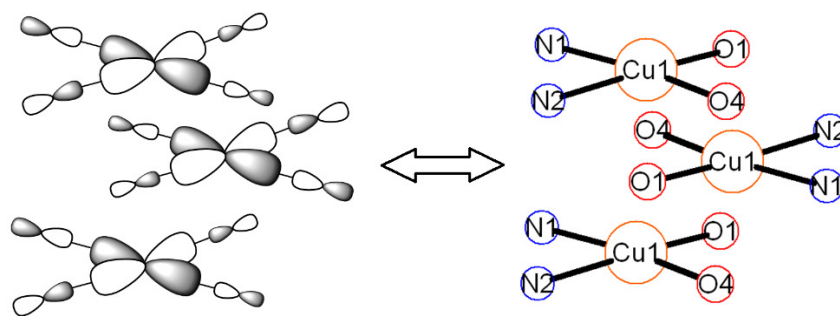


Figure 5.12 Localized magnetic orbitals on three nearest copper centers from three interlayer chains display a weak δ -interaction.

Negative J for the interchain interaction value indicates an antiferromagnetic interaction between the copper ions. Although the interaction within the chain is ferromagnetic, the layers of the chains are antiferromagnetically coupled.

In addition, the closest distance of intralayer-interchain copper centers is 9.5 Å (Figure 5.9, a), which is too long to have sufficient direct overlap of their wave functions. Furthermore, there is no ligand between the copper centers, and therefore, there would not be a long-range magnetic interaction either.

A similar one-dimensional zigzag structure of neodymium (III) by the pda linker with the empirical formula $[\text{Nd}_2(\text{pda})_3(\text{H}_2\text{O})] \cdot 2\text{H}_2\text{O}$ have the similar interdimer interaction ($J = 2.21 \text{ cm}^{-1}$)²⁸⁷. This value is consistent with the long-range magnetic coupling through pda ligand in **2**.

5.3. Conclusion

$[\text{Cu}(\text{phen})(\text{pda})][\text{H}_2\text{O}]_2$ (**2**) was synthesized by solvothermal reaction. The single-crystal structure of compound **2** shows a one-dimensional zigzag chain coordination polymer. The characterization was confirmed with IR, TGA and chemical analysis. Powder X-ray Diffraction

indicates compound **1** is a single phase. The χ^{-1} vs. T plot follows the Curie-Weiss law for the temperature higher than 100 K with $C = 0.305 \text{ cm}^3 \text{ mol}^{-1} \text{ K}$ and $\theta = +16.198 \text{ K}$. The temperature-dependent magnetic susceptibility experimental data was effectively fitted with the infinite chain model of Bonner-Fisher. The copper ions ferromagnetically interact within a chain through the phenylene diacetate (pda) ligand with a coupling constant of $J = +2.52 \text{ cm}^{-1}$. The interlayer-interchain interactions are antiferromagnetic with the magnitude of $zJ = -1.98 \text{ cm}^{-1}$. The intralayer-interchain unpaired electron magnetic moments of copper ions cannot be coupled due to the long distances between them. The intrachain and interchain magnetic exchanges cause the two-dimensional magnetic ordering.

Chapter 6. A Magnetic Study of a New Tetranuclear Copper(II) Complex with a Cu₄O₄

Cubane Core

6.1. Introduction

The binuclear copper(II) compounds with a bridging oxygen atom between the copper ions show a systematic relationship between the structure and the magnetic behavior, which allows the establishment of models^{54,136,288–290}. The coupling of the d⁹ unpaired electrons between the Cu(II) centers can result in a triplet (high spin) or a singlet (low spin) ground state or ferromagnetic (FM) and antiferromagnetic (AFM) behavior, respectively. Many studies have examined in depth the correlation between magnetic behavior and structural parameters. The first structural feature that affects the type and magnitude of magnetic coupling in binuclear copper(II) compounds with hydroxo bridge is the Cu^{II}-O-Cu^{II} angle (θ). A linear relationship has been established between the intradimer interaction and θ . The border between ferromagnetic (FM) and antiferromagnetic (AFM) exchange for the Cu^{II}-O-Cu^{II} angle, according to Hatfield *et al.*¹¹⁶ is $\theta = 97.5^\circ$. Antiferromagnetic behavior is found for the compounds with θ greater than 97.5° ; Ferromagnetic behavior emerges for the θ lower than this threshold. Compounds with alkoxo bridges show similar trends; stronger AFM coupling exists at larger Cu^{II}-O-Cu^{II} angles. The other effective feature is the out-of-plane shift angle (τ) of a coordinated atom to the bridging oxygen regarding the plane of four atoms in the dimeric unit (Figure 6.1). By decreasing the θ and increasing the out-of-plane displacement of the hydrogen atom (τ) in hydroxo type dimeric systems, the ferromagnetic interaction is more favored. The experimental results (for the θ angles smaller than 97.5° and τ values larger than 50°) aligns with the reported calculated data to show that the ferromagnetic coupling of copper(II) centers increases on decreasing of the θ values^{1,16}. The spatial distance between two copper(II) centers which is also affected by θ and τ has a great influence on the exchange coupling of a dimeric compound as well^{17,116,291}.

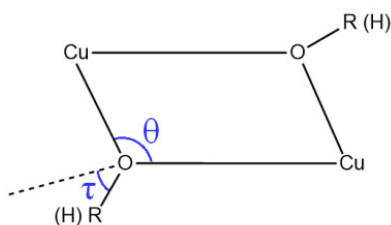


Figure 6.1 Out-of-plane displacement (τ) of the coordinated atom(s) to the bridging oxygen with respect to the dinuclear subunit plane and the Cu^{II}-O-Cu^{II} angle (θ).

If the structures of the binuclear compounds are developed on the six faces of a cube, cubane core complexes result in which four Cu(II) centers have six magnetic coupling pathways to one another. Cubane-like copper(II) based oxygen atom bridged coordination complexes with the Cu₄(μ_3 -OH)₄ or more generally the Cu₄O₄ core (oxygen atoms typically belong to alkoxo (-OR) or hydroxo (-OH) groups) have fascinating magnetic properties which arise from the specifics of the exchange coupling between the metal centers that is strongly affected by small cubane structural variations. Studies of the exchange coupling in the cubane type copper(II) structures with various geometries determined from X-ray diffraction have led to models that can be used to fit the experimental magnetic data. To do this successfully, it requires developing strategies to fully understand the different structural factors and their effect on the six coupling constants, (J values). For these cubane-like compounds, models are needed that account for the relationships between the structural geometries and the magnetic properties.

Different methods of classification of cubane complexes^{17,197,292} have been reported in order to better correlate the structure types and magnetic pathways and to predict the coupling constants (Figure 6.2). One of these classifications is based on Cu-O distances. Based on this classification both type I and type II classes contain eight short bonds, more likely shorter than $\sim 2 \text{ \AA}$ and four bonds longer than $\sim 2 \text{ \AA}$. The difference between these two types is the placement of each bond defined as short and long bonds. In type I class, the long Cu-O distances are between each dimeric Cu₂O₂ subunits, parallel to

each other. In type II, however, the long bonds are located within each pseudo-dinuclear units. The second type of classification is based on Cu...Cu distances. The short Cu...Cu distances are defined as less than $\sim 3 \text{ \AA}$ and the long ones are greater than $\sim 3 \text{ \AA}$. In this classification, the complexes with two short distances and four long ones are classified as 2+4 class which is equivalent to type I. The other the which contains four short Cu...Cu distances and two long ones are designated as 4+2 equivalent to type II. The third class in this classification corresponds to six similar Cu...Cu distances called 6+0 cubanes. The third classifications of cubane topologies consider elongated Cu-O distances as open edges and are named single or double open cubanes^{17,292}. The types of classification are not limited to the ones that are discussed here²⁹³. Several cubanes have been reported where different types of exchange pathways are correlated with their bond distances²⁹³⁻²⁹⁶.

A fundamental question in magnetic studies of the complexes is the type and strength of the interaction between the active centers. The classification of the cubane type complexes would specifically help to determine the J values relevant to the magnetic properties (Figure 6.2).

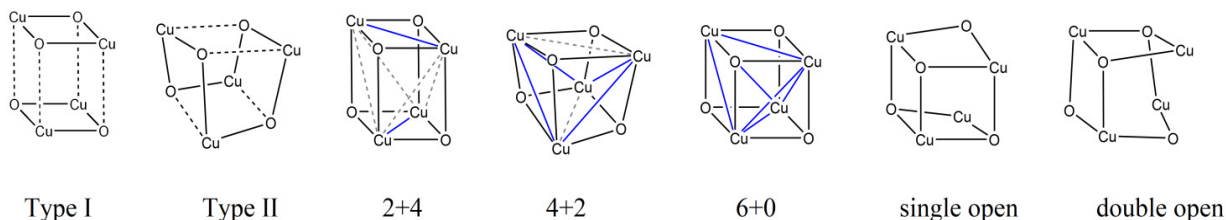


Figure 6.2 Schematic drawing of different models of Cu(II) cubane complexes.

In this context, a tetranuclear copper(II) complex, $[\{\text{Cu}(\text{OH})(\text{phen})\}_4] \cdot (\text{ClO}_4)_4$ (**3**), having a Cu_4O_4 cubane core was synthesized hydrothermally using the ligand 1,10-phenanthroline (phen) in a mildly acidic pH and structurally characterized by single-crystal X-ray crystallography. The copper centers are connected through four μ_3 -hydroxo bridges located at the vertices of a cubane like structure which allow the copper centers to magnetically communicate with each other. Further investigation of

3 was carried out using thermogravimetric analysis (TGA), CHN analysis and FT-IR spectroscopy; the purity of **3** was confirmed by powder X-ray diffraction. The magnetic susceptibility of **3** indicates overall antiferromagnetic coupling. To find the best fit for the experimental magnetic data and predict the exchange coupling constants the influence of several factors such as the coordination environment around the copper atoms, the bond lengths, and angles within the cubane core, the Cu...Cu distances and the displacement angle of hydroxo substituent were examined. The best fit is obtained with a 1+1+4 model for the exchange coupling among the copper(II) centers with $J_1 = -28.0 \text{ cm}^{-1}$, $J_2 = +72.2 \text{ cm}^{-1}$ and $J_3 = -15.3 \text{ cm}^{-1}$ corresponding to a medium, a short and four long exchange pathways. This model was derived the parameters known to be important in the classification of the cubane-like structures, and the study of the angle of the super-exchange pathways, such that all the signs and the magnitudes of the coupling constants were justified based on the different geometric factors. The predominant antiferromagnetic exchange through a Cu–O super-exchange pathway leads to the singlet total spin ground state.

6.2. Experimental

6.2.1. Synthesis of $[\{\text{Cu}(\text{OH})(\text{phen})\}_4] \cdot (\text{ClO}_4)_4$ (**3**)

This compound was synthesized several times using different poly-carboxylic acids. In all syntheses, a 0.2 M Cu(II) solution was prepared by dissolving $\text{Cu}(\text{ClO}_4)_2 \cdot 6\text{H}_2\text{O}$ salt in water and 1,10-phenanthroline (phen) was added to ethanol to make a 0.2 M solution. The poly-carboxylic acid (0.01-0.02 mmol) and 2mL of a solution of 0.1 M of $\text{LiOH} \cdot \text{H}_2\text{O}$ were added to 1 mL of the phenanthroline solution. The mixture was stirred for 15-20 minutes to make a clear solution. Copper perchlorate solution (0.1 mL) was then added to the solution. The whole solution was heated to 80-90 °C for 10-14 d in a sealed vial. The pH of the solution was 4.8-5.3. The acids that were used to synthesized **3** were phenylene diacetate (pda), 1,4-naphthalene dicarboxylate (1,4-ndc), 2,7-naphthalene dicarboxylate

(2,7-ndc) and 1,4,5,8- naphthalene tetracarboxylate (ntc). Blue rectangular single crystals were formed using 0.010 and 0.015 mmol (0.0019 and 0.0029 g) of pda (C₁₀H₁₀O₄) and 0.01 mmol (0.0030 g) of ntc (C₁₄H₈O₈). The quality of crystals prepared at 80 °C with ntc was sufficiently good for data collection, however the crystals were synthesized using pda were poor in quality. The crystals were washed with ethanol and immediately used to collect single-crystal X-ray diffraction data at -150 °C. Using pda, 1,4-ndc and ntc result in the formation of **3** mixed with an impurity as shown by powder X-ray diffraction. The only approach that results in forming the pure phase of **3** was using the 0.01 mmol of 2,7-ndc at 80 °C which results in pure light blue powder. Besides the powder X-ray diffraction, IR, TGA and CHN analyses were performed to characterize the compound.

Even though the polycarboxylic acids are absent from the product phases without their presence, the reaction results in the formation of cyan single crystals with the same unit cell parameters as [Cu(phen)₂(H₂O)](ClO₄)₂²⁸⁶.

6.2.2. Characterization of **3**

6.2.2.1. Powder X-ray Diffraction (PXRD)

The sample was prepared by washing with ethanol and acetone after filtration and then air-dried. Then the sample was ground using an agate mortar and pestle. The fine powder was spread over a zero-diffraction silicon sample holder. The experimental powder pattern is the same as the one simulated from the single crystal data except for small peak shifts due to the temperature difference and confirms the phase purity (Figure 6.3) (powder data were collected at room temperature; however, the single-crystal data were collected at -150 °C).

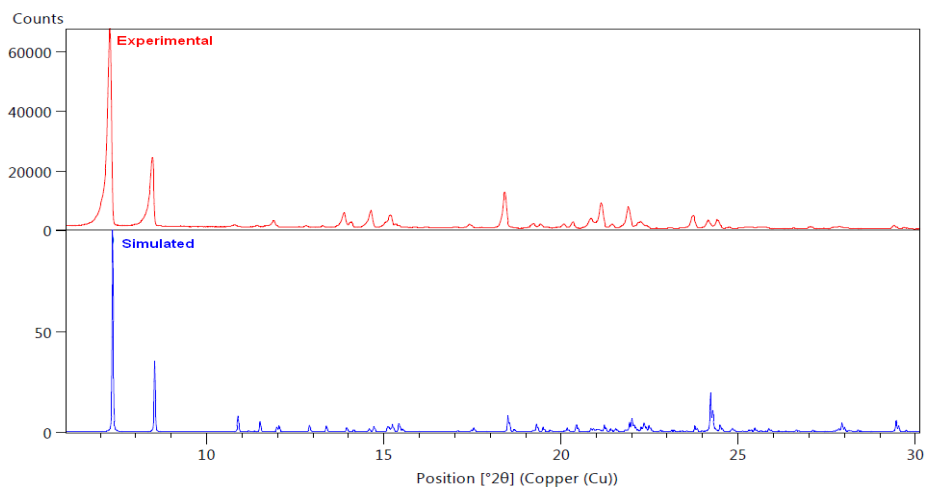


Figure 6.3 Experimental and simulated powder X-ray diffraction of compound **3**. The simulated pattern is based on the analysis of the single-crystal X-ray diffraction refined structure.

6.2.2.2. Single Crystal X-ray Diffraction (SCXRD)

A suitable blue rectangular plate single crystal was mounted on the tip of a Micromount mitegen loop using vacuum grease. A hemisphere of data (1272 frames at 6 cm detector distance) was collected using a narrow-frame algorithm with scan widths of 0.30 % in omega and an exposure time of 50 s frame⁻¹. Final cell constants were refined using 7230 reflections having $I > 4\sigma(I)$, and these, along with other information pertinent to data collection and refinement, are listed in Table 6.1. The Laue symmetry was determined to be -1 , and the space group was shown to be either P1 or P -1 . One of the perchlorate anions was found to be disordered over two slightly different orientations, and this was treated by refinement of ideal rigid body models. The population ratio of approximately 60:40 was estimated by comparison of isotropic displacement parameters.

Table 6.1 Crystal data and structure refinement for **3**.

Empirical formula	C ₄₈ H ₃₆ Cl ₄ Cu ₄ N ₈ O ₂₀
Formula Weight	1440.81
Temperature, Wavelength	123(2) K, 0.71073 Å
Crystal system, space group	Triclinic, P $\bar{1}$
Unit cell dimensions	a = 8.473(1) Å, b = 13.028(1) Å, c = 24.301(2) Å α = 79.184(1) °, β = 87.493(1) °, γ = 75.316(1) °
Cell Volume	2548.8(4)
Z, Calculated density	2, 1.877 g/cm ³
Crystal size	0.30 × 0.10 × 0.06 mm ³
Index ranges	-10 ≤ h ≤ 9, -14 ≤ k ≤ 15, -26 ≤ l ≤ 28
Theta range for data collection	1.64 to 25.03°
Absorption coefficient	1.947 mm ⁻¹
F(000)	1448
Reflections collected / unique	15335 / 8768 [R(int) = 0.0162]
Refinement method	Full-matrix least-squares on F ²
Data/restraints/parameters	7230 / 4 / 739
Goodness-of-fit on F ²	1.017
Final R indices [I > 4σ(I)]	R1 = 0.0290, wR2 = 0.0716
R indices (all data)	R1 = 0.0365, wR2 = 0.0776
Largest diff. peak and hole	1.031 and -0.980 e.Å ⁻³

6.2.2.3. Crystal Structure

The crystal structure of $[\{\text{Cu}(\text{OH})(\text{phen})\}_4] \cdot (\text{ClO}_4)_4$ (**3**), shows that the compound contains four copper centers. Cu(1) is five-coordinated in a distorted square-pyramidal coordinated by two nitrogen atoms (N(1) and N(2)) from the bidentate 1,10-phenanthroline (phen) ligand, and three bridging oxygen ions (O(1), O(2), and O(3)) from μ_3 -hydroxyl groups, one of them (O(3)) is in the apical position and links Cu1 to the two other copper ions (Cu(3) and Cu(4)). The other two oxygen (O(1) and O(2)) and two nitrogen atoms (N(1) and N(2)) form the basal plane. The coordination environment around Cu(2) is similar to that of Cu(1); the basal plane contains of two nitrogen atoms (N(3) and N(4)) from a different phen ligand and two oxygen ions (O(1) and O(2)) from μ_3 -hydroxyl groups that connect Cu(1) and Cu(2) to one another and make the first binuclear subunit. The other bridging oxygen ion (O(4)) is in the apical position of the Cu(2) square pyramid and connects it to the second binuclear subunit consisting of Cu(3) and Cu(4). In these distorted square pyramidal geometries, the copper ions are sitting above the basal plane in the direction of the apical oxygen ions, and the apical Cu-O bonds are longer than the corresponding basal Cu-O bonds, see Figure 6.4.

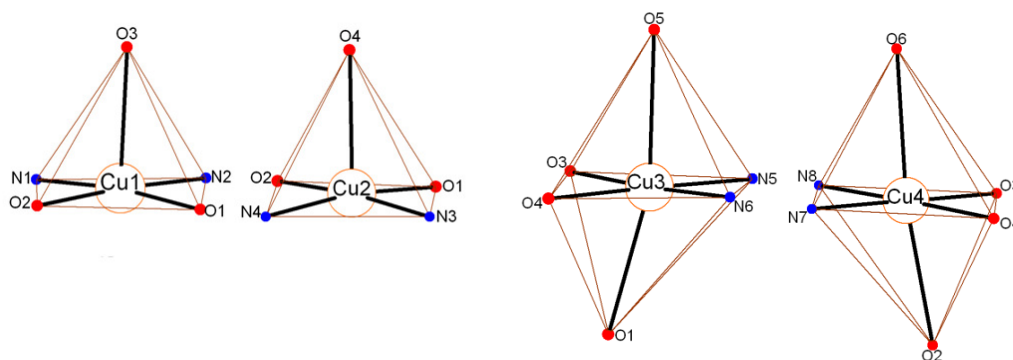


Figure 6.4 Coordination environment around Cu(II) centers; polyhedron of the Cu(1) and Cu(2) are distorted square pyramidal and the geometry of the Cu(3) and Cu(4) are distorted octahedral.

The coordination of the Cu(3) atom is distorted octahedral with long bonds to the axial oxygen ions (O(1) and O(5)). One of these two oxygen ions (O(1)) from the bridging μ_3 -hydroxyl group

belongs to the first binuclear subunit and the other oxygen ion (O(5)) is from the perchlorate group. The basal positions are occupied by oxygen ions from μ_3 -hydroxyl groups (O(3) and O(4)) that join the Cu(3) and Cu(4) to each other making the second binuclear subunit, and by two nitrogen atoms (N(5) and N(6)) from phen ligand. Cu(4) has a similar coordination environment and geometry. The bond length range of Cu-O basal and Cu-N are 1.945 (0) – 1.973 (4) Å and 1.992 (2) – 2.023 (2) Å, respectively. The Cu-O apical bond distances for first binuclear subunit (for Cu(1)-O(3) is 2.384 (2) Å and for Cu(2)-O(4) is 2.306 (2) Å) are shorter than axial bond distances for the second binuclear (Cu(3) – O(1), Cu(3) – O(5), Cu(4) – O(2), Cu(4) – O(6) are 2.566 (2) Å, 2.591 (2) Å, 2.468 (2) Å, and 2.577 (2) Å, respectively). The axial bond distances are longer than the basal ones for the Cu(3) and Cu(4) due to the Jahn-Teller distortion (Figure 6.4).

Cu(3) and Cu(4) attracts the oxygen ions of perchlorate, and that makes this second binuclear plane bends toward these oxygens and far apart from the opposite first binuclear subunit. In other word when the Cu(1)-O(1)-Cu(2)-O(2) is almost a perfect plane (with 0.0446 root mean square deviation of fitted atoms) the plane of Cu(3)-O(3)-Cu(4)-O(4) is bent (with 0.1317 roots mean square deviation of fitted atoms) toward the perchlorate group. The presence of this bond is also indicated by bond valence sum calculations (Table 6.2 and 6.3).

The four copper centers make a $\{\text{Cu}_4(\mu_3\text{-OH})_4\}$ cubane core in which the μ_3 -hydroxo bridges and copper(II) ions are located at the alternate vertices (Figure 6.5.a). The distortion (elongation of apical and axial positions) makes the four parallel Cu-O bonds that connect the first and second binuclear subunits to one another longer than the rest. Each oxygen ion from a hydroxo group acts as a basal position for two copper ions and apical for one other copper ion. A 1,10-phenanthroline (phen) as an aromatic bidentate ligand is linked to each copper through its nitrogen atoms that occupy the two other basal positions for each copper center (Figure 6.5.b). All the bond distances involved in the cubane are summarized in Table 6.4, and Figure 6.5.

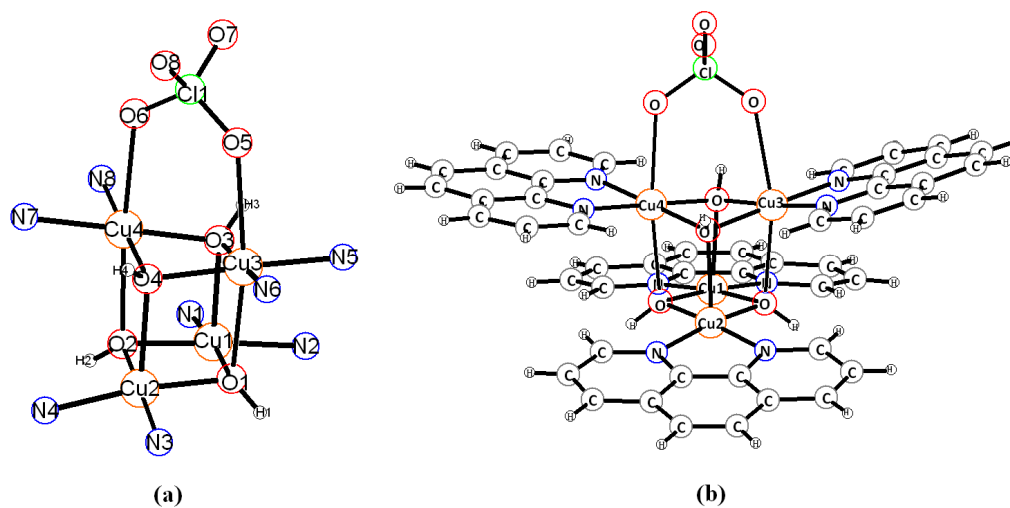


Figure 6.5 The coordination environment around copper centers (a) without and (b) with the phen ligands.

The perchlorates are connected to hydrogens of each μ_3 -hydroxo groups through weak hydrogen bonds with the $O\cdots H$ distance ranges of 1.9794 (2) – 2.3020 (1) Å and except for one perchlorate (Cl4) they are ordered (Figure 6.6). The perchlorate (Cl1) bonded to the copper ions having also a weak hydrogen bond to the hydroxide of the next unit.

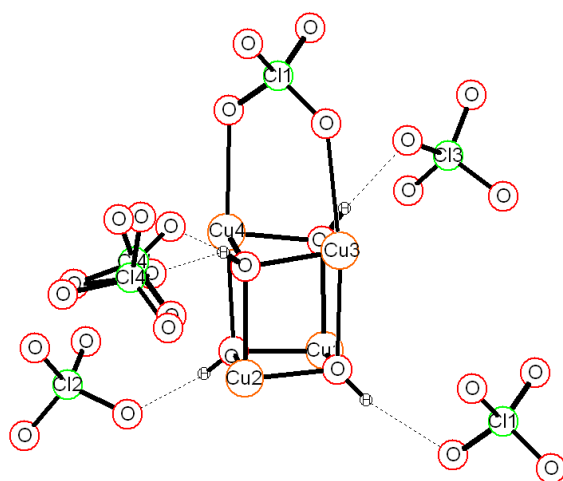


Figure 6.6 The hydrogen bond of the perchlorates to the μ_3 -hydroxo groups in vertices of the cubane core.

The packing in the b-c plane shows how the inversion center makes the space group of **3** centrosymmetric, $P\bar{1}$ (Figure 6.7). There are no π - π interactions between the phen ligands and the empty spaces are filled with perchlorate counterions. The shortest intermolecular distance between the copper centers from one cubane core to the other one is 5.8 Å.

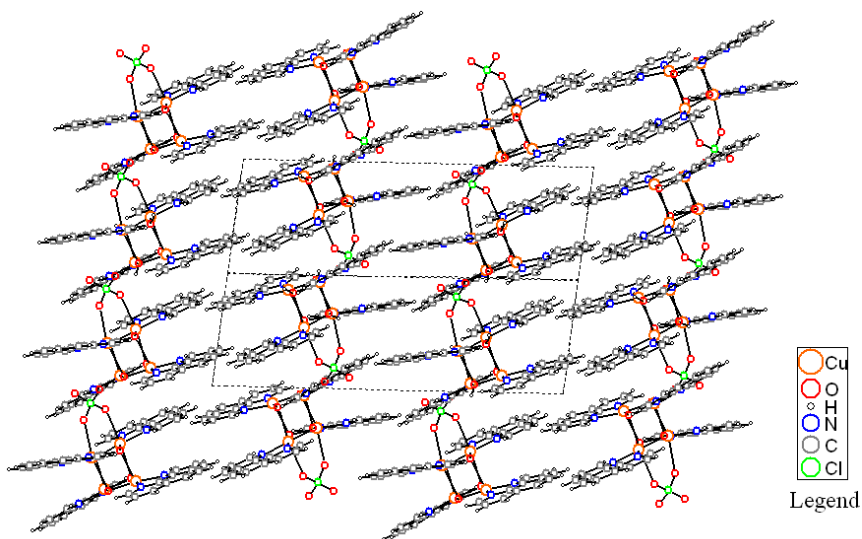


Figure 6.7 Packing of **3** with a centrosymmetric space group. The unit cell border is shown with dash lines.

6.2.2.4. Physical Measurements

The C, H and N values for the **3** compositions based on elemental analysis were 38.91%, 2.81% and 7.21% which are consistent with the calculated percentage of the carbon, hydrogen and nitrogen amounts from the X-ray crystallography that was 40%, 2.52%, and 7.78%, respectively.

Thermogravimetric analysis (TGA) and Derivative Thermogravimetry (DTG) were performed in air with a heating rate of 0.1 °C/min up to 420 °C (Figure 6.8). The experimental mass loss of the first two steps from 220 to 270 °C relates to the loss of perchlorate regarding the reported TGAs^{297,298}. Examination of the TGA and DTG is complex because of the explosive exothermic decomposition of perchlorate as a counterion that leads to breaking down of the whole structure and results in partial loss of the sample from the balance pan. The remaining powder after heating 400 °C was identified as copper(II) oxide by powder X-ray diffraction. The residual amount (3.68 moles of CuO per formula unit) was less than the expected theoretical amount (4 moles per formula unit) due to the loss at a lower temperature. This was confirmed by repeating the experiment at a faster heating rate (1 °C/min) which results in smaller CuO residue (2.4 moles) due to greater loss of sample when perchlorate decomposes.

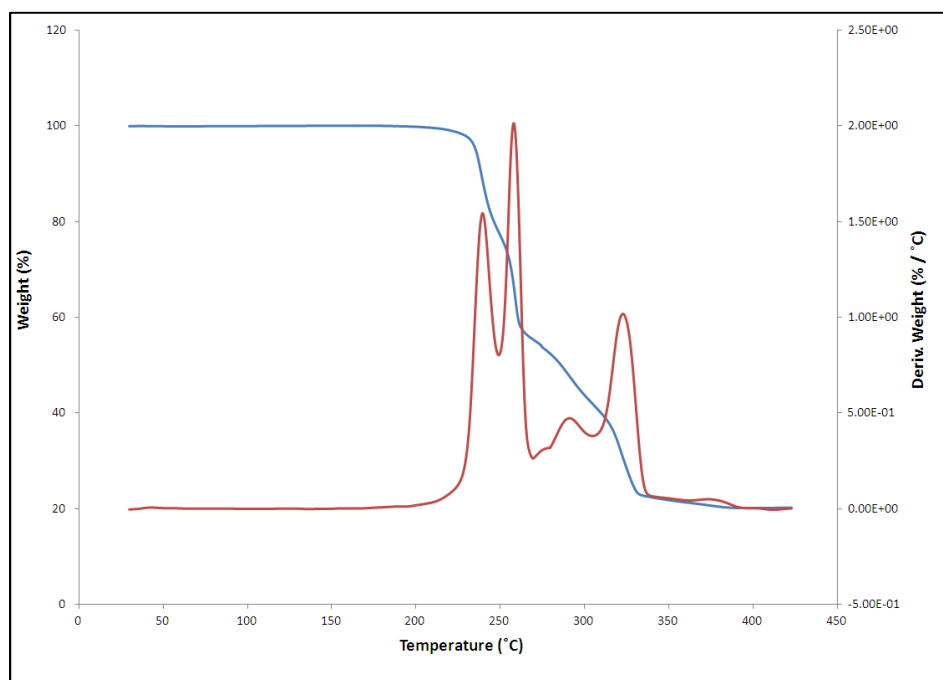


Figure 6.8 TGA and DTG of **3** in the air with a heating rate of 1 °C/min.

Through the bond valence sum, we assessed the copper oxidation state as Cu^{2+} for all four copper centers with 5 bonds for Cu(1) and Cu(2) and with 6 bonds for Cu(3) and Cu(4). Their electron configuration based on these calculations would be d^9 (Table 6.2 and 6.3).

Table 6.2 The oxidation states assignment of the copper ions from bond valence sums (BVS) in **3**

site	Bond Valence Sum			Assignment
	Cu(I)	Cu(II)	Cu(III)	
Cu1	1.398	1.990	2.313	Cu(II)
Cu2	1.435	2.042	2.373	Cu(II)
Cu3	1.190	1.941	2.258	Cu(II)
Cu4	1.191	1.955	2.274	Cu(II)

Table 6.3 Parameters used for the BVS calculations for **3**^{227,239}

		Cu ¹⁺	Cu ²⁺	Cu ³⁺
		O	R _o	1.504
	b	0.37	0.37	0.37
N	R _o	1.63	1.713	1.768
	b	0.37	0.37	0.37

FT-IR spectroscopic analysis of **3** is shown in Figure 6.9. The bands of Cu-O and Cu-N are observed at 473.7 and 562.4 cm⁻¹, respectively. The absorption peak at 720.3 cm⁻¹ is related to the O-Cu-N bending vibrations. The Cu-O-Cu stretching vibration group occurs at 618.7 cm⁻¹. The stretching vibrations of the Cu-OH group has three weak peaks at 650.2, 783.5, and 871.4 cm⁻¹. A weak absorption from ClO₄⁻ can be seen at 927.7 cm⁻¹. The out of plane bending vibration of the CH aromatic group appears at 739.9 cm⁻¹ and the CH aromatic in-plane vibrations are occur at 1033.3, 1054, and 1094 cm⁻¹. The peak in 1431 cm⁻¹ is related to stretching vibration of C=N group and the absorption peak at 1522.92 cm⁻¹ is related to stretching vibration of C=C group. The absorption peaks at 3074.8 and 3523.4 cm⁻¹ are related to stretching vibrations of CH and OH groups, respectively²⁹⁹. The assignments are made based on comparisons with IR spectra for similar compounds.

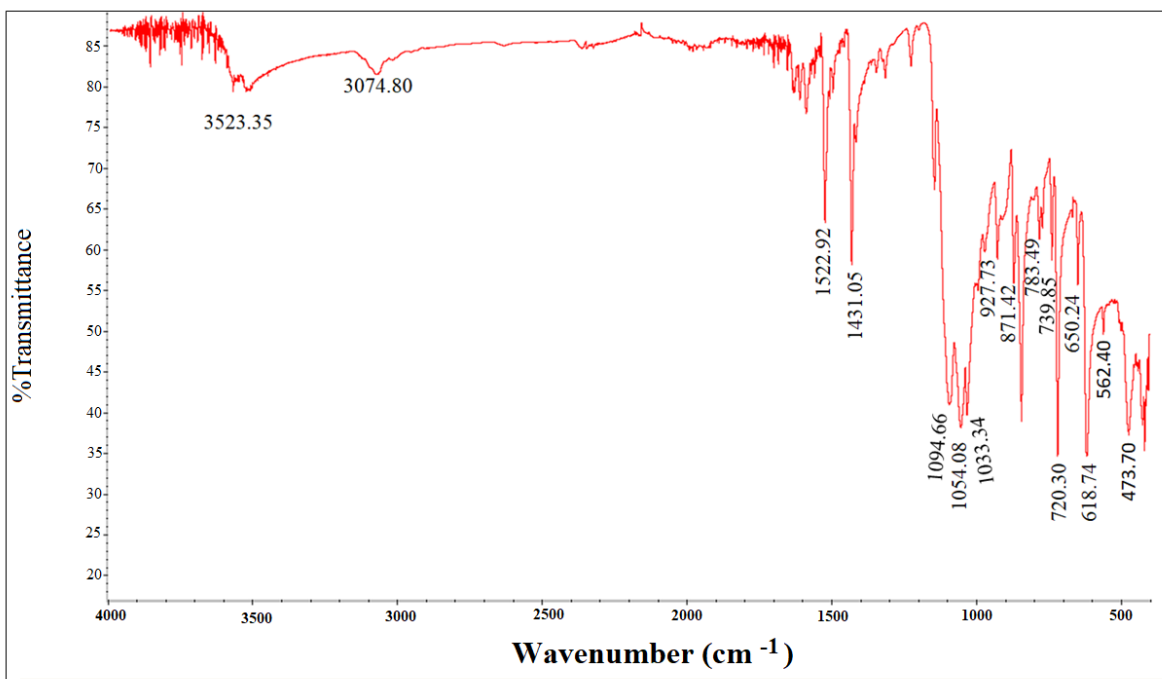


Figure 6.9 IR Spectroscopy of **3**.

6.2.3. Magnetic Studies

The magnetic susceptibility (χ) per tetranuclear Cu(II) cubane was measured in a field of 1 T in the temperature range of 2–300 K. The temperature dependence of χT product in this temperature range is shown in Figure 6.10. The χT at room temperature is $1.23 \text{ cm}^3 \text{ K mol}^{-1}$ which is slightly lower than that expected spin-only value for four uncoupled $S = 1/2$ spins ($1.40 \text{ cm}^3 \text{ mol}^{-1} \text{ K}$ with $g = 1.93$). On lowering the temperature, the χT product decreases slowly down to about 50 K, and then more rapidly to a value of $0.18 \text{ cm}^3 \text{ mol}^{-1} \text{ K}$ at 2 K indicating an antiferromagnetic coupling (Figure 6.11). The χ and $1/\chi$ vs. T plots confirm this overall magnetic behavior of **3** (Figure 6.10).

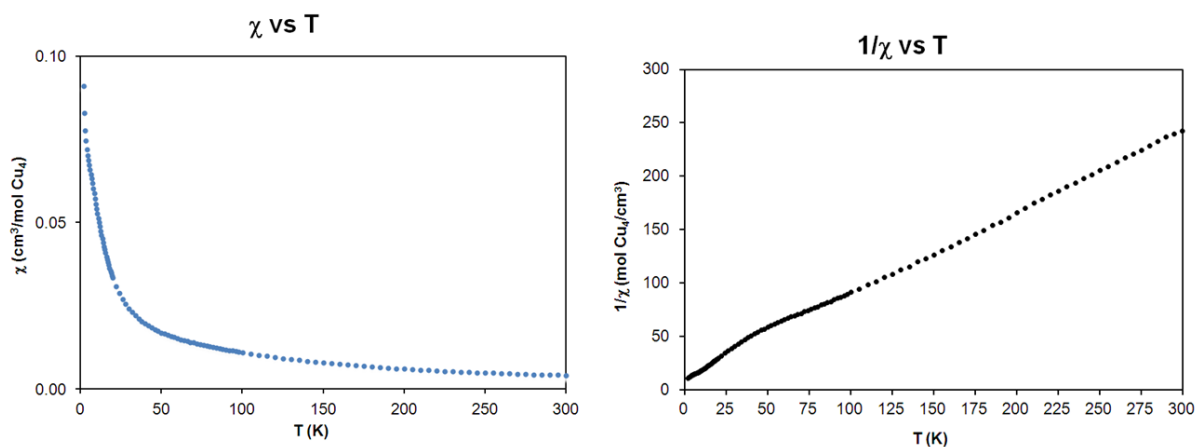


Figure 6.10 Plots of χ and $1/\chi$ vs. T for **3**.

The trend of χT at low temperature indicates a total spin-singlet ground state. According to the Equation (6.1) showing the spin only magnetic moment related to the total number of unpaired coupled electrons, the total $S=0$ at low temperature. This also confirms that the **3** magnetic behavior is predominantly antiferromagnetic. Based on Escuer *et. al.*²⁹³ in the models with two short and four longer Cu...Cu distances with the antiferromagnetic exchange along the diagonals of the cubane structure, the total ground state spin is always zero.

$$\mu_{\text{eff}} = \sqrt{8\chi T} = g\sqrt{S(S+1)}, \quad g=1.93 \quad (6.1)$$

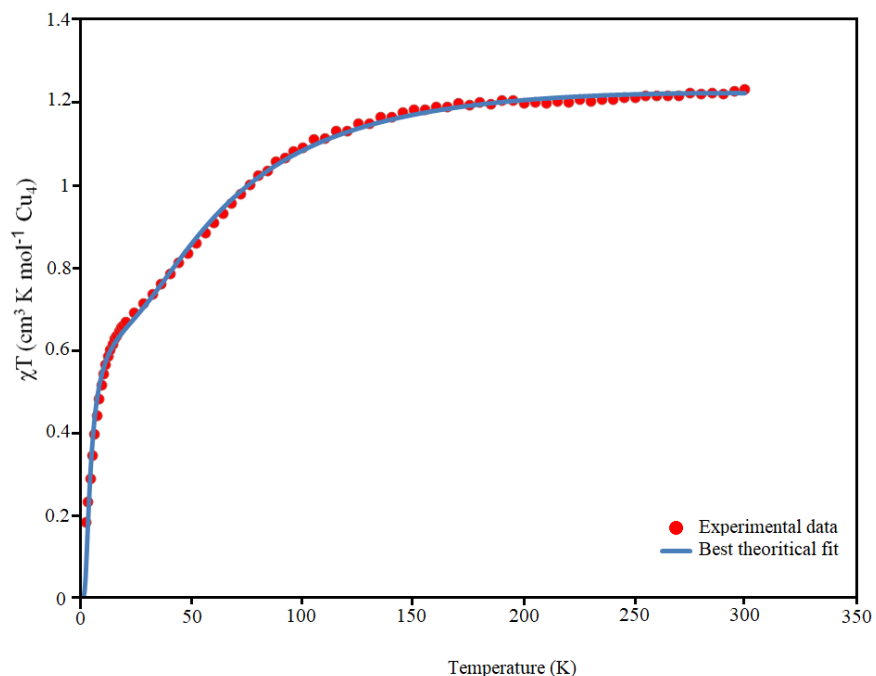


Figure 6.11 The experimental and best theoretical fit of the temperature dependence susceptibility, χT in a field of 1 T for **3**.

As discussed above, the Cu...Cu distance and the Cu-O bond lengths influence the exchange coupling of copper(II) centers in cubane type structures and determine which coupling constants are important in calculations. The other important parameters that are needed to decide on the important coupling constants are the Cu-O-Cu bond angle (θ) and the out-of-plane displacement angle (τ) between the hydroxide group and the dimeric subunit plane of the cubane. All these factors are summarized in Table 6.4. Based on all these characteristics **3** could classify in type I, with eight short Cu-O bonds and four long ones, or 2+4 class with two short Cu...Cu distances and four long ones. However, the best fitting approach using the computer program PHI for finding the J coupling constants based on the 2+4 model for the interaction between four coppers results in failure, no values were found for the J and g factors to fit this model to the experimental data. In order to find the best model and avoid over parameterizing the calculations and to take advantage of the models based on

previous studies, we reviewed the bond lengths and angles in the structure of **3**. In the classic 2+4 or type I model of cubanes the magnetic interactions are classified based only on the bond distances. In **3**, however, the two short Cu···Cu distances cannot be in the same group, as the Cu-O-Cu bond angles for Cu(1)-Cu(2) interactions are above (98.54 and 99.08°) the 97.5°³⁰⁰, the empirical threshold value for exchange coupling in hydroxo-bridged Cu(II) binuclear compounds³⁰⁰, and for Cu(2)-Cu(3) mentioned angles are below (96.34 and 97.41°) the threshold. All the bond lengths and angles in the cubane **3** are summarized in Figure 6.12 and Table 6.4.

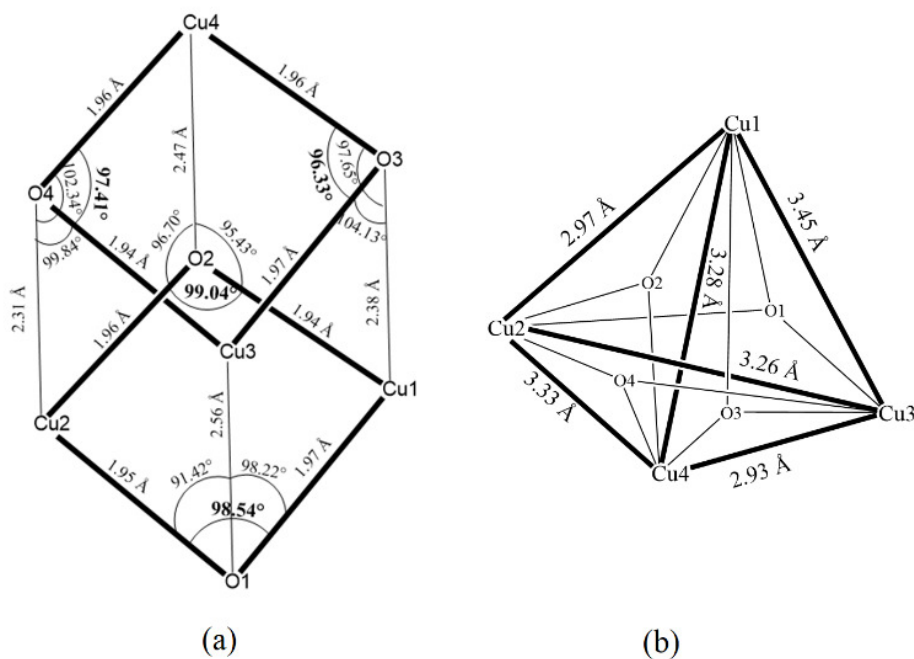


Figure 6.12 (a) Cu-O bond lengths and Cu-O-Cu angles (b) Cu···Cu distances of the cubane core of **3**.

Table 6.4 Important bond length and angles for **3** cubane core.

	Distance (Å) Cu...Cu	Angle θ (°) Cu-O-Cu	Angle τ (°) O-H & O-Cu-O- Cu	Distance (Å) Cu-O
Cu(1), Cu(2)	Cu(1)...Cu(2) 2.9745 (6)	Cu(1)-O(1)- Cu(2) 98.54 (8)	O(1)-H(1) & O(1)- Cu(1)- O(2)- Cu(2) 52.768(2)	Cu(1)- O(1) 1.9709 (2)
		Cu(1)- O(2)- Cu(2) 99.08 (9)	O(2)- H(2) & O(1)- Cu(1)- O(2)- Cu(2) 49.927 (2)	Cu(1)- O(2) 1.9423 (2)
				Cu(2)- O(1) 1.9544 (2)
				Cu(2)- O(2) 1.9670 (2)
Cu(1), Cu(3)	Cu(1)...Cu(3) 3.4498 (5)	Cu(1)- O(1)- Cu(3) 98.119 (8)	O(1)- H(1) & O(1)- Cu(1)- O(3)- Cu(3) 54.461 (2)	Cu(1)- O(1) 1.9709 (2)
		Cu(1)- O(3)- Cu(3) 104.284 (8)	O(3)- H(3) & O(1)- Cu(1)- O(3)- Cu(3) 52.489 (2)	Cu(1)- O(3) 2.3842 (2)
				Cu(3)- O(1) 2.5666 (2)
				Cu(3)- O(3) 1.9735 (2)
Cu(1), Cu(4)	Cu(1)... Cu(4) 3.2860 (6)	Cu(1)- O(2)- Cu(4) 95.590 (8)	O(2)- H(2) & O(3)- Cu(4)- O(2)- Cu(1) 59.864 (1)	Cu(1)- O(2) 1.9422 (2)
		Cu(1)- O(3)- Cu(4) 97.719 (8)	O(3)- H(3) & O(3)- Cu(4)- O(2)- Cu(1) 59.658 (2)	Cu(1)- O(3) 2.3842 (2)
				Cu(4)- O(2) 2.4682 (2)
				Cu(4)- O(3) 1.9636 (2)
Cu(2), Cu(3)	Cu(2)... Cu(3) 3.2611 (6)	Cu(2)- O(1)- Cu(3) 91.297 (8)	O(4)- H(4) & O(4)- Cu(2)- O(1)- Cu(3) 54.291 (1)	Cu(2)- O(1) 1.9544 (2)
		Cu(2)- O(4)- Cu(3) 99.846 (8)	O(1)- H(1) & O(4)- Cu(2)- O(1)- Cu(3) 57.361 (2)	Cu(2)- O(1) 2.3061 (2)
				Cu(3)- O(1) 2.5666 (2)
				Cu(3)- O(4) 1.9449 (2)

Table 6.4 Important bond length and angles for **3** cubane core (Cont).

Cu(2), Cu(4)	Cu(2)···Cu(4)	Cu(2)- Cu(4)	O(2)- H(2) & O(2)- Cu(2)- O(4)- Cu(4)	Cu(2)- O(2)
	3.3291 (6)	96.633 (8)	53.442 (2)	1.9670 (2)
		Cu(2)- O(4)- Cu(4)	O(4)- H(4) & O(2)- Cu(2)- O(4)- Cu(4)	Cu(2)- O(4)
		102.289 (8)	52.488 (2)	2.3061 (2)
				Cu(4)- O(2) 2.4682 (2) Cu(4)- O(4) 1.9598 (2)
Cu(3), Cu(4)	Cu(3)··· Cu(4)	Cu(3)- O(3)- Cu(4)	O(3)- H(3) & O(3)- Cu(3)- O(4)- Cu(4)	Cu(3)- O(3)
	2.9336 (5)	96.337 (8)	52.259 (2)	1.9735 (2)
		Cu(3)- O(4)- Cu(4)	O(4)- H(4) & O(3)- Cu(3)- O(4)- Cu(4)	Cu(3)- O(4)
		97.406 (8)	58.723 (2)	1.9449 (2)
				Cu(4)- O(3) 1.9636 (2) Cu(4)- O(4) 1.9598 (2)

So, we break down the six exchange interactions to three exchange interactions with a 1+1+4 categorization (Figure 6.13) and use the Heisenberg model with the spin Hamiltonian (Equation 6.2) to fit the data.

$$H = -J_1 (S_1 S_2) - J_2 (S_3 S_4) - J_3 (S_1 S_3 + S_1 S_4 + S_2 S_3 + S_2 S_4) \quad (6.2)$$

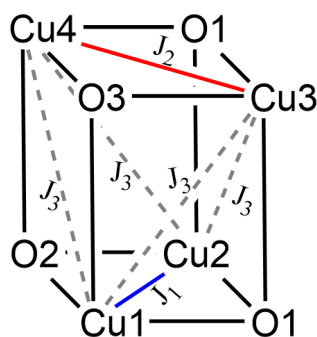


Figure 6.13 Schematic view of coupling exchange in **3**, between Cu(1)-Cu(2), J_1 , between Cu(2)-Cu(3), J_2 and between Cu(1)-Cu(3), Cu(1)-Cu(4), Cu(2)-Cu(3), Cu(2)-Cu(4), J_3 .

Using the program PHI the best fit of the experimental χT data gives the parameters $J_1 = -28.0 \text{ cm}^{-1}$, $J_2 = +72.2 \text{ cm}^{-1}$ and $J_3 = -15.3 \text{ cm}^{-1}$ and the isotropic g factor for all four copper centers is 1.93. The best fit (solid blue line) and the experimental data are shown in Figure 6.13. The temperature-independent paramagnetism (TIP) correction value is $-3.93 \times 10^{-4} \text{ cm}^3 \text{ mol}^{-1}$ per copper ion.

6.2.4. Magneto-Structural Correlations

The J_1 coupling constant is related to Cu(1)···Cu(2) with a distance of 2.97 Å and four short Cu-O bond distances (averaged ~ 1.96 Å). The strongest coupling constant, J_2 , corresponds to the shortest Cu(3)···Cu(4) distance, 2.93 Å with four short Cu-O bond lengths (averaged ~ 1.96 Å). The out-of-plane displacement angle of hydroxo group (τ) is higher than 50° for almost all exchanges (Table 6.4) and ferromagnetic behavior for smaller Cu-O-Cu angles and antiferromagnetic interaction for larger angles are predicted. The magnitudes of the coupling constants are consistent with the Cu···Cu and Cu-O distances (shorter distances, stronger interactions). The sign of the coupling constants shows the type of coupling exchanges in this normal style correspond to the structural parameters discussed for the dimer Cu-O-Cu bond angles. The coupling constant of Cu(1)-Cu(2) shows an antiferromagnetic ($J_1 = -28.0 \text{ cm}^{-1}$) interaction and the Cu(3)-Cu(4) coupling constant shows a ferromagnetic ($J_2 = +72.2 \text{ cm}^{-1}$) interaction.

For drawing the magnetic orbitals each copper ion is considered as an individual magnetic center. For Cu(1)-Cu(2), the copper ion geometry is elongated square pyramidal. Splitting of square pyramidal orbitals makes the $d_{x^2-y^2}$ orbital as the singly occupied molecular orbital (SOMO). For Cu(3)-Cu(4), the geometry of the copper ions is distorted octahedral. A Jahn-Teller distortion results in elongation of the Cu-O octahedral along z. The SOMO in this geometry is also the $d_{x^2-y^2}$ orbital (Figure 6.14). So, for both geometries, the $d_{x^2-y^2}$ orbital carrying an unpaired electron is the magnetic orbital for each Cu(II) center.

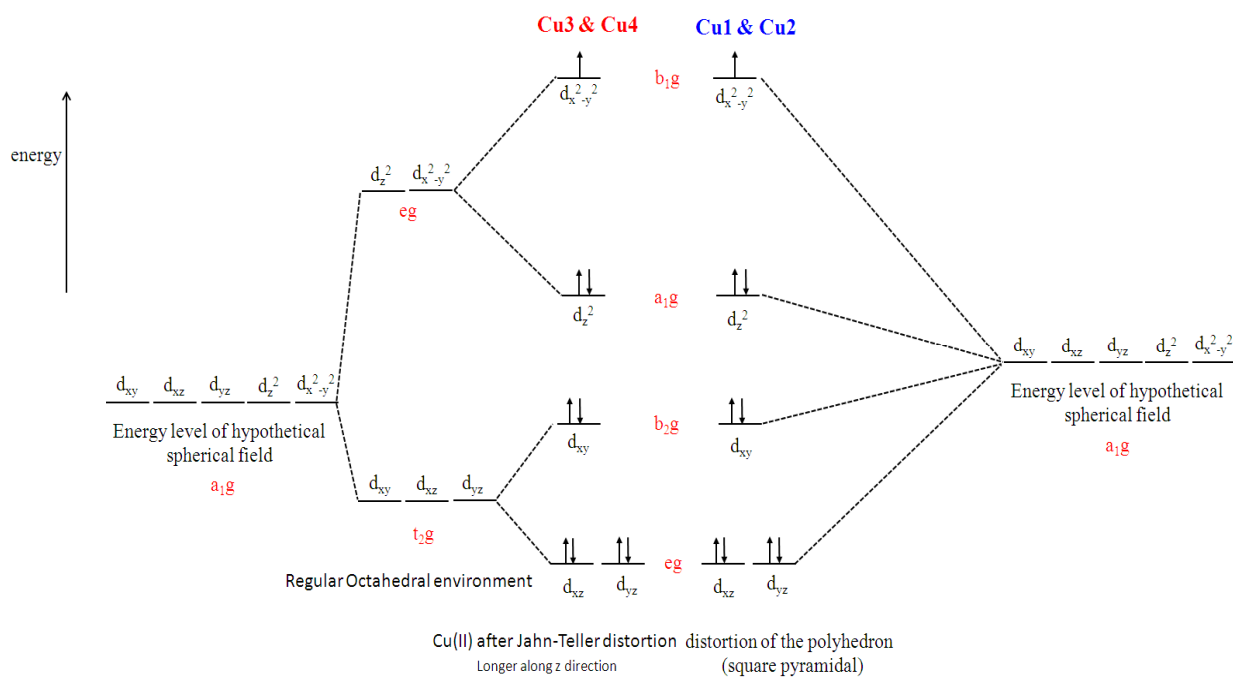


Figure 6.14 d^9 orbital splitting of square pyramidal and octahedral both with elongation along the z -axis.

As the coupling occurs through the bridging oxygen ions the copper(II) magnetic orbital lobes are directed toward these paramagnetic centers. Figure 6.15 shows the magnetic orbitals on copper centers considering the stronger exchange pathways and how they form by combining the magnetic orbitals of the binuclear subunit of the cubane core.

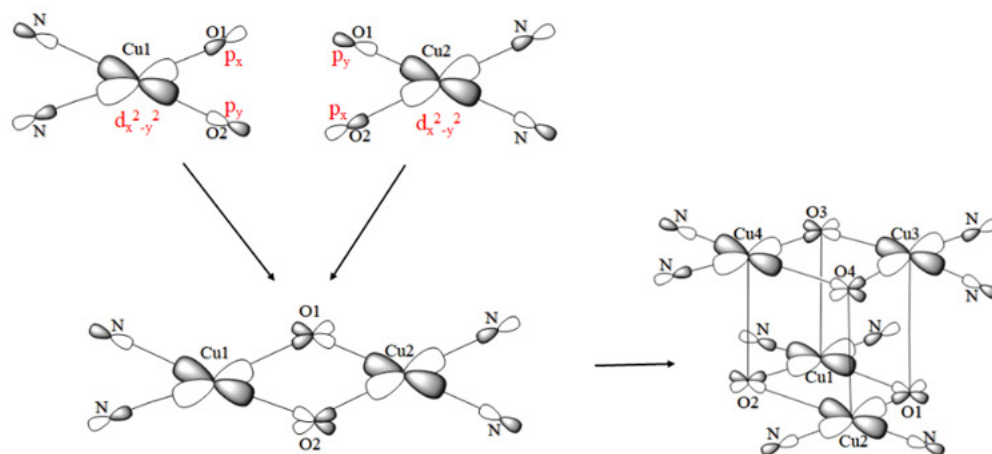


Figure 6.15 Schematic view of the magnetic orbitals on copper centers for the predominant exchange pathways in the cubane core consists of two individual subunits. The binuclear subunit coupling exchange pathway consists of each individual copper center and the connected atoms.

The four long Cu-O bonds are involved in four weaker exchanges with the J_3 coupling constant. The Cu-O-Cu bond angles corresponding to the J_3 exchange coupling constants are a mixture of above and below the empirical threshold value ($\theta = 97.5^\circ$) for FM or AFM coupling for Cu(1)-Cu(4), Cu(2)-Cu(3) and Cu(2)-Cu(4). For Cu(1)-Cu(3) both angles are above the threshold and are consistent with antiferromagnetic interactions. The reason for weaker exchanges of J_3 is Cu-O bonds that are defined as the long bonds comparing to the ones that are in intradimer units. In each diagonal exchange, one of the two Cu-O bonds that are responsible for the super-exchange pathway is longer than the other one. This causes less overlap and in consequence the weaker exchange.

6.3. Conclusion

A new compound, $[\{\text{Cu}(\text{OH})(\text{phen})\}_4] \cdot (\text{ClO}_4)_4$ (**3**), with a cubane core structure was synthesized hydrothermally and structurally characterized using single X-ray crystallography, powder X-ray diffraction, CHN analysis, TGA and FT-IR spectroscopy. The four copper centers are alternatively

located on the vertices of the cubane core and connect to each other through μ_3 -hydroxo groups which are also responsible for the super-exchange magnetic interaction between copper centers. The susceptibility measurement on **3** indicates the dominant antiferromagnetic behavior leads to the singlet total spin multiplicity. To fit this experimental data with the spin Hamiltonian the classic model (2+4) using bond lengths and distances combined with the binuclear units' magnetic exchange type prediction out of bond angles were considered. The exchange interactions break down to three exchange coupling constants and the model used for successfully fitting the experimental data was 1+1+4. The correlation between the structure and magnetic exchange among copper centers was investigated. Besides the Cu-O bond lengths and Cu...Cu distances, the Cu-O-Cu bond angle and O-H displacement angle regarding the binuclear subunits were studied. The exchange coupling constants for the three exchange pathways were determined by fitting the magnetic susceptibility data to be $J_1 = -28.0 \text{ cm}^{-1}$, $J_2 = +72.2 \text{ cm}^{-1}$ and $J_3 = -15.3 \text{ cm}^{-1}$. The orbital splitting due to the geometry around each copper results in the assignment of $d_{x^2-y^2}$ orbital as the magnetic orbital on each copper center. The magnetic orbital layout indicates that the main interaction between copper ions are controlled through super-exchange pathways.

Chapter 7. Four New Cu(II) Coordination Complexes Crystal Structure

7.1 Introduction

Using solvothermal reactions, a bridging linker, phenylene diacetate (pda), and chelating blocking ligand (phen) under different conditions several different coordination compounds were synthesized. All have similar stabilities and consequently finding conditions that result in the synthesis of a pure phase proved difficult. Besides the three compounds reported in previous chapters, four more phases are described in this chapter. Additional compounds shown in Figure 7.1 were synthesized by Helen Wang in our lab. One of the compounds (**HW1**) has the same composition as **1** but a different crystal structure. Another (**HW2**) is similar to **4.1**, (for more details see Section 7.2.3). Furthermore, there are some reported crystal structures of copper(II) compounds such as $[\text{Cu}(\text{phen})_2(\text{OH}_2)][\text{ClO}_4]_2$ ²²⁵ and $[\text{Cu}_2(\text{pda})_2(\text{phen})_2(\text{H}_2\text{O})_2] \cdot 6\text{H}_2\text{O}$ ³⁰¹ which is similar to **2**.

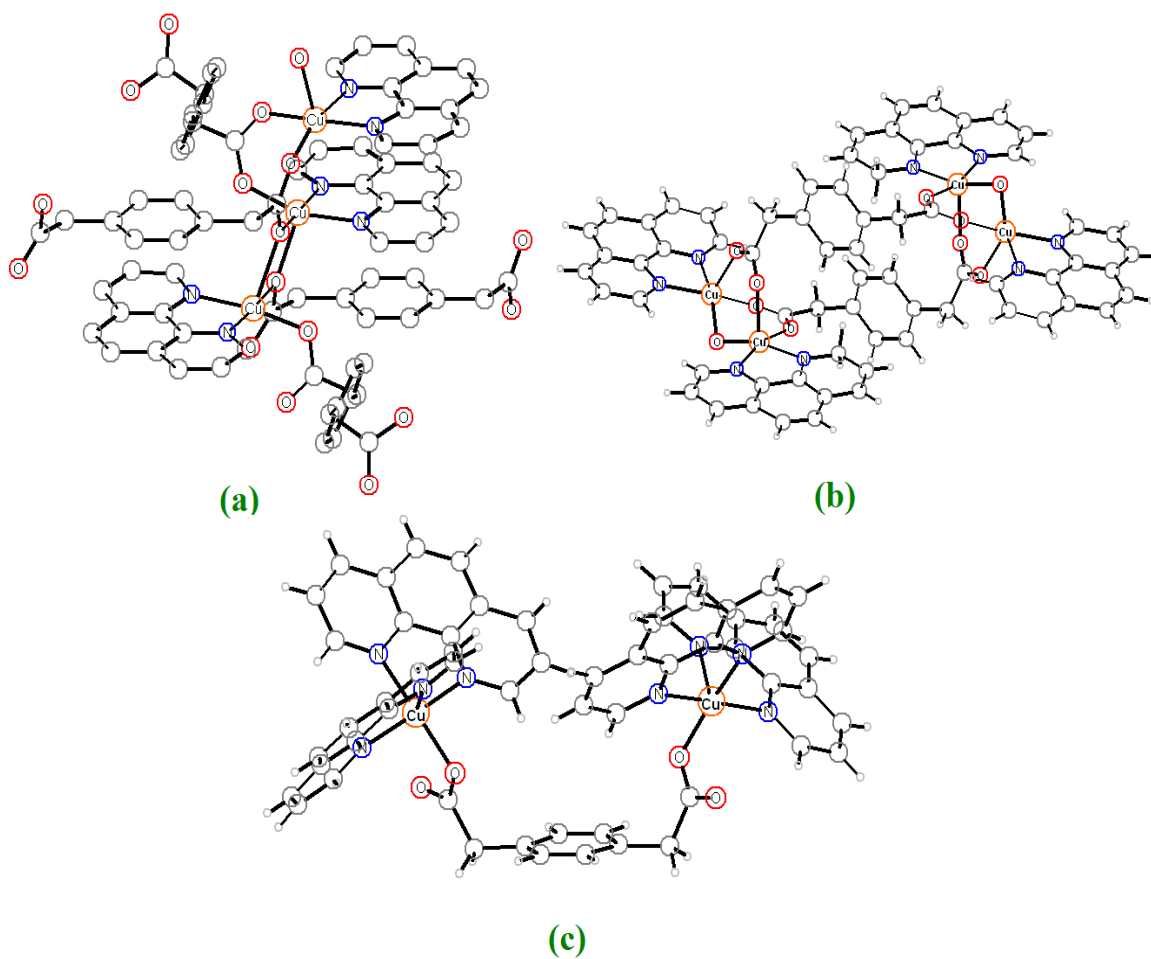


Figure 7.1 The copper(II) complexes synthesized by Helen Wang³⁰² using pda and phen ligands. (a) $[\text{Cu}_3(\text{phen})_3(\text{pda})_3(\text{H}_2\text{O})](\text{ClO}_4)_2(\text{H}_2\text{O})_x$ (**HW1**), (b) $[\text{Cu}_2(\text{phen})_4(\text{pda})](\text{ClO}_4)_2$ (**HW2**), and (c) $[\text{Cu}_4(\text{phen})_4(\text{pda})_2(\text{OH})_2](\text{ClO}_4)_2(\text{H}_2\text{O})_x$ (**HW3**).

In the synthesis sections below, the reactions gave the product as a major phase are described; the yields of the reactions were generally low. The impurity phase was identified in some cases.

7.2. Copper(II) Binuclear One-Dimensional Coordination Polymer

7.2.1. Synthesis of $[\text{Cu}_2(\text{phen})_2(\text{pda})(\text{H}_2\text{O})] \cdot [\text{H}_2\text{pda}] \cdot [\text{ClO}_4]_2 \cdot [\text{H}_2\text{O}]_4$ (**4.1**)

Compound **4.1** was synthesized by a one-pot solvothermal reaction. The starting solutions were made the same as Section 6.2.1. After the preparation of all three solutions, they were mixed together in order. 0.1 mmol (0.0194 g) of phenylene diacetic acid (H_2pda) was added to 1.5 mL of the solution of 0.1 M of $\text{LiOH} \cdot \text{H}_2\text{O}$ in the reaction vial. Then 7 mL of tetrahydrofuran (THF) was added. The mixture was stirred for an hour to make a clear solution. Then 1 mL of premade phen 0.2 M solution was added to the mixture and shaken well. By adding 1 mL of premade $\text{Cu}(\text{ClO}_4)_2 \cdot 6\text{H}_2\text{O}$ 0.2 M solution, the reaction mixture became blue. The reaction mixture was capped in a vial and sealed with a Teflon tape. The reaction mixture was heated in the oven at 65 °C for 10 to 14 d. Blue cubic crystals of **4.1** formed from the reaction mixture as a major phase, in < 30% yield. Cyan crystals with the same unit cell parameters as $[\text{Cu}(\text{phen})_2(\text{H}_2\text{O})](\text{ClO}_4)_2$, a blue unknown polycrystalline, and a dark green precipitate were present along with crystals of **4.1**.

Compound **4.1** was also obtained using the same reaction scheme but in a solvent mixture of 4 mL of ethanol and 3 mL of water at 120 °C in 10 d, the minor phase containing **1** and **5.2**.

7.2.2. Single Crystal X-ray Diffraction (SCXRD)

All measurements were made with a Bruker D8 platform diffractometer equipped with a 4K CCD APEX II detector. A hemisphere of data (1272 frames at 6 cm detector distance) was collected using a narrow-frame algorithm with scan widths of 0.30% in omega and an exposure time of 60 s frame⁻¹. The data were integrated using the Bruker-Nonius SAINT program, with the intensities corrected for Lorentz factor, polarization, air absorption, and absorption due to variation in the path length through the detector faceplate. The data were scaled, and an absorption correction was applied

using SADABS. Redundant reflections were averaged. Final cell constants were refined using 6579 reflections having $I > 4 \sigma(I)$, and these, along with other information pertinent to data collection and refinement, are listed in Table 7.1. The Laue symmetry was determined to be 2/m, and from the systematic absences noted the space group was shown unambiguously to be $P2_1/n$. The asymmetric unit consists of a di-cationic unit, a neutral hydrogen-bonded p-phenylene diacetic acid molecule, two perchlorate anions, and four water molecules of solvation. One of the perchlorate ions is disordered over three different orientations and was modeled using ideal rigid bodies with population factors estimated by comparison of isotropic displacement parameters. Three of the four water molecule sites were found to be only partially occupied, most likely due to solvent evaporation during crystal handling or perhaps undiscovered disorder. Since it is unlikely for these sites to be partially occupied the water molecule positions are assumed to be fully occupied for calculations of the molecular formula, formula weight, and density.

Table 7.1 Crystal data and structure refinement for **4.1**.

Empirical formula	C ₄₄ H ₄₄ Cl ₂ Cu ₂ N ₄ O ₂₁
Formula Weight	1162.81 g mol ⁻¹
Temperature, Wavelength	123(2) K, 0.71073 Å
Crystal system, space group	Monoclinic, P2 ₁ /n
Unit cell dimensions	$a = 18.599(4)$ Å, $b = 13.076(3)$ Å, $c = 20.603(5)$ Å $\alpha = 90^\circ$, $\beta = 112.198(3)^\circ$, $\gamma = 90^\circ$
Cell Volume	4639.3(18) Å ³
Z, Calculated density	4, 1.665 g/cm ³
Crystal size	0.40 × 0.30 × 0.20 mm ³
Index ranges	$-21 \leq h \leq 22$, $-15 \leq k \leq 14$, $-24 \leq l \leq 23$
Theta range for data collection	1.26 to 25.01°
Absorption coefficient	1.122 mm ⁻¹
F(000)	2384
Reflections collected / unique	22860 / 8141 [R(int) = 0.0184]
Refinement method	Full-matrix least-squares on F ²
Data/restraints/parameters	6579 / 2 / 640
Goodness-of-fit on F ²	1.037
Final R indices [I > 4σ(I)]	R1 = 0.0347, wR2 = 0.0863
R indices (all data)	R1 = 0.0431, wR2 = 0.0936
Largest diff. peak and hole	1.190d -847 e.Å ⁻³

7.2.3. Crystal Structure

The binuclear unit of the crystal structure of $[\text{Cu}_2(\text{phen})_2(\text{pda})(\text{H}_2\text{O})] \cdot [\text{H}_2\text{pda}] \cdot [\text{ClO}_4]_2 \cdot [\text{H}_2\text{O}]_4$ (**4.1**) consists of two copper atoms each attached to a bidentate phenanthroline (phen) ligand. The copper atoms are by a water molecule and two phenylene diacetate (pda) ligands. A phenylene diacetic acid (H_2pda) molecule is hydrogen-bonded to the coordinated water molecule. Figure 7.2 shows the binuclear part of the structure omitting the solvent, hydrogen atoms, and the counter anions.

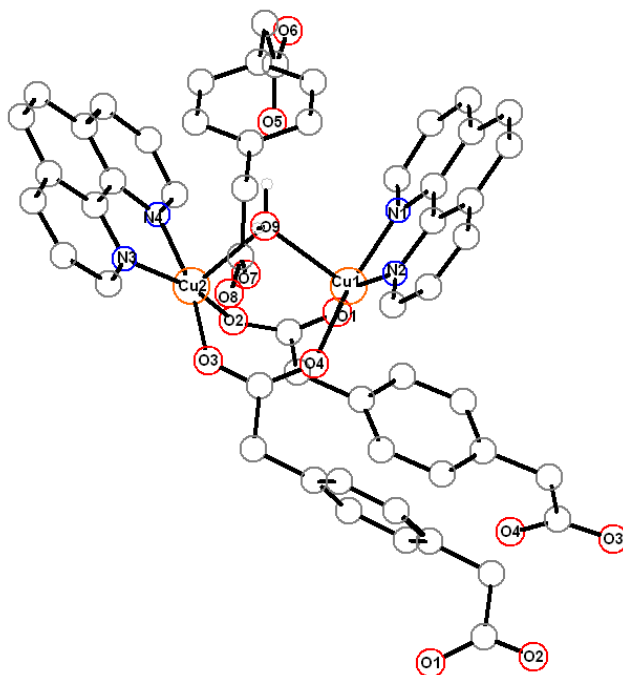


Figure 7.2 Coordination environment around copper centers in **4.1**. Lattice water molecules, perchlorate ions, and hydrogen atoms are removed for clarity. Gray spheres represent carbon atoms.

The Cu^{2+} ions are chelated by the nitrogen atoms of the phenanthroline ligands. Each pda ligand though acts as a tetradentate linker. Each pda oxygen atom is bonded to one copper ion, so each pda ligand links four copper ions together.

The coordination environment around the copper ions is distorted square pyramidal. Each copper ion is coordinated to two nitrogen atoms from the bidentate 1,10-phenanthroline ligand in the basal plane of the square pyramid and to three oxygen ions. Two of the oxygen ions that are connected to Cu(1) and Cu(2) are from two different phenylene diacetate (pda) ligands. The coordinated water molecule bridges two copper ions (Figure 7.3).

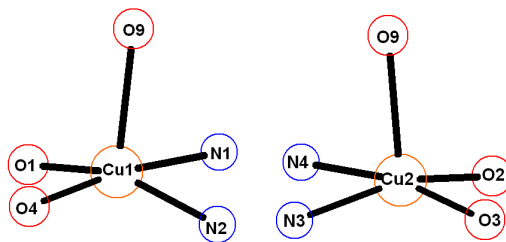


Figure 7.3 Geometry around Cu(1) and Cu(2) in **4.1**.

In these distorted square pyramids, the copper ions lie above the basal plane. The apical Cu-O bond lengths are longer than the corresponding basal Cu-O bond lengths. Selected bond lengths [\AA] and angles [$^\circ$] are summarized in Table 7.2.

Table 7.2 Selected bond lengths [Å] and angles [°] for **4.1**

Cu(1)-O(1)	1.930(2)	O(1)-Cu(1)-O(4)	92.75(9)
Cu(1)-O(4)	1.933(2)	O(1)-Cu(1)-N(1)	92.33(9)
Cu(1)-O(9)	2.285(2)	O(4)-Cu(1)-N(2)	90.69(9)
Cu(1)-N(1)	2.001(2)	N(1)-Cu(1)-N(2)	82.08(9)
Cu(1)-N(2)	2.015(2)	O(4)-Cu(1)-O(9)	94.73(7)
Cu(2)-O(3)	1.923(2)	O(1) -Cu(1)-O(9)	105.93(7)
Cu(2)-O(2)	1.935(2)	N(1) -Cu(1)-O(9)	90.44(8)
Cu(2)-O(9)	2.288(2)	N(2) -Cu(1)-O(9)	95.16(8)
Cu(2)-N(4)	2.002(2)	O(2)-Cu(2)-O(3)	93.41(8)
Cu(2)-N(3)	2.019(2)	O(2)-Cu(2)-N(4)	91.40(9)
		O(3)-Cu(2)-N(3)	90.40(8)
		N(4)-Cu(2)-N(3)	82.18(9)
		O(3)-Cu(2)-O(9)	94.75(7)
		O(2)-Cu(2)-O(9)	106.41(7)
		N(4)-Cu(2)-O(9)	93.25(8)
		N(3)-Cu(2)-O(9)	90.30(7)
		Cu(1)-O(9)-Cu(2)	96.00(6)

The two copper ions in a binuclear unit are linked by a coordinated water molecule and two pda ligands. These two pda ligands connect the binuclear unit to two different binuclear units forming a zigzag chain. The zigzag chain is shown in Figure 7.4 along with the perchlorate anions and water molecules. One of the perchlorate groups is disordered over three different positions.

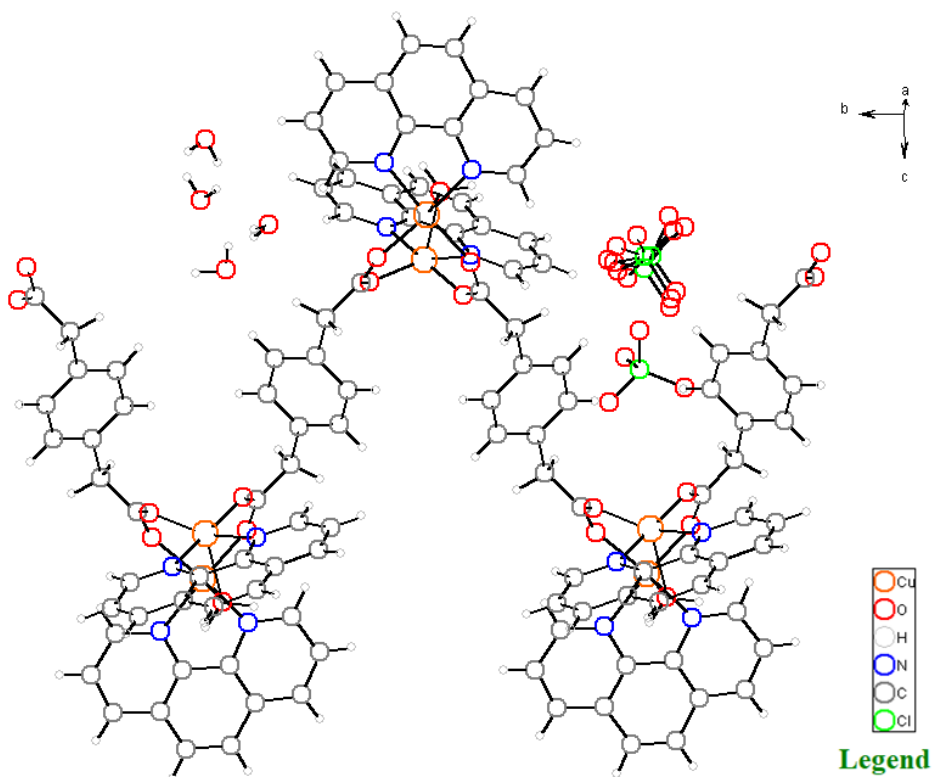


Figure 7.4 The zigzag chain of binuclear units of **4.1**. The hydrogen-bonded phenylene diacetic acid (H_2pda) molecule is removed for clarity, and the water molecules and the perchlorate counter ions are shown in two different sides of the figure.

The structure of **4.1** is similar to that of **HW2**. **HW2** was synthesized in the solvent mixture of water and methanol at 80 °C for 7 d with a ratio of 1:1 of all starting materials. The difference between the tetranuclear structure of **HW2** and the polymeric structure of **4.1** is shown in Figure 7.5. In **HW2** two pda ligands connect only one pair of binuclear units, whereas in **4.1** two pda ligands connect three binuclear units to make the zigzag chain.

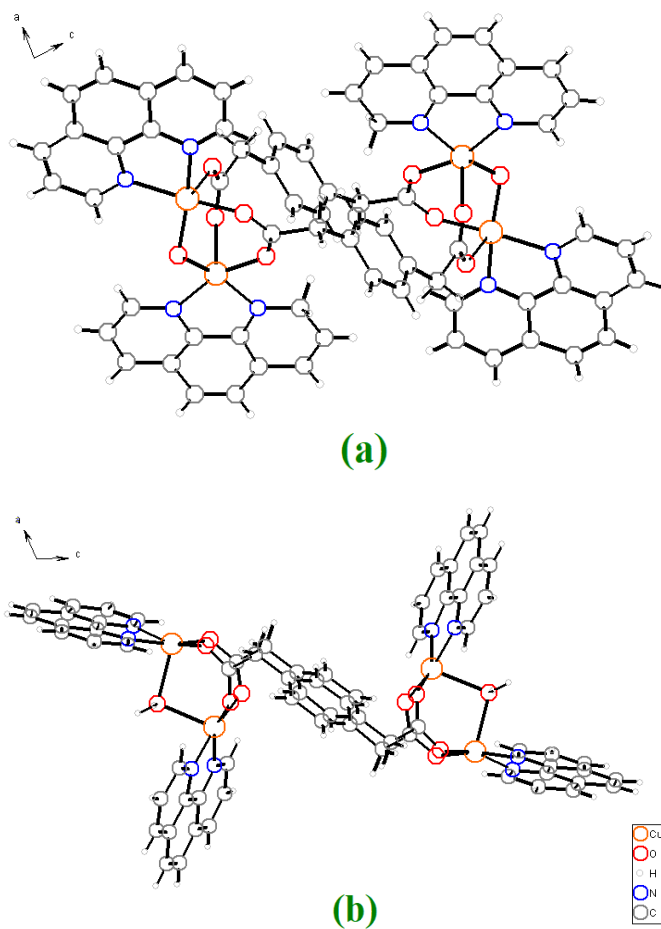


Figure 7.5 The tetranuclear unit consists of two binuclear parts connected through two pda ligands. Each binuclear unit contains copper centers with chelating phen ligand bridging by a water molecule and two pda ligands in ac-plane in (a) **HW2** structure and (b) **4.1**.

The aromatic phenanthroline rings are stacked on top of each other and hold the chains together. The distance between the aromatic planes $\approx 3.5 \text{ \AA}$ indicating a strong π - π interaction (Figure 7.6).

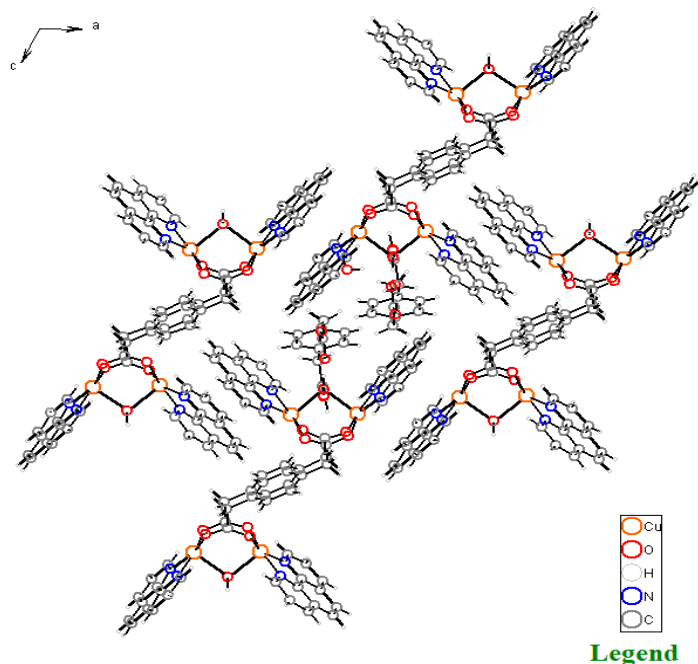


Figure 7.6 The π - π stacking interchain interactions.

7.3. Isolated Copper(II) Binuclear Coordination Compound

7.3.1. Synthesis of $[\text{Cu}_2(\text{phen})_2(\text{Hpda})_{0.175}(\text{CH}_3\text{CH}_2\text{pda})_{0.825}(\text{H}_2\text{O})] \cdot [\text{H}_2\text{O}]_{0.35} \cdot [\text{ClO}_4^-]_2$ (**4.2**)

Compound **4.2** was synthesized by a one-pot solvothermal reaction. The primary solutions were made the same as **3** (Section 6.2.1). 0.15 mmol (0.0291 g) of phenylene diacetic acid (H_2pda) was added to 1 mL of the solution of 0.1 M of $\text{LiOH} \cdot \text{H}_2\text{O}$ in the reaction vial. Then 7 mL of acetonitrile was added to the vial. The mixture was treated the same as **4.1**, and then was heated in the oven at 60 °C for 7 d. Blue blade-like crystals of **4.2** formed from the reaction mixture as a major phase, in < 35% yield, the minor phase contained the blue crystals of **1**, **4.1**, and an unknown light blue precipitate.

The **4.2** crystals were obtained from the reaction of the same starting materials in the solvent mixture of 4 mL of ethanol and 3 mL of water at 80 °C in 10 d.

7.3.2. Single Crystal X-ray Diffraction (SCXRD)

All measurements were made with the same method as described in Section 7.2.2. Final cell constants were refined using 5847 reflections having $I > 2\sigma(I)$, and these, along with other information pertinent to data collection and refinement, are listed in Table 7.3. The Laue symmetry was determined to be $2/m$, and from the systematic absences noted the space group was shown unambiguously to be $C2/c$. The asymmetric unit consists of one-half of a binuclear unit situated on a two-fold axis and one perchlorate anion. The metal-containing unit was found to be composed of two different species, one containing ethyl phenylene diacetate and the other containing phenylene diacetic acid hydrogen-bonded to solvent water molecules. Based on comparison of the isotropic displacement parameters involved, there is a ratio of 82.5:17.5 ethyl carboxylate:carboxylic acid molecules in this crystal. A strong π - π attraction exists between neighboring phenanthroline rings (with a distance of $\approx 3.5 \text{ \AA}$) along the c axis direction.

Table 7.3 Crystal data and structure refinement for **4.2**.

Empirical formula	$C_{47.3}H_{42.25}Cl_2Cu_2N_4O_{17.7}$
Formula Weight	1147.88 g mol ⁻¹
Temperature, Wavelength	123(2) K, 0.71073 Å
Crystal system, space group	Monoclinic, C2/c
Unit cell dimensions	$a = 22.397(3)$ Å, $b = 11.4243(1)$ Å, $c = 18.941(2)$ Å $\alpha = 90^\circ$, $\beta = 100.120(1)^\circ$, $\gamma = 90^\circ$
Cell Volume	4771.0(1) Å ³
Z, Calculated density	4, 1.598 g/cm ³
Crystal size	0.20 × 0.15 × 0.05 mm ³
Index ranges	$-27 \leq h \leq 29$, $-15 \leq k \leq 15$, $-23 \leq l \leq 25$
2 θ range for data collection	3.694 - 56.682°
Absorption coefficient	1.085 mm ⁻¹
F(000)	2351.0
Reflections collected / unique	14286 / 5847 [$R_{int} = 0.0275$, $R_{sigma} = 0.0379$]
Refinement method	Full-matrix least-squares on F ²
Data/restraints/parameters	5847 / 127 / 384
Goodness-of-fit on F ²	1.030
Final R indices [$I \geq 2\sigma(I)$]	$R_1 = 0.0418$, $wR_2 = 0.0928$
R indices (all data)	$R_1 = 0.0570$, $wR_2 = 0.0992$
Largest diff. peak and hole	0.77 and 0.45 e.Å ⁻³

7.3.3. Crystal Structure

The binuclear unit of the crystal structure of $[\text{Cu}_2(\text{phen})_2(\text{Hpda})_{0.35}(\text{CH}_3\text{CH}_2\text{pda})_{1.65}(\text{H}_2\text{O})] \cdot [\text{H}_2\text{O}]_{0.35} \cdot [\text{ClO}_4^-]_2$ (**4.2**) consists of two copper atoms each bonded to a bidentate phenanthroline ligand. The copper atoms are linked together through a water molecule and two 2-(4-(carboxymethyl)phenyl)acetate (Hpda) ligands. The Hpda ligand occupancy is 17.5%, with a hydrogen bond to $\text{H}_2\text{O}(8)$. This water molecule also has two hydrogen bonds to another water molecule ($\text{H}_2\text{O}(9)$) and the oxygen of the perchlorate ($\text{O}_3\text{Cl}-\text{O}(7)$) ion. The ethyl ester form of the pda has an occupancy of 82.5% (Figure 7.7).

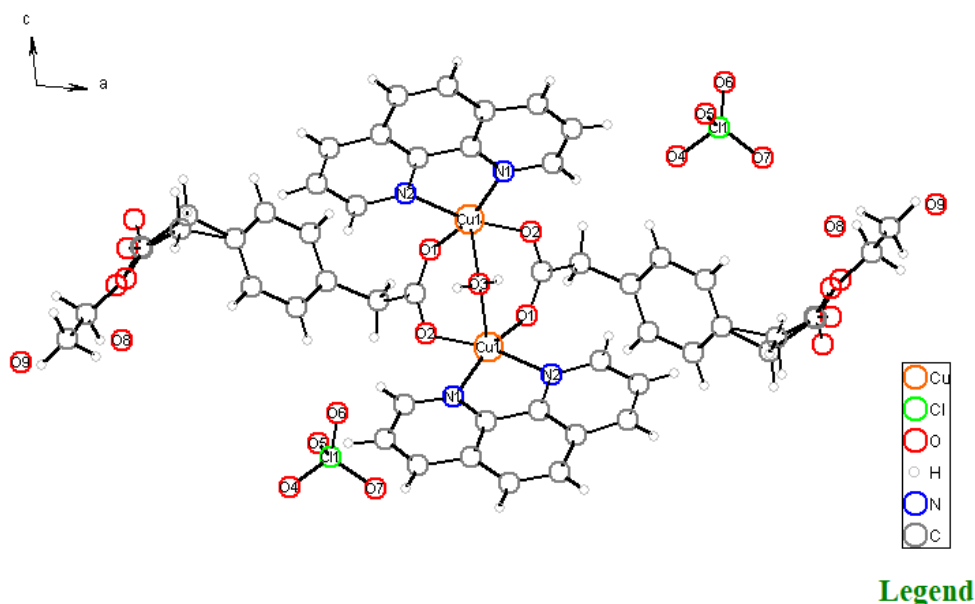


Figure 7.7 The view of the asymmetric unit of an isolated binuclear unit of **4.2** with two different occupancy percentages.

Each pda ligand in the **4.2** structure acts as a bidentate ligand. One end of the pda ligand is deprotonated and connects two copper ions. The other end of the pda (17.5% occupancy) remains protonated with hydrogen bonds to water molecules, 82.5% is occupied by the ethyl ester.

The coordination of the copper ion is distorted square pyramidal. The copper ion is coordinated to two nitrogen atoms from 1,10-phenanthroline ligand in the basal plane of the square pyramid and to two oxygen ions from two pda ligands. The O(3) from the coordinated water is the bridging oxygen ion is in the apical position (Figure 7.8).

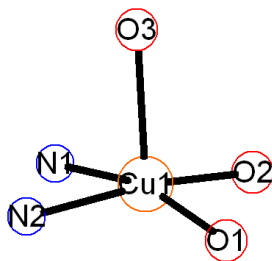


Figure 7.8 Geometry around Cu ion in **4.2**.

The copper ions lie above the basal plane and the apical Cu-O bond lengths are longer than the corresponding basal Cu-O bonds. Selected bond lengths [\AA] and angles [$^\circ$] are summarized in Table 7.4.

Table 7.4 Selected bond lengths [\AA] and angles [$^\circ$] for **4.2**

Cu(1)-O(1)	1.9359(2)	O(1)-Cu(1)-O(2)	90.52(7)
Cu(1)-O(2)	1.9391(2)	O(2)-Cu(1)-N(1)	91.33(8)
Cu(1)-O(3)	2.629(2)	O(1)-Cu(1)-N(2)	92.83(8)
Cu(1)-N(1)	2.004(2)	N(1)-Cu(1)-N(2)	82.79(8)
Cu(1)-N(2)	2.016(2)	O(2)-Cu(1)-O(3)	96.28(6)
Cu(2)-O(3)	1.923(2)	O(1) -Cu(1)-O(3)	105.13(7)
		N(1) -Cu(1)-O(3)	89.79(7)
		N(2) -Cu(1)-O(3)	92.71(7)

The oxygen atom on ethyl acetate or acetic acid from one binuclear unit is hydrogen bonded to the coordinated water molecule of another binuclear unit. The distances between O(3) \cdots O(4), O(3) \cdots O(4'), H(3) \cdots O(4), and H(3) \cdots O(4') are 2.71, 2.67, 2.02, and 1.96 \AA , respectively. Angles of O(3)-H(3) \cdots O(4) and O(4') are 170.16 $^\circ$ and 164.26 $^\circ$, respectively. The distances and angles display the intermolecular hydrogen bonds. (Figure 7.9).

The structure of **4.2** is similar to that of **4.1**. The difference between their structures is related to the complete deprotonation of phenylene diacetic acid in **4.1** and partial deprotonation in **4.2**. In **4.2**, 82.5% of the Hpda molecules react with the ethanol to form the ethyl ester.

A π - π stacking interaction between the phenanthroline ligands, connects the binuclear units. The distance between the aromatic planes is ≈ 3.3 \AA which indicates a strong π - π electrostatic interaction (Figure 7.10).

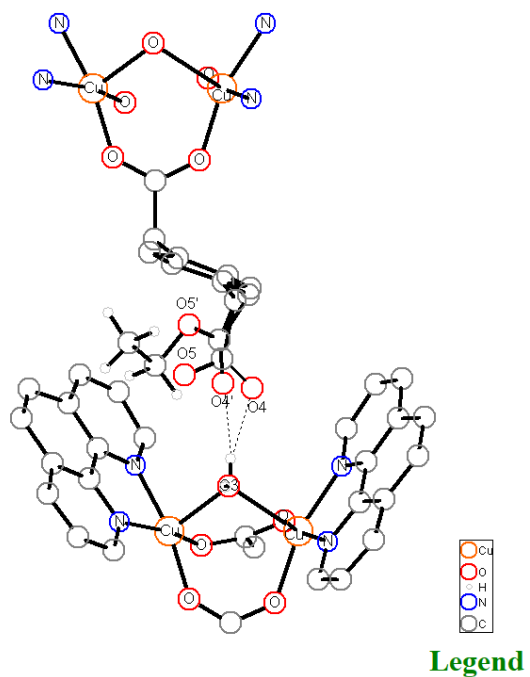


Figure 7.9. The hydrogen bond between a coordinated water molecule and O4 or O4' in **4.2**.

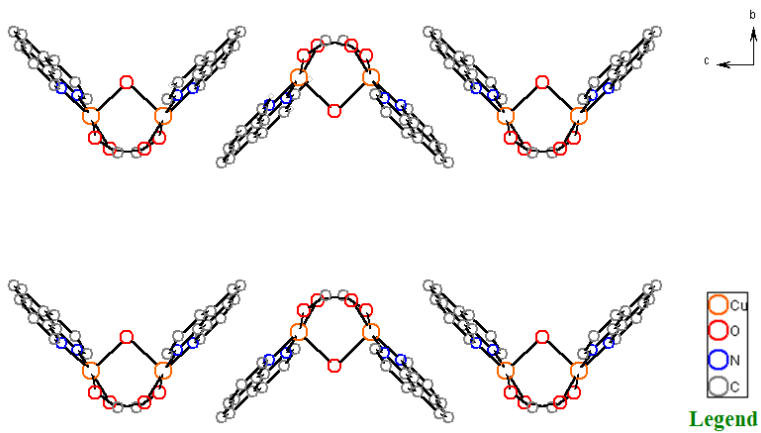


Figure 7.10 The π - π stacking intermolecular interaction along the c-axis.

7.4. Copper(II) Tetranuclear Coordination Polymer in Acetonitrile

7.4.1. Synthesis of $[\text{Cu}_4(\text{phen})_4(\text{pda})_2(\text{H}_2\text{O})_2] \cdot [\text{ClO}_4]_4 \cdot [\text{H}_2\text{O}]_2 \cdot [\text{CH}_3\text{CN}]_4$ (**5.1**)

Compound **5.1** was synthesized by a one-pot solvothermal reaction. The primary solutions were made the same as **3** (Section 6.2.1). 0.1 mmol (0.0194 g) of phenylene diacetate (pda) was added to 1 mL of the solution of 0.1 M of $\text{LiOH} \cdot \text{H}_2\text{O}$ in the reaction vial. Then 7 mL of acetonitrile was added. The mixture was treated the same as **4.1**, and then was heated in the oven at 65-70 °C for 7 d. Blue plate-like crystals of **5.1** formed from the reaction mixture as a major phase, in < 30% yield, the minor phase contained the blue crystals of **1**, and an unknown dark green precipitate.

7.4.2. Single Crystal X-ray Diffraction (SCXRD)

All measurements were made with the same method as described in Section 7.2.2. The exposure time was 90 s frame⁻¹. Final cell constants were refined using 4222 reflections having $I > 4\sigma(I)$, and these, along with other information pertinent to data collection and refinement, are listed in Table 7.5. The Laue symmetry was determined to be -1, and the space group was shown to be either P1 or P-1.

The asymmetric unit consists of one-half cation situated on inversion center, along with two perchlorate anions, two acetonitrile solvent molecules, and a solvent molecule water all in general positions. One of the perchlorates and the solvent water molecule were found to be disordered over two slightly different orientations. The disorder was modeled by the refinement of ideal rigid bodies, with the population factors estimated by comparison of isotropic displacement parameters. The disordered water molecule positions could not be refined independently due to the very small amount of electron density at the hydrogen locations, and so the hydrogens were fixed at positions which formed the most reasonable hydrogen bonding parameters.

Table 7.5 Crystal data and structure refinement for **5.1**

Empirical formula	$C_{76} H_{68} Cl_4 Cu_4 N_{12} O_{28}$
Formula Weight	1993.38 g mol ⁻¹
Temperature, Wavelength	123(2) K, 0.71073 Å
Crystal system, space group	Triclinic, $P\bar{1}$
Unit cell dimensions	$a = 9.808(1) \text{ \AA}$, $b = 12.935(1) \text{ \AA}$, $c = 16.538(2) \text{ \AA}$ $\alpha = 72.182(2)^\circ$, $\beta = 78.198(2)^\circ$, $\gamma = 89.386(2)^\circ$
Cell Volume	1952.2(3) Å ³
Z, Calculated density	1, 1.696 g/cm ³
Crystal size	0.25 × 0.15 × 0.04 mm ³
Index ranges	$-11 \leq h \leq 9$, $-15 \leq k \leq 15$, $-18 \leq l \leq 19$
Theta range for data collection	1.77 to 24.72°
Absorption coefficient	1.306 mm ⁻¹
F(000)	1016
Reflections collected / unique	9942 / 6597 [R(int) = 0.0258]
Refinement method	Full-matrix least-squares on F ²
Data/restraints/parameters	4222 / 14 / 536
Goodness-of-fit on F ²	1.008
Final R indices [I>4σ(I)]	R1 = 0.0443, wR2 = 0.1057
R indices (all data)	R1 = 0.0753, wR2 = 0.1279
Largest diff. peak and hole	1.080 and -1.150 e.Å ⁻³

7.4.3. Crystal Structure

The tetranuclear structure of $[\text{Cu}_4(\text{phen})_4(\text{pda})_2(\text{H}_2\text{O})_2] \cdot [\text{ClO}_4^-]_4 \cdot [\text{H}_2\text{O}]_2 \cdot [\text{CH}_3\text{CN}]_4$ (**5.1**) consists of two binuclear units of copper ions. Each copper(II) ion is attached to a bidentate 1,10-phenanthroline (phen) chelating ligand. The copper ions are linked together through phenylene diacetate (pda) ligands.

In a binuclear unit, the terminal copper ion is coordinated to a water molecule ($\text{H}_2\text{O}(1)$). The copper ions are connected through two pda ligands in a binuclear unit. An oxygen atom from a pda ligand (O(5)) connects the binuclear units to each other. Figure 7.11 shows the tetranuclear molecular structure of **5.1**.

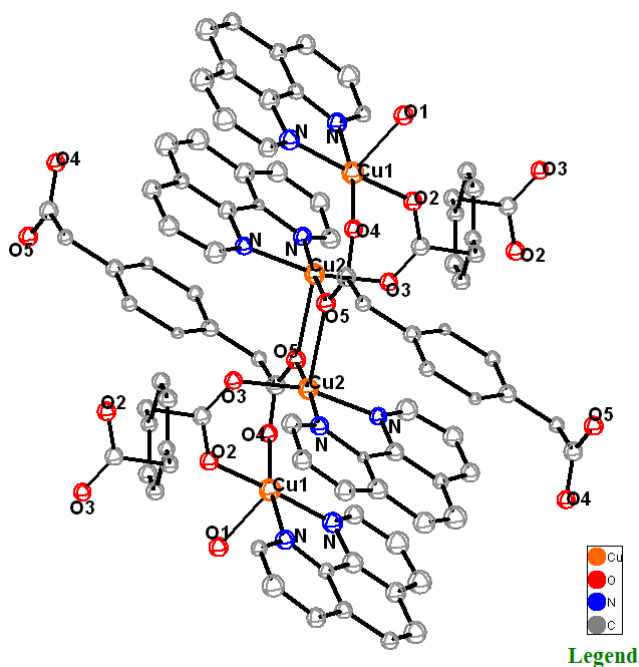


Figure 7.11 The view of the asymmetric unit of **5.1** with thermal ellipsoids at the probability of 50%.

Hydrogen atoms, solvent molecules, and counter ions are removed for clarity.

The copper ions coordination is distorted square pyramidal. Each copper ion is coordinated to two nitrogen atoms from the bidentate 1,10-phenanthroline (phen) ligand in the basal plane of the

square pyramid and to three oxygen ions. Two oxygen ions in the basal planes are from the pda ligands of the dinuclear unit. The apical position of Cu(1) is occupied by a coordinated water molecule. The third oxygen atom of the apical position of Cu(2) is from a pda ligand in the adjacent binuclear unit (O5') (Figure 7.12).

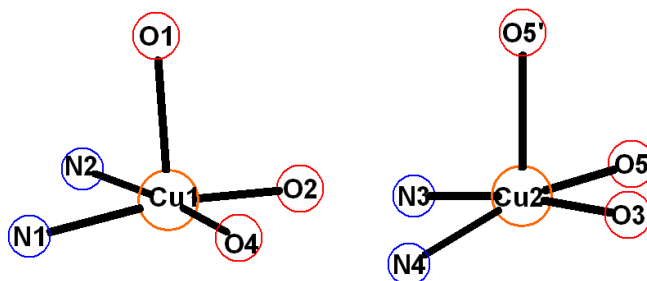


Figure 7.12 Geometry around Cu(1) and Cu(2) in **5.1**.

In these distorted square pyramidal geometries, the copper ions lie above the basal plane. The apical Cu-O bond lengths are longer than the corresponding basal Cu-O bond lengths. Selected bond lengths [\AA] and angles [$^\circ$] are summarized in Table 7.6.

Table 7.6 Selected bond lengths [Å] and angles [°] for **5.1**

Cu(1)-O(2)	2.001(1)	O(1)-Cu(1)-O(2)	98.14(3)
Cu(1)-O(4)	1.948(1)	O(1)-Cu(1)-O(4)	90.43(3)
Cu(1)-O(1)	2.212(1)	O(1)-Cu(1)-N(1)	92.39(4)
Cu(1)-N(1)	1.995(1)	O(1)-Cu(1)-N(2)	91.08(4)
Cu(1)-N(2)	2.001(1)	O(2)-Cu(1)-O(4)	93.25(4)
Cu(2)-O(3)	1.985(1)	O(2)-Cu(1)-N(2)	91.95(4)
Cu(2)-O(5)	1.959(1)	N(1)-Cu(1)-N(2)	82.47(4)
Cu(2)-O(5')	2.295(2)	O(4)-Cu(1)-N(1)	92.00(4)
Cu(2)-N(3)	2.008(1)	O(3)-Cu(2)-O(5')	79.54(3)
Cu(2)-N(4)	1.990(1)	O(5)-Cu(2)-O(5')	94.06(4)
		N(3)-Cu(2)-O(5')	106.78(4)
		N(4)-Cu(2)-O(5')	100.77(3)
		O(3)-Cu(2)-O(5)	89.63(4)
		O(5)-Cu(2)-N(3)	91.50(4)
		N(3)-Cu(2)-N(4)	82.94(4)
		N(4)-Cu(2)-O(3)	94.39(4)
		Cu(1)-O(5')-Cu(2)	100.46(4)

The coordinated water molecule is hydrogen-bonded to a solvent water molecule with the O...O distance of 2.7 Å. In a unit cell, besides the tetranuclear copper(II) coordination compound unit, there are four perchlorate anions, four acetonitrile and two water molecules (Figure 7.13).

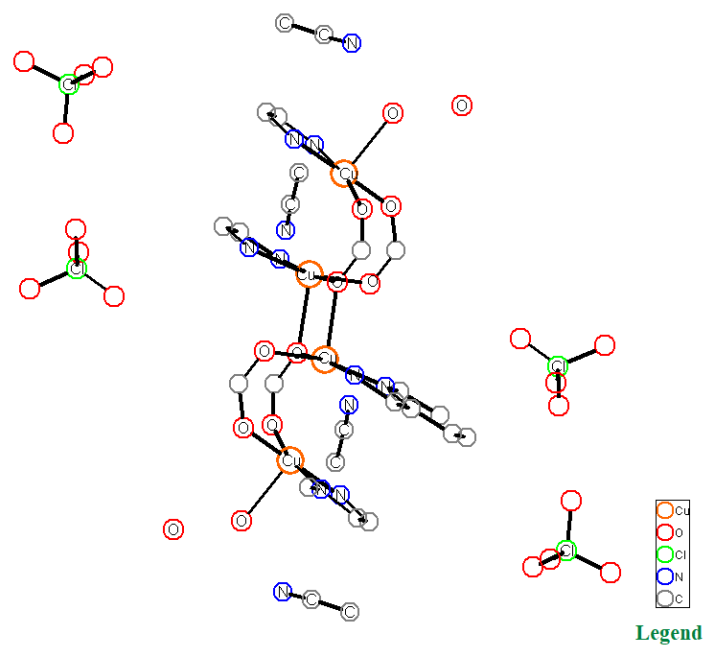


Figure 7.13 Solvent molecules of water and acetonitrile in unit cell and four perchlorate anions in **5.1**.

The carbon atoms of the organic ligands are removed for clarity.

Each pda ligand acts as tetra- or hexadentate linker. The pda ligands direct the crystal growth in two different directions to make a two-dimensional polymer. Figure 7.14 shows that how the pda linkers bridge the tetranuclear units and to form a two-dimensional coordination polymer.

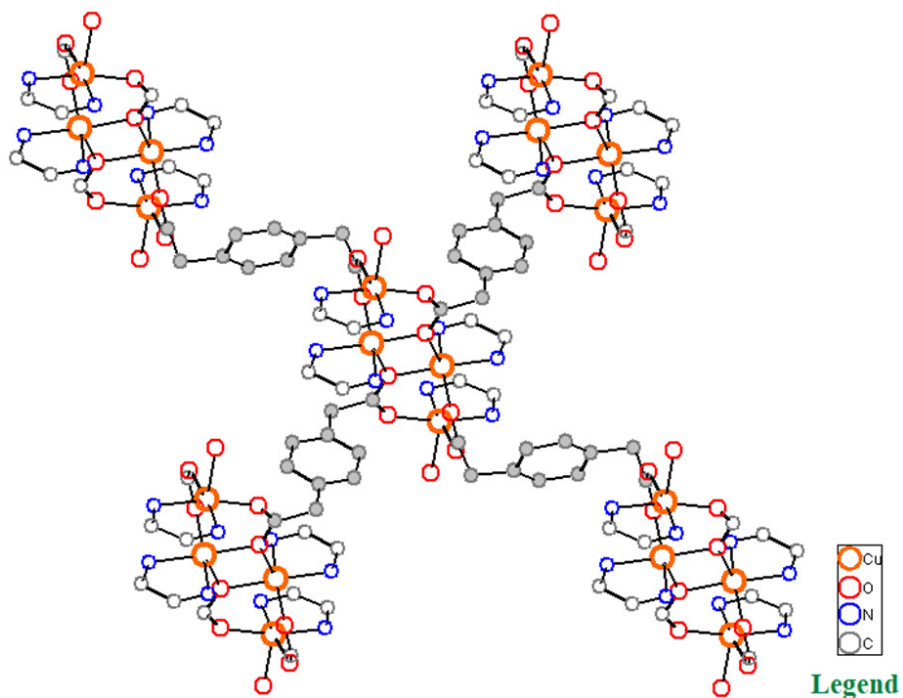


Figure 7.14 A tetranuclear unit connects to four tetranuclear units through phenylene diacetate (pda) ligands. The pda linkers are shown with filled gray circles.

The phenanthroline rings and two pda ligands phenyl rings stack to make the third dimension. The distance between the aromatic planes $\approx 3.4\text{-}3.6 \text{ \AA}$, which indicates strong $\pi\text{-}\pi$ stacking. Figure 7.15 shows the stacking of the aromatic rings.

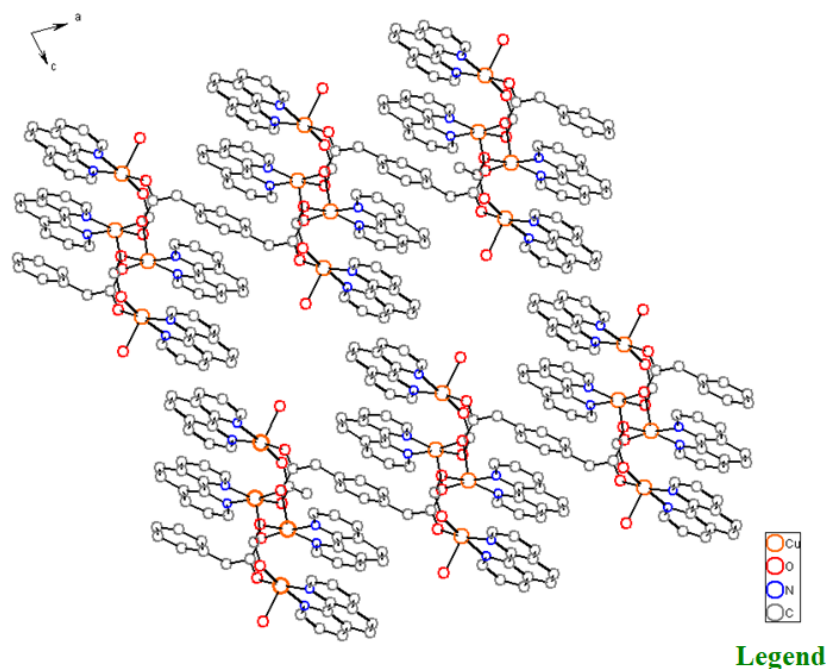


Figure 7.15 The π - π stacking interchain interactions of the aromatic ring in **5.1**.

7.5. Copper(II) Tetranuclear Coordination Polymer in Aqueous Solution

7.5.1. Synthesis of $[\text{Cu}_4(\text{phen})_4(\text{pda})_2(\text{H}_2\text{O})_2] \cdot [\text{ClO}_4]_4 \cdot [\text{H}_2\text{O}]_{0.24}$ (**5.2**)

Compound **5.2** was synthesized by a one-pot hydrothermal reaction. The primary solutions were made the same as **3** (Section 6.2.1). 0.1 mmol (0.0194 g) of phenylene diacid (pda) was added to 1 mL of the solution of 0.1 M of $\text{LiOH} \cdot \text{H}_2\text{O}$ in the Teflon liner. Then 4 mL of ethanol and 3 mL of water were added. The mixture was treated the same as **4.1**, and then was capped in a Teflon liner and sealed in a stainless-steel autoclave reactor. The reaction mixture was heated in the oven at 110 °C for 10-14 d. Blue needle-like crystals of **5.2** formed from the reaction mixture as a major phase, in < 30% yield, the minor phase contained the blue crystals of **1**, and **4.1** and unknown light blue precipitate.

7.5.2. Single Crystal X-ray Diffraction (SCXRD)

All measurements were made with the same method as described in Section 7.2.2. The exposure time was 40 s frame⁻¹. The quality of this crystal was poor due to the crystal cracks and twinning. Final cell constants were refined using 5841 reflections having $I > 2\sigma(I)$, and these, along with other information pertinent to data collection and refinement, are listed in Table 7.7.

The asymmetric unit consists of one-half cation situated on an inversion center, along with two perchlorate anions, and a molecule of solvent with 12% occupancy, most likely due to solvent evaporation during crystal handling.

Table 7.7 Crystal data and structure refinement for **5.2**

Empirical formula	$C_{34} H_{26} Cl_2 Cu_2 N_4 O_{13.12}$
Formula Weight	898.5 g mol ⁻¹
Temperature, Wavelength	123(2) K, 0.71073 Å
Crystal system, space group	Triclinic, $P\bar{1}$
Unit cell dimensions	$a = 10.214(4)$ Å, $b = 12.294(5)$ Å, $c = 15.802(6)$ Å $\alpha = 98.758(5)^\circ$, $\beta = 103.467(5)^\circ$, $\gamma = 114.142(5)^\circ$
Cell Volume	1691.2(1) Å ³
Z, Calculated density	2, 1.764 g/cm ³
Crystal size	0.2 × 0.05 × 0.01 mm ³
Index ranges	$-12 \leq h \leq 12$, $-14 \leq k \leq 14$, $-17 \leq l \leq 18$
Theta range for data collection	1.890 to 25.172°
Absorption coefficient	1.493 mm ⁻¹
F(000)	910
Reflections collected / unique	8252 / 5841 [R(int) = 0.0555]
Refinement method	Full-matrix least-squares on F ²
Data/restraints/parameters	5841 / 501 / 505
Goodness-of-fit on F ²	0.996
Final R indices [I>2σ(I)]	R1 = 0.0726, wR2 = 0.1619
R indices (all data)	R1 = 0.1356, wR2 = 0.1989
Largest diff. peak and hole	0.905 and -1.094 e.Å ⁻³

7.5.3. Crystal Structure

The connectivity of atoms in a tetranuclear structure of $[\text{Cu}_4(\text{phen})_4(\text{pda})_2(\text{H}_2\text{O})_2] \cdot [\text{ClO}_4^-]_4 \cdot [\text{H}_2\text{O}]_{0.24}$ (**5.2**) is similar to that in **5.1**, with four copper ions, each attached to a bidentate 1,10-phenanthroline (phen) ligand and linked together through phenylene diacetate (pda) ligands. The terminal copper ions are coordinated to a water molecule. The bond length and angles in the tetranuclear units of **5.1** and **5.2** are different (Figure 7.16).

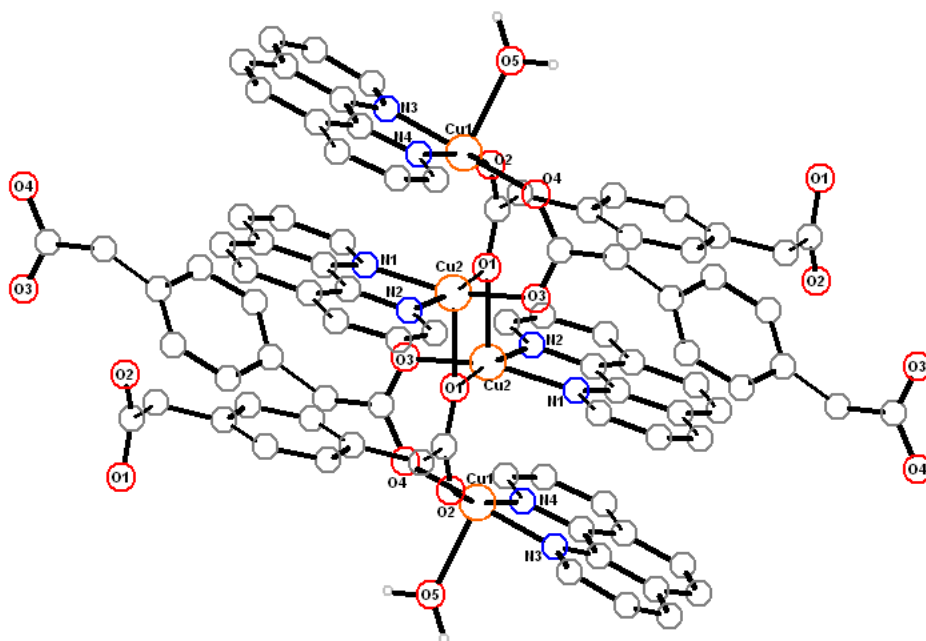


Figure 7.16 The view of the asymmetric unit of a tetranuclear unit of **5.2** Hydrogen atoms, solvent molecules, and counter ions are removed for clarity.

The copper ions coordination is distorted square pyramidal with the same atom connectivity found in **5.1** (Figure 7.17).

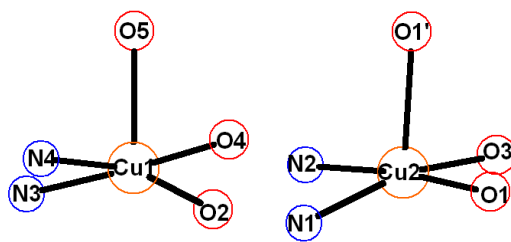


Figure 7.17 Geometry around Cu(1) and Cu(2) in **5.2**.

The copper ions lie above the basal plane and the apical Cu-O bond lengths are longer than the corresponding basal Cu-O bonds. The O(1) and O(1') are the oxygen atoms that connect the binuclear parts to each other. The O(5) atom is from the coordinated water molecule. Nitrogen atoms are from phen ligand. Selected bond lengths [\AA] and angles [$^\circ$] are summarized in Table 7.8.

Table 7.8 Selected bond lengths [\AA] and angles [$^\circ$] for **5.2**

Cu(1)-O(2)	1.971(5)	O(5)-Cu(1)-O(2)	90.87(1)
Cu(1)-O(4)	1.915(8)	O(5)-Cu(1)-O(4)	91.04(1)
Cu(1)-O(5)	2.176(7)	O(5)-Cu(1)-N(4)	102.11(2)
Cu(1)-N(4)	2.022(6)	O(5)-Cu(1)-N(3)	89.19(2)
Cu(1)-N(3)	1.968(8)	O(2)-Cu(1)-O(4)	93.82(2)
Cu(2)-O(1)	1.953(7)	O(2) -Cu(1)-N(3)	91.44(2)
Cu(2)-O(3)	1.957(8)	N(3) -Cu(1)-N(4)	82.72(2)
Cu(2)-O(1')	2.315(9)	O(4) -Cu(1)-N(4)	92.09(2)
Cu(2)-N(2)	1.994(7)	O(1)-Cu(2)-O(1')	77.42(1)
Cu(2)-N(1)	2.003(8)	O(3)-Cu(2)-O(1')	97.73(2)
		N(2)-Cu(2)-O(1')	106.39(2)
		N(1)-Cu(2)-O(1')	97.73(1)
		O(1)-Cu(2)-O(3)	95.59(2)
		O(3)-Cu(2)-N(2)	92.32(2)
		N(1)-Cu(2)-N(2)	82.84(2)
		N(1)-Cu(2)-O(1)	91.25(2)
		Cu(1)-O(1')-Cu(2)	102.58(2)

The unit cell contains the tetranuclear unit, four perchlorate anion and two water molecules. No acetonitrile molecules are present in **5.2** in contrast to **5.1** (Figure 7.18).

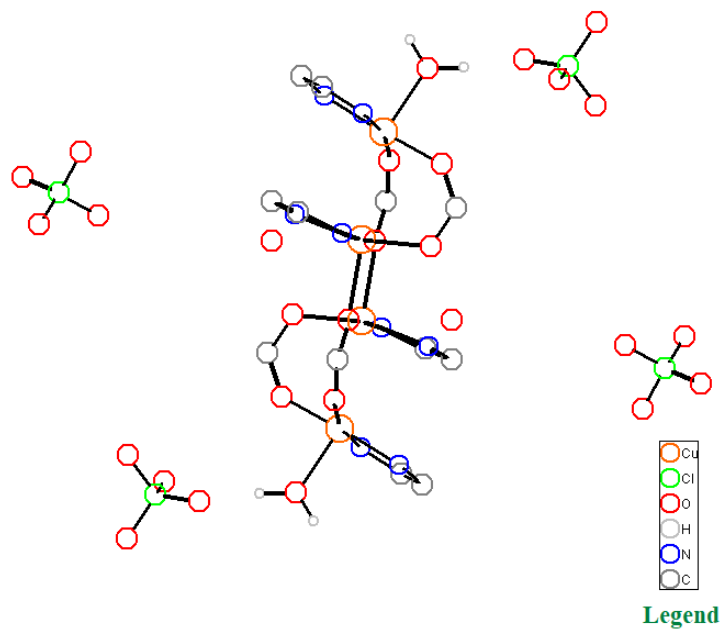


Figure 7.18 Water molecules and four perchlorate anions in the unit cell of **5.2**. The carbon atoms of the organic ligands are removed for clarity.

In **5.2**, the directionality of two types of pda ligands are different from **5.1**. Figure 7.19 shows the difference of the directionality of the pda ligands in **5.1** and **5.2**.

Each pda ligand acts as a tetra- or hexadentate linker. Each tetranuclear entity is connected to other tetranuclear units through pda linkers, hence, each tetranuclear molecule connects to four other tetranuclear units. Figure 7.20 shows that how the pda linkers are bridging between the tetranuclear units and make the two-dimensional (2-D) structure of **5.2**.

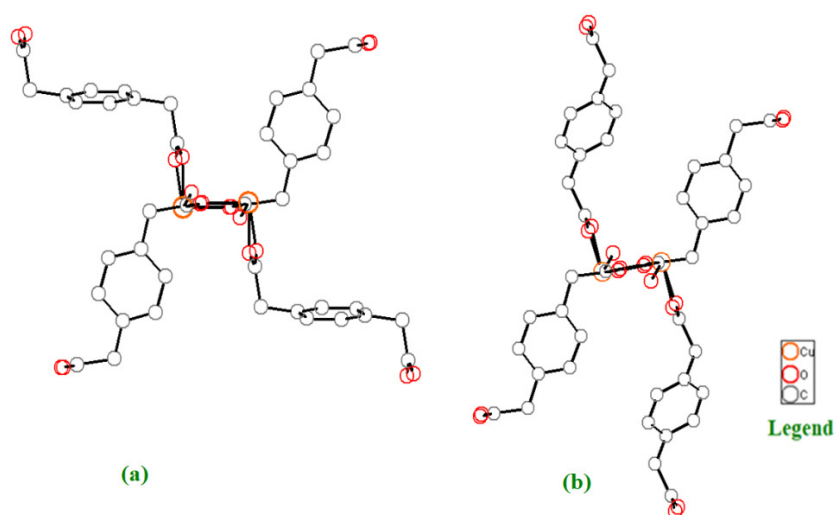


Figure 7.19 The view of the pda ligands directions in a tetranuclear unit of (a) **5.1** and (b) **5.2**.

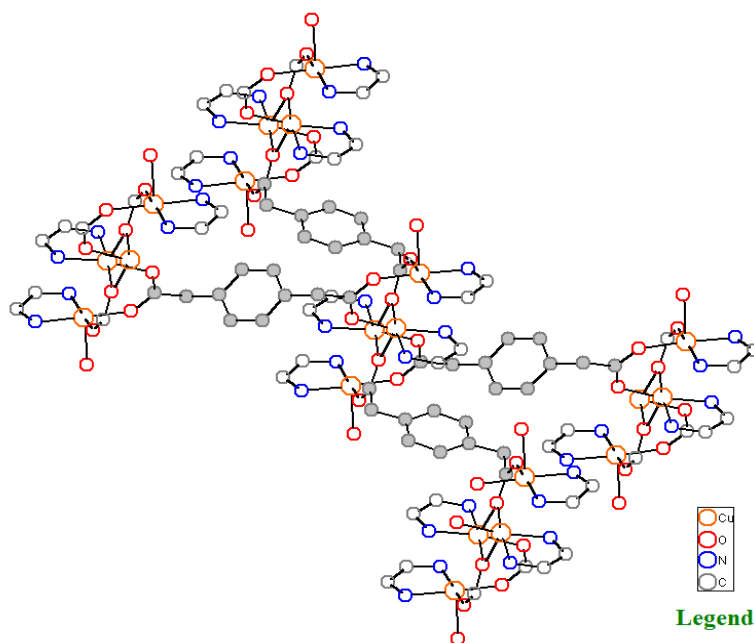


Figure 7.20 A tetranuclear unit in **5.2** connects to four tetranuclear units through phenylene diacetate (pda) ligands, making 2-D coordination polymer. The pda linkers are shown with filled gray circles.

The coordinated water molecule is hydrogen bonded to two perchlorate anions and each anion is hydrogen bonded to the other water molecule from an adjacent tetranuclear unit. The phenanthroline rings and the phenyl groups from two pda ligands stack. The distance between the aromatic planes \approx

3.3-3.5 Å indicates a strong π - π interaction. The hydrogen bonding and the π - π interactions in **5.2** further extend the structure. Figure 7.21 shows the stacking of the aromatic rings and the hydrogen bond.

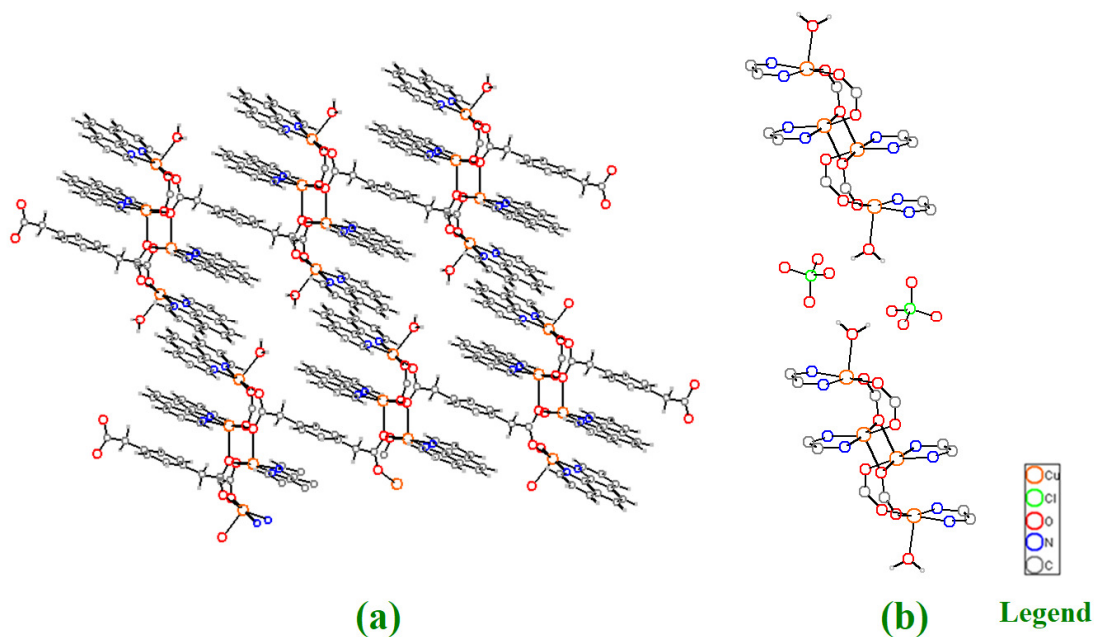


Figure 7.21 (a) The π - π stacking interactions of the aromatic ring and (b) the hydrogen bond of terminal coordinated water to perchlorate ions in **5.2**.

7.6. Conclusion

Four new Copper(II) coordination compounds were synthesized using two ligands of pda and phen. **4.1** and **4.2** consist of a binuclear copper(II) units. This unit is linked to the other units in a zigzag chain manner with the pda linker in **4.1**. However, due to the incomplete deprotonation of pda ligand in the units are remained isolated in the **4.2** structure.

5.1 and **5.2** are the tetranuclear two-dimensional copper(II) coordination polymers with the different solvent molecules in their unit cell. They both contain lattice water, and **5.1** comprises

acetonitrile as well. The electrostatic π - π stacking interactions and the hydrogen bonds are making the third dimension of their structure.

These four compounds cannot be synthesized in a single phase. All of them crystallized along with impure phases, such as **1**. Clearly there is not much difference in the stability of them. Therefore, secluding a condition to synthesize a single phase of them would not be simple.

Chapter 8. Conclusion and Future Work

8.1 Conclusion

Polynuclear coordination compounds attract attention due to their diverse structural properties and a wide range of potential applications in biology, physics, and materials science^{303–307}. In recent years, remarkable progress has been made in determining magneto-structural correlations in these compounds. Different types of ligands can be used to build new structures^{308–310}. Among transition metal complexes, the chemistry of the copper compounds due to their interesting structures arising from various coordination modes and often unusual magnetic properties has been of interest for many years^{103,118,311}. Furthermore, anticancer effects is one of the fundamental subjects of recent researches^{12,26,312}. The magnetic characteristics arise from the exchange coupling established between the Cu²⁺ centers with singly occupied orbitals. These compounds are applicable as molecular conductors, single-molecule transistors, and molecular magnet memories^{313,314}.

Much of the attention on polynuclear metal compounds has been dedicated to the magnetic properties of di- or polynuclear copper(II) ions with flexible coordination spheres together with multidentate ligands. The magnetic properties originate from the local interactions between all the active centers. A vast effort has been devoted to the assessment, explanation, and understanding of the factors leading to the magnitude and sign of these local interactions and how they result in the overall magnetic behavior^{118,315–319}.

The first chapter of this dissertation has a closer look at the transition metal complexes and specifically copper(II) coordination compounds. The structural features and the applications of copper(II) complexes in porous coordination polymers and pharmacy are discussed in the first chapter. The motivation for the research stems from earlier work in our group, which led to the successful

synthesis and anticancer investigation on two copper coordination compounds ¹⁰³. Later, the compounds which were synthesized using two specific ligands, phen (1,10-phenanthroline) and pda (1,4-phenylene diacetate) had interesting magnetic properties. The second chapter provides a comprehensive literature review on the magnetic behavior of copper(II) complexes based on their structural features, and the models proposed to study their magnetic behavior. Some examples of each type of structure and their coupling constants are documented in the second chapter.

In this work, the syntheses of seven new copper(II) coordination compounds have been reported. All syntheses took place in two steps, preparing the initial solvents and mixing them in order. To optimize the conditions to produce phase pure compounds in high yield and high-quality single crystals, different variables were investigated. The concentrations of the initial solutions, the order of addition, the amount of solvent and the reaction time were optimized by designing several series of reactions. Then the optimized values of these variables were kept constant and the type of solvent, temperature and amount of starting materials varied. The main synthesis conditions used for compounds **1** to **5.2** are summarized in Table 8.1.

Table 8.1 The main syntheses condition with the highest yield of compounds.

Compound	Cu(ClO ₄) ₂ .6H ₂ O (mmol)	pda (mmol)	phen (mmol)	LiOH (mmol)	Solvent (mL)	Temperature (°C)
1	0.2	0.1	0.2	0.1	ethanol:water 4:3	r.t
2	0.2	0.2	0.2	0.4	acetonitrile 7	60
3	0.2	0.01	0.2	0.2	ethanol:water 4:3	80
4.1	0.2	0.1	0.2	0.2	THF 7	60
4.2	0.2	0.15	0.2	0.2	acetonitrile 7	60
5.1	0.2	0.1	0.2	0.2	acetonitrile 7	70
5.2	0.2	0.1	0.2	0.2	Ethanol:water 4:3	110

In reactions that result in the formation of **1**, higher temperature leads to impurity phases. The major impurity phases in water and ethanol mixture at 80, 110 and 120 °C are **4.1**, **4.2** and **5.2**, respectively. In acetonitrile, by changing the temperature from 60 to 70 °C, the major phase is changed from **1** to **5.1**. The molar ratio of pda/LiOH is higher in a synthesis method forming **4.2** as a major phase in compare with **4.1**. This causes the pda ligand in **4.2** to make individual molecules. These individual molecules in **4.2** are attached to make the zigzag chains in **4.1**. Compound **2** was synthesized using more lithium hydroxide. This may cause complete pda deprotonation which results in the zigzag chain of compound **2**. The pda ligand is not including in the structure of **3**, however, the presence of a little amount of pda or any of 1,4-naphthalene dicarboxylic acetate (1,4-ndc), 2,7-naphthalene dicarboxylic acetate (2,7-ndc) or 1,4,5,8- naphthalene tetracarboxylic acetate (ntc) dicarboxylate is necessary to form **3**. The pure phase of **3** was attained using 0.01 mmol of 2,7-ndc.

Compound **1-3** could be obtained as a single-phase using a solvothermal reaction, a simple filtration and washing with a solvent afterward. Powder X-ray Diffraction (PXRD) indicates the phase purity of **1**, **2**, and **3**. IR, Raman, TGA and chemical analysis confirmed the structural characterization. The magnetic susceptibility of these three compounds was measured. Based on their structure, models were selected to fit the experimental data. The coupling constants were determined from the fitting and were assigned by reviewing data for similar compounds.

Compound **1** is a trinuclear copper(II) coordination polymer and each copper is in a distorted square-pyramidal coordination environment. **1** could be synthesized as a single-phase compound at room temperature. The three copper centers in **1** interact magnetically. A 2-J model fitted well ($J_1 = -51.8 \text{ cm}^{-1}$, $J_2 = +22.9 \text{ cm}^{-1}$) the experimental data well and showed one ferromagnetic interaction through super-exchange through an oxygen bridging atom, and another antiferromagnetic interaction. The first J value was explained with the copper acetate model. The Goodenough–Kanamori–Anderson (GKA) rule gives a good model to describe the second J-value. The magnetic data shows that the total spin of the ground state is $1/2$.

Compound **2**, consists of copper(II) zigzag chains. The chains are parallel within a layer, and anti-parallel with a slight shift by moving in between the layers. The chains are considered as one-dimensional compounds. Three different magnetic interactions can be considered in **2**; within a chain through pda ligands (intrachain), within a layer between the chains (intralayer), and between the layers (interchain). However, because of the long-distance (9.5 \AA) between the intralayer copper centers and the absence bridging linkers to mediate the magnetic interactions between the chains of a layer, no coupling constant were considered for intralayer copper centers. The χ^{-1} vs. T plot above 100 K follows the Curie-Weiss law. The positive value of θ (Weiss constant) shows an intramolecular (intrachain) coupling constant. The model that was used to analyze the magneto-structure of **2**, was the Bonner-Fisher²¹⁶ model for equally spaced chains. This model was modified with the interchain interaction

exchange (zJ). The long-range intrachain interaction through para-phenylene diacetate bridge is a weak, but not negligible, ferromagnetic interaction, with $J = +2.52 \text{ cm}^{-1}$ and the interchain interaction, is antiferromagnetic with the $zJ = -1.98 \text{ cm}^{-1}$. Due to the parallel magnetic orbitals of the intrachain copper centers, a weak δ -interaction could be considered.

Compound **3** is a tetranuclear copper(II) complex, having a Cu_4O_4 cubane core. The magnetic susceptibility of **3** indicates overall antiferromagnetic coupling. To find the best fit for the experimental magnetic data and predict the exchange coupling the cubane models were studied and the effect of Hatfield¹¹⁶ correlation (considering the $\text{Cu}^{\text{II}}\text{-O-Cu}^{\text{II}}$ angle (θ) in hydroxo-bridged copper dimers as the first structural effect on type and magnitude of magnetic exchanges) were investigated in the structure of **3**. The best fit is obtained with a 1+1+4 model for the six exchange coupling among the copper(II) centers with short exchange pathways with strong ferromagnetic interaction, a medium and four long pathway with medium antiferromagnetic coupling exchange ($J_1 = -28.0 \text{ cm}^{-1}$, $J_2 = +72.2 \text{ cm}^{-1}$ and $J_3 = -15.3 \text{ cm}^{-1}$). This model is similar to the type (I) or 2+4 model, with two short and four long $\text{Cu}\cdots\text{Cu}$ distances, or eight short and four long Cu-O bonds. However, due to the different $\text{Cu}^{\text{II}}\text{-O-Cu}^{\text{II}}$ angles in each binuclear set, these 2 interactions cannot be classified in the same group, according to Hatfield correlation for the first set $\theta > 97.5^\circ$ which antiferromagnetic interaction is expected, and for the second set $\theta < 97.5^\circ$ which is predicted as ferromagnetic exchange. Based on this statement the two stronger J values obtained from the fitting model are consistent with the structural features.

In the last experimental chapter, four other copper(II) coordination complexes were structurally explored. The **4.1** and **4.2** contain the polymeric and single binuclear units, respectively. **5.1**, and **5.2** are the tetranuclear copper(II) compounds with acetonitrile and water molecules in their unit cell, respectively.

8.2 Future Work

The resistance of cancer cells to Cis-platin and its serious side effects and overall toxicity have limited its usage in chemotherapy ³¹². Hence, considerable research has been made to change this medication with less toxic and more efficacious drugs. In the last decade, anticancer properties of numerous copper(II) coordination complexes have been investigated ³²⁰⁻³²².

The starting point of motivation in this research was the successful synthesis of two copper(II) coordination polymers in our lab and their in vitro cytotoxicity effect specifically against human-derived liver and pancreatic cancer cells ¹⁰³. Compounds **1**, **2**, and **3** may potentially have interesting anticancer properties. Evaluation of potent anticancer activity is suggested for the future work on these compounds.

Furthermore, the interesting structural features of binuclear units of **4.1** and **4.2**, and tetranuclear polymers of **5.1** and **5.2** with the possible interesting magnetic interactions, are good reasons for making more effort to obtain these compounds. For instance, the **4.1** magnetic behavior could contain a short-range coupling within a binuclear unit and a long range coupling through the chain. As it was discussed above, these materials are highly sensitive to temperature and concentration variations. By regulating the temperature changes more accurately or by controlling the concentration changes more precisely the reactions may lead to synthesis of pure phase of these compounds.

Bibliography

- (1) Munoz-Becerra, K. Aravena, D.; Ruiz, E.; Spodine, E.; Soto-Donoso, N.; Paredes-García, V.; Venegas-Yazigi, D. Models to Predict the Magnetic Properties of Single- and Multiple-Bridged Phosphate Cu^{II} Systems: A Theoretical DFT Insight. *Inorg. Chem. Front.* **2017**, *4*, 509–520.
- (2) Lu, J. Y. Crystal Engineering of Cu-Containing Metal-Organic Coordination Polymers under Hydrothermal Conditions. *Coord. Chem. Rev.* **2003**, *246*, 327–347.
- (3) Qiao, Y.; Schelter, E. J. Lanthanide Photocatalysis. *Acc. Chem. Res.* **2018**, *51*, 2926–2936.
- (4) Nielsen, L. G.; Junker, A. K. R.; Sørensen, T. J. Composed in the F-Block: Solution Structure and Function of Kinetically Inert Lanthanide(III) Complexes. *Dalt. Trans.* **2018**, *47*, 10360–10376.
- (5) Marsh, M. L.; White, F. D.; Meeker, D. S.; McKinley, C. D.; Dan, D.; Van Alstine, C.; Poe, T. N.; Gray, D. L.; Hobart, D. E.; Albrecht-Schmitt, T. E. Electrochemical Studies of Selected Lanthanide and Californium Cryptates. *Inorg. Chem.* **2019**, *58*, 9602–9612.
- (6) Farrell, N. *Metal Complexes as Drugs and Chemotherapeutic Agents*, 2018.
- (7) Ayad, M. I.; Boraey, H. A. E. Characterization, Thermal and Electrical Conductivity of Some Transition Metal Adducts. *Int. J. ChemTech Res.* **2014**, *6*, 266–275.
- (8) Zhu, C.; Xia, H. Carbolong Chemistry: A Story of Carbon Chain Ligands and Transition Metals. *Acc. Chem. Res.* **2018**, *51*, 1691–1700.
- (9) Alig, L.; Fritz, M.; Schneider, S. First-Row Transition Metal (De)Hydrogenation Catalysis Based on Functional Pincer Ligands. *Chem. Rev.* **2019**, *119*, 2681–2751.
- (10) Malik, M. A.; Dar, O. A.; Gull, P.; Wani, M. Y.; Hashmi, A. A. Heterocyclic Schiff Base Transition Metal Complexes in Antimicrobial and Anticancer Chemotherapy. *Med. Chem.*

Comm. **2018**, *9*, 409–436.

- (11) Cotton, F. A.; Wilkinson, G. *Advanced Inorganic Chemistry*; New York: Wiley, 1980.
- (12) Santini, C.; Pellei, M.; Gandin, V.; Porchia, M.; Tisato, F.; Marzano, C.; Sez, T.; Camerino, U.; Agostino, S.; Padova, U. Advances in Copper Complexes as Anticancer Agents. *Chem. Rev.* **2014**, *114*, 815–862.
- (13) Holm, R. H.; Kennepohl, P.; Solomon, E. I. Structural and Functional Aspects of Metal Sites in Biology. *Chem. Rev.* **1996**, *96*, 2239–2314.
- (14) Zhou, J. H.; Cheng, R. M.; Song, Y.; Li, Y. Z.; Yu, Z.; Chen, X. T.; Xue, Z. L.; You, X. Z. Syntheses, Structures, and Magnetic Properties of Unusual Nonlinear Polynuclear Copper(II) Complexes Containing Derivatives of 1,2,4-Triazole and Pivalate Ligands. *Inorg. Chem.* **2005**, *44*, 8011–8022.
- (15) Sheppard, C. L.; Tandon, S. S.; Thompson, L. K.; Bridson, J. N.; Miller, D. O.; Handa, M.; Lloret, F. Polynuclear Copper(II) Complexes with 1,1-Azide Bridges. Structural and Magnetic Properties. *inorganica Chhnica Acta* **1996**, *250*, 227–239.
- (16) Boulsourani, Z.; Tangoulis, V.; Raptopoulou, C. P.; Psycharis, V.; Dendrinou-Samara, C. Ferromagnetic and Antiferromagnetic Copper(II) Complexes: Counterplay between Zero-Field Effects of the Quartet Ground State and Intermolecular Interactions. *Dalton Trans.* **2011**, *40*, 7946–7956.
- (17) Tercero, J.; Ruiz, E.; Alvarez, S.; Rodríguez-Forteza, A.; Alemany, P. Density Functional Study of Magnetostructural Correlations in Cubane Complexes Containing the Cu₄O₄ Core. *J. Mater. Chem.* **2006**, *16*, 2729–2735.
- (18) Wenzel, M.; Forgan, R. S.; Faure, A.; Mason, K.; Tasker, P. A.; Piligkos, S.; Brechin, E. K.;

- Plieger, P. G. A New Polynuclear Coordination Type for (Salicylaldoxime) Copper(II) Complexes : Structure and Magnetic Properties of an (Oxime) Cu₆ Cluster. *Eur. J. Inorg. Chem.* **2009**, 2, 4613–4617.
- (19) Anson, F. C.; Collins, T. J.; Richmond, T. G.; Santarsiero, B. D.; Toth, J. E.; T Treco, B. G. R. Highly Stabilized Copper(III) Complexes. *J. Am. Chem. Soc.* **1987**, 109, 2974–2979.
- (20) Schnell, J. P.; Fourquet, J. L. Electrical Conductivity Measurements on HNbO₃. *Mater. Res. Bull.* **1986**, 21, 1045–1050.
- (21) DeSilva, A. W.; Katsouros, J. D. Electrical Conductivity of Dense Copper and Aluminum Plasmas. *Phys. Rev. E - Stat. Physics, Plasmas, Fluids, Relat. Interdiscip. Top.* **1998**, 57, 5945–5951.
- (22) Lu, L.; Shen, Y.; Chen, X.; Qian, L.; Lu, K. Ultrahigh Strength and High Electrical Conductivity in Copper. *Science* **2004**, 304, 422–426.
- (23) Berman, R.; Macdonald, D. K. C. The Thermal and Electrical Conductivity of Copper at Low Temperatures. *Proc. R. Soc. London. Ser. A.* **1952**, 211, 122–128.
- (24) Takata, N.; Lee, S.; Tsuji, N. Ultra Fine Grained Copper Alloy Sheets Having Both High Strength and High Electric Conductivity. *Mater. Lett.* **2009**, 63, 1757–1760.
- (25) Kraatz, H.; Metzler-Nolte, N. *Concepts and Models in Bioinorganic Chemistry*; New York: Wiley-Vch, 2006.
- (26) Chakraborty, A.; Kumar, P.; Ghosh, K.; Roy, P. Evaluation of a Schiff Base Copper Complex Compound as Potent Anticancer Molecule with Multiple Targets of Action. *Eur. J. Pharmacol.* **2010**, 647, 1–12.
- (27) Chaudhuri, P.; Kataev, V.; Büchner, B.; Klauss, H. H.; Kersting, B.; Meyer, F. Tetranuclear

Complexes in Molecular Magnetism: Targeted Synthesis, High-Field EPR and Pulsed-Field Magnetization. *Coord. Chem. Rev.* **2009**, *253*, 2261–2285.

- (28) Miller, J. S.; Gatteschi, D. Molecule-Based Magnets Themed Issue. *Chem. Soc. Rev.* **2011**, *40*, 3065–3066.
- (29) Winpenny, R. E. P. Quantum Information Processing Using Molecular Nanomagnets as Qubits. *Angew. Chemie - Int. Ed.* **2008**, *47*, 7992–7994.
- (30) Casitas, A.; Ribas, X. The Role of Organometallic Copper(III) Complexes in Homogeneous Catalysis. *Chem. Sci.* **2013**, *4*, 2301–2318.
- (31) Rizvi, M. A.; Akhoun, S. A.; Maqsood, S. R.; Peerzada, G. M. Synergistic Effect of Perchlorate Ions and Acetonitrile Medium Explored for Extension in Copper Redoximetry. *J. Anal. Chem.* **2015**, *70*, 633–638.
- (32) Rizvi, M. A. Complexation Modulated Redox Behavior of Transition Metal Systems (Review). *Russ. J. Gen. Chem.* **2015**, *85*, 959–973.
- (33) Zou, X. H.; Cai, J. W.; Feng, X. L.; Hu, X. P.; Yang, G.; Zhang, H.; Ji, L. N. Crystal Structure of [Cu₄(Pytp)₂(SO₄)₂(H₂O)] and Vibrational Spectroscopic Studies of Some Copper(I) Thiourea Complexes. *Transit. Met. Chem.* **2001**, *26*, 704–708.
- (34) Freiser, B. S.; Woodin, R. L.; Beauchamp, J. L. Characterization of a Readily Accessible Copper(III)-Peptide Complex. *J. Am. Chem. Soc.* **1975**, *97*, 6894–6896.
- (35) McDonald, M. R.; Scheper, W. M.; Lee, H. D.; Margerum, D. W. Copper(III) Complexes of Tripeptides with Histidine and Histamine as the Third Residue. *Inorg. Chem.* **1995**, *34*, 229–237.
- (36) Kochem, A.; Molloy, J. K.; Gellon, G.; Leconte, N.; Philouze, C.; Berthiol, F.; Jarjayes, O.;

- Thomas, F. A Structurally Characterized Cu^{III} Complex Supported by a Bis(Anilido) Ligand and Its Oxidative Catalytic Activity. *Chem. - A Eur. J.* **2017**, *23*, 13929–13940.
- (37) Hanss, J.; Krieger, H.-J. The First Stable Copper(III) Complex Containing Aliphatic Thiolates as Ligands: Structural and Spectroscopic Evidence for Cu(II) and Cu(III) Ions in Complexes with Square-Planar CuN₂S₂ Coordination Environments. *Angew. Chemie - Int. Ed.* **1995**, *35*, 2827–2830.
- (38) Zhang, S. L.; Xiao, C.; Wan, H. X. Diverse Copper(III) Trifluoromethyl Complexes with Mono-, Bi- and Tridentate Ligands and Their Versatile Reactivity. *Dalton Trans.* **2018**, *47*, 4779–4784.
- (39) Hickman, A. J.; Sanford, M. S. High-Valent Organometallic Copper and Palladium in Catalysis. *Nature* **2012**, *484*, 177–185.
- (40) Sinha, W.; Sommer, M. G.; Deibel, N.; Ehret, F.; Bauer, M.; Sarkar, B.; Kar, S. Experimental and Theoretical Investigations of the Existence of Cu^{II}, Cu^{III}, and Cu^{IV} in Copper Corrolato Complexes. *Angew. Chemie - Int. Ed.* **2015**, *54*, 13769–13774.
- (41) Mannschreck, B. A.; Jonas, V.; Kolb, B. Proof of the Chirality of Rapidly Interconverting Enantiomers. *Angew. Chemie. Int. Ed.* *12*, 583–585, 1973.
- (42) Harnischmacher, V. W.; Hoppe, R. Vierwertiges Kupfer : Cs₂ [CuF₆]. *Angew. Chem.* **1973**, *85*, 590.
- (43) Popova, T. V.; Aksenova, N. V. Complexes of Copper in Unstable Oxidation States. *Russ. J. Coord. Chem.* **2003**, *29*, 743–765.
- (44) Mikhailov, O. V.; Chachkov, D. V. About Possibility of Stabilization of Unusual Copper(IV) Oxidation State in Complexes with Porphyrazine and Two Fluorine Ligands: Quantum-

Chemical Design. *Inorg. Chem. Commun.* **2019**, *106*, 224–227.

- (45) Chaurin, V.; Constable, E. C.; Housecroft, C. E. What Is the Coordination Number of Copper(II) in Metallosupramolecular Chemistry? *New J. Chem.* **2006**, *30*, 1740–1744.
- (46) Pirsiavash, F.; Amani, V.; Abedi, A. Coordination Number in Copper(II) Complexes with Bipyridine-Dicarboxylate Anion and Diamine Derivatives. *Res. Chem. Intermed.* **2018**, *44*, 7411–7426.
- (47) Dahl, E. W.; Szymczak, N. K. Hydrogen Bonds Dictate the Coordination Geometry of Copper: Characterization of a Square-Planar Copper(I) Complex. *Angew. Chemie - Int. Ed.* **2016**, *55*, 3101–3105.
- (48) Haas, K. L.; Franz, K. J. Application of Metal Coordination Chemistry to Explore and Manipulate Cell Biology. *Chem. Rev.* **2009**, *109*, 4921–4960.
- (49) Fujisawa, K.; Tobita, K.; Sakuma, S.; Savard, D.; Leznoff, D. B. Binuclear and Mononuclear Copper(II) Chlorido Complexes with Hindered Neutral N₃ Type Ligands: Influence of Ligand Framework and Charge on Their Structure and Physicochemical Properties. *Inorganica Chim. Acta* **2019**, *486*, 582–588.
- (50) Large, T. A. G.; Mahadevan, V.; Keown, W.; Stack, T. D. P. Selective Oxidation of Exogenous Substrates by a Bis-Cu(III) Bis-Oxide Complex: Mechanism and Scope. *Inorganica Chim. Acta* **2019**, *486*, 782–792.
- (51) Keller, H.; Bussmann-holder, A.; Müller, K. A. Jahn–Teller Physics and High-T_c Superconductivity. *Mater. Today* **2008**, *11*, 38–46.
- (52) Allmann, R.; Henke, W.; Reinen, D. Presence of a Static Jahn-Teller Distortion in Copper(II) Terpyridine Complexes. 1. Crystal Structure of Cu(Terpy)₂(NO₃)₂. *Inorg. Chem.* **1978**, *17*, 378–

382.

- (53) Brewster, J. T.; Anguera, G.; Moore, M. D.; Dolinar, B. S.; Zafar, H.; Thiabaud, G. D.; Lynch, V. M.; Humphrey, S. M.; Sessler, J. L. Synthesis and Characterization of a Binuclear Copper(II) Naphthoisoamethyrin Complex Displaying Weak Antiferromagnetic Coupling. *Inorg. Chem.* **2017**, *56*, 12665–12669.
- (54) Lv, H. M.; Wang, S. N.; Li, D. C.; Dou, J. M. A One-Dimensional Coordination Polymer with a Capped [Cu₄O₄] Cubane Core Assembled from 2-(Hydroxymethyl)Pyridine. *Acta Crystallogr. Sect. C Struct. Chem.* **2014**, *70*, 843–846.
- (55) Robin, A. Y.; Fromm, K. M. Coordination Polymer Networks with O- and N-Donors: What They Are, Why and How They Are Made. *Coord. Chem. Rev.* **2006**, *250*, 2127–2157.
- (56) Kaufman, G. B. Inorganic Chemistry: Principles of Structure and Reactivity. *J. Chem. Educ.* **1993**, *70*, A279.
- (57) Halcrow, M. A. Interpreting and Controlling the Structures of Six-Coordinate Copper(II) Centres-When Is a Compression Really a Compression? *J. Chem. Soc. Dalt. Trans.* **2003**, *3*, 4375–4384.
- (58) Pearson, R. The Second Order Jahn-Teller Effect. *J. Mol. Struct.* **1983**, *103*, 25–34.
- (59) Árkosi, Z.; Szabó-Plánka, T.; Rockenbauer, A.; Nagy, N. V.; Lázár, L.; Fulöp, F. An Electron Paramagnetic Resonance Study of Copper(II)- β -Substituted β -Amino Acid Systems by the Two-Dimensional Simulation Method: First Evidence of Primarily Steric Effects of Substituents on Equilibria of Metal Complexes. *Inorg. Chem.* **2003**, *42*, 4842–4848.
- (60) Hitchman, M. A.; Yablokov, Y. V.; Petrashen, V. E.; Augustyniak-Jablokov, M. A.; Stratemeier, H.; Riley, M. J.; Lukaszewicz, K.; Tomaszewski, P. E.; Pietraszko, A. Dynamic

Behavior of the Jahn-Teller Distorted $\text{Cu}(\text{H}_2\text{O})_6^{2+}$ Ion in Cu^{2+} Doped $\text{Cs}_2[\text{Zn}(\text{H}_2\text{O})_6](\text{ZrF}_6)_2$ and the Crystal Structure of the Host Lattice. *Inorg. Chem.* **2002**, *41*, 229–238.

- (61) Savarimuthu, V.; Anthonisamy, X.; Murugesan, R. EPR of Hexakis (1-Propyltetrazole) Copper(II) Tetrafluoroborate and Cu(II) -Doped Hexakis (1-Propyltetrazole) Zinc (II) Tetrafluoroborate. Dynamic to Static Jahn–Teller Distortion. *Chem. Phys. Lett.* **1998**, *287*, 353–358.
- (62) Wagner, B.; Warda, S. A.; Hitchman, M. A.; Reinen, D. Geometry and Electronic Structure of CuCl_6 -Polyhedra Doped into $(3\text{-Chloroanilinium})_8[\text{CdCl}_6]\text{Cl}_4^-$ An EPR and Structural Investigation. *Inorg. Chem.* **1996**, *35*, 3967–3974.
- (63) Bertini, I.; Gatteschi, D.; Scozzafava, A. Jahn-Teller Distortions of Tris(Ethylenediamine) Copper(II) Complexes. *Inorg. Chem.* **1977**, *16*, 1973–1976.
- (64) Bhunia, A.; Vojtišek, P.; Bertolasi, V.; Manna, S. C. Tridentate Schiff Base Coordinated Trigonal Bipyramidal / Square Pyramidal Copper(II) Complexes: Synthesis, Crystal Structure, DFT/TD-DFT Calculation, Catecholase Activity and DNA Binding. *J. Mol. Struct.* **2019**, *1189*, 94–101.
- (65) Karipcin, F.; Dede, B.; Caglar, Y.; Hür, D.; Ilican, S.; Caglar, M.; Şahin, Y. A New Dioxime Ligand and Its Trinuclear Copper(II) Complex: Synthesis, Characterization and Optical Properties. *Opt. Commun.* **2007**, *272*, 131–137.
- (66) Drewry, J. A.; Gunning, P. T. Recent Advances in Biosensory and Medicinal Therapeutic Applications of Zinc(II) and Copper(II) Coordination Complexes. *Coord. Chem. Rev.* **2011**, *255*, 459–472.
- (67) Ouellette, W.; Liu, H.; O'Connor, C. J.; Zubieta, J. Solid-State Coordination Chemistry of

Copper(II) Tetrazolates: Anion Control of Frameworks Constructed from Trinuclear Copper(II) Building Blocks. *Inorg. Chem.* **2009**, *48*, 4655–4657.

- (68) Kato, M. Factors Affecting the Magnetic of Dimeric Copper(II) Complexes Properties. *Coord. Chem. Rev.* **1988**, *92*, 45–83.
- (69) Katwal, R.; Kaur, H.; Kapur, B. K. Applications of Copper – Schiff's Base Complexes. *Sci. Rev. Chem. Commun.* **2013**, *3*, 1–15.
- (70) Bednorz, J. G.; Müller, K. A.; Takashige, M. Superconductivity in Alkaline Earth-Substituted $\text{La}_2\text{CuO}_{4-y}$. *Science* **2019**, *236*, 73–75.
- (71) Auni, N.; Mustafa, M.; Kechik, A.; Atikah, N.; Soo, C.; Baqiah, H.; Nabilah, N.; Yusuf, M.; Halim, A.; Hashim, A. Impact of Carbon Nanotubes Addition on Transport and Superconducting Properties of $\text{YBa}_2\text{Cu}_3\text{O}_{7-8}$ Ceramics. *Ceram. Int.* **2018**, *44*, 9568–9573.
- (72) Egami, T. Local Structural Distortion and Superconductivity in Doped La_2CuO_4 and $\text{YBa}_2\text{Cu}_8\text{O}_7$. *Solid State Commun.* **1987**, *63*, 1019–1022.
- (73) Koura, N.; Shoji, H. BSCCO Superconductor Coating by the Electrophoretic Deposition Method. *Phys. C* **1992**, *200*, 50–54.
- (74) You, A.; Be, M. A. Y.; In, I. Superconducting Superlattices : Verification of Two-Dimensional Nature in High T_c $\text{Bi}_2\text{Sr}_2(\text{Ca}_{1-x}\text{Y}_x)\text{Cu}_2\text{O}_8$ Superconductors. *Appl. Phys. Lett.* **1998**, *2*, 2–5.
- (75) Sözeri, H. Enhancement in the High- T_c Phase of BSCCO Superconductors by Nb. *Supercond. Sci. Technol.* **2007**, *20*, 522.
- (76) Harlingen, V. Experimental Determination of the Superconducting Pairing State in YBCO from the Phase Coherence of YBCO-Ph Dc SQUIDS. *Phys. Rev. Lett.* **1993**, *71*, 2134–2137.

- (77) Kim, H. High- T_c Mechanism through Analysis of Diverging Effective Mass for $YBa_2Cu_3O_{6+x}$ and Pairing Symmetry in Cuprate Superconductors. *Int. J. Mod. Phys. B* **2017**, *17*, 1840031.
- (78) Chen, X.; Hao, X. S.; Goodhue, C. E.; Yu, J. Q. Cu(II)-Catalyzed Functionalizations of Aryl C-H Bonds Using O_2 as an Oxidant. *J. Am. Chem. Soc.* **2006**, *128*, 6790–6791.
- (79) Guo, X. X.; Gu, D. W.; Wu, Z.; Zhang, W. Copper-Catalyzed C-H Functionalization Reactions: Efficient Synthesis of Heterocycles. *Chem. Rev.* **2015**, *115*, 1622–1651.
- (80) Allen, S. E.; Walvoord, R. R.; Padilla-Salinas, R.; Kozlowski, M. C. Aerobic Copper-Catalyzed Organic Reactions. *Chem. Rev.* **2013**, *113*, 6234–6458.
- (81) Collman, J. P.; Zhong, M.; Zhang, C.; Costanzo, S. Catalytic Activities of Cu(II) Complexes with Nitrogen-Chelating Bidentate Ligands in the Coupling of Imidazoles with Arylboronic Acids. *J. Org. Chem.* **2001**, *66*, 7892–7897.
- (82) Kolesnichenko, I. V.; Anslyn, E. V. Practical Applications of Supramolecular Chemistry. *Chem. Soc. Rev.* **2017**, *46*, 2385–2390.
- (83) Constable, E. C.; Housecroft, C. E.; Price, J. R.; Zampese, J. A. When Five Are Six: The Myth of Five-Coordinate Copper(II) in Supramolecular Chemistry. *Cryst. Eng. Comm.* **2010**, *12*, 3163–3171.
- (84) Nugent, P.; Giannopoulou, E. G.; Burd, S. D.; Elemento, O.; Giannopoulou, E. G.; Forrest, K.; Pham, T.; Ma, S.; Space, B.; Wojtas, L.; et al. Porous Materials with Optimal Adsorption Thermodynamics and Kinetics for CO_2 Separation. *Nature* **2013**, *495*, 80–84.
- (85) Du, M.; Li, C. P.; Chen, M.; Ge, Z. W.; Wang, X.; Wang, L.; Liu, C. Sen. Divergent Kinetic and Thermodynamic Hydration of a Porous Cu(II) Coordination Polymer with Exclusive CO_2 Sorption Selectivity. *J. Am. Chem. Soc.* **2014**, *136*, 10906–10909.

- (86) Storr, T.; Thompson, K. H.; Orvig, C. Design of Targeting Ligands in Medicinal Inorganic Chemistry. *Chem. Soc. Rev.* **2006**, *35*, 534–544.
- (87) Fricker, S. P. Metal Based Drugs: From Serendipity to Design. *Dalton Trans.* **2007**, *43*, 4903–4917.
- (88) Navarro, M.; Gabbiani, C.; Messori, L.; Gambino, D. Metal-Based Drugs for Malaria, Trypanosomiasis and Leishmaniasis: Recent Achievements and Perspectives. *Drug Discov. Today* **2010**, *15*, 1070–1078.
- (89) Lloyd, N. C.; Morgan, H. W.; Nicholson, B. K.; Ronimus, R. S. The Composition of Ehrlich's Salvarsan: Resolution of a Century-Old Debate. *Angew. Chemie - Int. Ed.* **2005**, *44*, 941–944.
- (90) İspir, E.; Toroğlu, S.; Kayraldız, A. Syntheses, Characterization, Antimicrobial and Genotoxic Activities of New Schiff Bases and Their Complexes. *Transit. Met. Chem.* **2008**, *33*, 953–960.
- (91) Prashanthi, Y.; Raj, S. Synthesis and Characterization of Transition Metal Complexes with N,O; N,N and S,N-Donor Schiff Base Ligands. *J. Sci. Res.* **2009**, *2*, 114–126.
- (92) Yadav, L.; Tripathi, R. M.; Prasad, R.; Pudake, R. N.; Mittal, J. Antibacterial Activity of Cu Nanoparticles against E. Coli, Staphylococcus Aureus and Pseudomonas Aeruginosa. *Nano Biomed. Eng.* **2017**, *9*, 9–14.
- (93) Rosenberg, B.; Vancamp, L.; Trosko, J. E.; Mansour, V. H. Platinum Compounds: A New Class of Potent Antitumour Agents. *Nature* **1969**, *222*, 385–386.
- (94) Elie, M.; Mahoro, G. U.; Duverger, E.; Renaud, J. L.; Daniellou, R.; Gaillard, S. Cytotoxicity of Cationic NHC Copper(I) Complexes Coordinated to 2,2'-Bis-Pyridyl Ligands. *J. Organomet. Chem.* **2019**, *893*, 21–31.
- (95) Allardyce, C. S.; Dyson, P. J. Metal-Based Drugs That Break the Rules. *Dalt. Trans.* **2016**, *45*,

3201–3209.

- (96) Heidari, A. Cheminformatics and System Chemistry of Cisplatin, Carboplatin, Nedaplatin, Oxaliplatin, Heptaplatin and Lobaplatin as Anti-Cancer Nano Drugs: A Combined Computational and Experimental Study. *J. Informatics Data Min.* **2016**, *1*, 9–11.
- (97) Alderden, R. A.; Hall, M. D.; Hambley, T. W. The Discovery and Development of Cisplatin. *J. Chem. Educ.* **2006**, *83*, 728–734.
- (98) Thompson, K. H.; Orvig, C. Metal Complexes in Medicinal Chemistry: New Vistas and Challenges in Drug Design. *Dalt. Trans.* **2006**, *6*, 761–764.
- (99) Zhang, S.; Zhu, Y.; Tu, C.; Wei, H.; Yang, Z. A Novel Cytotoxic Ternary Copper(II) Complex of 1 , 10-Phenanthroline and L -Threonine with DNA Nuclease Activity. **2004**, *98*, 2099–2106.
- (100) Mahendiran, D.; Amuthakala, S.; Bhuvanesh, N. S. P.; Kumar, R. S.; Rahiman, A. K. Copper Complexes as Prospective Anticancer Agents:: In Vitro and in Vivo Evaluation, Selective Targeting of Cancer Cells by DNA Damage and S Phase Arrest. *RSC Adv.* **2018**, *8*, 16973–16990.
- (101) Maroń, A.; Czerwińska, K.; Machura, B.; Raposo, L.; Roma-Rodrigues, C.; Fernandes, A. R.; Małecki, J. G.; Szłapa-Kula, A.; Kula, S.; Krompiec, S. Spectroscopy, Electrochemistry and Antiproliferative Properties of Au(III), Pt(II) and Cu(III) Complexes Bearing Modified 2,2':6',2''-Terpyridine Ligands. *Dalton Trans.* **2018**, *47*, 6444–6463.
- (102) Armaroli, N. Photoactive Mono- and Polynuclear Cu(I)-Phenanthrolines. A Viable Alternative to Ru(II)-Polypyridines? *Chem. Soc. Rev.* **2001**, *30*, 113–124.
- (103) Wang, H.; Sorolla, M.; Wang, X.; Jacobson, A. J.; Wang, H.; Pillai, A. K. Synthesis, Crystal Structures and in Vitro Anticancer Activities of Two Copper(II) Coordination Compounds.

Transit. Met. Chem. **2019**, *44*, 237–245.

- (104) Cornia, A.; Seneor, P. Spintronics: The Molecular Way. *Nat. Mater.* **2017**, *16*, 505–506.
- (105) Wolf, S. A.; Awschalom, D. D.; Buhrman, R. A.; Daughton, J. M.; Von Molnár, S.; Roukes, M. L.; Chtchelkanova, A. Y.; Treger, D. M. Spintronics: A Spin-Based Electronics Vision for the Future. *Science* **2001**, *294*, 1488–1495.
- (106) Castro, I.; Luisa, M.; Yuste, C.; Castellano, M.; Ruiz-garcía, R.; Cano, J.; Faus, J.; Verdager, M.; Lloret, F. Dinuclear Copper(II) Complexes as Testing Ground for Molecular Magnetism Theory. *Polyhedron* **2019**, *169*, 66–77.
- (107) Campbell, V. E.; Tonelli, M.; Cimatti, I.; Moussy, J. B.; Tortech, L.; Dappe, Y. J.; Rivière, E.; Guillot, R.; Delprat, S.; Mattana, R.; et al. Engineering the Magnetic Coupling and Anisotropy at the Molecule-Magnetic Surface Interface in Molecular Spintronic Devices. *Nat. Commun.* **2016**, *7*, 1–10.
- (108) Kato, M.; Jonassen, H. B.; Fanning, J. Copper(II) Complexes with Subnormal Magnetic Moments. *Chem. Rev.* **1963**, *64*, 99–128.
- (109) Guha, B. C. Magnetic Properties of Some Paramagnetic Crystals at Low Temperatures. *Proc. R. Soc. A* **1945**, *155*, 364.
- (110) Bleaney, B. Anomalous Paramagnetism of Copper Acetate. *Rev. Mod. Phys.* **1953**, *25*, 161–162.
- (111) Niekerk, J. N.; Schoening, R. L. A New Type of Copper Complex as Found in the Crystal Structure of Cupric Acetate, $\text{Cu}_2(\text{CH}_3\text{COO})_4 \cdot 2\text{H}_2\text{O}$. *Acta Cryst.* **1953**, *6*, 227.
- (112) Guvelioglu, G. H.; Pingping, M.; Xiaoyi, H.; Forrey, R. C.; Cheng, H. First Principles Studies on the Growth of Small Cu Clusters and the Dissociative Chemisorption of H_2 . *Phys. Rev. B* **2006**, *73*, 1–10.

- (113) Dirac, P. A. M. Quantum Mechanics of Many-Electron Systems. *Proc. R. Soc. A Math. Phys. Eng. Sci.* **1929**, *123*, 714–733.
- (114) Hatfield, W. E.; Morrison, J. C. Substituted Pyridine N-Oxide Complexes of Copper(II) Halides. II. Magnetic Properties of Complexes with 3-Picoline N-Oxide, 2,6-Lutidine N-Oxide, and 2,4,6-Collidine N-Oxide. *Inorg. Chem.* **1966**, *5*, 1390–1394.
- (115) Heisenberg, W. Zur Theorie Des Ferromagnetismus. *Zeitschrift für Phys.* **1928**, *49*, 619–636.
- (116) Crawford, V. A. N. H.; Richardson, H. W.; Wasson, J. R.; Hatfield, W. E. Relationship between the Singlet-Triplet Splitting and the Cu-O-Cu Bridge Angle in Hydroxo-Bridged Copper Dimers. *Inorg. Chem.* **1976**, *15*, 2107–2110.
- (117) Dubicki, L.; Martin, R. L.; Harris, C. M.; Kokot, E. Magnetic Studies with Copper(II) Salts. VII. The Structure of Copper(II) α,ω -Dicarboxylates and Their Amine Derivatives. *Inorg. Chem.* **1966**, *5*, 93–100.
- (118) Phys, J. C.; Calzado, C. J.; Maynau, D. Evaluation of Magnetic Terms in Cu_4O_4 Cubane-like Systems from Selected Configuration Interaction Calculations : A Case Study of Polynuclear Transition-Metal Systems. *J. Chem. Phys.* **2011**, *135*, 194704.
- (119) Castro, I.; Luisa, M.; Yuste, C.; Castellano, M.; Ruiz-garcía, R.; Cano, J.; Faus, J.; Verdager, M.; Lloret, F. Dinuclear Copper(II) Complexes as Testing Ground for Molecular Magnetism Theory. *Polyhedron* **2019**, *169*, 66–77.
- (120) Kanamori, J. Superexchange Interaction and Symmetry Properties of Electron Orbitals. *J. Phys. Chem. Solids* **1959**, *10*, 87–98.
- (121) Goodenough, J. B. An Interpretation of the Magnetic Properties of the Perovskite-Type Mixed Crystals $\text{La}_{1-x}\text{Sr}_x\text{CoO}_{3-\lambda}$. *J. Phys. Chem. Solids* **1958**, *6*, 287–297.

- (122) Weihe, H.; Güdel, H. U. Quantitative Interpretation of the Goodenough - Kanamori Rules: A Critical Analysis. *Inorg. Chem.* **1997**, *36*, 3632–3639.
- (123) Atanasov, M.; Angelov, S. Angular Overlap Model Parameterisation of Anderson's Superexchange Theory. I. A Quantification of Goodenough-Kanamori Rules. *Chem. Phys.* **1991**, *150*, 383–393.
- (124) Anderson, P. W. New Approach to the Theory of Superexchange Interactions. *Phys. Rev.* **1959**, *115*, 2–13.
- (125) Oleś, A. M.; Horsch, P.; Feiner, L. F.; Khaliullin, G. Spin-Orbital Entanglement and Violation of the Goodenough-Kanamori Rules. *Phys. Rev. Lett.* **2006**, *96*, 1–4.
- (126) Ohmura, T.; Mori, W.; Hasegawa, Ā. M.; Takei, T.; Yoshizawa, A. Gas-Occlusion Properties of a Novel Compound : Mononuclear Copper(II) Terephthalate-Pyridine. *Chem. Lett.* **2003**, *32*, 7–8.
- (127) Getova, V. T.; Bontchev, R. P.; Mehandjiev, D. R.; Bontchev, P. R. Complexes of 1-[2-[2-Hydroxy-3-(Propylamino)Propoxy]Phenyl]-3-Phenyl-1-Propanone (Propafenone) with Copper(II): Crystal Structure of the Mononuclear Cu(II) Complex with Propafenone. *Polyhedron* **2006**, *25*, 2254–2260.
- (128) Ohmura, T. Structure and Magnetic Behaviour of Mononuclear and Dinuclear Cu(II)/Zn (II) Monocarboxylate-Pyridine Derivatives Studied by Crystal Engineering. *Mater. Sci.* **2005**, *23*, 719–736.
- (129) Wei, H. H.; Wang, Y. Reinvestigation of the Crystal Structure and Cryomagnetic Behaviour of Copper(II) Propionates. *Polyhedron* **1998**, *17*, 449–755.
- (130) Liao, C. Structure and Magnetic Properties of Mononuclear Copper(II) Complexes Based

Ligands. *Inorg. Chem.* **2005**, 707–716.

- (131) Dominguez-vera, J. M.; Camara, F.; Moreno, J. M.; Colacio, E.; Stoeckli-evans, H. A New Mononuclear Copper(II) Complex Containing Two Imidazolyl Moieties as Precursor of Self-Assembled and Ni^{II}Cu^{II}Ni^{II} Heterobimetallic Complexes. *Inorg. Chem.* **2000**, 1669, 3046–3050.
- (132) Barnes, J. A.; Hodgson, D. J.; Hatfield, W. E. The Magnetic Properties of a Series of Hydroxo-Bridged Complexes of 2,2' -Dipyridyl and Copper(II). *Inorg. Chem.* **1972**, 11, 144–148.
- (133) Carlisle, G. O.; Hatfield, W. E. The Importance of Out-of-Plane Interactions in the Dimer N,N'-Ethylenebis(Salicylideneiminato) Copper(II). *Inorg. Nucl. Chem. Lett.* **1970**, 6, 633–637.
- (134) Jeter, D. Y.; Hatfield, W. E. The Magnetism of Potassium Dioxalatocuprate (II) Dihydrate and Ammonium Dioxalatocuprate(II) Dihydrate. *Inorganica Chim. Acta* **1971**, 6, 523–525.
- (135) Richardson, H. W.; Wasson, J. R.; Hatfield, W. E. Spectral and Magnetic Properties of Copper(II) Furoate and Copper(II) Thiophene-2-Carboxylate. *J. Mol. Struct.* **1977**, 36, 83–91.
- (136) Rodríguez-Fortea, A.; Alemany, P.; Alvarez, S.; Ruiz, E. Exchange Coupling in Halo-Bridged Dinuclear Cu(II) Compounds : A Density Functional Study. *Inorg. Chem.* **2002**, 41, 3769–3778.
- (137) Elmali, A. The Magnetic Super-Exchange Coupling in Copper(II) Acetate Monohydrate and a Redetermination of the Crystal Structure. *Turkish J. Phys.* **2000**, 24, 667–672.
- (138) Rodriguez, M.; Llobet, A.; Corbella, M.; Martell, A. E.; Reibenspies, J. Synthesis, Structure, and Magnetic Properties of a New Chloro-Bridged Dimer [Cu₂(Dpt)₂Cl₂]Cl₂ with an Unusual Structure and Ferromagnetic Coupling. *Inorg. Chem.* **1999**, 38, 2328–2334.
- (139) Chailuecha, C.; Youngme, S.; Pakawatchai, C.; Chaichit, N.; van Albada, G. A.; Reedijk, J. Dinuclear Triply Bridged Copper(II)-Carboxylato Compounds with Different Bischelating Ligands: Synthesis, Crystal Structure, Spectroscopic and Magnetic Properties. *Inorganica Chim.*

Acta **2006**, 359, 4168–4178.

- (140) Gungor, E.; Kara, H. Chiral One-Dimensional Hydrogen Bonded, Antiferromagnetic Chloro-Bridged Dinuclear Copper(II) Complex with Tridentate Schiff Base Ligand. *Inorganica Chim. Acta* **2012**, 384, 137–142.
- (141) Koohzad, S.; Golchoubian, H.; Jagličić, Z. Structural, Solvatochromism and Magnetic Properties of Two Halogen Bridged Dinuclear Copper(II) Complexes: A Density Functional Study. *Inorganica Chim. Acta* **2018**, 473, 60–69.
- (142) Banerjee, I.; Samanta, P. N.; Das, K. K.; Ababei, R.; Kalisz, M.; Girard, A.; Mathonière, C.; Nethaji, M.; Clérac, R.; Ali, M. Air Oxygenation Chemistry of 4-TBC Catalyzed by Chloro Bridged Dinuclear Copper(II) Complexes of Pyrazole Based Tridentate Ligands: Synthesis, Structure, Magnetic and Computational Studies. *Dalton Trans.* **2013**, 42, 1879–1892.
- (143) Muñoz-Becerra, K.; Aravena, D.; Ruiz, E.; Spodine, E.; Soto-Donoso, N.; Paredes-García, V.; Venegas-Yazigi, D. Models to Predict the Magnetic Properties of Single- and Multiple-Bridged Phosphate Cu_{II} Systems: A Theoretical DFT Insight. *Inorg. Chem. Front.* **2017**, 4, 509–520.
- (144) Noshiranzadeh, N.; Emami, M.; Bikas, R.; Ślepokura, K. Synthesis, Crystal Structure, Spectroscopic Studies and Magnetic Behavior of a New Diphosphonate-Bridged Dinuclear Copper(II) Complex. *Polyhedron* **2017**, 133, 155–161.
- (145) Viola; Muhammad, N.; Ikram, M.; Rehman, S.; Ali, S.; Akhtar, M. N.; AlDamen, M. A.; Schulzke, C. A Paddle Wheel Dinuclear Copper(II) Carboxylate: Crystal Structure, Thermokinetic and Magnetic Properties. *J. Mol. Struct.* **2019**, 1196, 754–759.
- (146) Wood, L. Magnetic Properties of Some Aryl-Carboxylates of Copper II. *Nature* **1963**, 200, 468–469.

- (147) Rodríguez-Fortea, A.; Alemany, P.; Alvarez, S.; Ruiz, E. Exchange Coupling in Carboxylato-Bridged Dinuclear Copper(II) Compounds: A Density Functional Study. *Chem. - A Eur. J.* **2001**, *7*, 627–637.
- (148) Herringer, S. N.; Landee, C. P.; Turnbull, M. M.; Ribas-Ariño, J.; Novoa, J. J.; Polson, M.; Wikaira, J. L. Ferromagnetic Exchange in Bichloride Bridged Cu(II) Chains: Magnetostructural Correlations between Ordered and Disordered Systems. *Inorg. Chem.* **2017**, *56*, 5441–5454.
- (149) Estes, W. E.; Wasson, J. R.; Hall, J. W.; Hatfield, W. E. Characterization of Some Mixed-Halide Copper(II) Dimers of the General Formula $[\text{Cu}_2\text{X}_n\text{X}'_{6-n}]^{2-}$ ($\text{X} = \text{Cl}^-$ and $\text{X}' = \text{Br}^-$): Evidence for the Preference of Chloride Bridges in the Mixed-Halide Spe. *Inorg. Chem.* **1978**, *17*, 3657–3664.
- (150) Willett, R. D.; Haugen, J. A.; Lebsack, J.; Morrey, J. Thermochromism in Copper(II) Chlorides. Coordination Geometry Changes in Tetrachlorocuprate(2-) Anions. *Inorg. Chem.* **1974**, *13*, 2510–2513.
- (151) Rodríguez-Fortea, A.; Alemany, P.; Alvarez, S.; Ruiz, E. Exchange Coupling in Halo-Bridged Dinuclear Cu(II) Compounds : A Density Functional Study. *Inorg. Chem.* **2002**, *41*, 3769–3778.
- (152) Bannon, G. O.; Willett, R. D. A Redetermination of the Crystal Structure of $\text{NH}_4\text{-CuCl}_3$ and a Magnetic Study of NH_4CuX_3 ($\text{X} = \text{Cl}, \text{Br}$). *Inorganica Chim. Acta* **1981**, *53*, 131–132.
- (153) Landee, C. P.; Djili, A.; Mudgett, D. F.; Newhall, M.; Place, H.; Scott, B.; Willett, R. D. Alternating Exchange in Homonuclear Ferrimagnetic Linear Chains. Tetrakis(Tetramethylene Sulfoxide)Copper(II) Hexahalodicuprate(II) (Halo = Chloro, Bromo): Crystal Structures and Magnetic Susceptibilities. *Inorg. Chem.* **1988**, *27*, 620–627.
- (154) Estes, W. E.; Gavel, D. P.; Hatfield, W. E.; Hodgson, D. J. Magnetic and Structural

- Characterization of Dibromo-and Dichlorobis(Thiazole)Copper(II). *Inorg. Chem.* **1978**, *17*, 1415–1421.
- (155) Handa, M.; Koga, N.; Kida, S. Study of the Effect of Structural Factors on Magnetism of Di- μ -Alkoxodicopper(II) Complexes by Ab Initio MO Calculations. *Bull. Chem. Soc. Jpn.* **1988**, *61*, 3853–3857.
- (156) Moreno, Y.; Vega, A.; Ushak, S.; Baggio, R.; Peña, O.; Le Fur, E.; Pivan, J. Y.; Spodine, E. Magnetic Properties of Phosphate-Bridged Copper(II) Organic-Inorganic Hybrid Compounds. *J. Mater. Chem.* **2003**, *13*, 2381–2387.
- (157) Briat, B.; Russel, M. F.; Rivoal, J. C.; Chapelle, J. P.; Kahn, O. Exchange Interactions in Polynuclear Complexes. *Mol. Phys.* **1975**, *34*, 268–281.
- (158) Aravena, D.; Ruiz, E.; Spodine, E.; Soto-donos, N. Models to Predict the Magnetic Properties of Single- and Multiple-Bridged Phosphate Cu^{II} Systems : A Theoretical DFT Insight. *Inorg. Chem. Front.* **2017**, *4*, 509–520.
- (159) Pardo, E.; Carrasco, R.; Ruiz-garcía, R.; Julve, M.; Lloret, F.; Mun, M. C.; Journaux, Y.; Ruiz, E.; Cano, J.; Vale, D.; et al. Structure and Magnetism of Dinuclear Copper(II) Metallacyclophanes with Oligoacenebis (Oxamate) Bridging Ligands : Theoretical Predictions on Wirelike Magnetic Coupling. *J. Am. Chem. Soc.* **2008**, *130*, 576–585.
- (160) Pardo, E.; Faus, J.; Julve, M.; Lloret, F.; Mun, M. C.; Cano, J.; Ottenwaelder, X.; Journaux, Y.; Carrasco, R.; Blay, G.; et al. Long-Range Magnetic Coupling through Extended π -Conjugated Aromatic Bridges in Dinuclear Copper(II) Metallacyclophanes. **2003**, *91*, 10770–10771.
- (161) Sarma, R.; Boudalis, A. K.; Baruah, J. B. Aromatic N -Oxide Bridged Copper(II) Coordination Polymers : Synthesis , Characterization and Magnetic Properties. *Inorganica Chim. Acta* **2010**,

363, 2279–2286.

- (162) Tiana, D.; Hendon, C. H.; Walsh, A. Ligand Design for Long-Range Magnetic Order in Metal-Organic Frameworks. *Chem. Commun.* **2014**, *50*, 13990–13993.
- (163) Todaro, M.; Buscarino, G.; Sciortino, L.; Alessi, A.; Messina, F.; Taddei, M.; Ranocchiari, M.; Cannas, M.; Gelardi, F. M. Decomposition Process of Carboxylate MOF HKUST-1 Unveiled at the Atomic Scale Level. *J. Phys. Chem. C* **2016**, *120*, 12879–12889.
- (164) Ghosh, S. K.; El, M. S.; Ribas, J.; Bharadwaj, P. K. Coordination Polymers Built from Cu(II) and Tricarboxylate : Structural and Magnetic Studies. *Inorganica Chim. Acta* **2006**, *359*, 468–474.
- (165) Shen, L.; Yang, S.; Xiang, S.; Liu, T.; Zhao, B.; Ng, M. Origin of Long-Range Ferromagnetic Ordering in Metal – Organic Frameworks with Antiferromagnetic Dimeric-Cu(II) Building Units. *J. Am. Chem. Soc.* **2012**, *134*, 17286-17290.
- (166) Dey, C.; Das, R.; Krishna, B.; Banerjee, R. Design and in Situ Synthesis of a Cu-Based Porous Framework Featuring Isolated Double Chain Magnetic Character. *Chem. Comm.* **2011**, *47*, 11008–11010.
- (167) Gutierrez, L.; Alzuet, G.; Real, J. A.; Cano, J.; Borrás, J.; Castiñeiras, A. Countercomplementarity and Strong Ferromagnetic Coupling in a Linear Mixed μ -Acetato, μ -Hydroxo Trinuclear Copper(II) Complex. Synthesis, Structure, Magnetic Properties, EPR, and Theoretical Studies. *Inorg. Chem.* **2000**, *39*, 3608–3614.
- (168) González-Álvarez, M.; Alzuet, G.; Borrás, J.; Macías, B.; Castiñeiras, A. Oxidative Cleavage of DNA by a New Ferromagnetic Linear Trinuclear Copper(II) Complex in the Presence of H₂O₂/Sodium Ascorbate. *Inorg. Chem.* **2003**, *42*, 2992–2998.

- (169) Zhu, Q.; Tian, C.; Shen, C.; Sheng, T.; Hu, S.; Wu, X. A Three-Dimensional Coordination Polymer Based on Linear Trinuclear Copper(II) Clusters Featuring a Ferromagnetic Exchange Interaction. *Cryst. Eng. Comm.* **2013**, *15*, 2120–2126.
- (170) Song, Y.; Gamez, P.; Roubeau, O.; Lutz, M.; Spek, A. L.; Reedijk, J. Structural and Magnetic Characterization of a Linear Trinuclear Copper Complex Formed through Ligand Sharing. *Eur. J. Inorg. Chem.* **2003**, 2924–2928.
- (171) Driessen, W. L.; Chang, L.; Finazzo, C.; Gorter, S.; Rehorst, D.; Reedijk, J.; Lutz, M.; Spek, A. L. Two Pyrazolato-Bridged, Linear Trinuclear Cu(II) Complexes. Crystal Structures and Magnetic Properties. *Inorganica Chim. Acta* **2003**, *350*, 25–31.
- (172) Aznar, E.; Ferrer, S.; Borrás, J.; Lloret, F.; Liu-González, M.; Rodríguez-Prieto, H.; García-Granda, S. Coordinative Versatility of Guanazole [3,5-Diamino-1,2,4-Triazole]: Synthesis, Crystal Structure, EPR, and Magnetic Properties of a Dinuclear and a Linear Trinuclear Copper(II) Complex Containing Small Bridges and Triazole Ligands. *Eur. J. Inorg. Chem.* **2006**, 5115–5125.
- (173) Liu, J.; Song, Y.; Yu, Z.; Zhuang, J.; Huang, X.; You, X. A Novel Linear Trinuclear Copper(II) Compound with 4-(2-Pyridyl)-1,2,4-Triazole as a Bridging Ligand. *Polyhedron* **1999**, *18*, 1491–1494.
- (174) Piovesana, O.; Chiari, B.; Tarantelli, T.; Zanazzi, P. F. Exchange Interaction in Multinuclear Transition-Metal Complexes. Synthesis, X-Ray Structure, and Magnetic Properties of $\text{Cu}_3\text{L}_2(\text{CH}_3\text{COO})_4$ (LH = N-Methyl-N'-(4-Methoxysalicylidene)-1,3-Propanedianiine. *Inorg. Chem.* **1985**, *24*, 4615–4619.
- (175) Van Koningsbruggen, P. J.; Van Hal, J. W.; De Graaff, R. A. G.; Haasnoot, J. G.; Reedijk, J. Synthesis, Crystal Structure and Magnetic Properties of a Linear Trinuclear Copper(II)

Compound with Chloride and 4-Amino-3,5-Bis(Hydroxymethyl)-1,2,4-Triazole as Bridging Ligands. *J. Chem. Soc. Dalton Trans.* **1993**, 2163–2167.

- (176) Baker, W. A.; Helm, F. T. Linear Trinuclear Copper(II) Complex with a Spin-Doublet Ground State. *J. Am. Chem. Soc.* **1975**, *97*, 2295–2296.
- (177) Davydenko, Y. M.; Demeshko, S.; Pavlenko, V. A.; Dechert, S.; Meyer, F.; Fritsky, I. O. Synthesis, Crystal Structure, Spectroscopic and Magnetically Study of Two Copper(II) Complexes with Pyrazole Ligand. *Zeitschrift fur Anorg. und Allg. Chemie* **2013**, *639*, 1472–1476.
- (178) Di Nicola, C.; Forlin, E.; Garau, F.; Gazzano, M.; Lanza, A.; Monari, M.; Nestola, F.; Pandolfo, L.; Pettinari, C.; Zorzi, A.; et al. Coordination Polymers Based on the Trinuclear Triangular Secondary Building Unit $[\text{Cu}_3(\mu_3\text{-OH})(\mu\text{-Pz})_3]^{2+}$ (Pz = Pyrazolate) and Succinate Anion. *Cryst. Growth Des.* **2013**, *13*, 126–135.
- (179) Contaldi, S.; Di Nicola, C.; Garau, F.; Karabach, Y. Y.; Martins, L. M. D. R. S.; Monari, M.; Pandolfo, L.; Pettinari, C.; Pombeiro, A. J. L. New Coordination Polymers Based on the Triangular $[\text{Cu}_3(\mu_3\text{-OH})(\mu\text{-Pz})_3]^{2+}$ Unit and Unsaturated Carboxylates. *J. Chem. Soc. Dalton Trans.* **2009**, *3*, 4928–4941.
- (180) Di Nicola, C.; Garau, F.; Gazzano, M.; Lanza, A.; Monari, M.; Nestola, F.; Pandolfo, L.; Pettinari, C. Interaction of the Trinuclear Triangular Secondary Building Unit $[\text{Cu}_3(\mu_3\text{-OH})(\mu\text{-Pz})_3]^{2+}$ with 4,4'-Bipyridine. Structural Characterizations of New Coordination Polymers and Hexanuclear CuII Clusters. 2°. *Cryst. Growth Des.* **2015**, *15*, 1259–1272.
- (181) Di Nicola, C.; Karabach, Y. Y.; Kirillov, A. M.; Monari, M.; Pandolfo, L.; Pettinari, C.; Pombeiro, A. J. L. Supramolecular Assemblies of Trinuclear Triangular Copper(II) Secondary Building Units through Hydrogen Bonds. Generation of Different Metal-Organic Frameworks,

Valuable Catalysts for Peroxidative Oxidation of Alkanes. *Inorg. Chem.* **2007**, *46*, 221–230.

- (182) Casarin, M.; Corvaja, C.; Di Nicola, C.; Falcomer, D.; Franco, L.; Monari, M.; Pandolfo, L.; Pettinari, C.; Piccinelli, F.; Tagliatesta, P. Spontaneous Self-Assembly of an Unsymmetric Trinuclear Triangular Copper(II) Pyrazolate Complex, $[\text{Cu}_3(\mu_3\text{-OH})(\mu\text{-Pz})_3(\text{MeCOO})_2(\text{Hpz})]$ (Hpz = Pyrazole). Synthesis, Experimental and Theoretical Characterization, *Reac. Inorg. Chem.* **2004**, *43*, 5865–5876.
- (183) Ferrer, S.; Haasnoot, J. G.; Reedijk, J.; Müller, E.; Biagini Cingi, M.; Lanfranchi, M.; Manotti Lanfredi, A. M.; Ribas, J. Trinuclear N,N-Bridged Copper(II) Complexes Involving a Cu_3OH Core: $[\text{Cu}_3(\mu_3\text{-OH})\text{L}_3\text{A}(\text{H}_2\text{O})_2]\text{A}, (\text{H}_2\text{O})_x$ Synthesis, X-Ray Structures, Spectroscopy, and Magnetic Properties. *Inorg. Chem.* **2002**, *39*, 1859–1867.
- (184) Pandolfo, L.; Pettinari, C. Trinuclear Copper(II) Pyrazolate Compounds: A Long Story of Serendipitous Discoveries and Rational Design. *Cryst. Eng. Comm.* **2017**, *19*, 1701–1720.
- (185) Angaridis, P. A.; Baran, P.; Boča, R.; Cervantes-Lee, F.; Haase, W.; Mezei, G.; Raptis, R. G.; Werner, R. Synthesis and Structural Characterization of Trinuclear CuII-Pyrazolato Complexes Containing $\mu_3\text{-OH}$, $\mu_3\text{-O}$, and $\mu_3\text{-Cl}$ Ligands. Magnetic Susceptibility Study of $[\text{PPN}]_2[(\mu_3\text{-O})\text{Cu}_3(\mu\text{-Pz})_3]$. *Inorg. Chem.* **2002**, *41*, 2219–2228.
- (186) Kintzel, B.; Böhme, M.; Liu, J.; Burkhardt, A.; Mrozek, J.; Buchholz, A.; Ardavan, A.; Plass, W. Molecular Electronic Spin Qubits from a Spin-Frustrated Trinuclear Copper Complex. *Chem. Commun.* **2018**, *54*, 12934–12937.
- (187) Ferrer, S.; Lloret, F.; Bertomeu, I.; Alzuet, G.; Borrás, J.; García-Granda, S.; Liu-González, M.; Haasnoot, J. G. Cyclic Trinuclear and Chain of Cyclic Trinuclear Copper(II) Complexes Containing a Pyramidal $\text{Cu}_3\text{O}(\text{H})$ Core. Crystal Structures and Magnetic Properties of $[\text{Cu}_3(\mu_3\text{-OH})(\text{Aaat})_3(\text{H}_2\text{O})_3](\text{NO}_3)$. *Inorg. Chem.* **2002**, *41*, 5821–5830.

- (188) Ouellette, W.; Yu, M. H.; O'Connor, C. J.; Hagrman, D.; Zubieta, J. Hydrothermal Chemistry of the Copper-Triazolate System: A Microporous Metal-Organic Framework Constructed from Magnetic $\{Cu_3Materials(\mu_3-OH)(Triazolate)_3\}^3$ Building Blocks, and Related. *Angew. Chemie - Int. Ed.* **2006**, *45*, 3497–3500.
- (189) Lloret, F.; Julve, M.; Journaux, Y. Molecular Topology and Exchange Interaction: Synthesis and Magnetic Properties of $[Cu^{II}_3M^{II}]$ (M = Cd, Ni, Mn) Tetranuclear Species. *Inorg. Chem.* **1990**, *29*, 3967–3972.
- (190) Anwar, M. U.; Al-Harrasi, A.; Pilkington, M.; Gavey, E. L.; Rawson, J. M. A Linear Tetranuclear Cu(II) Complex Exhibiting Both Ferro and Antiferromagnetic Couplings: Synthesis, Characterization and Magneto-Structural Studies. *Polyhedron* **2019**, *165*, 63–67.
- (191) Martínez-Benito, C.; Pasán, J.; Martín, T.; Lago, A. B.; Julve, M.; Ruiz-Pérez, C. Tailor-Made Copper(II) Coordination Polymers Based on the C_3 Symmetric Methanetriacetate as a Ligand. *Cryst. Eng. Comm.* **2017**, *19*, 376–390.
- (192) Colacio, E.; López-magaña, C.; Romerosa, A. Novel Square-Planar Cyclic Tetranuclear Copper(II) Complex Containing Oximate Bridges. Synthesis, Crystal Structure and Magnetic Properties of Tetrakis[Diaqua(μ -1,3-Dimethylviolurato)-Copper(II)] Tetraperchlorate Dihydrate. *J. Chem. Soc., Dalton Trans.* **1999**, 2923–2926.
- (193) Aouaidjia, F.; Messai, A.; Siab, R.; Ayes, A. I. A New Tetranuclear Copper(II) Complex Using a Schiff Base Ligand: Synthesis, Structural, and Magnetic Studies. *Polyhedron* **2017**, *133*, 257–263.
- (194) Zaltariov, M.-F.; Alexandru, M.; Cazacu, M.; Shova, S.; Novitchi, G.; Train, C.; Dobrov, A.; Kirillova, M. V.; Alegria, E. C. B. A.; Pombeiro, A. J. L.; et al. Tetranuclear Copper(II) Complexes with Macrocyclic and Open-Chain Disiloxane Ligands as Catalyst Precursors for

- Hydrocarboxylation and Oxidation of Alkanes and 1-Phenylethanol. *Eur. J. Inorg. Chem.* **2014**, *2014* (29), 4946–4956.
- (195) Asadi, Z.; Golchin, M.; Eigner, V.; Dusek, M.; Amirghofran, Z. A Novel Water-Soluble Tetranuclear Copper(II) Schiff Base Cluster Bridged by 2, 6-Bis-[(2-Hydroxyethylimino)Methyl]-4-Methylphenol in Interaction with BSA: Synthesis, X-Ray Crystallography, Docking and Cytotoxicity Studies. *J. Photochem. Photobiol. A Chem.* **2018**, *361*, 93–104.
- (196) Nanda, P. K.; Aromí, G.; Ray, D. Tetranuclear Cu(II) Complex Supported by a Central μ_4 -1,1,3,3 Azide Bridge. *Chem. Commun.* **2006**, 3181–3183.
- (197) Gungor, E.; Kara, H.; Colacio, E.; Mota, A. J. Two Tetranuclear Copper(II) Complexes with Open Cubane-like Cu_4O_4 Core Framework and Ferromagnetic Exchange Interactions between Copper(II) Ions: Structure, Magnetic Properties, and Density Functional Study. *Eur. J. Inorg. Chem.* **2014**, *9*, 1552–1560.
- (198) Gungor, E. A New Stepped Tetranuclear Copper(II) Complex: Synthesis, Crystal Structure and Photoluminescence Properties. *Acta Crystallogr. Sect. C Struct. Chem.* **2017**, *73*, 393–398.
- (199) Borisova, N. E.; Kostin, A.; Magdesieva, T. V.; Reshetova, M. D.; Nikitin, O.; Paredes-García, V.; Garland, M. T.; Hermosilla-Ibáñez, P.; Cañon-Mancisidor, W.; Rodionov, A.; et al. Solvent Switchable CuII Complexes. *New J. Chem.* **2014**, *38*, 709–716.
- (200) Kahn, O. *Molecular Magnetism*; Wiley-VCH, New York.: Orsay, 1993.
- (201) Spielberg, E. T.; Gilb, A.; Plaul, D.; Geibig, D.; Hornig, D.; Schuch, D.; Buchholz, A.; Ardavan, A.; Plass, W. A Spin-Frustrated Trinuclear Copper Complex Based on Triaminoguanidine with an Energetically Well-Separated Degenerate Ground State. *Inorg. Chem.* **2015**, *54*, 3432–3438.

- (202) Anwar, M. U.; Thompson, L. K.; Dawe, L. N. Spin Frustration in a Cu(II)₃ Triangle Frustrated? *Dalt. Trans.* **2011**, *40*, 1437–1440.
- (203) Chaudhuri, P.; Karpenstein, I.; Winter, M.; Butzlaff, C.; Bill, E.; Alfred, X.; Florkec, U.; Hauptc, H. Isolation of a Spin-Frustrated Imidazolate-Bridged Trinuclear Copper(II) Complex Potentially Relevant to the Multicopper Oxidases. *J. Chem. Soc. Chem. Commun* **1992**, 321–322.
- (204) Padilla, J.; Gatteschi, D.; Chaudhuri, P. Single-Crystal EPR Studies of a Spin-Frustrated Imidazolate-Bridged Trinuclear Copper(II) Complex. *Inorganica Chim. Acta* **1997**, *260*, 217–220.
- (205) Bhattacharyya, A.; Bauzá, A.; Sproules, S.; Natrajan, L. S.; Frontera, A.; Chattopadhyay, S. A Polynuclear and Two Dinuclear Copper(II) Schiff Base Complexes: Synthesis, Characterization, Self-Assembly, Magnetic Property and DFT Study. *Polyhedron* **2017**, *137*, 332–346.
- (206) Provó Kluit, H. A. J.; Spek, A. L.; Agterberg, F. P. W.; Oevering, H.; Driessen, W. L.; Reedijk, J.; Buijs, W.; Lakin, M. T. Dinuclear Paddle-Wheel Copper(II) Carboxylates in the Catalytic Oxidation of Carboxylic Acids. *Inorg. Chem.* **1997**, *36*, 4321–4328.
- (207) Speed, S.; Vicente, R.; Aravena, D.; Ruiz, E.; Roubeau, O.; Teat, S. J.; El Fallah, M. S. Hexanuclear Copper(II) Cages Built on a Central { μ_3 -O \cdots H \cdots μ_3 -O} Moiety, 1,3-Bis(Dimethylamino)-2-Propanolato and Capping R-Phosphonates: Crystal Structures, Magnetic Behavior, and DFT Studies. *Inorg. Chem.* **2012**, *51*, 6842–6850.
- (208) Zhang, J.; Li, A. H.; Liu, B. L.; Tao, R. J. Synthesis, Structures and Magnetic Properties of Dissymmetrical Schiff-Base Copper(II) Complexes: [(Cu₂L)₂(H₂O)₄] \cdot (CuL)₂ \cdot 4H₂O and [Cu₂L(Dca)]N. *Inorg. Chem. Commun.* **2013**, *35*, 333–336.

- (209) Alves, W. A.; Cerchiaro, G.; Paduan-Filho, A.; Tomazela, D. M.; Eberlin, M. N.; Da Costa Ferreira, A. M. Infinite Zig-Zag and Cyclic-Tetranuclear Isomeric Imidazolate-Bridged Polynuclear Copper(II) Complexes: Magnetic Properties, Catalytic Activity and Electrospray Mass and Tandem Mass Spectrometry Characterization. *Inorganica Chim. Acta* **2005**, *358*, 3581–3591.
- (210) Dîrtu, M. M.; Boland, Y.; Gillard, D.; Tinant, B.; Robeyns, K.; Safin, D. A.; Devlin, E.; Sanakis, Y.; Garcia, Y. New Mononuclear Cu(II) Complexes and 1D Chains with 4-Amino-4H-1,2,4-Triazole. *Int. J. Mol. Sci.* **2013**, *14*, 23597–23613.
- (211) Landee, C. P.; Turnbull, M. M. Recent Developments in Low-Dimensional Copper(II) Molecular Magnets. *Eur. J. Inorg. Chem.* **2013**, 2266–2285.
- (212) Yang, Y. S.; Liu, L. J.; Ju, H. Y.; Liu, X. Y.; Li, Y. G.; Shi-Ping, Y. Dicyanamide Bridged Cu(II)₃₆-Metallacrown-6 Complex with 1,4,7-Triisopropyl-1,4,7-Triazacyclononane and Binding Properties with DNA. *Molecules* **2018**, *23*, 1269.
- (213) Zyga, L. Researchers Engineer Molecular Magnets to Act as Long-Lived Qubits. *Phys. Rev. Lett.* **2012**, *108*, 2–3.
- (214) Baker, M. L.; Timco, G. A.; Piligkos, S.; Mathieson, J. S.; Mutka, H.; Tuna, F.; Kozłowski, P.; Antkowiak, M.; Guidi, T.; Gupta, T.; et al. A Classification of Spin Frustration in Molecular Magnets from a Physical Study of Large Odd-Numbered-Metal, Odd Electron Rings. *Proc. Natl. Acad. Sci. U. S. A.* **2012**, *109*, 19113–19118.
- (215) Sun, H. L.; Wang, Z. M.; Gao, S. Strategies towards Single-Chain Magnets. *Coord. Chem. Rev.* **2010**, *254* (9–10), 1081–1100.
- (216) Bonner, J. C.; Fisher, M. E. Linear Magnetic Chains with Anisotropic Coupling. *Phys. Rev.*

1964, 135.

- (217) Baker, G. A.; Rushbrooke, G. S.; Gilbert, H. E. High-Temperature Series Expansions for the Spin--, Heisenberg Model by the Method of Irreducible Representations of the Symmetric Group. **1964**, 135, 1272–1277.
- (218) Su, F.; Lu, L.; Feng, S.; Zhu, M.; Gao, Z.; Dong, Y. Synthesis, Structures and Magnetic Properties in 3d-Electron-Rich Isostructural Complexes Based on Chains with Sole Syn-Anti Carboxylate Bridges. *Dalt. Trans.* **2015**, 44, 7213–7222.
- (219) Gao, W.; Zhang, X. M.; Liu, J. P.; Gao, E. Q. Structures and Magnetism of Two Copper(II) Compounds with Mixed Hydroxido-Carboxylate Bridges Derived from Isomeric Pyridylbenzoate N-Oxide Ligands. *Inorganica Chim. Acta* **2016**, 440, 21–25.
- (220) Dalgarno, S. J.; Power, N. P.; Atwood, J. L. Metallo-Supramolecular Capsules. *Coord. Chem. Rev.* **2008**, 252, 825–841.
- (221) Machado, V.; Turnbull, M. M.; Dawe, L. N. Structure and Magnetic Properties of a 1d Alternating Cu(II) Monomer—Paddlewheel Chain. *Crystals* **2018**, 8.
- (222) Turba, S.; Foxon, S. P.; Beitat, A.; Heinemann, F. W.; Petukhov, K.; Müller, P.; Walter, O.; Lloret, F.; Julve, M.; Schindler, S. Syntheses, Characterization, and Magnetic Studies of Copper(II) Complexes with the Ligand N,N,N',N'-Tetrakis(2-Pyridylmethyl)-1,3-Benzenediamine (1,3-Tpbd) and Its Phenol Derivative 2,6-Bis[Bis(2-Pyridylmethyl) Amino]-p-Cresol] (2,6-Htpcd). *Inorg. Chem.* **2012**, 51 (1), 88–97.
- (223) Valencia, S.; Vargas, X.; Rios, L.; Restrepo, G.; Marín, J. M. Sol-Gel and Low-Temperature Solvothermal Synthesis of Photoactive Nano-Titanium Dioxide. *J. Photochem. Photobiol. A Chem.* **2013**, 251, 175–181.

- (224) Demazeau, G. Solvothermal Reactions : An Original Route for the To Cite This Version : HAL Id : Hal-00269253. *J. Mater. Sci.* **2008**, 7, 2104–2114.
- (225) Murphy, G.; Murphy, C.; Murphy, B.; Hathaway, B. Crystal Structures, Electronic Properties and Structural Pathways of Two $[\text{Cu}(\text{Phen})_2(\text{OH}_2)][\text{Y}]_2$ Complexes (Phen = 1,10-Phenanthroline, $\text{Y}=\text{CF}_3\text{SO}_3$ or ClO_4). **1997**, 2, 2653–2660.
- (226) Sheldrick, G. M. Crystal Structure Refinement with SHELXL. *Acta Crystallogr. Sect. C Struct. Chem.* **2015**, 71, 3–8.
- (227) Shields, G. P.; Raithby, P. R.; Allen, F. H.; Samuel Mothewell, W. D. The Assignment and Validation of Metal Oxidation States in the Cambridge Structural Database. *Acta Crystallogr. Sect. B Struct. Sci.* **2000**, 455–465.
- (228) Chilton, N. F.; Anderson, R. P.; Turner, L. D.; Soncini, A.; Murray, K. S. PHI: A Powerful New Program for the Analysis of Anisotropic Monomeric and Exchange-Coupled Polynuclear d- and f-Block Complexes. *J. Comput. Chem.* **2013**, 34, 1164–1175.
- (229) Chen, J.; Wang, X.; Shao, Y.; Zhu, J.; Zhu, Y.; Li, Y.; Xu, Q.; Guo, Z. A Trinuclear Copper(II) Complex of 2,4,6-Tris(Di-2-Pyridylamine)-1,3,5-Triazine Shows Prominent DNA Cleavage Activity. *Inorg. Chem.* **2007**, 46, 3306–3312.
- (230) Goodenough, J. B. Theory of the Role of Covalence in the Perovskite-Type Manganites $[\text{La},\text{M}(\text{II})]\text{MnO}_3$. *Phys. Rev.* **1955**, 100 (2), 564–573.
- (231) P. W. Anderson. Antiferromagnetism. Theory of Superexchange. *Phys. Rev.* **1950**, 79, 350–355.
- (232) Zhang, F.; Kong, Y.-C.; Pang, R.; Hu, L.; Gong, P.-L.; Shi, X.-Q.; Tang, Z.-K. Super-Exchange Theory for Polyvalent Anion Magnets. *New J. Phys.* **2019**, 21, 053033.
- (233) Geertsma, W.; Khomskii, D. Influence of Side Groups on 90° Superexchange: A Modification of the Goodenough-Kanamori-Anderson Rules. *Phys. Rev. B - Condens. Matter Mater. Phys.* **1996**, 54, 3011–3014.

- (234) Streltsov, S. V.; Khomskii, D. I. Orbital Physics in Transition Metal Compounds: New Trends. *Uspekhi Fiz. Nauk* **2017**, *187*, 1205–1235.
- (235) Saparov, B.; Mitzi, D. B. Organic-Inorganic Perovskites: Structural Versatility for Functional Materials Design. *Chem. Rev.* **2016**, *116* (7), 4558–4596.
- (236) Hadouchi, M.; Assani, A.; Saadi, M.; Saadoune, I.; Lahmar, A.; Bouyanfif, H.; El Marssi, M.; El Ammari, L. Synthesis, Crystal Structure and Properties of a New Phosphate, $\text{Na}_2\text{Co}_2\text{Cr}(\text{PO}_4)_3$. *J. Inorg. Organomet. Polym. Mater.* **2018**, *28*, 2854–2864.
- (237) Zeisel, L.; Szimhardt, N.; Wurzenberger, M. H. H.; Klapötke, T. M.; Stierstorfer, J. 2-Methyl-Substituted Monotetrazoles in Copper(II) Perchlorate Complexes: Manipulating Coordination Chemistry and Derived Energetic Properties. *New J. Chem.* **2019**, *43*, 609–616.
- (238) Xiao, X.; Peng, B.; Cai, L.; Zhang, X.; Liu, S.; Wang, Y. The High Efficient Catalytic Properties for Thermal Decomposition of Ammonium Perchlorate Using Mesoporous ZnCo_2O_4 Rods Synthesized by Oxalate Co-Precipitation Method. *Sci. Rep.* **2018**, *8*, 1–13.
- (239) Brown, I. D.; Altermatt, D. Bond-Valence Parameters Obtained from a Systematic Analysis of the Inorganic Crystal Structure Database. *Acta Cryst.* **1985**, 244–247.
- (240) Balaji, S. S.; Sathish, M. Supercritical Fluid Processing of Nitric Acid Treated Nitrogen Doped Graphene with Enhanced Electrochemical Supercapacitance. *RCS Adv.* **2014**, *47*, 7634–7639.
- (241) Chu, S.; Subrahmanyam, A. V.; Huber, G. W. The Pyrolysis Chemistry of a β -O-4 Type Oligomeric Lignin Model Compound. *Green Chem.* **2013**, *15*, 125–136.
- (242) Dong, Z.; Mi, Z.; Shi, W.; Jiang, H.; Zheng, Y.; Yang, K. High Pressure Effects on Hydrate Cu-BTC Investigated by Vibrational Spectroscopy and Synchrotron X-Ray Diffraction. *RSC Adv.* **2017**, *7*, 55504–55512.
- (243) Knop, S.; Jansen, T. L. C.; Lindner, J.; Vöhringer, P. On the Nature of OH-Stretching Vibrations in Hydrogen-Bonded Chains: Pump Frequency Dependent Vibrational Lifetime.

- Phys. Chem. Chem. Phys.* **2011**, *13*, 4641–4650.
- (244) Mohr, S.; Schmitt, T.; Döpfer, T.; Xiang, F.; Schwarz, M.; Görling, A.; Schneider, M. A.; Libuda, J. Coverage-Dependent Anchoring of 4,4'-Biphenyl Dicarboxylic Acid to CoO(111) Thin Films. *Langmuir* **2017**, *33*, 4178–4188.
- (245) Zafiu, C.; Trettenhahn, G.; Pum, D.; Sleytr, U. B.; Kautek, W. Structural Control of Surface Layer Proteins at Electrified Interfaces Investigated by in Situ Fourier Transform Infrared Spectroscopy. *Phys. Chem. Chem. Phys.* **2011**, *13*, 13232–13237.
- (246) Akgul, F. A.; Akgul, G.; Yildirim, N.; Unalan, H. E.; Turan, R. Influence of Thermal Annealing on Microstructural, Morphological, Optical Properties and Surface Electronic Structure of Copper Oxide Thin Films. *Mater. Chem. Phys.* **2014**, *147*, 987–995.
- (247) Simone, E.; Nagy, Z. K. A Link between the ATR-UV/Vis and Raman Spectra of Zwitterionic Solutions and the Polymorphic Outcome in Cooling Crystallization. *Cryst. Eng. Comm.* **2015**, *17*, 6538–6547.
- (248) Maurice, R.; Sivalingam, K.; Ganyushin, D.; Guihéry, N.; De Graaf, C.; Neese, F. Theoretical Determination of the Zero-Field Splitting in Copper Acetate Monohydrate. *Inorg. Chem.* **2011**, *50*, 6229–6236.
- (249) Kawamori, A. Exchange Interaction in Copper Acetate Monohydrate Studied by Nuclear Quadrupole Resonance. *J. Magn. Reson.* **1978**, *31*, 423–430.
- (250) de Loth, P.; Cassoux, P.; Daudey, J. P.; Malrieu, J. P. Ab Initio Direct Calculation of the Singlet-Triplet Separation in Cupric Acetate Hydrate Dimer. *J. Am. Chem. Soc.* **1981**, *103*, 4007–4016.
- (251) Fallis, A. . The Insignificance of Metal-Metal Bonding in the Antiferromagnetism of Copper(II) Carboxylate Dimers. *J. Chem. Inf. Model.* **2013**, *53*, 1689–1699.
- (252) Kyuzou, M.; Mori, W.; Tanaka, J. Electronic Structure and Spectra of Cupric Acetate Mono-

- Hydrate Revisited. *Inorganica Chim. Acta* **2010**, *363*, 930–934.
- (253) Suzuki, M.; Suzuki, I. S. Lecture Note on Solid State Physics: Mean-Field Theory. *System* **2006**, *6000*, 1–15.
- (254) Gatteschi, D. Molecular Magnetism: A Basis for New Materials. *Adv. Mater.* **1994**, *6*, 635–645.
- (255) Guo, F. S.; Bar, A. K.; Layfield, R. A. Main Group Chemistry at the Interface with Molecular Magnetism. *Chem. Rev.* **2019**, *119*, 8479–8505.
- (256) Jiang, W.; Jiao, C.; Meng, Y.; Zhao, L.; Liu, Q.; Liu, T. Switching Single Chain Magnet Behavior: Via Photoinduced Bidirectional Metal-to-Metal Charge Transfer. *Chem. Sci.* **2018**, *9*, 617–622.
- (257) Liu, X.; Wang, Y. X.; Han, Z.; Han, T.; Shi, W.; Cheng, P. Tuning the Magnetization Dynamics of TbIII-Based Single-Chain Magnets through Substitution on the Nitronyl Nitroxide Radical. *Dalton Trans.* **2019**, *48*, 8989–8994.
- (258) Long, Q. Q.; Hu, Z. B.; Wang, H. S.; Yin, C. L.; Chen, Y.; Song, Y.; Zhang, Z. C.; Xia, B. T.; Pan, Z. Q. Field-Induced Single Molecule Magnet Behavior of a Dy^{III}-Na^I One-Dimensional Chain Extended by Acetate Ions. *Inorg. Chem. Commun.* **2018**, *98*, 127–131.
- (259) Degayner, J. A.; Wang, K.; Harris, T. D. A Ferric Semiquinoid Single-Chain Magnet via Thermally-Switchable Metal-Ligand Electron Transfer. *J. Am. Chem. Soc.* **2018**, *140*, 6550–6553.
- (260) Kharwar, A. K.; Mondal, A.; Konar, S. Field Induced Slow Magnetic Relaxation in a Non Kramers Tb(III) Based Single Chain Magnet. *Magnetochemistry* **2018**, *4*, 59.
- (261) Colacio, E.; Ghazi, M.; Kivekäs, R.; Klinga, M.; Lloret, F.; Moreno, J. M. A Rational Design for Imidazolate-Bridged Linear Trinuclear Compounds from Mononuclear Copper(II) Complexes with 2-[[[(Imidazol-2-ylmethylidene)Amino]Ethyl]Pyridine (HL): Syntheses, Structures, and Magnetic Properties of [Cu(L)(Hfac)M(Hfac)₂Cu(Hfac)(L)] (M. *Inorg. Chem.*

2000, 39, 2770–2776.

- (262) Liu, C. M.; Gao, S.; Zhang, D. Q.; Huang, Y. H.; Xiong, R. G.; Liu, Z. L.; Jiang, F. C.; Zhu, D. Ben. A Unique 3D Alternating Ferro- and Antiferromagnetic Manganese Azide System with Threefold Interpenetrating (10,3) Nets. *Angew. Chemie - Int. Ed.* **2004**, 43, 990–994.
- (263) Liu, X.; Sun, L.; Zhou, H.; Cen, P.; Jin, X.; Xie, G.; Chen, S.; Hu, Q. Single-Ion-Magnet Behavior in a Two-Dimensional Coordination Polymer Constructed from Co^{II} Nodes and a Pyridylhydrazone Derivative. *Inorg. Chem.* **2015**, 54, 8884–8886.
- (264) Ferlay, S.; Mallah, T.; Ouahès, R.; Veillet, P.; Verdaguer, M. A Room-Temperature Organometallic Magnet Based on Prussian Blue. *Nature* **1995**, 378, 701–703.
- (265) Liu, X.; Qu, X.; Zhang, S.; Ke, H.; Yang, Q.; Shi, Q.; Wei, Q.; Xie, G.; Chen, S. High-Performance Energetic Characteristics and Magnetic Properties of a Three-Dimensional Cobalt(II) Metal-Organic Framework Assembled with Azido and Triazole. *Inorg. Chem.* **2015**, 54, 11520–11525.
- (266) Pardo, E.; Train, C.; Boubekour, K.; Gontard, G.; Cano, J.; Lloret, F.; Nakatani, K.; Verdaguer, M. Topological Versatility of Oxalate-Based Bimetallic One-Dimensional (1D) Compounds Associated with Ammonium Cations. *Inorg. Chem.* **2012**, 51, 11582–11593.
- (267) Zeng, Y. F.; Hu, X.; Liu, F. C.; Bu, X. H. Azido-Mediated Systems Showing Different Magnetic Behaviors. *Chem. Soc. Rev.* **2009**, 38, 469–480.
- (268) Mezei, G.; Zaleski, C. M.; Pecoraro, V. L. Structural and Functional Evolution of Metallacrowns. *Chem. Rev.* **2007**, 107, 4933–5003.
- (269) Lescouëzec, R.; Toma, L. M.; Vaissermann, J.; Verdaguer, M.; Delgado, F. S.; Ruiz-Pérez, C.; Lloret, F.; Julve, M. Design of Single Chain Magnets through Cyanide-Bearing Six-Coordinate Complexes. *Coord. Chem. Rev.* **2005**, 249, 2691–2729.
- (270) Batten, S. R.; Murray, K. S. Structure and Magnetism of Coordination Polymers Containing

- Dicyanamide and Tricyanomethanide. *Coord. Chem. Rev.* **2003**, *246*, 103–130.
- (271) Girovsky, J.; Nowakowski, J.; Ali, M. E.; Baljovic, M.; Rossmann, H. R.; Nijs, T.; Aeby, E. A.; Nowakowska, S.; Siewert, D.; Srivastava, G.; et al. Long-Range Ferrimagnetic Order in a Two-Dimensional Supramolecular Kondo Lattice. *Nat. Commun.* **2017**, *8*, 15388.
- (272) Liu, X.; Li, F.; Ma, X.; Cen, P.; Luo, S.; Shi, Q.; Ma, S.; Wu, Y.; Zhang, C.; Xu, Z.; et al. Coligand Modifications Fine-Tuned the Structure and Magnetic Properties of Two Triple-Bridged Azido-Cu(II) Chain Compounds Exhibiting Ferromagnetic Ordering and Slow Relaxation. *Dalton Trans.* **2017**, *46*, 1207–1217.
- (273) Chen, M.; Zhao, H.; Sañudo, E. C.; Liu, C. Sen; Du, M. Two Isostructural Coordination Polymers Showing Diverse Magnetic Behaviors: Weak Coupling (Ni^{II}) and an Ordered Array of Single-Chain Magnets (Co^{II}). *Inorg. Chem.* **2016**, *55*, 3715–3717.
- (274) Liu, X.; Liu, H.; Cen, P.; Chen, X.; Zhou, H.; Song, W.; Hu, Q. Auxiliary Ligand-Triggered Assembly of Two Dinuclear Cu(II) Compounds with a Pyridylhydrazone Derivative: Synthesis, Crystal Structure and Magnetic Property. *Inorganica Chim. Acta* **2016**, *447*, 12–17.
- (275) Castellano, M.; Fortea-Pérez, F. R.; Stiriba, S. E.; Julve, M.; Lloret, F.; Armentano, D.; De Munno, G.; Ruiz-Garci, R.; Cano, J. Very Long-Distance Magnetic Coupling in a Dicopper(II) Metallacyclophane with Extended π -Conjugated Diphenylethyne Bridges. *Inorg. Chem.* **2011**, *50*, 11279–11281.
- (276) Brown, I. D. *The Chemical Bond in Inorganic Chemistry: The Bond Valence Model*; 2nd ed. Oxford University Press, Oxford, 2016.
- (277) Sanda, S.; Parshamoni, S.; Adhikary, A.; Konar, S. A Family of Metal-Organic Frameworks Based on Carboxylates and a Neutral, Long, and Rigid Ligand: Their Structural Revelation, Magnetic, and Luminescent Property Study. *Cryst. Growth Des.* **2013**, *13*, 5442–5449.
- (278) Han, L. L.; Wang, S. N.; Jagličić, Z.; Zeng, S. Y.; Zheng, J.; Li, Z. H.; Chen, J. S.; Sun, D.

- Synthesis, Structural Versatility and Magnetic Properties of a Series of Copper(II) Coordination Polymers Based on Bipyrazole and Various Dicarboxylate Ligands. *Cryst. Eng. Comm.* **2015**, *17*, 1405–1415.
- (279) Liu, D.; Chang, Y. J.; Lang, J. P. Ligand Geometry-Driven Formation of Different Coordination Polymers from $Zn(NO_3)_2$, 1,4-Bpeb and Phenylenediacetic Acids. *Cryst. Eng. Comm.* **2011**, *13*, 1851–1857.
- (280) Ahn, S. H.; Lee, H. Copper(II) Complexes Containing N,N'-Bidentate-(Pyridin-2-Ylmethyl) Aniline and Its Derivatives: Synthesis, Structure and Magnetic Property. *Bull. Korean Chem. Soc.* **2016**, *37*, 27–32.
- (281) Świtlicka, A.; Czerwińska, K.; Machura, B.; Penkala, M.; Bieńko, A.; Bieńko, D.; Zierkiewicz, W. Thiocyanate Copper Complexes with Pyrazole-Derived Ligands-Synthesis, Crystal Structures, DFT Calculations and Magnetic Properties. *Cryst. Eng. Comm.* **2016**, *18*, 9042–9055.
- (282) Estes, W. E.; Weller, R. R.; Hatfield, W. E. Preparation and Magnetic Characterization of the Linear-Chain Series $M^{II}L_2Cl_2$ with $M = Mn^{2+}$, Cu^{2+} , and Ni^{2+} and $L = 4$ -Phenylpyridine. *Inorg. Chem.* **1980**, *19*, 26–31.
- (283) Salunke-Gawali, S.; Rane, S. Y.; Puranik, V. G.; Guyard-Duhayon, C.; Varret, F. Three Dimensional Hydrogen-Bonding Network in a Copper Complex of 2-Hydroxy-1,4-Naphthoquinone: Structural, Spectroscopic and Magnetic Properties. *Polyhedron* **2004**, *23*, 2541–2547.
- (284) Ikeue, T.; Furukawa, K.; Hata, H.; Aratani, N.; Shinokubo, H.; Kato, T.; Osuka, A. The Importance of a b – b Bond for Long-Range Antiferromagnetic Coupling in Directly Linked Copper(II) and Silver(II) Diporphyrins. *Angew. Chemie* **2005**, *44*, 6899–6901.
- (285) Rabu, P.; Rueff, J. M.; Huang, Z. L.; Angelov, S.; Souletie, J.; Drillon, M. Copper(II) and

- Cobalt (II) Dicarboxylate-Based Layered Magnets : Influence of π -Electron Ligands on the Long Range Magnetic Ordering. *Polyhedron* **2001**, *20*, 1677–1685.
- (286) Burger, K.; Chaudhuri, P.; Wieghardt, K.; Nuber, B. Intramolecular Long-Range Exchange Coupling in Dinuclear Copper(II) Complexes with Cu...Cu Separations Greater than 10 Å. *Chem. Eur. J.* **1995**, 583–593.
- (287) Chen, Z.; Xiong, W.; Zhang, Z.; Liang, F. Structure and Magnetic Properties of Two Lanthanide 1, 4-Phenylenediacetate Compounds. *Z. Anorg. Allg. Chem.* **2010**, *636*, 1392–1396.
- (288) Mcgregor, K. T.; Watkins, N. T.; Lewis, D. L.; Drake, R. T.; Hodgson, D. J.; Hatfield, W. E. Magnetic Properties of Di- μ -Hydroxobis(2,2'-Bipyridyl) Dicopper(II) Nitrate, and the Correlation Between the Singlet-Triplet Splitting and the Cu-O-Cu Angle in Hydroxo-Bridged Copper(II) Complexes. *Inorg. Nucl. Chem. Lett.* **1973**, *9*, 423–428.
- (289) Titi, H. M.; Karmakar, A.; Goldberg, I. Coordination Polymers and Hydrogen-Bonded Assemblies of 2,2'-[2,5-Bis-(Carboxymethoxy)-1,4-Phenylene]-Diacetic Acid with Ammonium, Lanthanum and Zinc Cations. *Acta Crystallogr. Sect. C Cryst. Struct. Commun.* **2010**, *66* (9), 238–244.
- (290) Reger, D. L.; Debreczeni, A.; Smith, M. D. Synthesis and Structure of a Cu₄O₄ Cubane Core Complex from a Carboxylate Ligand Containing a Strong π ... π Stacking Supramolecular Synthone. *Inorganica Chim. Acta* **2012**, *386*, 102–108.
- (291) Ruiz, E.; Cano, J.; Alvarez, S.; Alemany, P.; Barcelona, U. V. De. Magnetic Coupling in End-On Azido-Bridged Transition Metal Complexes : A Density Functional Study. *J. Chem. Am. Soc.* **1998**, *10*, 11122–11129.
- (292) Dias, S. S. P.; Kirillova, M. V; Julia, K.; Kirillov, A. M. New Tetracopper(II) Cubane Cores Driven by a Diamino Alcohol: Self- Assembly Synthesis, Structural and Topological Features, and Magnetic and Catalytic Oxidation Properties. *Inorg. Chem.* **2015**, *54*, 5204–5212.

- (293) Escuer, A.; Mayans, J.; Font-Bardia, M. Copper(II) Cubanes with a {Cu₄O} Core and Well Defined S = 1 Ground State. *Dalt. Trans.* **2016**, 45 (4), 1604–1613.
- (294) Banerjee, A.; Singh, R.; Mondal, P.; Colacio, E.; Rajak, K. K. Tetranuclear Copper(II) Complexes Bearing Cu₄O₆ and Cu₄O₄ Cores: Synthesis, Structure, Magnetic Properties, and DFT Study. *Eur. J. Inorg. Chem.* **2010**, 4 (5), 790–798.
- (295) Sun, J.; Xu, H. Synthesis, Structures and Properties of Cu(II) and Mn(II) Complexes with 1,10-Phenanthroline-2-Carboxylic Acid and 2,2'-Bipyridine Ligands. **2010**, 8349–8359.
- (296) Ardizzoia, G. A.; Brenna, S. Hydroxo-Bridged Copper(II) Cubane Complexes. *Coord. Chem. Rev.* **2016**, 311, 53–74.
- (297) Mallick, L.; Kumar, S.; Chowdhury, A. Thermal Decomposition of Ammonium Perchlorate — A TGA – FTIR – MS Study : Part I. *Thermochim. Acta* **2015**, 610, 57–68.
- (298) Wojtas', M.; Czupinski, O.; Tylczyn, Z.; Isakov, D.; Belsley, M.; Jakubas, R. Optical Nonlinearity and Piezoelectricity in 2,4,6-Trimethylpyridinium Perchlorate. **2014**, 441, 59–65.
- (299) Donald L. Pavia, Gary M. Lampman, G. S. K. *Introduction to Spectroscopy*; Cengage Learning: Bellingham, 2008.
- (300) Fielden, J.; Sprott, J.; Long, D.; Ko, P. Controlling Aggregation of Copper(II) -Based Coordination Compounds : From Mononuclear to Dinuclear, Tetranuclear ,and Polymeric Copper Complexes. **2006**, 45, 2886–2895.
- (301) Zhang, M.; Wu, Y.; Wang, J.; Ren, Y.; Hou, X. Crystal Structure and Magnetic Properties of a Novel Helical Coordination Polymer [Cu₂(Pda)₂(Phen)₂(H₂O)₂].6H₂O. *J. Inorg. Organomet. Polym. Mater.* **2010**, 20, 862–866.
- (302) Wang, H.; Jacobson, A. J. Unpublished Work. 2018.
- (303) Lu, Z.; Fan, T.; Guo, W.; Lu, J.; Fan, C. Synthesis, Structure and Magnetism of Three Cubane Cu(II) and Ni(II) Complexes Based on Flexible Schiff-Base Ligands. *Inorganica Chim. Acta*

2013, 400, 191–196.

- (304) Xie, Y.; Bu, W.; Xu, X.; Jiang, H.; Liu, Q.; Xue, Y.; Fan, Y. Crystal Structure and Magnetic Properties of a Cu₄O₄ Cubane Complex with N-(2-Hydroxybenzyl)-Propanolamine. *Inorg. Chem. Commun.* **2001**, 4 (10), 558–560.
- (305) Quintanar, L.; Gebhard, M.; Wang, T.; Kosman, D. J.; Solomon, E. I. Ferrous Binding to the Multicopper Oxidases *Saccharomyces Cerevisiae* Fet3p and Human Ceruloplasmin: Contributions to Ferroxidase Activity. *J. Am. Chem. Soc.* **2004**, 9 (1), 6579–6589.
- (306) Lin, J.; Liang, X.; Cao, X.; Wei, N.; Ding, Y. An Octanuclear Cu(II) Cluster with a Bio-Inspired Cu₄O₄ Cubic Fragment for Efficient Photocatalytic Water Oxidation. *Chem. Commun.* **2018**, 54 (88), 12515–12518.
- (307) Crispini, A.; Cretu, C.; Aparaschivei, D.; Andelescu, A. A.; Sasca, V.; Badea, V.; Aiello, I.; Szerb, E. I.; Costisor, O. Influence of the Counterion on the Geometry of Cu(I) and Cu(II) Complexes with 1, 10-Phenanthroline. *Inorganica Chim. Acta* **2018**, 470, 342–351.
- (308) Ruiz, E.; Alemany, P.; Alvarez, S.; Cano, J. Structural Modeling and Magneto-Structural Correlations for Hydroxo-Bridged Copper(II) Binuclear Complexes. *Inorg. Chem.* **1997**, 36, 3683–3688.
- (309) Triki, S.; Gómez-García, C. J.; Ruiz, E.; Sala-Pala, J. Asymmetric Azido-Copper(II) Bridges: Ferro- or Antiferromagnetic? Experimental and Theoretical Magneto-Structural Studies. *Inorg. Chem.* **2005**, 44, 5501–5508.
- (310) Mukherjee, A.; Raghunathan, R.; Saha, M. K.; Nethaji, M.; Ramasesha, S.; Chakravarty, A. R. Magnetostructural Studies on Ferromagnetically Coupled Copper(II) Cubanes of Schiff-Base Ligands. *Chem. - A Eur. J.* **2005**, 11, 3087–3096.

- (311) Gupta, S.; Pal, S.; Barik, A. K.; Hazra, A.; Roy, S.; Mandal, T. N.; Peng, S. M.; Lee, G. H.; Salah El Fallah, M.; Tercero, J.; et al. Synthesis, Characterization and Magnetostructural Correlation Studies on Three Binuclear Copper Complexes of Pyrimidine Derived Schiff Base Ligands. *Polyhedron* **2008**, *27*, 2519–2528.
- (312) Trans, S. O. C. D.; Structure, C. D.; Nuclear, D.; Resonance, M.; Darriet, J.; Villeneuve, G.; Porter, D. B.-. Magnetostructural Correlations in Parallel Square-Planar Chloride Bridged Copper(II) Dimers: Structure, Dynamic Nuclear Magnetic Resonance Study, and Magnetic Properties of $[\text{Cu}_2(\text{Terpy})_2\text{Cl}_2][\text{PF}_6]_2$. *Dalton Trans.* **1987**, *2*, 285–291.
- (313) Herringer, S. N.; Landee, C. P.; Turnbull, M. M.; Ribas-Ariño, J.; Novoa, J. J.; Polson, M.; Wikaira, J. L. Ferromagnetic Exchange in Bichloride Bridged Cu(II) Chains: Magnetostructural Correlations between Ordered and Disordered Systems. *Inorg. Chem.* **2017**, *56*, 5441–5454.
- (314) Shiga, T.; Oshio, H.; Shiga, T.; Oshio, H. Molecular Cubes with High-Spin Ground States. *Sci. Technol. Adv. Mater.* **2006**, *6996*, 2005.
- (315) Christou, G.; Gatteschi, D.; Hendrickson, D. N.; Sessoli, R. Single-Molecule Magnets. *Mrs Bull.* **2019**, *25*, 66–71.
- (316) Constantinos, J.; Vinslava, A.; Wood, P. A.; Parsons, S.; Wernsdorfer, W.; Christou, G.; Perlepes, S. P.; Brechin, E. K. A Single-Molecule Magnet with a “Twist”. *J. Am. Chem. Soc.* **2007**, *129*, 8–9.
- (317) Willett, R. D.; Gatteschi, D.; Kahn, O. Magneto-Structural Correlations in Exchange Coupled Systems; 1985.
- (318) Cristallografia, S.; Perugia, U.; Interaction, E.; Structural, T. C.; Chiari, B.; Helms, J. H.; Piovesana, O.; Tarantelli, T.; Zanazzi, P. F. Exchange Interaction in Multinuclear Transition-

Metal Complexes. Structural and Magnetic Studies on $\text{Cu}_2\text{L}_2(\text{CH}_3\text{COO})_2\cdot 2\text{H}_2\text{O}$ (LH = N-Methyl-N'-(5-methoxysalicylidene)-1,3-propanediamine), a Novel “Structural” Ladderlike Compound with “Magnetic” Alternating-Chain Behavior. *Inorg. Chem.* **1986**, *25*, 870–874.

(319) Kou, H.; Liao, D.; Cheng, P.; Jiang, Z.; Yan, S.; Wang, G.; Yao, X.; Wang, H. Crystal Structure and Magnetic Behaviour of a Two-Dimensional Step-Shaped Cyano-Bridged Complex $[\text{Cu}(\text{Dien})]_3[\text{Fe}(\text{CN})_6]_2\cdot 6\text{H}_2\text{O}$ (Dien = Diethylenetriamine). *J. Chem. Soc., Dalton Trans.* **1997**, *9*, 1503–1506.

(320) Pandey, P.; Verma, A.; Bretosh, K.; Sutter, J.; Sunkari, S. S. Template Directed Synthesis of Half Condensed Schiff Base Complexes of Cu(II) and Co (III): Structural and Magnetic Studies. *Polyhedron* **2019**, *164*, 80–89.

(321) Baryshnikova, A. T.; Minaev, B. F.; Baryshnikov, G. V; Hans, Å. Computational Study of the Structure and Magnetic Properties of the Weakly- Coupled Tetranuclear Square-Planar Complex of Cu(II) with a Tetraporphyrin Sheet. **2019**, *485*, 73–79.

(322) Qi, J.; Liang, S.; Gou, Y.; Zhang, Z.; Zhou, Z.; Yang, F.; Liang, H. Synthesis of Four Binuclear Copper(II) Complexes: Structure, Anticancer Properties and Anticancer Mechanism. *Eur. J. Med. Chem.* **2015**, *96*, 360–368.

(323) Boodram, J. N.; Mcgregor, I. J.; Bruno, P. M.; Cressey, P. B.; Hemann, M. T.; Suntharalingam, K. Breast Cancer Stem Cell Potent Copper(II)-Non-Steroidal Anti-Inflammatory Drug Complexes. *Angew. Chemie - Int. Ed.* **2016**, *55*, 2845–2850.

(324) Duff, B.; Reddy Thangella, V.; Creaven, B. S.; Walsh, M.; Egan, D. A. Anti-Cancer Activity and Mutagenic Potential of Novel Copper(II) Quinolinone Schiff Base Complexes in Hepatocarcinoma Cells. *Eur. J. Pharmacol.* **2012**, *689*, 45–55.

(325) Muralisankar, M.; Sujith, S.; Bhuvanesh, N. S. P.; Sreekanth, A. Synthesis and Crystal Structure of New Monometallic and Bimetallic Copper(II) Complexes with N-Substituted Isatin Thiosemicarbazone Ligands: Effects of the Complexes on DNA/Protein-Binding Property, DNA Cleavage Study and in Vitro Anticancer Activity. *Polyhedron* **2016**, *118*, 103–117.